

INVESTIGATING THE BOTTOM FREE SURFACE NAPPE (OGEE PROFILE) ACROSS A SHARP-CRESTED WEIR INFLUENCED BY THE FLOW IN AN ASYMMETRICAL APPROACH CHANNEL

GERT LOUIS COETZEE

04428986

A dissertation submitted in fulfilment of the requirements for the degree of

MASTER OF ENGINEERING
WATER RESOURCES ENGINEERING

In the

FACULTY OF ENGINEERING

DEPARTMENT OF CIVIL ENGINEERING

UNIVERSITY OF PRETORIA

March 2013

DISSERTATION

INVESTIGATING THE BOTTOM FREE SURFACE NAPPE
(OGEE PROFILE) ACROSS A SHARP-CRESTED WEIR
INFLUENCED BY THE FLOW IN AN ASYMMETRICAL
APPROACH CHANNEL

Gert Louis Coetzee

Supervisor: Professor Doctor SJ van Vuuren

Department: Civil Engineering

University: University of Pretoria

Degree: Master of Engineering (Water Resources Engineering)

When the well is dry, we know the worth of water.

BENJAMIN FRANKLIN, (1706-1790)

EXECUTIVE SUMMARY

The shape of an Ogee spillway is based on the shape of the lower nappe of water flowing over a sharp-crested weir for the selected design discharge. At the design discharge, the shape minimises the possibility of sub-atmospheric pressure occurring on the spillway and maximise the discharge across the spillway for the given energy condition.

Currently used formulae that were developed to approximate this shape consider the following 2-dimensional flow parameters (USBR, 1987):

- depth of flow over the spillway crest (H_d);
- the inclination of the upstream wall face (F_s); and
- the pool depth upstream of the spillway (P).

These 2-dimensional flow parameters are graphically depicted in **Figure i**.

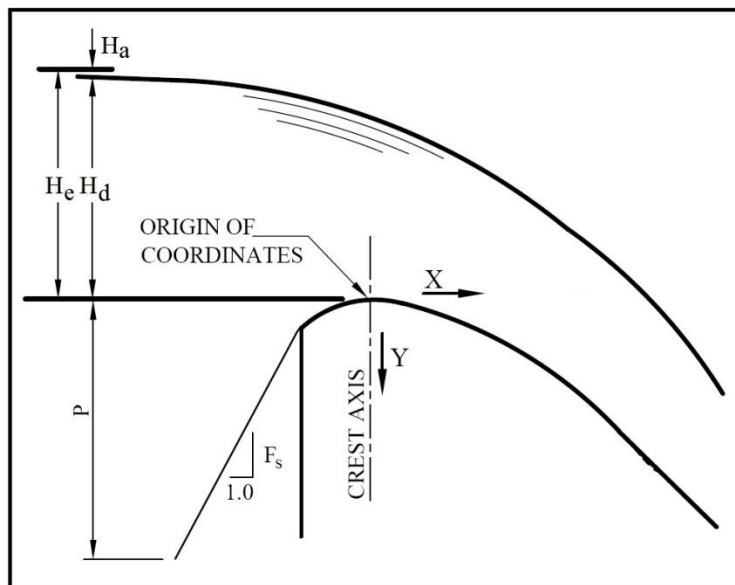


Figure i: Definition sketch of current formulae parameters

The upstream pool depth can also be related to the average approach velocity in the channel (Velocity head – H_a). Current formulations to determine the Ogee shape, do not consider the influence of 3-dimensional flow parameters. The most significant 3-dimensional flow parameters that could affect the shape of the nappe are:

- the flow velocity distribution upstream of the spillway;
- the orientation or angle of the water approaching the spillway in relation to the centreline of the spillway;
- the asymmetrical cross-section of the approach channel upstream from the spillway; as well as
- the curvature of the dam wall.

This research project reflects the results from a model study in which some of these 3-dimensional flow parameters were evaluated to determine their influence on the shape of the Ogee profile. The Ogee profile was simulated by the bottom nappe for water flowing freely across a sharp-crested weir. The study also compares the measured nappe profile with the currently used design relationships to determine the Ogee profile.

It was found that changes in the asymmetrical upstream cross-section, affects the shape of the bottom nappe which differs from the shape proposed by the known Ogee formulae. This dissertation highlights the shortcomings of a two dimensional assessment of the Ogee spillway.

DECLARATION OF ORIGINALITY



UNIVERSITEIT VAN PRETORIA
UNIVERSITY OF PRETORIA
YUNIBESITHI YA PRETORIA
Denkleiers • Leading Minds • Dikgopolo tša Dihalefi

Full names of student: GERT LOUIS COETZEE

Student number: 04428986

Topic of work: INVESTIGATING THE BOTTOM FREE SURFACE NAPPE (OGEE PROFILE) ACROSS A SHARP-CRESTED WEIR INFLUENCED BY THE FLOW IN AN ASYMMETRICAL APPROACH CHANNEL

Declaration

1. I understand what plagiarism is and I am also aware of the University's policy in this regard.
2. I declare that this dissertation is my own original work. Where other people's work has been used (either from a printed source, Internet or any other source), this has been properly acknowledged and referenced in accordance with Departmental requirements.
3. I have not used work previously produced by another student or any other person to hand in as my own.
4. I have not allowed, and will not allow, anyone to copy my work with the intention of passing it off as his or her own work.

A handwritten signature in black ink, appearing to read 'G. Coetzee'.

GL COETZEE

8712075053084

ACKNOWLEDGEMENTS

I wish to express my appreciation and indebtedness to the following organizations and persons who made this dissertation possible (in no particular order):

1. Professor SJ van Vuuren (University of Pretoria), my supervisor for all his guidance, encouragement, patience and assistance during the course of this study;
2. Dr P Wessels (Department of Water Affairs) senior specialist engineer, hydrological services, my co-supervisor all his guidance and assistance during the course of this study;
3. Neil van Rensburg and all the other staff members of Interlock Systems who assisted in the construction of the aluminium frame, sharp-crested weir and profile measuring apparatus;
4. Mark-Andrew Beukes who assisted in the construction of the profile measuring apparatus;
5. Interlock Systems for sponsoring the sharp-crested weir, aluminium frame and profile measuring apparatus;
6. The University of Pretoria for the use of the Proefplaas Hydraulic Laboratory during preliminary evaluation of the study with the aid of undergraduate students Cameron Fynn and Hayden Armstrong;
7. Jerry Nkosi, artisan from the University of Pretoria for construction of the steel frames, and painting and welding of the steel structures;
8. Johannes Matlala and Pieter Mynardt, both supervisors of the Department of Water Affairs Hydraulic Laboratory for assistance in the construction of the physical model;
9. Freddie Khoza, Patrick Mpyana, Alfred Mothombeni, Joseph Sithole and Joseph Nkosi, artisans from the Department of Water Affairs Hydraulic Laboratory for their help with the construction of the brick structures;
10. Prof Louis Coetzee, my father, for his help in construction of the sharp-crested weir and many hours of proofreading of my dissertation;
11. Laetitia Coetzee, my mother, for all the inventive paint work on the physical model to reflect a better visual impression of my results;
12. Jacobus Coetzee, my young brother, for his many hours of dedication in assisting me with the construction of the physical model at the Department of Water Affairs, helping with technical ideas and supporting me at all times;
13. The rest of my family for their continual encouragement, and support during the study; and
14. The Lord Almighty who is my only salvation and saviour for giving me the ability to complete this research topic in the regulated time set.

INVESTIGATING THE BOTTOM FREE SURFACE NAPPE (OGEE PROFILE) ACROSS A SHARP-CRESTED WEIR INFLUENCED BY THE FLOW IN AN ASYMMETRICAL APPROACH CHANNEL

TABLE OF CONTENTS

1	INTRODUCTION	1-1
1.1	BACKGROUND	1-1
1.2	HYPOTHESIS	1-6
1.3	OBJECTIVES OF THE STUDY.....	1-10
1.4	SCOPE OF THE STUDY	1-10
1.5	METHODOLOGY.....	1-12
1.6	ORGANISATION OF THE DISSERTATION	1-14
2	LITERATURE REVIEW	2-1
2.1	SPILLWAYS	2-1
2.2	BACKGROUND ON THE OGEE SPILLWAY	2-6
2.3	THE OGEE SPILLWAY.....	2-7
2.3.1	<i>Approximation of the Ogee curve by means of first principles of projectile movement.....</i>	<i>2-10</i>
2.3.1.1	The relationship of the Ogee curve as approximated by Ven te Chow from 1 st Principles of projectile movement	2-11
2.3.1.2	The relationship of the Ogee curve as approximated by Ven te Chow (Modified)	2-14
2.3.1.3	The relationship of the Ogee curve as approximated by Wahl et al. (2008).....	2-16
2.3.2	<i>Approximation of the Ogee curve by means of experimental methods</i>	<i>2-19</i>
2.3.2.1	The relationship of the Ogee curve as approximated by the USBR (1987).....	2-19
2.3.2.2	The relationship of the Ogee curve as approximated by the UASCE (1970)	2-26
2.3.2.3	The relationship of the Ogee curve as approximated by USACE (b) (1987)	2-28
2.3.2.4	The relationship of the Ogee curve as approximated by Hager (1987)	2-31
2.3.2.5	The relationship of the Ogee curve as approximated by Creager, 1917 (Chanson, 2004).....	2-34
2.3.2.6	The relationship of the Ogee curve as approximated by Scimeni, 1930 (Chanson, 2004)	2-34
2.3.2.7	The relationship of the Ogee curve as approximated by Montes, 1992 (Chanson, 2004)	2-34
2.3.2.8	The relationship of the Ogee curve as approximated by Knapp, 1960 (Chanson, 2004).....	2-36
2.3.2.9	The relationship of the Ogee curve as approximated by CE-05016 (Ministry of Science and Technology, 2007)	2-37
2.3.3	<i>Summary and comparison of Ogee profile formulae</i>	<i>2-38</i>
2.4	OGEE CURVE APPROXIMATIONS OF ACTUAL DAMS (ŞENTÜRK, 1994).....	2-41
2.5	TANGENT POINT ON DOWNSTREAM SLOPE OF THE OGEE CURVE.....	2-44

2.6	3-DIMENSIONAL FLOW PARAMETERS TO BE CONSIDERED WHEN APPROXIMATING THE OGEE CURVE.....	2-47
2.6.1	<i>Introduction</i>	2-47
2.6.2	<i>Velocity distribution of approach channel</i>	2-49
2.6.3	<i>The orientation of approach velocity relative to the spillway structure</i>	2-56
2.6.4	<i>Effects of asymmetry of the upstream cross-section</i>	2-58
2.6.5	<i>Effects of the radius of the wall</i>	2-60
2.6.6	<i>Comparison of opinions of 3-D effects</i>	2-62
2.7	SEPARATION FROM SPILLWAY	2-64
2.8	CREST PRESSURES (MELSHEIMER & MURPHY, 1970).....	2-65
2.9	CAVITATION	2-67
2.9.1	<i>CAVITATION INDEX</i>	2-72
2.10	INTERNATIONAL DESIGN STANDARDS OF SHARP-CRESTED WEIRS	2-74
2.10.1	<i>MORE DISCHARGE COEFFICIENTS OF SHARP-CRESTED WEIRS</i>	2-80
2.11	CALIBRATION OF SHARP-CRESTED WEIR	2-81
2.12	CASE STUDIES	2-84
2.13	SCALED MODELS	2-86
3	METHOD	3-1
3.1	EXPERIMENTAL SETUP AT THE DEPARTMENT OF WATER AFFAIRS HYDRAULIC LABORATORY	3-1
3.1.1	<i>Introduction</i>	3-1
3.1.2	<i>Existing layout at the Department of Water Affairs Hydraulic Laboratory</i>	3-1
3.1.3	<i>Preliminary design of the model</i>	3-6
3.2	CONSTRUCTION OF THE PHYSICAL MODEL	3-10
3.2.1	<i>Construction of the outer boundary of the physical model</i>	3-10
3.2.2	<i>Installation of the wall structure utilized to dam the water</i>	3-12
3.2.3	<i>Levelling the wall structure of the sharp-crested weir</i>	3-13
3.2.4	<i>Waterproofing and sealing of the wall structure of the sharp-crested weir</i>	3-15
3.2.5	<i>Construction and plastering of fill-in walls</i>	3-16
3.2.6	<i>Attachment of the stainless steel sharp-crested weir's crest</i>	3-18
3.2.7	<i>Assembly of the aluminium frame for the Ogee profile measuring apparatus</i>	3-19
3.2.8	<i>Painting and measuring position markers on the sharp-crested weir</i>	3-24
3.2.9	<i>Installation of Plexiglas contractions sheets on the crest of the sharp-crested weir</i>	3-26
3.2.10	<i>Installation of flow straighteners in the approach channel of the physical model</i>	3-28
3.2.11	<i>Levelling of the upstream pool</i>	3-30
3.2.12	<i>Fitment of the wooden slope at the toe of the sharp-crested weir</i>	3-31

3.2.13	<i>Construction of the variable side angle walls used to alter the symmetricity of the approach channel</i>	3-34
3.2.14	<i>Sliding mechanism for Ogee profile measuring instrument (OPMI)</i>	3-39
3.2.15	<i>Construction of the Ogee profile measuring instrument (OPMI)</i>	3-41
3.2.16	<i>Installation of the water level sensor to the OPMI</i>	3-45
3.2.17	<i>Definition of Cartesian co-ordinate system</i>	3-47
3.2.18	<i>Installation of the stage depth meters with OTT-point gauges in stilling columns</i>	3-50
3.3	OTHER OGEE PROFILE MEASURING TECHNIQUES INVESTIGATED	3-52
3.3.1	<i>Laser measuring apparatus</i>	3-52
3.3.2	<i>PhotoModeler® Scanner</i>	3-58
3.3.3	<i>Ultra-sonic sensors</i>	3-61
3.4	PROCEDURE FOLLOWED DURING THE EXECUTION OF MEASURING THE OGEE PROFILE	3-62
3.5	MOTIVATION FOR THE EXPERIMENTAL METHOD USED	3-69
3.6	OBSTACLES FACED DURING THE PROJECT	3-71
4	ANALYSIS OF EXPERIMENTAL RESULTS AND COMPARISON WITH THEORY	4-1
4.1	DISCUSSION OF RESULTS	4-1
4.1.1	<i>Scenario 1: Symmetrical Approach Channel with flow rate at 60 l/s</i>	4-3
4.1.2	<i>Scenario 2A: Symmetrical Approach Channel with flow rate at 80 l/s</i>	4-9
4.1.3	<i>Scenario 2B: Asymmetrical Approach Channel with side wall inclined at 45° with flow rate at 80 l/s</i>	4-14
4.1.4	<i>Scenario 2C: Asymmetrical Approach Channel with side wall inclined at 60° with flow rate at 80 l/s</i>	4-21
4.1.5	<i>Scenario 3A: Asymmetrical Approach Channel with side wall inclined at 45° with flow rate at 130 l/s</i>	4-29
4.1.6	<i>Scenario 3B: Asymmetrical Approach Channel with side wall inclined at 60° with flow rate at 115 l/s</i>	4-37
5	CONCLUSIONS AND RECOMMENDATIONS	5-1
6	REFERENCES	6-1
	APPENDIX A: POPULATED DATA SHEETS	6-1

INVESTIGATING THE BOTTOM FREE SURFACE NAPPE (OGEE PROFILE) ACROSS A SHARP-CRESTED WEIR INFLUENCED BY THE FLOW IN AN ASYMMETRICAL APPROACH CHANNEL

LIST OF FIGURES

Figure 1-1: Blyderiverpoort Dam, Mpumalanga, South Africa (Ogee spillway with Robertson Splitters) (Yahoo! Inc., 2011).....	1-2
Figure 1-2: Cavitation damage at a spillway chute exposing the reinforcement of the hydraulic structure (Smoak, 1997).....	1-4
Figure 1-3: Example of cavitation erosion damage on a spillway (Tropea, et al., 2007)	1-5
Figure 1-4: The presence of sub-atmospheric pressure was indicated by purple dye downstream of the Ogee crest during the physical model study of the Neckartal Dam (van Vuuren, et al., 2011)	1-6
Figure 1-5: Free overfall spillway (Kouga Dam, Eastern Cape, A) and Ogee Spillway (Blyderiverpoort Dam, Mpumalanga, B).....	1-7
Figure 1-6: The velocity distribution in an asymmetrical channel with the colour scale depicting the magnitude of the water’s velocity: A. the relative orientation of the cross-section in relation to the approach channel and B. the asymmetrical approach channel’s velocity distribution (Figures modified from Riley & Rhoads, 2012).....	1-8
Figure 1-7: Curvature of dam wall influencing the geometric shape of the Ogee profile at the Neckartal dam, Namibia (van Vuuren, <i>et al.</i> , 2011).....	1-9
Figure 1-8: Rectangular symmetrical approach channel with flow line perpendicular to the crest section used to determine a baseline Ogee profile (ASTM International, 2001)	1-11
Figure 1-9: Symmetrical approach channel (A) and Asymmetrical approach channel (B)	1-11
Figure 1-10: Lower nappe of the water trajectory flowing over a sharp-crested weir simulates the profile of an Ogee spillway (Ministry of Science and Technology, 2007).....	1-12
Figure 1-11: Positions of the Ogee profile measurements	1-13
Figure 2-1: Grand Coulee Dam Ogee spillway spilling 2011 (Yahoo! Inc., 2011)	2-2
Figure 2-2: Mohale dam spilling February 2006 (International Water Power and Dam Construction, 2009)	2-2
Figure 2-3: Hoover Dam side channel spillway overflowing 1983 (Wiltshire, et al., 2010).....	2-3
Figure 2-4: Limited service spillway (in foreground) to be constructed and auxiliary spillway (ogee crest) in background at New Waddle Dam , Arizona (LaBoon, et al., 2011)	2-4

Figure 2-5: Arabie Dam, now called Flag Boshielo Dam in the Crocodile River, South Africa with limited service spillway embankment to be flushed away under large floods without damaging the main spillway structure2-4

Figure 2-6: Curved streamlines with its origin of curvature below the flow (Lv, et al., 2011)2-6

Figure 2-7: Shape of the Ogee Spillway (Anon., 2006).....2-8

Figure 2-8: Trajectory of a particle following a projectile movement.....2-11

Figure 2-9: Derivation of the nappe profile of a water particle flowing over a sharp-crested weir by the principle of projectile movement (Chow, 1959).....2-12

Figure 2-10: Position of the turning point of curvature at the maximum elevation of the Ogee profile..2-13

Figure 2-11: Comparison of the USBR compound curve for insignificant upstream velocity head is compared with the modified Vent te Chow equation (Chow, 1959)2-16

Figure 2-12: Comparison of computed jet trajectories and Ogee crest profile representing experimental data (Wahl, et al., 2008).....2-18

Figure 2-13: Ogee profile approximation by the USBR (1987) for negligible approach velocity2-21

Figure 2-14: Ogee profile approximation by the USBR (1987) for measurable approach velocities2-22

Figure 2-15: Standard shape of Ogee curve for a vertical upstream spillway face with measurable velocity head (Chow, 1959).....2-23

Figure 2-16: Design charts to determine values for K and n for power function curve (USBR, 1987)...2-24

Figure 2-17: Factors for definition of Ogee profile compound curve's radii for the case of measurable approach velocities (USBR, 1987).....2-25

Figure 2-18: The coordinates for the upstream quadrant of the Ogee curve as defined by the USACE (1987).....2-27

Figure 2-19: Elliptical curve method for determining the Ogee curve (USACE (b), 1987)2-30

Figure 2-20: Definition sketch of parameters for Ogee Profile (Chanson, 2004).....2-32

Figure 2-21: The Ogee curve as defined by Hager (1987) and USACE (1987)2-33

Figure 2-22: Comparitive plot of Creager's, Scimemi's and Montes' Ogee profiles (Chanson, 2004) ..2-35

Figure 2-23: Comparitive plot of Creager's, Knapp's, Hager's and Montes' Ogee profiles for the crest region only (Chanson, 2004).....2-36

Figure 2-24: Definition sketch of parameters for Ogee Profile2-37

Figure 2-25: K and n constants for the approximation of the downstream quadrant of the Ogee curve (Ministry of Science and Technology, 2007).....2-38

Figure 2-26: The upstream quadrant as defined by the aforementioned methods for defining the Ogee curve.....2-40

Figure 2-27: The downstream quadrant as defined by the aforementioned methods for defining the Ogee curve.....	2-41
Figure 2-28: Schematic section of a dam wall used to calculate the downstream slope of the hydraulic structure	2-44
Figure 2-29: Example of an Ogee spillway with reverse curve at the bottom for dissipation of energy. The tangent point is indicated and located at the orange dot (Anon., 2006).....	2-45
Figure 2-30: Slope function graph of the tangents X and Y to the downstream quadrant of Ogee spillways (USACE (a), 1987)	2-46
Figure 2-31: Upstream topography of approach channel influencing the velocity distribution over the spillway (Chow, 1959).....	2-48
Figure 2-32: Asymmetry of approach channel for the Neckertal Dam (van Vuuren, 2010)	2-49
Figure 2-33: Velocity distribution upstream of a sharp-crested weir (Horton, 1907).....	2-51
Figure 2-34: Velocity distribution of a rectangular open channel as given by ISO 1438 (2008)	2-54
Figure 2-35: Hypothetical scenario where the Ogee curve is approximated by the USACE (a) (1987) ..	2-55
Figure 2-36: Angles of river approaching a spillway.....	2-57
Figure 2-37: Symmetry of upstream cross-section in the approach channel	2-59
Figure 2-38: Velocity distribution of a straight spillway compared to a curved spillway	2-61
Figure 2-39: Influence of curvature visible at the Blydepoortriver Dam indicating a larger trajectory of water flowing over the center of the spillway compared to the sides.	2-62
Figure 2-40: Nappe separation for spillway at heads exceeding 3 times the design head (Thandaveswara, 2006)	2-64
Figure 2-41: Crest pressures on Ogee spillways evaluated by Melsheimer & Murphy (1970)	2-66
Figure 2-42: Shock-wave formation during collapse of an air void particle	2-67
Figure 2-43: Micro-jet collapse edited from Knapp <i>et al.</i> (1970).....	2-68
Figure 2-44: Damage in a spillway tunnel at Glen Canyon Dam as a result of cavitation (Morris, 2012).....	2-69
Figure 2-45: Examples of basic aeration devices as given by Asawa (2008).....	2-70
Figure 2-46: Cavitation damage on the Karun dam, Iran (Kramer, 2009).....	2-71
Figure 2-47: Extract from the 2011/2012 Dam Safety Office Report of South Africa indicate the 80 cases of cavitation damage to spillways (DWA, 2012).....	2-72
Figure 2-48: Vapour pressure as a function of temperature.....	2-74
Figure 2-49: Approach channel requirements for designing a fully contracted sharp-crested weir (ISO 1438, 2008)	2-76

Figure 2-50: Plate requirements for a sharp-crested weir (ASTM International, 2001; ISO 1438, 2008).....	2-77
.....	2-77
Figure 2-51: Estimation of effective weir widths for ratios of b/B (ISO 1438, 2008).....	2-79
Figure 2-52: Estimation of discharge coefficients for ratios of h/p (ISO 1438, 2008)	2-79
Figure 2-53: Calibration methods for sharp-crested weirs by Johnson & Green (1977)	2-82
Figure 2-54: Keenleyside Dam cavitation damage on the sluiceway crest near the gate slots (Tatro, et al., 1994)	2-85
Figure 2-55: Neglecting the 3-dimensional effect being caused by the contraction of side walls at a sharp-crested weir, a relative good approximation of the Ogee curve is obtained by means of a CFD analysis (Ferrari, 2010).....	2-88
Figure 3-1: Three centrifugal pumps installed at DWA Hydraulic Laboratory (Pump no. 1, KSB ETA250/29 was utilized for the experimental setup)	3-2
Figure 3-2: Pump curve of pump no. 1, KSB ETA250/29 (KSB Pumps, 2005)	3-3
Figure 3-3: Flow regulated to physical model by adjusting the full-bore butterfly valve.....	3-4
Figure 3-4: Calibration of the magnetic flow meter by making use of the provided crump weir and volumetric tank	3-5
Figure 3-5: Configuration of the constant-head tank layout	3-6
Figure 3-6: Plan view of proposed sharp-crested weir.....	3-8
Figure 3-7: Downstream view of the proposed sharp-crested weir	3-8
Figure 3-8: Side view of the proposed sharp-crested weir model and detail of the crest-configuration....	3-9
Figure 3-9: 44 mm x 44 mm aluminium support beams (PRO-VEY (Pty) Ltd., 2012)	3-20
Figure 3-10: 63 mm x 63 mm aluminium angle support brackets (PRO-VEY (Pty) Ltd., 2012).....	3-20
Figure 3-11: Plan view with dimensions of the aluminium frame and its position relative to the sharp-crested weir	3-21
Figure 3-12: Cross-section of the laminated Plexiglas contraction attached to the crest of the sharp-crested weir	3-26
Figure 3-13: Upstream view of approach channel with steel frame made from 25 mm square tubing used to alter the symmetricity of the approach channel	3-34
Figure 3-14: The upstream cross-sectional view of the asymmetrical approach channel with side wall inclined at 45° (A) and 60° (B) respectively.....	3-35
Figure 3-15: Insize vernier height gauge with fine adjustment (accuracy ±0.05 mm, model no. 1250-450)	3-42
.....	3-42
Figure 3-16: KEMO® <i>M158 Waterswitch</i> with geometric dimensions (KEMO®, 2012)	3-45
Figure 3-17: Water level sensor circuit (KEMO®, 2011)	3-46

Figure 3-18: Conducting Silver used to coat the copper tip of the OPMI (KEMO®, 2012).....	3-46
Figure 3-19: Existing physical model of free falling weir at the Department of Water Affairs Hydraulic Laboratory.....	3-53
Figure 3-20: Schematic layout of making use of a Laser Pointer to measure the Ogee profile.....	3-54
Figure 3-21: Laser triangulation sensor: optoNCDT 2300 by Mirco-Epsilon.....	3-55
Figure 3-22: The optoNCDT 2300-100 measuring a co-ordinate on the Ogee profile from above the water surface at a sharp-crested weir.....	3-56
Figure 3-23: Confocal displacement measurement system: optoNCDT 2410 by Micro-Epsilon.....	3-57
Figure 3-24: Laser Profile Sensor (CC3100) by Cross Check.....	3-58
Figure 3-25: PhotoModeler® Scanner software package (PhotoModeler®, 2012).....	3-59
Figure 3-26: View of lower nappe from guide channel in which the camera was secured.....	3-60
Figure 3-27: Guide channel in which the camera was secured constructed from plywood and Plexiglas.....	3-60
Figure 3-28: Ultra-sonic displacement sensor (UC 500-30GM-IU-V1) by Pepperl + Fuchs GmbH.....	3-61
Figure 3-29: Offset of the copper tip of the OPMI relative to the crest of the weir (vertical - left, rotated - right).....	3-63
Figure 3-30: Vertical displacement of the copper tip of the OPMI relative to the crest of the weir (vertical - left, rotated - right).....	3-64
Figure 3-31: “Reference surface” for scenario 2 with the green surface reflecting the case of the rotated copper tip and the red surface that of the case of the vertical copper tip.....	3-65
Figure 3-32: Measurements of the Ogee profile was recorded at 10 mm intervals.....	3-66
Figure 3-33: Upstream view of the layout for the symmetrical approach channel.....	3-66
Figure 3-34: Protractor indicating the inclination of the installed plywood sidewall at 45° and 60° respectively.....	3-67
Figure 3-35: Datasheet complete for each scenario conducted (Afrikaans version).....	3-68
Figure 3-36: Gust of wind causing fluctuation in the Ogee profile at measuring location Yellow 1.....	3-73
Figure 4-1: 2-dimensional plot of measured Ogee profile for scenario 1.....	4-4
Figure 4-2: Prominent flow pattern visible at boundaries due to change in flow direction caused by contraction of the weir.....	4-5
Figure 4-3: Smooth water surface of the approach channel evidence of no prominent flow patterns existing in the channel.....	4-6
Figure 4-4: Measured Ogee surface for scenario 1.....	4-8
Figure 4-5: Measured Ogee surface for scenario 1 compared with theoretical Ogee profile a given by the USACE (1970).....	4-9

Figure 4-6: 2-dimensional plot of measured Ogee profile for scenario 2A	4-10
Figure 4-7: Measured Ogee surface for scenario 2A	4-13
Figure 4-8: Measured Ogee surface for scenario 2A compared with theoretical Ogee profile a given by the USACE (1970).....	4-13
Figure 4-9: 2-dimensional plot of measured Ogee profile for scenario 2B	4-15
Figure 4-10: Measured Ogee surface for scenario 2B (including outlier measurements).....	4-16
Figure 4-11: Measured Ogee surface for scenario 2B (including outlier measurements).....	4-17
Figure 4-12: Measured Ogee surface for scenario 2B compared with theoretical Ogee profile a given by the USACE (1970).....	4-21
Figure 4-13: 2-dimensional plot of measured Ogee profile for scenario 2C	4-22
Figure 4-14: High flow velocities experienced at boundary of sharp-crested weir's crest caused by the steep inclination of the 60° side wall	4-23
Figure 4-15: Measured Ogee surface for scenario 2C (including outlier measurements).....	4-24
Figure 4-16: Measured Ogee surface for scenario 2C (including outlier measurements).....	4-25
Figure 4-17: Measured Ogee surface for scenario 2C compared with theoretical Ogee profile a given by the USACE (1970).....	4-29
Figure 4-18: 2-dimensional plot of measured Ogee profile for scenario 3A	4-30
Figure 4-19: Measured Ogee surface for scenario 3A (including outlier measurements)	4-31
Figure 4-20: Measured Ogee surface for scenario 3A (including outlier measurements)	4-32
Figure 4-21: Measured Ogee surface for scenario 3A compared with theoretical Ogee profile a given by the USACE (1970).....	4-37
Figure 4-22: 2-dimensional plot of measured Ogee profile for scenario 3B	4-38
Figure 4-23: Measured Ogee surface for scenario 3B (including outlier measurements).....	4-39
Figure 4-24: Measured Ogee surface for scenario 3B (including outlier measurements).....	4-40
Figure 4-25: Measured Ogee surface for scenario 3B compared with theoretical Ogee profile a given by the USACE (1970).....	4-44
Figure 5-1: The upstream cross-sectional view of the asymmetrical approach channel reflecting the region where the increased Ogee profile is experienced.....	5-1

INVESTIGATING THE BOTTOM FREE SURFACE NAPPE (OGEE PROFILE) ACROSS A SHARP-CRESTED WEIR INFLUENCED BY THE FLOW IN AN ASYMMETRICAL APPROACH CHANNEL

LIST OF TABLES

Table 2-1: Methods for approximation of the Ogee curve.....	2-9
Table 2-2: Ogee profile approximation by the USBR (1987) for negligible approach velocity.....	2-20
Table 2-3: Standard shape of Ogee curve for a vertical upstream spillway face with measurable velocity head (Chow, 1959).....	2-22
Table 2-4: 2-dimensional flow parameters required to approximate Ogee curve.....	2-39
Table 2-5: Examples of Ogee spillways with second degree parabola curves to prevent sub-atmospheric conditions under high flow conditions (Şentürk, 1994).....	2-42
Table 2-6: Hypothetical scenario where the Ogee profile is approximated by the USACE (a) (1987)...	2-54
Table 2-7: Examples of spillway orientation relative to the approach channel for selected South African Dams (images form Google Earth 6.2)	2-58
Table 2-8: Visual comparison of symmetrical approach channels versus asymmetrical approach channels for selected South African Dams (Dam Contours, 2010)	2-60
Table 2-9: Discharge coefficient for un-contracted (full width) weirs (Bagheri & Heidarpour, 2010; ISO 1438, 2008).....	2-80
Table 2-10: Discharge coefficient for contracted weirs (Bagheri & Heidarpour, 2010)	2-81
Table 2-11: Conditions required and range of calibration head for different calibration methods by Johnson & Green (1977).....	2-83
Table 2-12: Spillways that has damaged due to cavitation damage (Tatro, et al., 1994).....	2-84
Table 3-1: Comparison of proposed models geometric ratios to ISO 1438 (2008).....	3-7
Table 3-2: Construction of the outer boundary of the physical model.....	3-10
Table 3-3: Installation of the wall structure utilized to dam the water	3-12
Table 3-4: Levelling the wall structure of the sharp-crested weir.....	3-14
Table 3-5: Waterproofing and sealing of the wall structure of the sharp-crested weir	3-15
Table 3-6: Construction and plastering of fill-in walls	3-17
Table 3-7: Attachment of the stainless steel sharp-crested weir's crest.....	3-19
Table 3-8: Assembly of the aluminium frame for the Ogee profile measuring apparatus.....	3-21

Table 3-9: Colour coded locations where the Ogee curve was measured along the crest of the sharp-crested weir	3-24
Table 3-10: Painting measuring position markers on the sharp-crested weir	3-25
Table 3-11: Installation of the Plexiglas contraction sheets on the crest of the sharp-crested weir.....	3-27
Table 3-12: Installation of flow straighteners in the approach channel of the physical model.....	3-29
Table 3-13: Levelling of the upstream pool depth.....	3-31
Table 3-14: Fitment of the wooden slope at the toe of the sharp-crested weir	3-32
Table 3-15: Construction of the variable angle side walls used to alter the symmetry of the approach channel	3-36
Table 3-16: Sliding mechanism for Ogee profile measuring instrument (OPMI)	3-39
Table 3-17: Construction of the Ogee profile measuring instrument (OPMI).....	3-43
Table 3-18: Installation of the water level sensor to the OPMI	3-47
Table 3-19: Definition of Cartesian co-ordinate system.....	3-48
Table 3-20: Installation of water level meters in stilling columns	3-50
Table 3-21: Various scenarios executed with allocated notation.....	3-67
Table 4-1: Maximum variance of the measured Ogee profile during scenario 1 at the different measuring locations	4-7
Table 4-2: Maximum variance of the measured Ogee profile during scenario 2A at the different measuring locations	4-11
Table 4-3: Maximum variance of the measured Ogee profile during scenario 2B at the different measuring locations (excluding outlier measurements)	4-18
Table 4-4: Maximum variance of the measured Ogee profile during scenario 2C at the different measuring locations (excluding outlier measurements)	4-26
Table 4-5: Maximum variance of the measured Ogee profile during scenario 3A at the different measuring locations (excluding outlier measurements).....	4-33
Table 4-6: Maximum variance of the measured Ogee profile during scenario 3B at the different measuring locations (excluding outlier measurements)	4-41

INVESTIGATING THE BOTTOM FREE SURFACE NAPPE (OGEE PROFILE) ACROSS A SHARP-CRESTED WEIR INFLUENCED BY THE FLOW IN AN ASYMMETRICAL APPROACH CHANNEL

1 INTRODUCTION

1.1 BACKGROUND

The Ogee spillway relationship (USBR, 1987; Vischer & Hager, 1999) is used to define the recurred profile of the spillway section of a dam or hydraulic structure (**Figure 1-1**). The Ogee relationship describes the bottom nappe associated with a sharp-crested weir. The current relationship accommodates the influence of the unit discharge, the angle of inclination of the upstream wall face, as well as the relationship of upstream pool depth to the total upstream energy at the apex of the structure.

In cases where the discharge flow rate exceeds the design flow rate the nappe coheres to surface of the spillway and a sub-atmospheric pressure region is generated that could lead to cavitation (Savage & Johnson, 2001; Momber, 2000). Cavitation usually occurs during a unit discharge, in excess of the design head, where the surface pressure can be reduced at positions along the spillway to sub-atmospheric pressure. This may cause the formation of vapour cavities. Vapour cavities may also be formed on the spillway where an irregularity in the surface exists. The vapour cavities (also referred to as miniscule air bubbles) will progress along the flow path due to the high flow velocity on the spillway to a region downstream where sufficient pressure is available leading to the collapse of the air vacuum. This generates localized high pressures. Should these vapour cavities collapse near the spillway structure, there will be some superficial damage to the spillway's surface where the vapour bubble has collapsed. This cavitation damage can ultimately result in substantial erosion and, if ignored, will subsequently cause failures of the spillway chute. Minute cracks, offsets and increased surface roughness intensify this cavitation process. The extent of cavitation damage is a function of the cavitation indices at key locations on the spillway chute and the duration of flow over the spillway. This emphasizes the need for a geometric, accurate and precise spillway profile to reduce the possibility of sub-atmospheric pressure formation (U.S. Army Corps of Engineers, 2009).

The current Ogee spillway relationship lacks to incorporate the asymmetrical cross sectional upstream geometry of the spillway, the relative orientation of the spillway with regard to the approaching flow and the curvature of the spillway in relation to the depth of the structure.



Figure 1-1: Blyderiverpoort Dam, Mpumalanga, South Africa (Ogee spillway with Robertson Splitters) (Yahoo! Inc., 2011)

“While dams are no longer considered the sole answer to improving access to water resources, there is no denying the role that these impressive structures have played in the history and development of South Africa. The country’s estimated 500 large dams hold back millions upon millions of litres of water, allowing us to pursue activities that would otherwise have been near impossible in a semi-arid climate. Dams bring us water for consumption in our large cities, irrigation to grow our crops, water to drive our main economic ventures and to generate power, all while holding back huge volumes of floodwaters that might have otherwise engulfed our settlements.”

Dhesigen Naidoo (van Vuuren, 2012a)

This quote by Mr Dhesigen Naidoo, Chief Executive Officer (CEO) of the Water Research Commission of South Africa during the launch of a new book titled: *In the Footsteps of Giants – Exploring the history of South Africa’s Large Dams* by Lani van Vuuren (van Vuuren, 2012c) emphasizes the need to maintain large water infrastructure in South Africa and to further research ways to maintain a sustainable water resource system for future generations. This precious idea should be combined with Mr Danie Badenhorst, Chairperson of SANCOLD (South African National Committee on Large Dams) and Technical director of BKS consulting engineers South Africa (alias AECOM) that stipulated:

“South Africa has developed a large percentage of its water resources and there will be limited dam developments in the future. However, we need to look after our multi-billion Rand dam assets by way of maintenance and rehabilitation. Dam safety is cardinal in this respect. Highly developed skills are required for rehabilitation, which is often more difficult than constructing a new dam. SANCOLD and ICOLD (International Committee on Large Dams) resources are in place to assist with such skills and information transfer”.

Danie Badenhorst (van Vuuren, 2012b)

The importance of large water infrastructure, with dams in particular, is an essential component for the successful economic and sustainable development of any country. The research into the influence of the 3-dimensional flow parameters that may alter the geometric shape of the Ogee spillway is reviewed and may prove to be one of the highly developed skills that are required for rehabilitation of dams in South Africa, as was suggested by Badenhorst (van Vuuren, 2012b).

One of the principal aims of including the upstream geometry was to increase the efficiency of the discharge of the spillway by considering the topographical layout of the spillway approach channel in

relation to the spillway chute and, at the same time preventing the formation of any possible sub-atmospheric pressure on the spillway that may lead to cavitation and concrete erosion. Both of these factors considered, discharge and cavitation damage are both closely linked to substantial financial implications. If the supply discharge is decreased, then the cost to the provider would be great. Similarly, the cost to repair cavitation damaged concrete would be considerable. The USBR suggests that the cost of replacing a damaged concrete spillway chute may be as much as ten times the initial cost of preventing cavitation damage on a newly built spillway. **Figure 1-2** indicates cavitation damage where the reinforcement of the hydraulic structure is visible (Smoak, 1997).

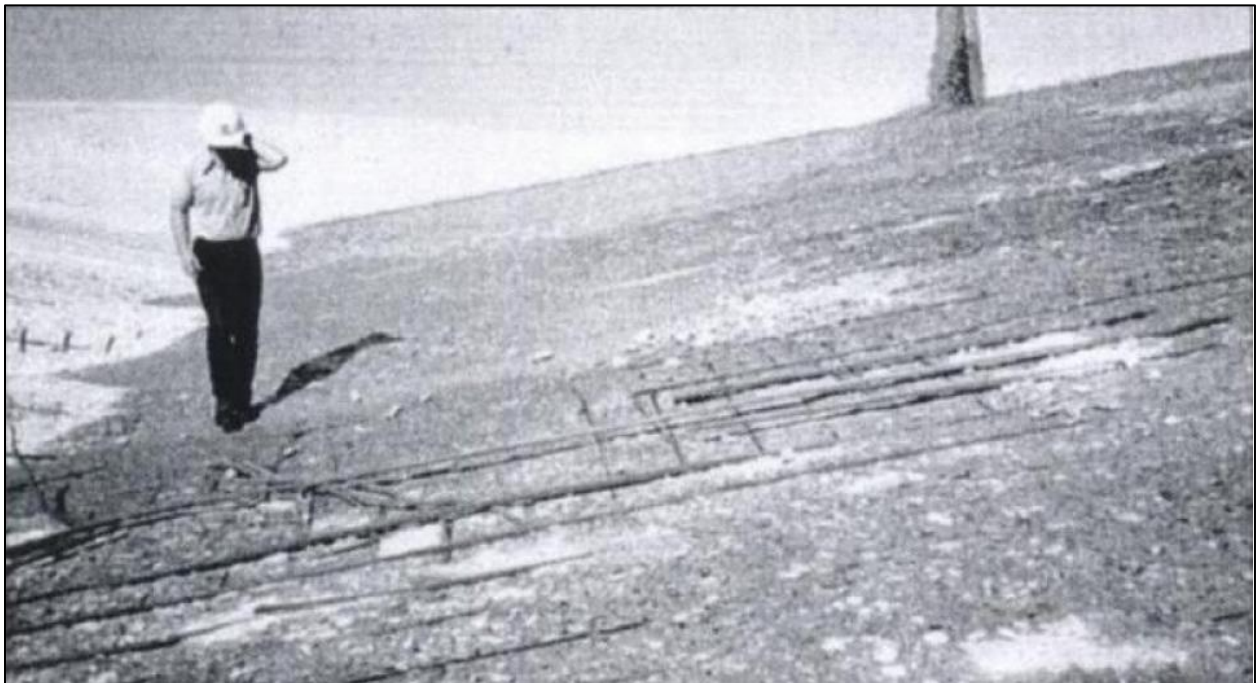


Figure 1-2: Cavitation damage at a spillway chute exposing the reinforcement of the hydraulic structure (Smoak, 1997)

The extent of cavitation erosion can range from a relatively minor amount of pitting after years of service to catastrophic failures in a relatively short period of time. **Figure 1-2** and **Figure 1-3** illustrates the damage that can occur on a spillway caused by cavitation damage due to improper geometric design of the spillway chute. The damage in **Figure 1-3** occurred after only four hours of operation during an extreme flood event. This destruction caused by the cavitation was evident when comparing the size of the eroded concrete with the size of the workmen in the figures (Smoak, 1997 and Tropea, et al., 2007).

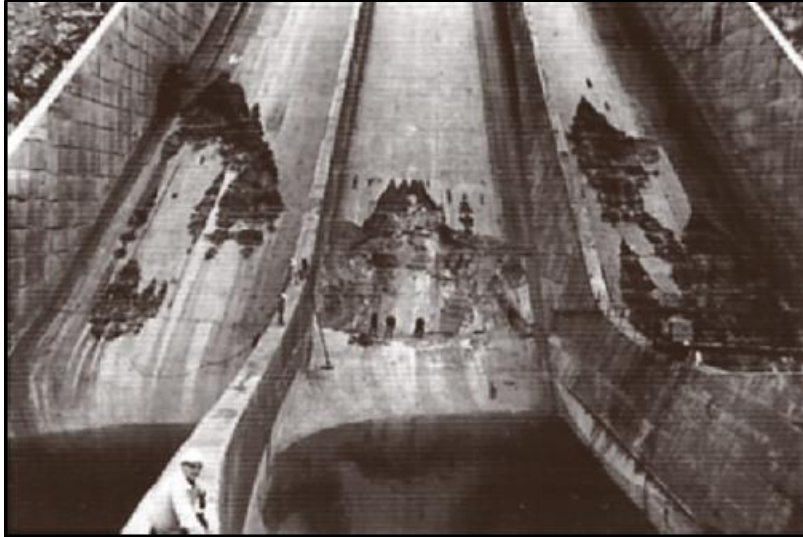


Figure 1-3: Example of cavitation erosion damage on a spillway (Tropea, et al., 2007)

In the reviewed design of the proposed Neckartal Dam (van Vuuren, 2010) to be constructed in Namibia, the physical model reflected that sub-atmospheric pressure were generated downstream of the Ogee spillway crest. These negative pressures were identified by introducing purple dye into the water and where stagnation of the dye occurred, the existence of sub-atmospheric pressure was present (**Figure 1-4**). The explanation of this phenomenon was that the curvature of the dam wall, relative orientation of the wall to the flow direction and approach channel yielded an asymmetrical layout of the system that was causing an increased flow on the one halve of the spillway. Restricted to this specific region on the spillway, the flow rate produced an overdesign of the system for the spillway chute at this location, resulting in sub-atmospheric pressure to exist just downstream of the Ogee crest. Further investigation indicated that with an altered Ogee profile, the sub-atmospheric pressure at this location could be decreased and even eliminated, therefore reducing the potential formation of cavitation and subsequent concrete erosion at this explicit location. The result of this physical model study has led to the conclusion that there still remained unconsidered factors that might have an influence on the required Ogee profile. Van Vuuren (2010) concluded with the recommendation that these parameters should be further studied, hence the existence of this specific research project (van Vuuren, et al., 2011).

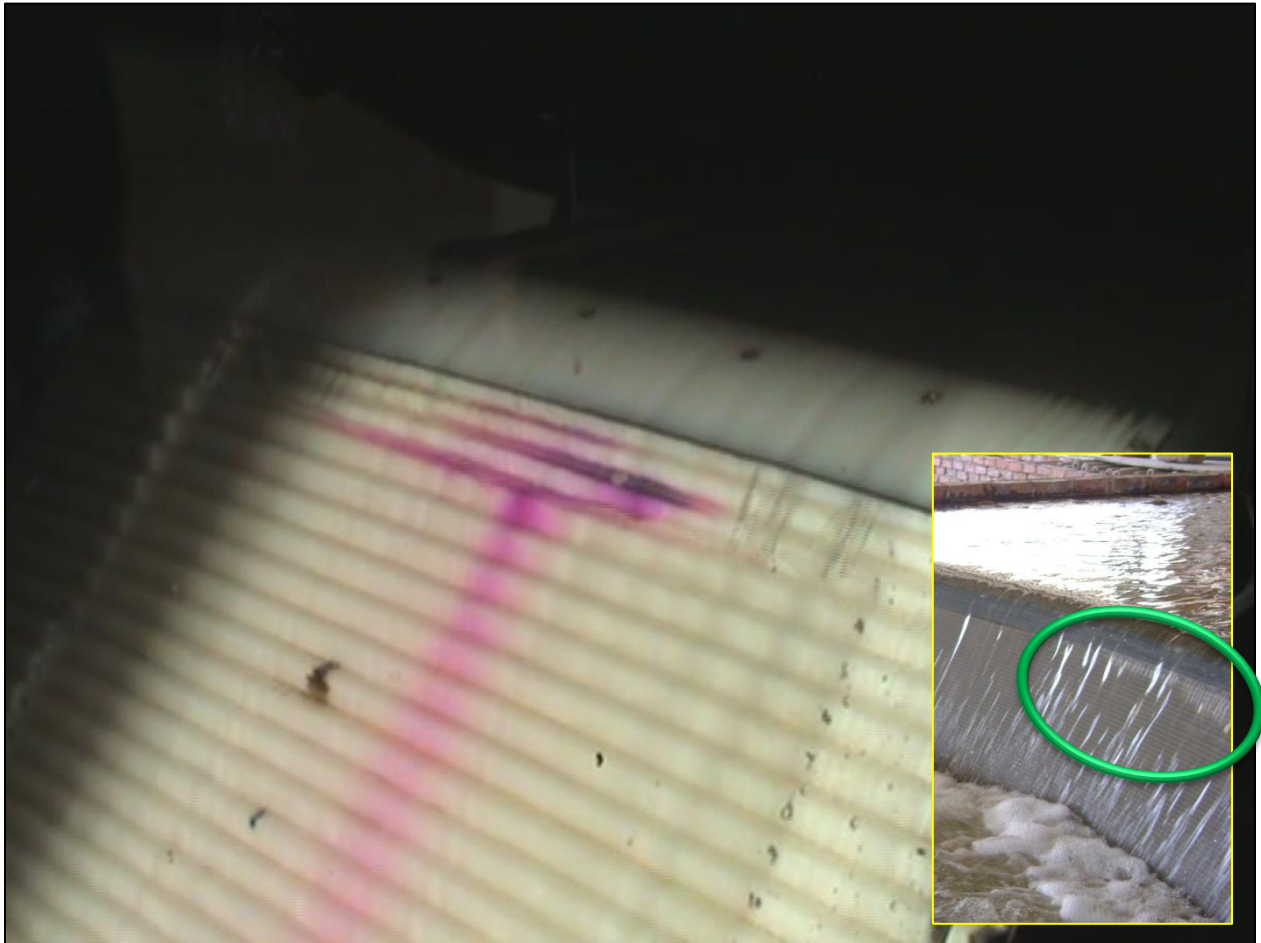


Figure 1-4: The presence of sub-atmospheric pressure was indicated by purple dye downstream of the Ogee crest during the physical model study of the Neckartal Dam (van Vuuren, et al., 2011)

1.2 HYPOTHESIS

The Ogee spillway profile is commonly used in conjunction with dam walls and hydraulic structures. It is widely used with gravity dams, arch dams and buttress dams and may in some cases even be applied at earth and rockfill dams, provided the spillway is a separate structure apart from the dam wall. Compared with the free overfall spillway in which the water drops vertically as a free jet clear from the downstream face of the hydraulic structure (**Figure 1-5 A**), the Ogee spillway is an improvement in the sense that the water flowing over the crest is guided smoothly and is made to move smoothly over the downstream face of the spillway without any obstructions (**Figure 1-5 B**) (Ministry of Science and Technology, 2007).



Figure 1-5: Free overfall spillway (Kouga Dam, Eastern Cape, A) and Ogee Spillway (Blyderiverpoort Dam, Mpumalanga, B)

The Ogee profile is used for spillway geometry to minimise the possibility of the occurrence of sub-atmospheric pressure, as well as to maximise the capacity of the spillway because of its effective discharge characteristics (Ministry of Science and Technology, 2007). The Ogee profile was historically determined by defining the shape of the spillway by first principles for projectile movement (Chow, 1959). This projectile movement of a free falling jet of water was determined from computing the trajectory of the free falling water. Many improvements and/or alterations are available to the original trajectory formula as discussed in Chapter 2 of this study. Research on this principle for the projectile movement of a free falling jet of water was further researched and it was discovered that the shape of the lower nappe of a jet of water flowing over a sharp-crested weir also provided the shape of an Ogee spillway (Chow, 1959; Hager, 1987; Knapp, et al., 1970; Melsheimer & Murphy, 1970; Ministry of Science and Technology, 2007; Murphy, 1973; USACE (a), 1987; USACE (b), 1987; USBR, 1987; Wahl, *et al.*, 2008). However, both the numerical relationships for the flow over a sharp-crested weir and the principle for the projectile movement of a free falling jet of water describing this shape, only consider the two-dimensional characteristics of the flow, namely: the available energy (i.e. depth and velocity of water flowing over the spillway crest); the angle of inclination of the upstream wall face; and the height of the spillway above the natural ground level (Hager, 1987; USACE (a), 1987; USACE (b), 1987; USBR, 1987). This approximation of co-planar (2-dimensional) flow neglects the 3-dimensional flow parameters which are occurring upstream of the spillway. These three-dimensional flow parameters being: the radius of the curved dam wall; the cross-sectional shape of the approach channel upstream of

the spillway; and the orientation of the spillway with regards to the angle of the approaching flow velocity.

It is hypothesized that the Ogee spillway will also be influenced by the following factors:

- a. The asymmetrical cross sectional approach channel upstream from the spillway (**Figure 1-6 B**);
- b. The relative orientation of the spillway with regard to the approaching flow (**Figure 1-6 A**); and;
- c. The curvature of the spillway in relation to the depth of the structure (**Figure 1-7**).

Note: *b. and c. was not considered for this study.*

If this hypothesis is proven correct, the Ogee spillway relationship can be extended to incorporate the 3-dimensional flow parameters. Incorporating these 3-dimensional flow parameters will prevent the development of possible cavitation that is initiated by the high velocity of the overflowing sheet of water that tends to pull away from the spillway crest for flow rates exceeding the design discharge (USBR, 1987). This phenomenon causes the formation of specific regions where sub-atmospheric pressure voids exist or develop on the spillway that may cause some cavitation and subsequent concrete erosion of the spillway.

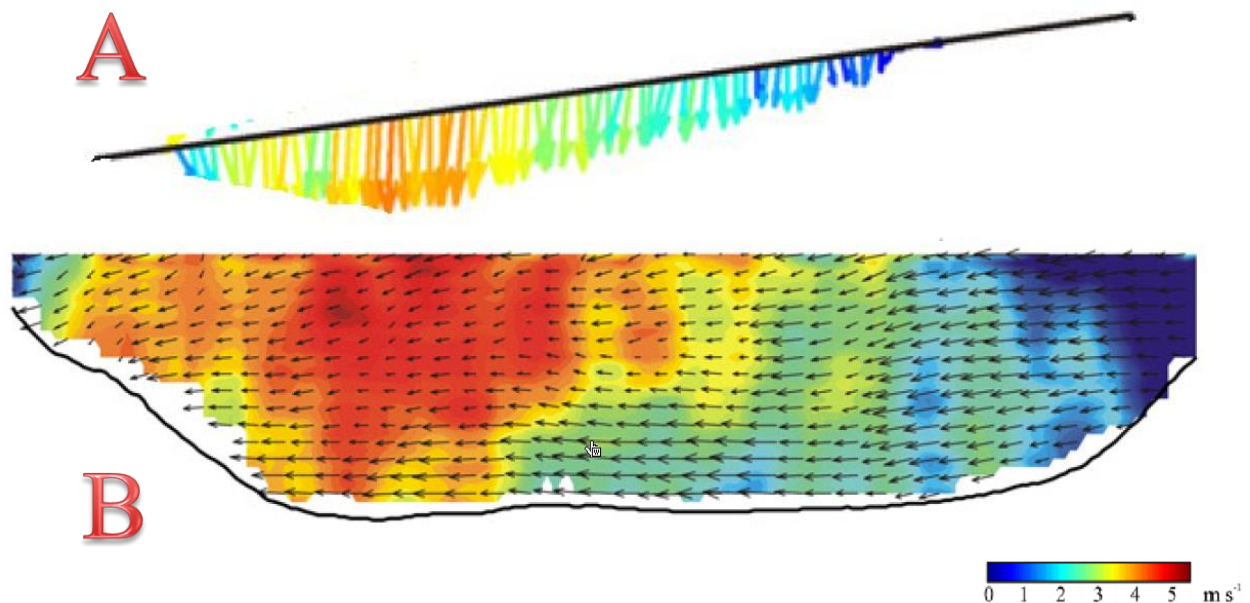


Figure 1-6: The velocity distribution in an asymmetrical channel with the colour scale depicting the magnitude of the water's velocity: A. the relative orientation of the cross-section in relation to the approach channel and B. the asymmetrical approach channel's velocity distribution (Figures modified from Riley & Rhoads, 2012)

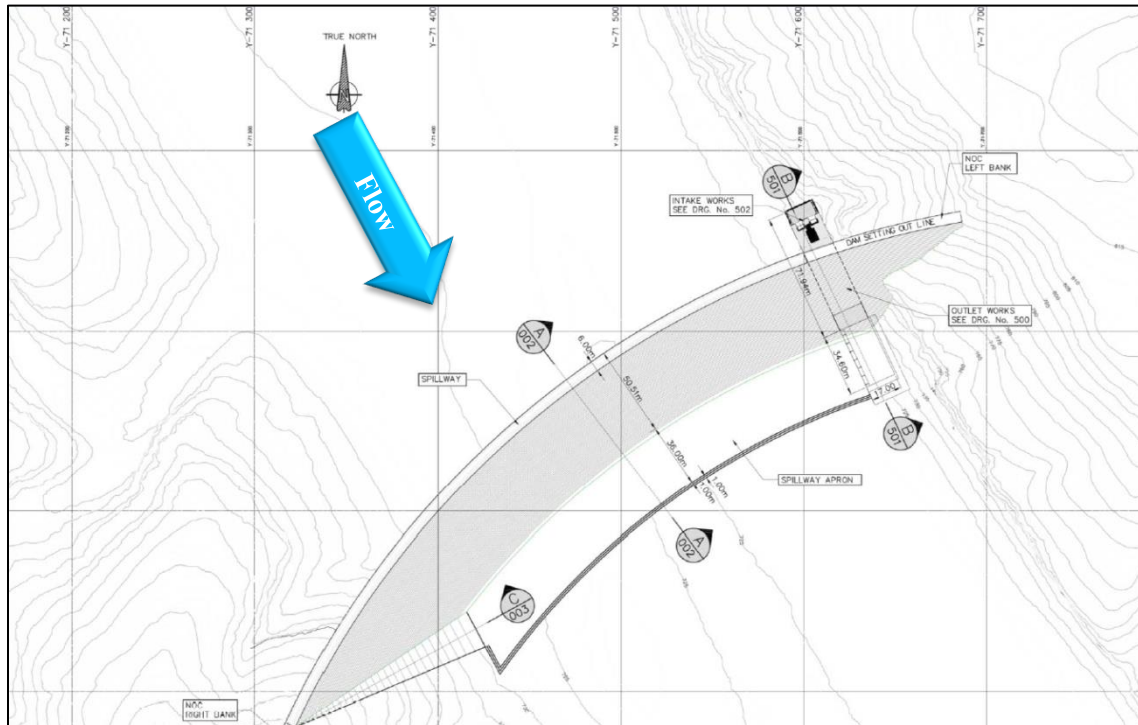


Figure 1-7: Curvature of dam wall influencing the geometric shape of the Ogee profile at the Neckertal dam, Namibia (van Vuuren, *et al.*, 2011)

Cavitation on concrete structures will result in the removal of the superficial concrete material and for that reason alters the original design shape of the spillway structure. Savage *et al.* (2001) cited that any discontinuity on a spillway crest can cause a region of sub-atmospheric pressure downstream of this discontinuity; accordingly repeating the cycle to increase the effect of cavitation on the spillway and, ultimately causing a failure of the structure. Momber (2000) indicated that it is not only the occurrence of long-term cavitation that is harmful to concrete structures. Even short-term cavitation exposure in the order of 2 seconds, can alter the concrete spillway profile causing a discontinuity on the spillway. The contribution of this research topic can be of international importance in dam design and may result in the minimization of cavitation damage to spillways and also lowering the risk of potential failure of hydraulic structures.

1.3 OBJECTIVES OF THE STUDY

The objectives of this study were:

- To determine the influence of the upstream channel's asymmetry on the bottom free surface nappe (Ogee profile) for water flowing across a sharp-crested weir; and
- Determine if the formulae provided in existing literature for the approximation of the Ogee profile, considering only two-dimensional flow over the hydraulic structure, were sufficient when compared with actual three-dimensional flow behaviour.

1.4 SCOPE OF THE STUDY

It is postulated that there are three 3-dimensional flow parameters influencing factors on the geometry of the Ogee profile: 1. the symmetry of the approach channel cross-section upstream of the spillway; 2. the angle of the approach channel in relation to the spillway; and 3. the curvature of the spillway structure (Section 1.3). However, only the symmetry of the approach channel as a parameter of three-dimensional flow has been considered in this study.

The scope of this study was to evaluate the Ogee relationship, considering in particular the three-dimensional flow parameters resembling in the asymmetrical approach channel. The following phases were included in the study:

- Review previous research undertaken to determine the geometrical shape of a free falling trajectory of water on which the Ogee shape is based upon; this includes previous relationships for the Ogee Spillway considering only two-dimensional flow parameters (Chapter 2 of this dissertation);
- Conduct a physical model study with an asymmetrical and rectangular approach channel considering design standards: ASTM Designation: D 5242 – 92 (Standard Test Method for Open-Channel Flow Measurement of Water with Thin-Plate Weirs (ASTM International, 2001)) and ISO 1438: Hydrometry - Open channel flow measurement using thin-plate weirs (International Organization for Standardization, 2008); and also considering the flow lines to be perpendicular to the spillway section in order to determine the baseline Ogee profile of two-dimensional flow parameters (**Figure 1-8**);

- Alter the physical model approach channel to simulate an asymmetrical approach channel, and to record the influence of change by measuring the geometric change of the Ogee profile (**Figure 1-9**);
- Compare previous results for the designing of Ogee spillways that are based on two-dimensional flow parameters with geometric measurements of the Ogee profile obtained from the inclusion of the three-dimensional flow parameters from the physical model study;

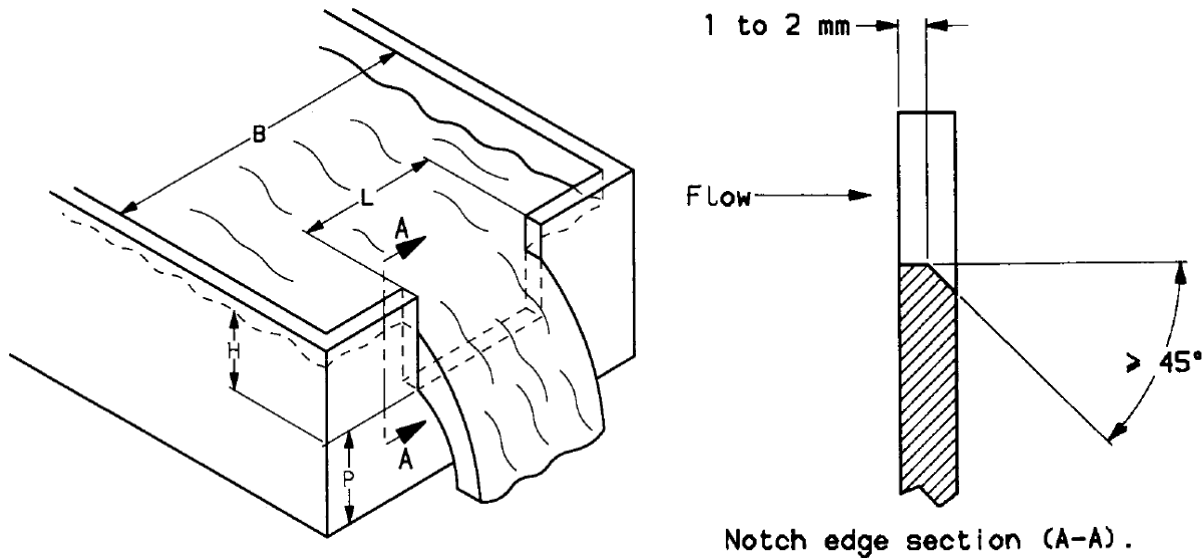


Figure 1-8: Rectangular symmetrical approach channel with flow line perpendicular to the crest section used to determine a baseline Ogee profile (ASTM International, 2001)



Figure 1-9: Symmetrical approach channel (A) and Asymmetrical approach channel (B)

1.5 METHODOLOGY

In order to complete the research study efficaciously and to meet the anticipated objectives, it was necessary to consider the available literature to obtain more knowledge on Ogee spillways. This includes the historical background, as well as some of the newest developments in the field including new relationships developed for determining the Ogee profile (Chow, 1959; Hager, 1987; Knapp, et al., 1970; Melsheimer & Murphy, 1970; Ministry of Science and Technology, 2007; Murphy, 1973; USACE (a), 1987; USACE (b), 1987; USBR, 1987; Wahl, et al., 2008). These topics include the technical formulae for calculating the Ogee profile, aspects on scaled physical models, calibration of weirs, international design standards and cavitation of spillways. These features were discussed in more detail in Chapter 2 of this dissertation.

On completion of the literature study (Chapter 2) a physical model of a sharp-crested weir was constructed at the Department of Water Affairs hydraulic laboratory in Pretoria-West. The physical model was based on all the appropriate literature and appropriate data collected and summarized in Chapter 2. The lower nappe of the water trajectory flowing over the sharp-crested weir simulates the profile of an Ogee spillway (**Figure 1-10**) (Ministry of Science and Technology, 2007). The Ogee profile was measured by means of a self-developed measuring instrument (discussed in more detail in Chapter 3).

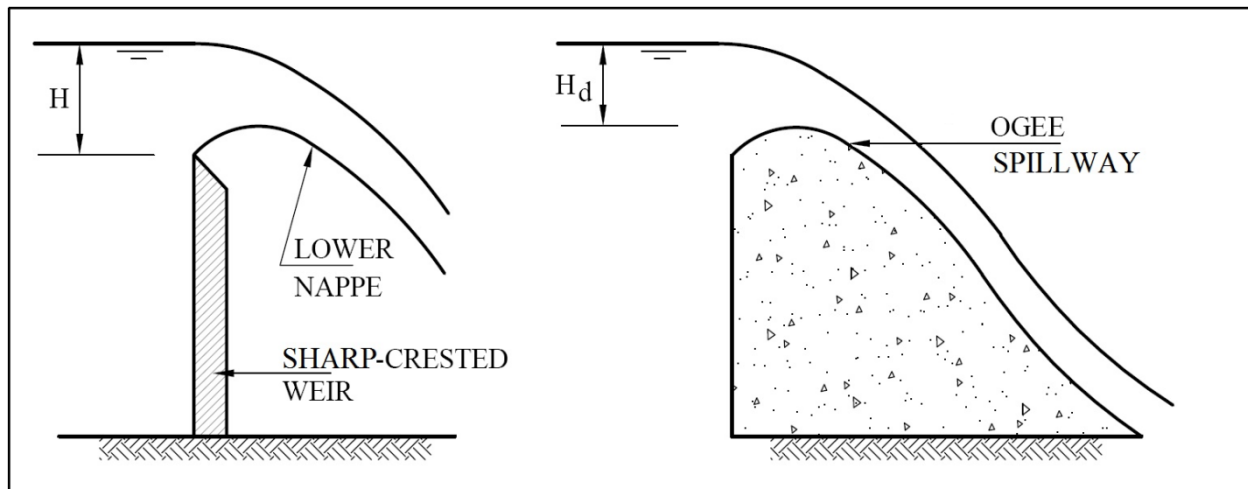


Figure 1-10: Lower nappe of the water trajectory flowing over a sharp-crested weir simulates the profile of an Ogee spillway (Ministry of Science and Technology, 2007)

The Ogee profile was measured for different symmetricity layouts of the approach channel. This was undertaken for different unit flow rates and the Ogee profile was measured for each specific layout

scenario at the centerline (Φ) of the spillway, as well as at a distance of $1/3^{\text{rd}}$, $2/3^{\text{rd}}$ and $5/6^{\text{th}}$ away for the centerline to either side to include and exclude any boundary conditions (**Figure 1-11**). The total length of the sharp-crested weir was 1201 mm.

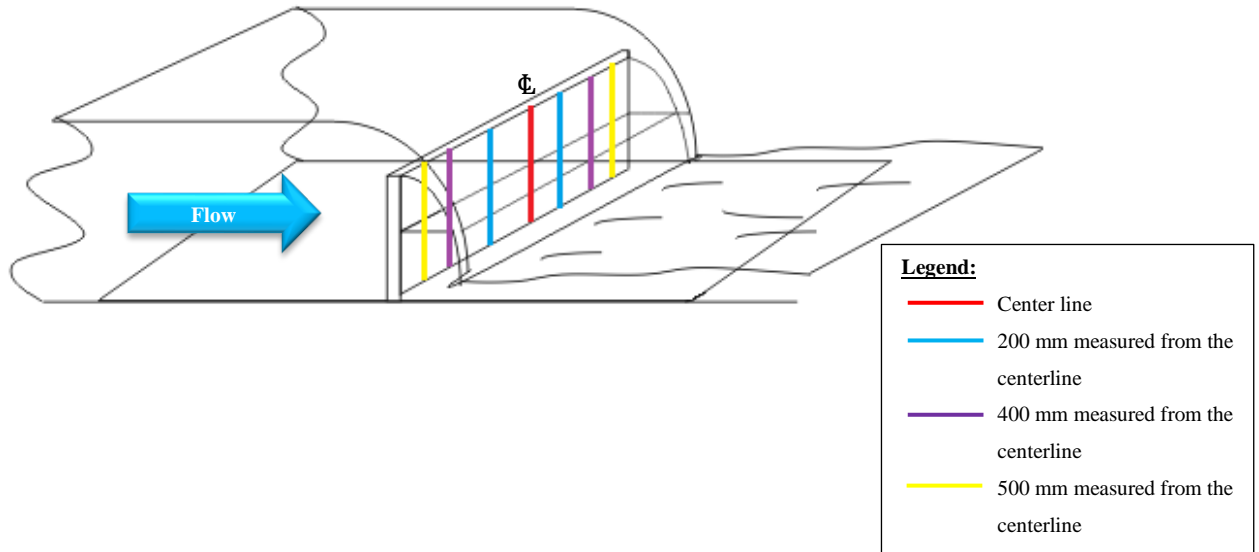


Figure 1-11: Positions of the Ogee profile measurements

- Note:** * *The Ogee profile was measured at 5 locations along the sharp-crested weir for the symmetrical (baseline) approach channel layout.*
- ** *The Ogee profile was measured at 7 locations along the sharp-crested weir for the asymmetrical approach channel layout.*

The geometric shape of the Ogee profile was measured by means of a Linear Variable Differential Transformer (LVDT) and verified with a Vernier scale (**Chapter 3**). The results were plotted in a spreadsheet and various graphs of the Ogee profile at the various positions along the crest of the sharp-crested weir were populated both in XY- and XYZ-coordinate systems. These graphs were analysed as follow:

1. Each layout scenario's Ogee profiles was measured at the different positions along the sharp-crested weir and data points were plotted to reflect the Ogee profiles;
2. All the scenarios were plotted together to determine the most severe scenario; and
3. The measured profiles were analysed with respect to theoretical curves.

Positions were designated where the sheet of water flowing over the weir may separate from the Ogee spillway for the selected design flow rate and were populated to evaluate the severity of the influence of the asymmetrical approach channel.

1.6 ORGANISATION OF THE DISSERTATION

The dissertation consists of the following chapters and appendices:

- Chapter 1 (This chapter) is an introduction to the study and provides the background to the problem statement; the problem statement is in the form of a hypothesis; the scope and limitations of the study; and the methodology that was followed during completion of the study.
- Chapter 2 is a technical introduction based on research that has been done pertaining to the current literature to ascertain the level of knowledge on the relationship of the Ogee spillway, and the effects that 3-dimensional flow parameters have on the geometric shape of the Ogee spillway. Design standards, scaled physical models, point of tangency, the phenomenon of cavitation and effect of velocity distribution upstream of the spillway are also discussed.
- Chapter 3 explains the experimental setup of the physical model, and also particular field observations that were performed and recorded during the study. It includes the method and the setup that was used to measure the Ogee profile (i.e. the bottom nappe of the water trajectory flowing over the sharp-crested weir). Included in chapter 3 are also motivations for why certain measuring instruments proved to be more feasible than others. Setbacks faced during the study are also included.
- Chapter 4 describes the results obtained, and explains how these results were analysed and compared with expected theoretical results.
- Chapter 5 serves as a conclusion to the hypothesized outcome, and includes recommendations on the implementation of the findings and possible further study;
- Chapter 6 contains the list of references.
- Appendix A on the supporting CD contains the populated datasheets for measuring the Ogee profile

2 LITERATURE REVIEW

2.1 SPILLWAYS

Aging hydraulic infrastructure in both developed and developing countries requires refurbishment, upgrading or total replacement of system components. These renovations include the upgrading or alteration of some of the older spillways to ensure that the structure is safe to convey a “larger” design discharge or to protect it against abrasive erosion and cavitation. Some of the older structures that have been constructed have not been design in accordance with modern standards. Recently, most dams are being constructed in developing countries to cater for the demands of irrigation, drinking water and energy generation. These structures should be designed on a sound hydraulic basis to ensure that the appropriateness of the geometric layout of the spillway has been accomplished in order to prevent excessive negative pressures occurring on the spillway chute and also to ensure a safe, cavitation free design (Vischer & Hager, 1999).

The USACE has classified spillways into four distinct categories. These categories relates to the specific site conditions and the anticipated function and discharge requirements of the structure (USACE, 1992). However, some of these spillway categories overlapped and it is thus possible that for a specific spillway structure, a combination of two or more of these categories may apply. In the following paragraphs the different spillway classifications are briefly reflected.

- *Overflow Spillway.* These spillways are typically constructed as part of the dam wall and may either form part of a gated or un-gated system. The construction of the spillway forms in most cases part of the dam wall itself and thus will be frequently seen in conjunction with a concrete gravity dam. An example of such a structure is shown in **Figure 2-1**;



Figure 2-1: Grand Coulee Dam Ogee spillway spilling 2011 (Yahoo! Inc., 2011)

- *Chute Spillway.* In most cases chute spillways will be in combination with an earth- or rock-filled dam. Though, it is also used with concrete gravity. In the case of concrete gravity dams the dam is usually located in a narrow valley with insufficient crest length available for an overflow spillway. A chute spillway may be located either through the abutment adjacent to the dam or in a saddle away from the dam structure. A typical chute spillway is shown in **Figure 2-2**;



Figure 2-2: Mohale dam spilling February 2006 (International Water Power and Dam Construction, 2009)

- *Side Channel Spillway.* A side channel spillway is usually located in a narrow valley where insufficient crest length is available for an overflow spillway. The side channel spillway may be located either on a narrow abutment of the dam or in a saddle away from the dam structure. Side channel spillways are generally un-gated; however, there is no reason why they may not be gated. **Figure 2-3** reflects the side spillway at the well renowned Hoover Dam.



Figure 2-3: Hoover Dam side channel spillway overflowing 1983 (Wiltshire, et al., 2010)

- *Limited Service Spillway.* A limited service spillway is designed with the understanding that the spillway will only be functional under extreme flood conditions. It is also sometimes been referred to as an emergency spillway. Thus, allowance is made for apparent damage that may occur to the structure; however, this damage may not be to the extent that it would cause a catastrophic or unsafe release of water from the dam. These spillways are also referred to as *Emergency Spillways*. Typical examples of this hydraulic structure is given in **Figure 2-4** and **Figure 2-5**;



Figure 2-4: Limited service spillway (in foreground) to be constructed and auxiliary spillway (ogee crest) in background at New Waddle Dam, Arizona (LaBoon, et al., 2011)



Figure 2-5: Arabie Dam, now called Flag Boshielo Dam in the Crocodile River, South Africa with limited service spillway embankment to be flushed away under large floods without damaging the main spillway structure

When designing a new dam and spillway system, considering the above mentioned spillway classification it is clear that all spillways require a unique spillway crest design that will be appropriate for its operational conditions and design head. USACE (1992) indicated that the capacity of the spillway is a

function of its crest shape (discharge coefficient), the crest length, and the hydraulic head available (i.e. available potential energy). The hydraulic head and effective spillway length may be modified by approach conditions, pier and/or abutment effects, and submergence conditions. These approach conditions refer to the approach channel symmetry and approach velocity upstream of the spillway's crest. The basic purpose of a spillway is to convey a large volume of water through a predefined area without sustaining unacceptable damage to either the upstream or the downstream face of the spillway. An acceptable spillway design is accomplished by minimizing the cost subject to the following norms (USACE, 1992):

- The crest length should be of adequate length in order to convey the required design discharge;
- During design discharge, pressures acting on the crest boundary should be limited to acceptable minimum pressures;
- The velocity head component and design discharge on the spillway crest should be restricted to tolerable maximum energy head;
- Velocities should be acceptable to reduce the possibility of cavitation formation;
- Flow characteristics through the spillway system should form uniform flow lines to prevent any standing waves or unsafe flow conditions; and
- Environmental release should be considered, together with acceptable aesthetic conditions.

According to USACE's (1992) engineering-economic investigations for optimal economic design of spillways, the general requirement of a spillway is a narrow spillway system with a high unit discharge. This implies that the most economic spillway designs will produce an outflow system that includes a large energy head on the crest (high velocity head component), a moderate design head (water depth at the crest), and a large unit discharge. However, contrary to economical feasible spillway designs, it should be considered that higher head spillways create excessive abutment and pier contractions. This may result in energy dissipation problems, and also increase the possibility of cavitation or the formation of a pulsating nappe on the spillway crest. All these factors, combined with poor flow characteristics through the whole spillway system may result in excessive eroding and decrease the normal life span of the outflow system. This emphasizes the demands that are placed on the design engineer for an economical spillway design, yet ensuring that the use of a high head, high-efficiency spillway which, in turn, requires a sound design methodology (precise geometrical layout of the spillway's crest).

2.2 BACKGROUND ON THE OGEE SPILLWAY

In order to determine the shape of a spillway's crest, different methods are available to determine the geometry of the spillway's crest. These methods are depending on the relative height of the structure, the available design head and upstream face slope of the spillway. Other factors that should also be considered are the approach channel symmetry, approach channel depth, orientation of the spillway relative to the flow path and the curvature (if applicable) of the hydraulic structure (van Vuuren, *et al.*, 2011). Literature reflects that in 1888, some of the first research has been undertaken to investigate the study of the Ogee shape. Ever since then, the Ogee spillway has been the most studied spillway geometry (Savage & Johnson, 2001 and Thandaveswara, 2006).

The Ogee spillway, also known as the Standard crest shape is derived from the trajectory of the lower nappe of flow over a ventilated sharp-crested weir. The flow generates curved streamlines with its origin of curvature below the flow (**Figure 2-6**). The design geometry of the Ogee spillway relates to the bottom nappe across a sharp-crested weir with an equivalent unit discharge. The upper surface of the spillway is properly shaped to form the crest. The nappe-shaped profile is an ideal profile because at the design discharge, water flowing over the crest of the spillway always remains in contact with the surface of the spillway as it glides over it. Moreover, for this shape there will be no negative pressure that will develop on the spillway surface at the design discharge.

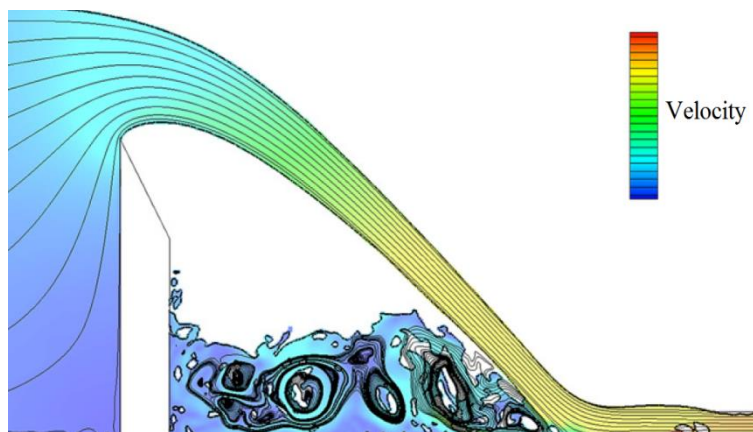


Figure 2-6: Curved streamlines with its origin of curvature below the flow (Lv, et al., 2011)

In the case where the energy head exceeds the design head (i.e. in the case of an extreme flood event), the bottom nappe of water tends to break contact with the spillway's surface and a zone of separation is formed on the spillway leading to sub-atmospheric or negative pressures. This may cause vibration of the

system that could result in pitting and cavitation of the spillway's surface. During high flow conditions the coefficient of discharge of the spillway will increase and thus will result in an increased discharge for an equivalent energy head. This process is called under-designing of the spillway and increases the efficiency of the spillway up to the point before cavitation damage occurs (Savage & Johnson, 2001). The limit to where under-designing of Ogee spillways may be acceptable is to the point before cavitation is experienced; this occurs when the pressure decreases to the saturated vapour pressure of the liquid, which is dependent on temperature (Koivula, 2000). Under-designing an Ogee spillway is unsafe and is not recommended because catastrophic failure of the spillway due to subsequent cavitation is possible. A positive hydrostatic pressure is exerted on the spillway when the flow rate is less than the design discharge because the nappe tends to be depressed onto the spillway. As the spillway surface supports the sheet of flowing water which creates a backwater effect downstream, energy is lost as friction is exerted between the sheet of water flowing over the structure and the spillway's surface, this results in the coefficient of discharge to be reduced (USACE, 1992). Under ideal conditions, the head should be equal to the design head of the Ogee spillway. For this condition the Ogee will be shaped accordingly and maximum efficiency of the spillway will be retained without any detrimental effect (Anon., 2006).

2.3 THE OGEE SPILLWAY

Chadwick *et al.* (2004) described a spillway as a structure that is a *carefully designed passage* used to provide for the controlled release of water from a dam into a downstream area, typically being the river that was being dammed. Spillways release floods safely so that the water does not overtop the structure which could lead to damage or even failure of the dam. The Ogee spillway is commonly used and the typical profile is shown in **Figure 2-7**. The nappe trajectory on which the Ogee spillway is based, varies with head (H_d), implying that the crest profile is derived on a specific head or discharge (i.e. the design head).

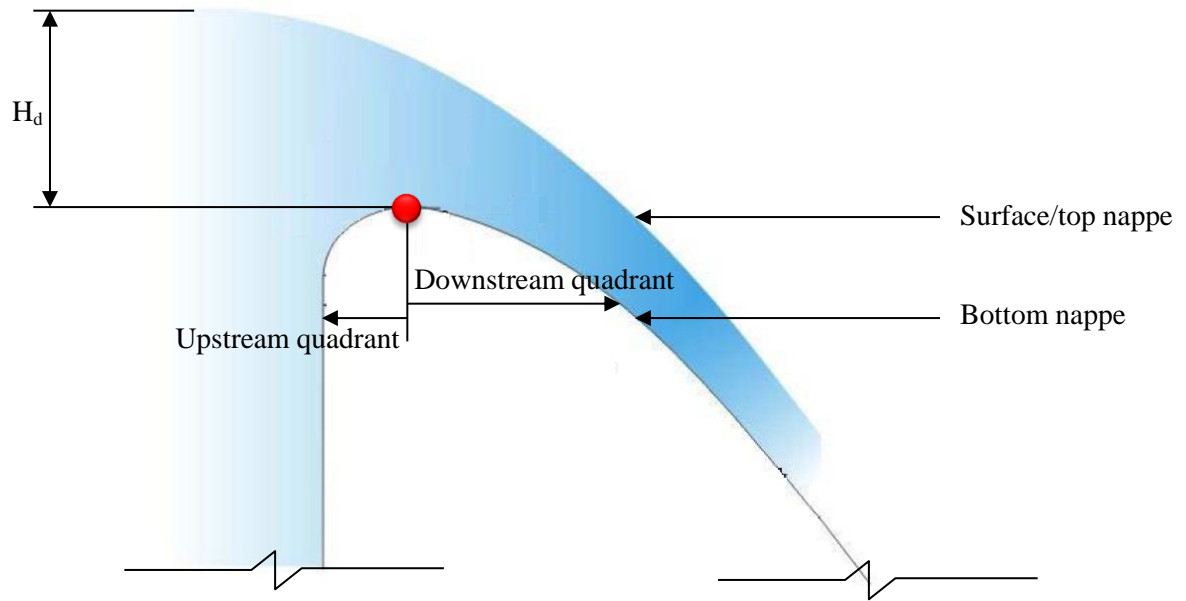


Figure 2-7: Shape of the Ogee Spillway (Anon., 2006).

The geometry of an Ogee spillway profile is based on a physical analysis of the shape produced by a ventilated jet of water flowing over a sharp-crested weir. The shape of the curve is determined by measuring the vertical distance from a datum to the underlying nappe of the jet flowing over the weir along the length of the jet in the direction of flow. Difficulties existed when a single equation was fitted to the upstream quadrant (i.e. the crest) of the spillway. The United States Bureau of Reclamation (USBR, 1987) and US Army Corps of Engineers (USACE, 1970) estimated the profile by means of a series of circular curves. The efficiency of the Ogee spillway is vastly dependent on the curvature of the crest immediately upstream of the highest point on the crest defined as the crest axis. With any sudden change in curvature or slight discontinuity it will cause a disruption of the boundary layer sheet of water and could lead to flow separation and cavitation. According to Murphy (1973), removing any small discontinuities (intersection points of circular curves) between the upstream face and upstream quadrant of the spillway could result in a three percent increase of the coefficient of discharge (USACE, 1992).

A wealth of literature is available on the approximation of the Ogee profile for spillway design and several endeavours have been made developing a relationship that would be able to mathematically describe the shape of the Ogee curve considering 2-dimensional flow parameters. Unfortunately in most cases the flow over an Ogee spillway cannot be considered merely as a 2-dimensional flow condition. The asymmetry of valleys and topographical approach channels where spillways are constructed will influence the flow pattern and velocity distribution upstream of the spillway. Neglecting these 3-

dimensional flow behaviours may result in an insufficient design of the Ogee spillway structure. The most obvious 3-dimensional flow parameters that influence the geometry of the Ogee profile include (van Vuuren, et al., 2011):

- The relative orientation of the spillway with regard to the approaching flow (not considered for this study) (**Figure 1-6 A**);
- The asymmetrical cross sectional approach channel upstream from the spillway (**Figure 1-6 B**); (included in this study) and
- The curvature of the spillway in relation to the depth of the structure (not considered for this study).

Some of the well-regarded approximations are described in the following section and are grouped according to two categories:

- a. Approximation of the Ogee curve by means of first principles of projectile movement; and
- b. Approximation of the Ogee curve by means of empirical methods (**Table 2-1**).

Table 2-1: Methods for approximation of the Ogee curve

Approximation of the Ogee curve based on the principles of projectile movement		Approximation of the Ogee curve based on experimental methods	
Description	Reference in dissertation	Description	Reference in dissertation
Ven te Chow (1st Principles) (Chow, 1959)	Section 2.3.1.1	United States Bureau of Reclamation (USBR, 1987)	Section 2.3.2.1
Ven te Chow (Modified) (Chow, 1959)	Section 2.3.1.2	United States Army Corps of Engineers (USACE, 1970)	Section 2.3.2.2
Brink Velocity (Wahl, et al., 2008)	Section 2.3.1.3	United States Army Corps of Engineers (USACE (b), 1987)	Section 2.3.2.3
		Hager (1987)	Section 2.3.2.4
		Creager (Chanson, 2004)	Section 2.3.2.5
		Scimeni (Chanson, 2004)	Section 2.3.2.6
		Montes (Chanson, 2004)	Section 2.3.2.7
		Knapp (Chanson, 2004)	Section 2.3.2.8
		CE-05016 (Ministry of Science and Technology, 2007)	Section 2.3.2.9

2.3.1 Approximation of the Ogee curve by means of first principles of projectile movement

Projectile movement of any particle is defined as a form of motion where a particle is moving obliquely near the earth's surface due to an initial force exerted onto it. The particle will move along a curved path under the action of gravity. From the equation of motion (**Equation 2-1**) it is possible to determine the two-dimensional displacement of a particle assuming constant acceleration acts onto it and neglecting all external forces (drag force etc.):

$$s = v_0 t + \frac{1}{2} a t^2$$

Equation 2-1

Where

- s - displacement of the particle for a time duration of t seconds (m)
- v_0 - the initial velocity of the particle (m/s)
- a - constant acceleration acting onto the particle (m/s^2)
- t - time duration of acceleration acting onto the particle (sec.)

Assuming that gravitational acceleration is constant and act only in the vertical direction, it is possible to determine the trajectory of a projectile by breaking it up into two components: a. horizontal displacement (x) and b. vertical displacement (y) as illustrated in **Figure 2-8**. Making use of **Equation 2-1** the horizontal and vertical components of the trajectory can be estimated in 2-dimensions by combining **Equation 2-2** and **Equation 2-3**.

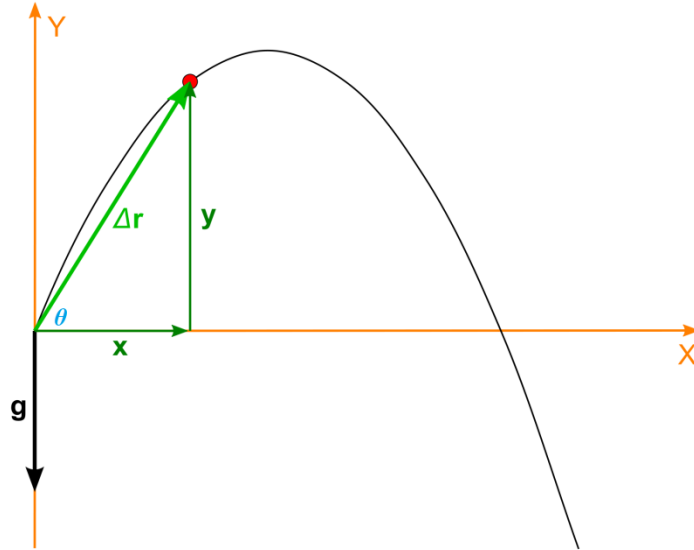


Figure 2-8: Trajectory of a particle following a projectile movement

$$x = v_0 t \cos \theta$$

Equation 2-2

$$y = v_0 t \sin \theta + \frac{1}{2} a t^2$$

Equation 2-3

Where:

θ - projectile launch angle (degrees)

The trajectory of the projectile can be determined by eliminating the time component (t) from **Equation 2-2** and **Equation 2-3** to obtain **Equation 2-4**.

$$y = \tan \theta \cdot x + \frac{a}{2v_0 \cos^2 \theta} \cdot x^2$$

Equation 2-4

2.3.1.1 *The relationship of the Ogee curve as approximated by Ven te Chow from 1st Principles of projectile movement*

Vent te Chow (1959) indicated that the geometric shape of a water particle flowing over a sharp-crested weir can be interpreted by the principle of projectile movement (**Figure 2-9**). Similar to the assumption of projectile movement in section 2.3.1 it was assumed that the horizontal velocity component of the flow particle is not experiencing any gravitational forces implying a constant horizontal movement. The only force acting onto the water particle would be in the vertical direction that is caused by gravity.

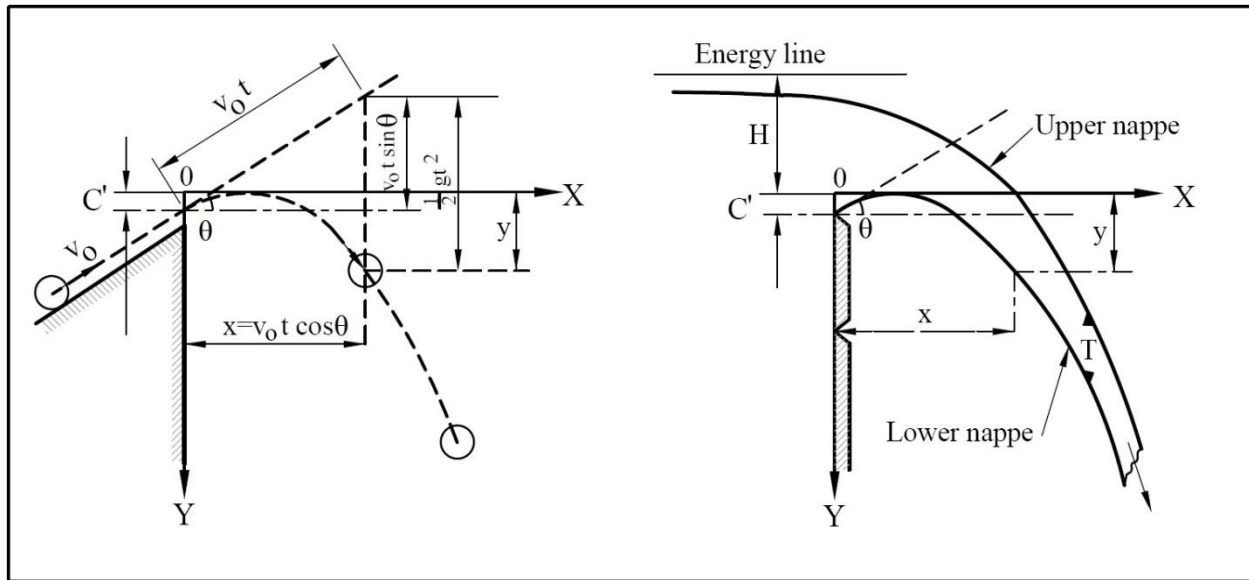


Figure 2-9: Derivation of the nappe profile of a water particle flowing over a sharp-crested weir by the principle of projectile movement (Chow, 1959)

For a predefined time duration the water particle at the lower nappe will experience a movement in the horizontal (x) and vertical (y) plane as expressed by **Equation 2-5** and **Equation 2-6**.

$$x = v_0 t \cos \theta$$

Equation 2-5

$$y = -v_0 t \sin \theta + \frac{1}{2} g t^2 + C'$$

Equation 2-6

Where:

- x - horizontal displacement during a time duration t (m)
- y - vertical displacement during a time duration t (m)
- v_0 - the initial velocity of the water particle (m/s)
- g - gravitational acceleration acting onto the water particle (m/s^2)

- t - time duration for assessment of particle (sec.)
 θ - angle of inclination (degrees)
 C' - the vertical displacement of the particle at $x = 0$ m (m)

Research indicated that the vertical displacement of the particle at $x = 0$ m (C') is equal to the vertical distance between the highest point of the nappe and the elevation of the crest (Chow, 1959). Rajaratnam *et al.* (1968) indicated that the vertical position C' can be empirically estimated by **Equation 2-7** and the horizontal distance (f') to this co-ordinate measured from the crest can be estimated by **Equation 2-8**. These experiments by Rajaratnam *et al.* (1968) were done for a confined weir (un-contracted). This position is known as the turning point of curvature (T_p) and is depicted in **Figure 2-10**.

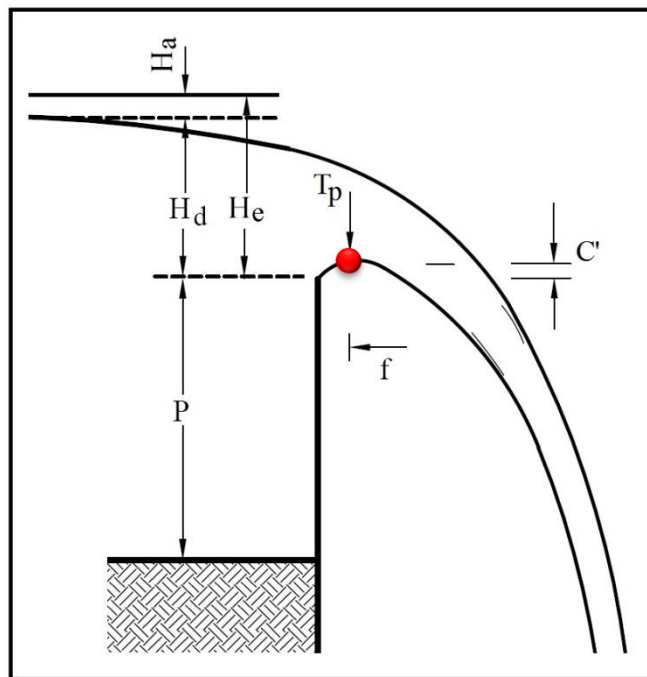


Figure 2-10: Position of the turning point of curvature at the maximum elevation of the Ogee profile

$$C' = 0.112 \cdot H_d - \frac{0.4v_0^2}{2g}$$

Equation 2-7

$$f' = 0.250 \cdot H_d - \frac{0.4v_0^2}{2g}$$

Equation 2-8

Where:

H_d - measured water depth on the crest (m)

The lower surface of the nappe can be determined by eliminating the time component (t) from **Equation 2-5** and **Equation 2-6**. A normalized form of the equation can be obtained by dividing each term by the total energy head upstream of the crest (**Equation 2-9**).

$$\frac{Y}{H_e} = A \left(\frac{x}{H_e} \right)^2 + B \frac{x}{H_e} + C$$

Equation 2-9

Where:

A - $\frac{gH_e}{2v_0^2 \cos^2 \theta}$

B - $-\tan \theta$

C - $\frac{C'}{H_e}$

H_e - total energy head upstream of crest (m)

2.3.1.2 *The relationship of the Ogee curve as approximated by Ven te Chow (Modified)*

From the normalized form of the projectile trajectory of the nappe over an aerated vertical sharp-crested (**Equation 2-9**) as derived by Ven te Chow (1959), a general parabolic equation for the Ogee curve was proposed by Chow, **Equation 2-10**. By adding the term D to the equation, the upper surface of the Ogee nappe can also be determined. Chow (1959) has derived the parabolic equation to determine the Ogee nappe curve for ratios of $x/H_e > 0.5$ and $H_w/H_e > 0.2$ based on the experimental data taken from the USBR, Hinds, Creager and Justin, Ippen and Blaisdell. The values for the constants for A, B, C and D can be determined from **Equation 2-11** to **Equation 2-14**. Chow (1959) indicated that for ratios of $x/H_e < 0.5$ the hydrostatic pressure within the nappe in the vicinity of the weir crest is above atmospheric pressure because of the convergence of the stream lines. Consequently, forces other than gravity are acting onto the nappe, which makes the principle of projectile movement invalid.

$$\frac{Y}{H_e} = A \left(\frac{x}{H_e} \right)^2 + B \frac{x}{H_e} + C + D$$

Equation 2-10

With:

$$A = -0.425 + 0.25 \frac{H_a}{H_e}$$

Equation 2-11

$$B = 0.411 - 1.603 \frac{H_a}{H_e} - \sqrt{1.568 \left(\frac{H_a}{H_e}\right)^2 - 0.892 \frac{H_a}{H_e} + 0.127}$$

Equation 2-12

$$C = 0.150 - 0.45 \frac{H_a}{H_e}$$

Equation 2-13

$$D = 0.57 - 0.02(10\text{m})^{0.2} e^{10m}$$

Equation 2-14

Where:

$$m = \frac{H_a}{H_e} - 0.208$$

H_a - velocity head $\left(\frac{v^2}{2g}\right)$ (m)

H_e - total energy head upstream of crest

A comparison of the USBR (**Figure 2-13**) compound curve for insignificant upstream velocity head is compared with the modified Vent te Chow relationship (**Equation 2-10**) in **Figure 2-11**. The modified Vent te Chow relationship (**Equation 2-10**) seems to underestimate the gravitation acceleration exerted onto the particle resulting in the trajectory of the nappe of water particle to be more conservative.

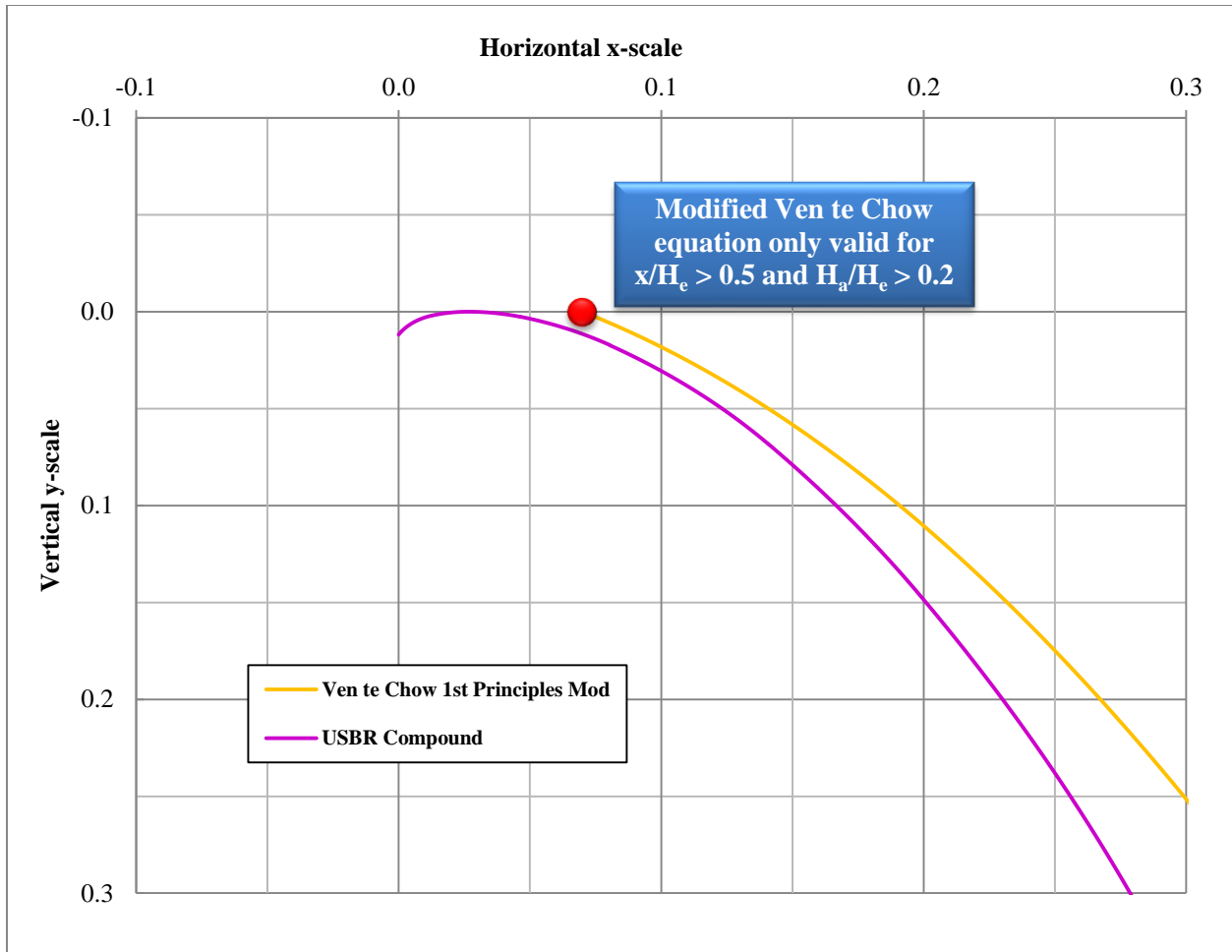


Figure 2-11: Comparison of the USBR compound curve for insignificant upstream velocity head is compared with the modified Vent te Chow equation (Chow, 1959)

2.3.1.3 The relationship of the Ogee curve as approximated by Wahl et al. (2008)

Wahl et al. (2008) indicated that the prediction of the trajectory of a free falling jet of water described by Vent te Chow (1959) may be flawed, producing a water jet trajectory that is much too flat. This may be a valid argument by Wahl et al. (2008), as one of the principal assumption made during the derivation of **Equation 2-9** was that no external force is acting onto the water particle. Through algebraic manipulation, the trajectory equation can be restated in terms of the velocity head (**Equation 2-15**). Wahl et al. (2008) stipulate that using **Equation 2-9** as it is may overestimate the jet trajectory by as much as 70% if the flow is exactly critical at the crest overtopping position. In an ideal environment, this would have not been a problem; however, since this is reality external forces like the drag force (air's resistance to movement) will be acting onto the lower nappe of water, and should thus be considered.

$$y = x \tan \theta_o - \frac{x^2}{4H_a \cos^2 \theta_o}$$

Equation 2-15

Where:

x	-	horizontal displacement (m)
y	-	vertical displacement (m)
H _a	-	the velocity head (m)
θ _o	-	angle of inclination (degrees)

However, the USBR (1987) has also noticed a discrepancy with the equation and considered including the depth of flow and a coefficient, K in the denominator (**Equation 2-16**). The notion of including the coefficient was to account for the external forces acting onto the water nappe, such as jet breakup and wind resistance.

$$y = x \tan \theta_o - \frac{x^2}{4K(d + H_a) \cos^2 \theta_o}$$

Equation 2-16

Where:

d	-	the depth of flow over the crest (m)
K	-	constant less or equal to 1

When comparing **Equation 2-16** and **Equation 2-15**, which was both derived from the projectile motion equation, it is clear that they are not equivalent, even when K = 1. According to Wahl *et al.* (2008) **Equation 2-16** would only be accurate if the total overtopping head could be converted to velocity head. However, in most cases this is not possible since a nearly hydrostatic pressure profile exists in the flow until the flow passes over the crest and part of the energy is in the form of pressure head.

Instead of including all the external forces acting onto the jet of water mathematically, Wahl *et al.* (2008) considered an empirical relationship known as the “brink velocity” that reflects the velocity when the water flows over the edge of the crest. The brink velocity was derived experimentally by (Rouse, 1936) and is approximated by **Equation 2-17**.

$$v_b = 0.808 \sqrt{2gH_d}$$

Equation 2-17

Where:

- v_b - brink velocity (m/s)
- H_d - water depth on the crest (m)

Wahl et al. (2008) recommends that **Equation 2-15** should be used in conjunction with the brink velocity head as reflected by **Equation 2-17**. It is also further suggested that a 7° downward deflection (θ) of the flow streamlines should be considered for the mid-section of the trajectory (Henderson, 1966). The trajectory estimated by Wahl et al. (2008) closely matches the profile of the Ogee geometry estimated by the compound curves as determined by USBR (1987). A comparison of these curves is depicted in **Figure 2-12**.

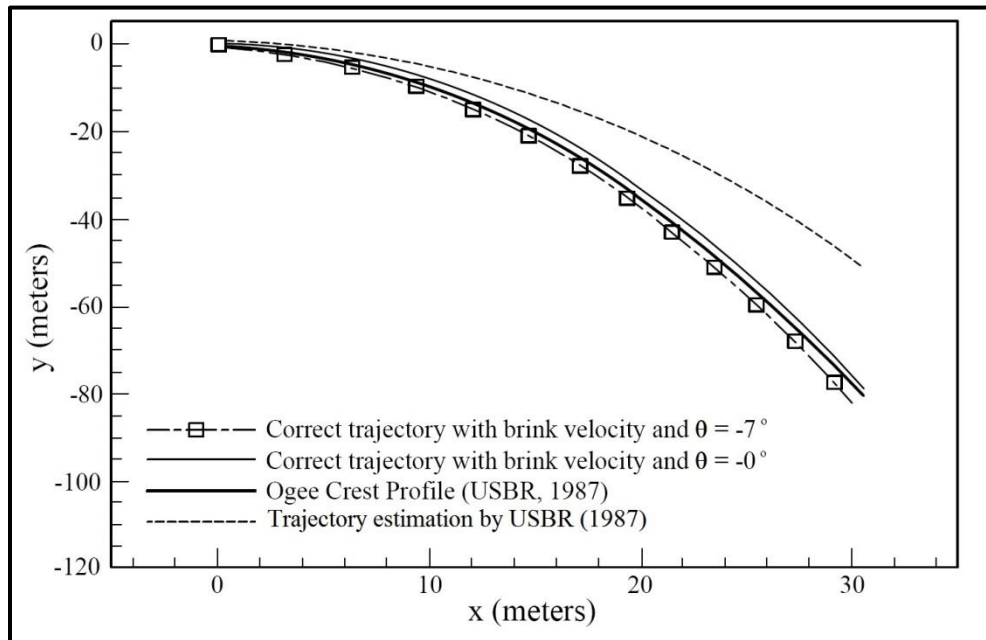


Figure 2-12: Comparison of computed jet trajectories and Ogee crest profile representing experimental data (Wahl, et al., 2008)

2.3.2 Approximation of the Ogee curve by means of experimental methods

Profiles of Ogee's have been experimentally developed for a range of dam heights and operating heads (H_o/P ratios). This information has mainly been published by the US Bureau of Reclamation and the US Army Waterways Experimental Station (Chadwick, et al., 2004). The relationship of the Ogee curve approximated by different experimental setups and researchers are described in the following paragraphs.

2.3.2.1 *The relationship of the Ogee curve as approximated by the USBR (1987)*

Research conducted by the United States Bureau of Reclamation (USBR, 1987) has resulted in the approximation of the Ogee profile by means of a series of compound circular curves. The conclusion of this research resulted in the formation of a relationship that numerically describes the shape of the Ogee curve with relation to the design head of the system. According to the USBR (1987), the shape of the Ogee profile is dependent on the following factors:

- Design head;
- Upstream wall face inclination; and
- Pool depth, which in turn influences the approach velocity.

All these factors are 2-dimensional flow parameters requiring the extension of the relationship to include 3-dimensional flow parameters. The relationship for the curve derived by the USBR consists of two quadrants: the first being that portion upstream of the apex of the Ogee profile, and the second being that downstream of the apex of the Ogee profile. The upstream quadrant can be defined in two manners, namely as a single curve in combination with a tangent (section 2.3.2.3), or as a compound circular curve; but is most often defined using the latter. The downstream portion can also be described in two manners, namely as a power function or a compound circular curve.

The approximate Ogee profile for a crest with a vertical upstream face and negligible approach velocity can be estimated by the compound circular curve configuration that comprises for the upstream quadrant of the spillway of two arcs of differing radii and points of origin, as shown in **Figure 2-13**. The downstream quadrant of the profile is estimated by five circular curves of differing radii and points of origin. Vischer & Hager (1999), indicated that the ratio of velocity head to design head is negligible, provided the head over the weir is greater than 100 mm and smaller than half of the pool depth. **Table**

2-2 depicts the Ogee profile's numeric approximation by the USBR (1987) for negligible approach velocity numerically.

Table 2-2: Ogee profile approximation by the USBR (1987) for negligible approach velocity

Radius	Radius magnitude (x·H _o) (m)	x-coordinate origin (x·H _o) (m)	y-coordinate origin (y·H _o) (m)	x-coordinate start (x·H _o) (m)	x-coordinate end (x·H _o) (m)	y-coordinate start (y·H _o) (m)	y-coordinate end (y·H _o) (m)
R ₁	0.235	-0.082	0.247	-0.284	-0.147	0.127	0.021
R ₂	0.530	0.000	0.530	-0.147	0.000	0.021	0.000
R ₃	0.825	0.000	0.825	0.000	0.217	0.000	0.029
R ₄	1.410	-0.153	1.389	0.217	0.583	0.029	0.187
R ₅	2.800	-0.880	2.575	0.583	1.230	0.187	0.734
R ₆	6.500	-3.668	5.007	1.230	1.840	0.734	1.556
R ₇	12.000	-8.329	7.927	1.840	2.758	1.556	3.336

Note: H_o - water depth measured upstream of the crest (m)
 H_e - total energy head upstream of crest, depicted as H_o in **Figure 2-13** (m)
 H_d = H_e - approach velocity negligible (m)

The USBR (1987) approximate the Ogee curve in cases where the approach velocity cannot be neglected by means of a compound circular curve configuration that comprises of two arcs of differing radii and points of origin, as shown in **Figure 2-14** for the upstream quadrant of the spillway and a power function curve for the downstream quadrant of the spillway. For the most general form of Ogee profiles, like in the case of a vertical upstream spillway face, the USACE has developed on the basis of the USBR several standard shapes (Chow, 1959). An example of such a standard shape is depicted in **Figure 2-15** and numerically reflected in **Table 2-3**. Determining the radii of the compound curves for any other configuration, **Figure 2-16** can be used that relate the ratio of approach velocity and the measured crest water depth to the specific radii of the compound circular curves to yield the Ogee profile USBR (1987).

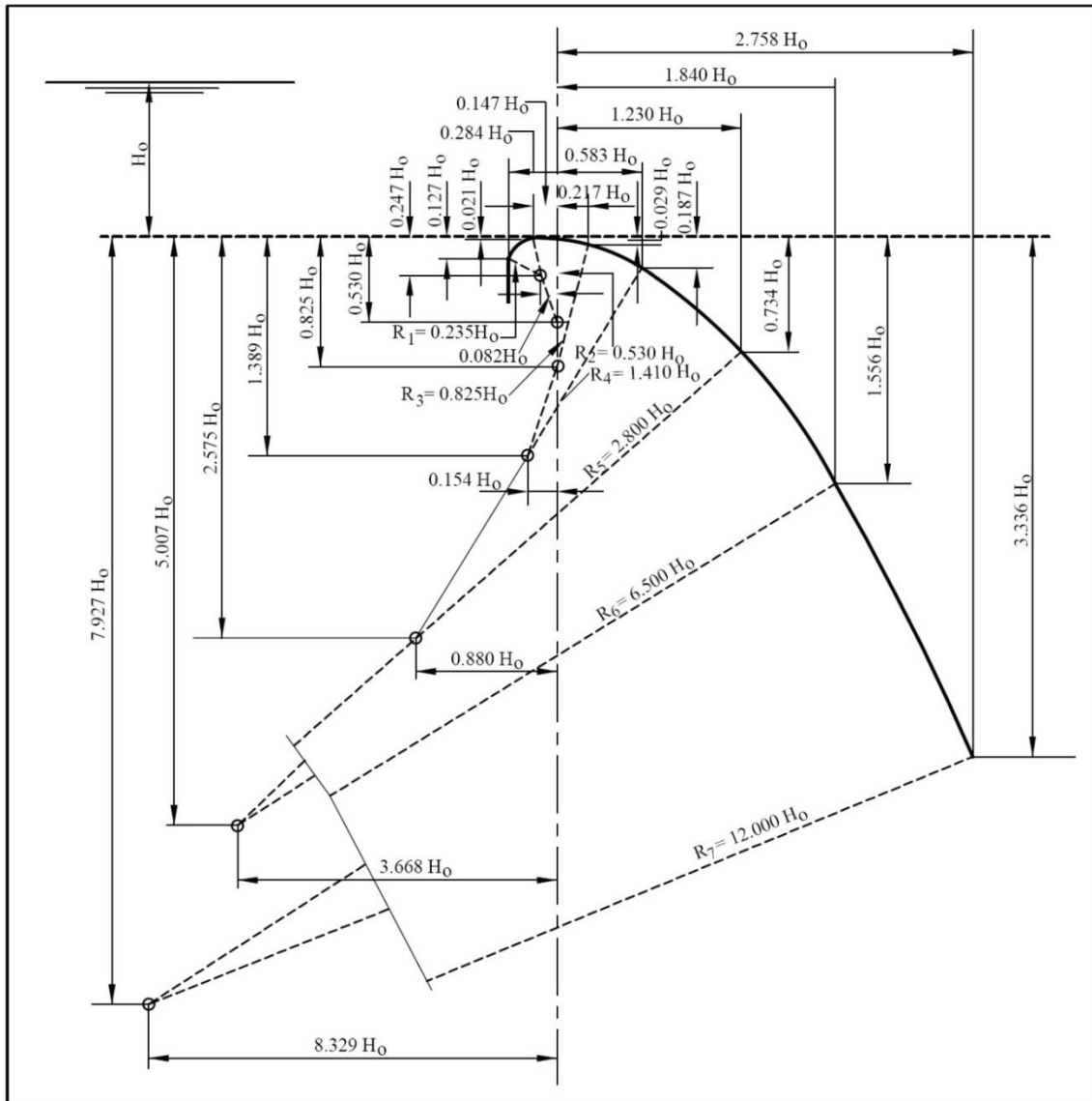


Figure 2-13: Ogee profile approximation by the USBR (1987) for negligible approach velocity

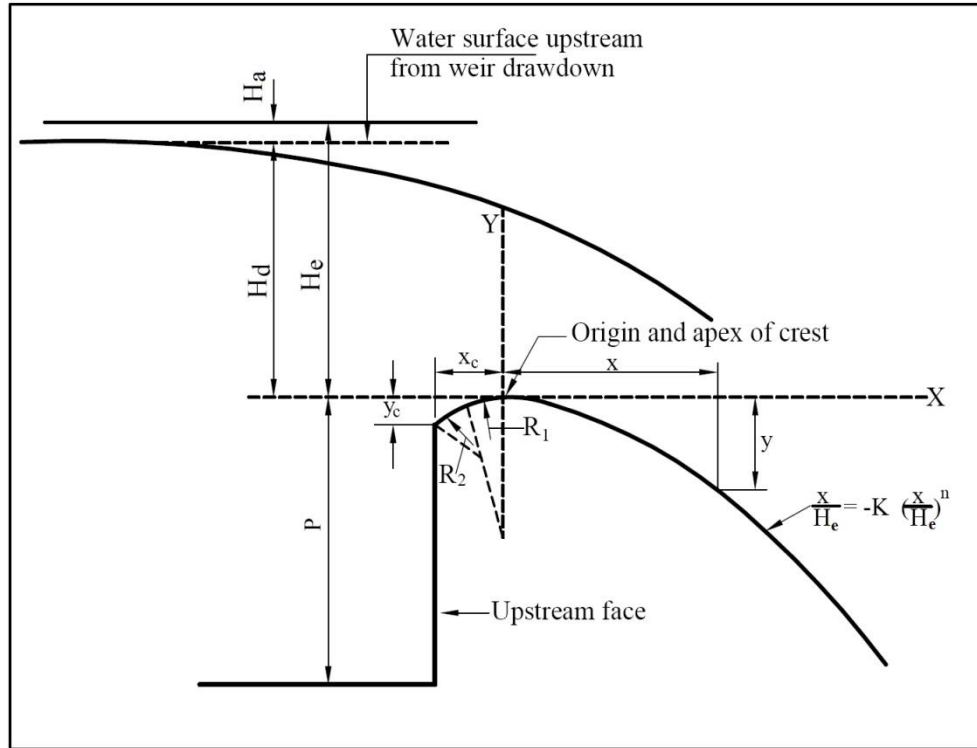


Figure 2-14: Ogee profile approximation by the USBR (1987) for measurable approach velocities

Table 2-3: Standard shape of Ogee curve for a vertical upstream spillway face with measurable velocity head (Chow, 1959)

Radius	Radius magnitude ($x \cdot H_d$) (m)	x-coordinate start ($x \cdot H_d$) (m)	x-coordinate end ($x \cdot H_d$) (m)
R_1	0.200	-0.282	-0.175
R_2	0.500	-0.175	0.000

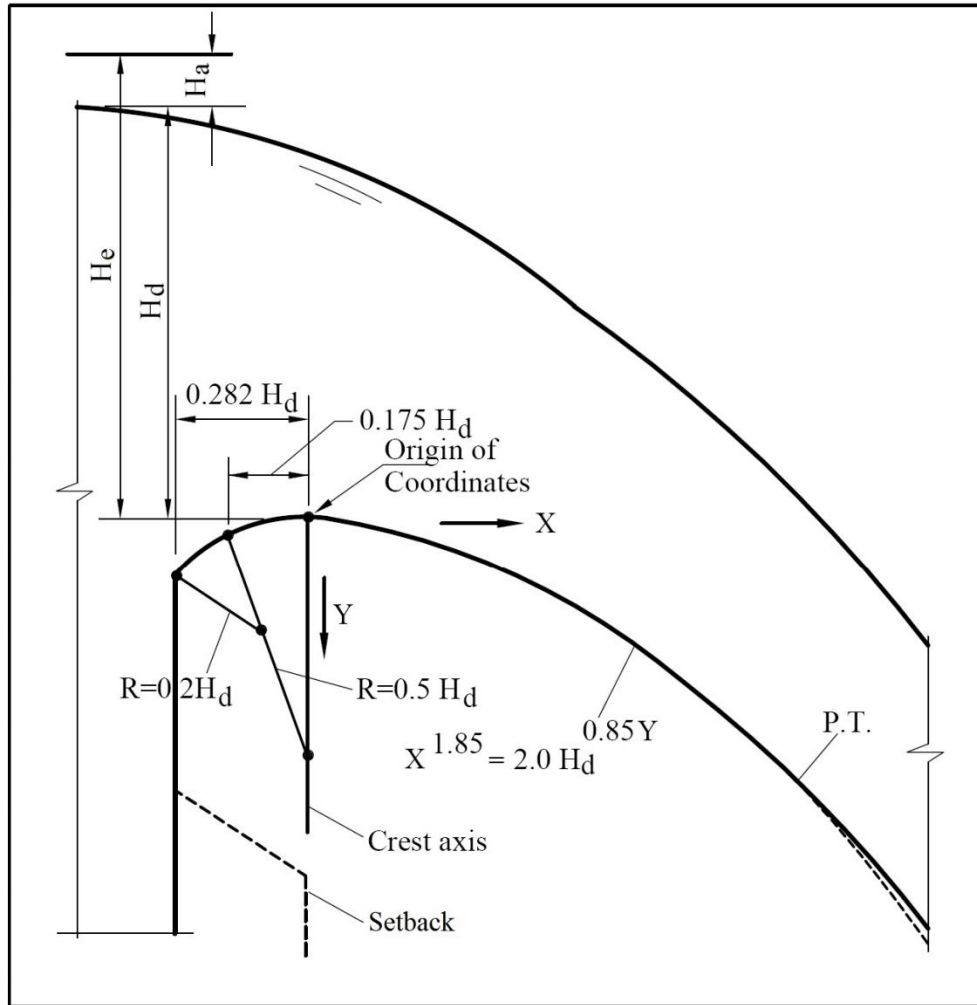


Figure 2-15: Standard shape of Ogee curve for a vertical upstream spillway face with measurable velocity head (Chow, 1959)

The power function describing the downstream quadrant of the Ogee curve is given by **Equation 2-18** and includes variables K and n that is a function of the upstream face geometry of the spillway (USBR, 1987). The values of K and n can be graphically derived from **Figure 2-16**. The power function describing the downstream quadrant of the Ogee curve the same as that of the USACE and IS: 6934-1998 downstream quadrant, as explained in greater detail in the section 2.3.2.2 and section 2.3.2.3 respectively.

$$\frac{y}{H_e} = -K \cdot \left(\frac{x}{H_e} \right)^n$$

Equation 2-18

Where:

- y - Vertical distance from the apex to the curve (m)
- H_e - total energy head upstream of crest, depicted as H_o in **Figure 2-16** (m)
- K - Constant, dependent on the upstream inclination and approach velocity
- x - Horizontal distance from the apex to the curve (m)
- n - Constant, dependent on the upstream inclination and approach velocity

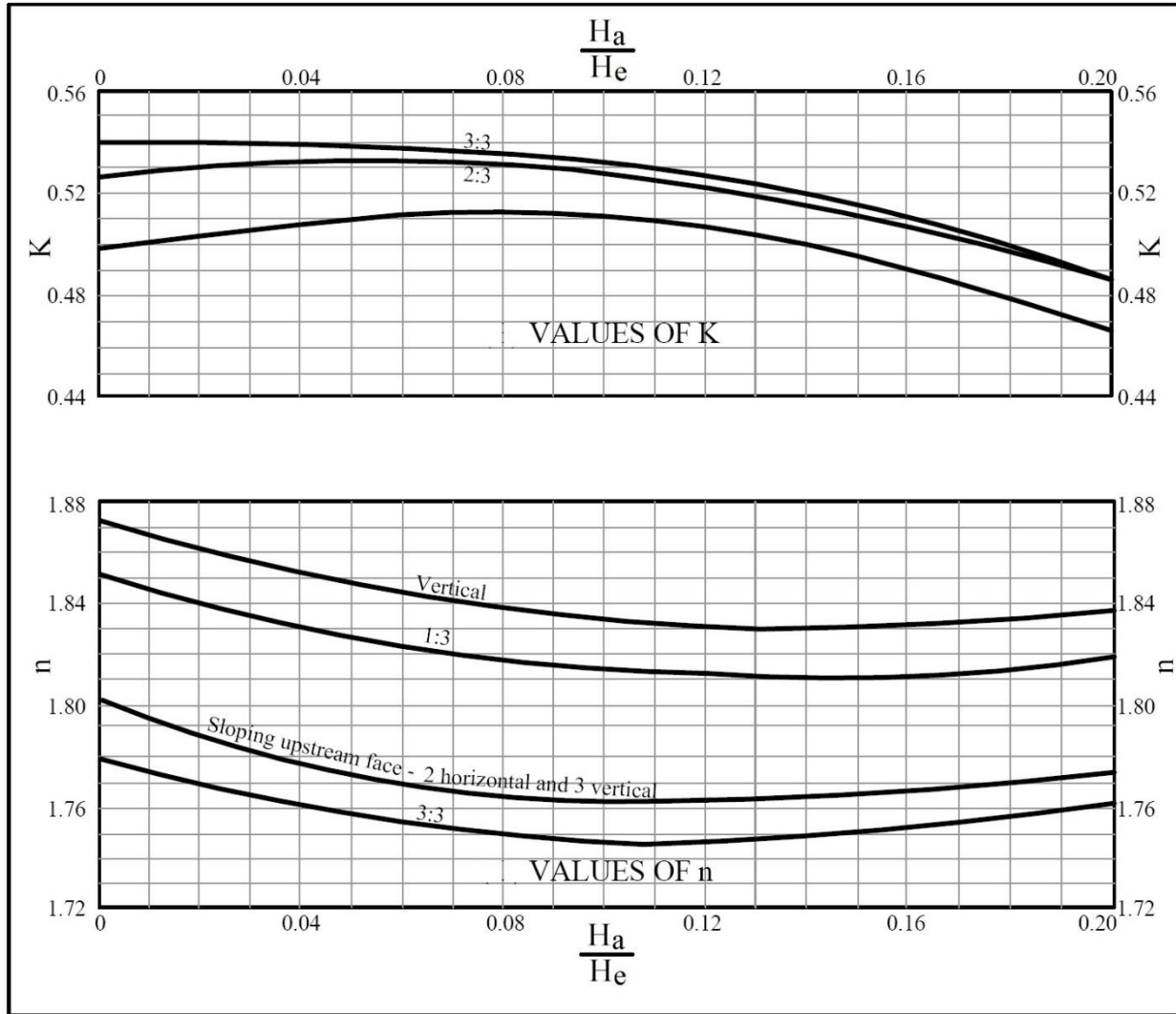


Figure 2-16: Design charts to determine values for K and n for power function curve (USBR, 1987)

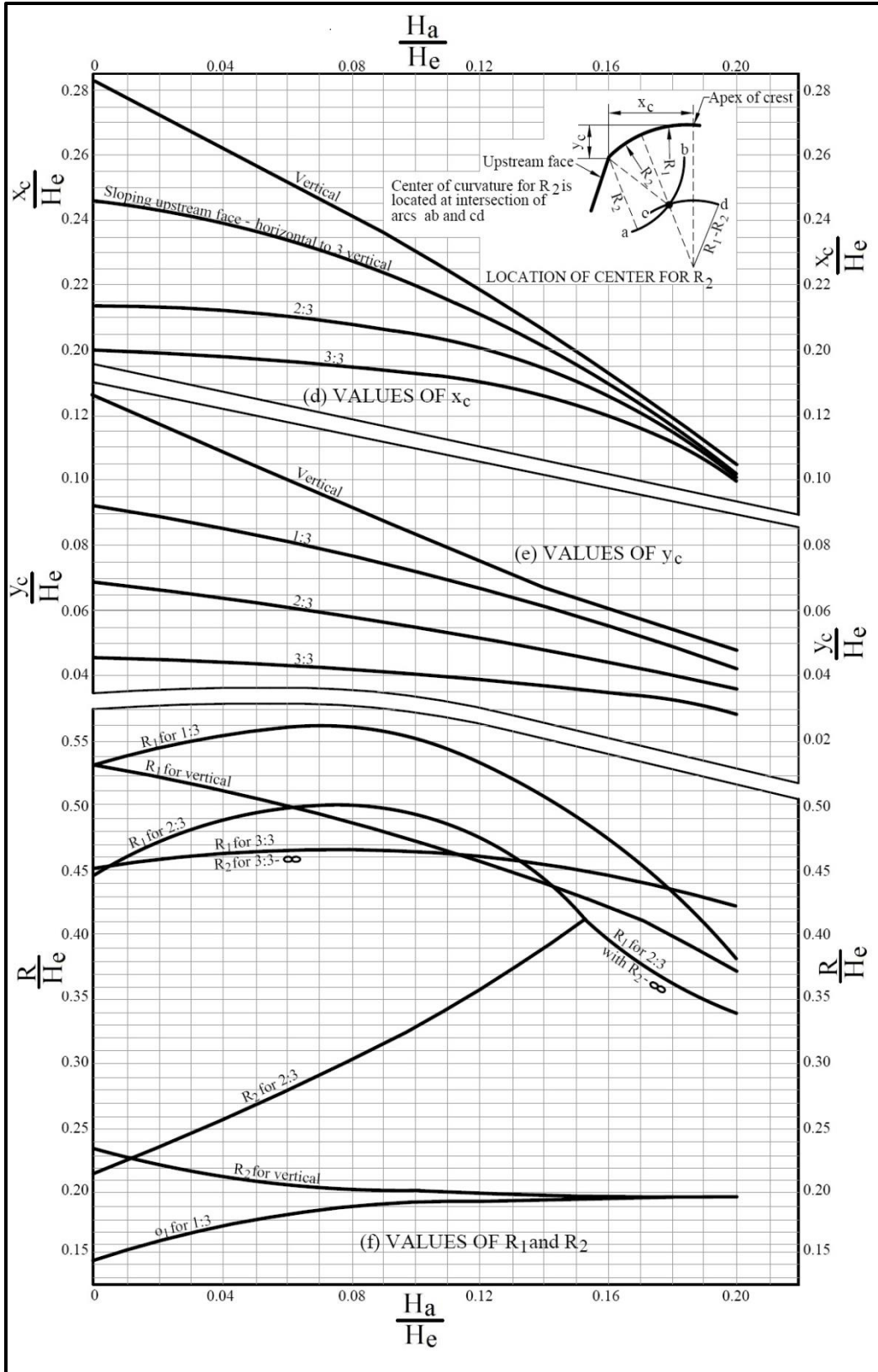


Figure 2-17: Factors for definition of Ogee profile compound curve's radii for the case of measurable approach velocities (USB, 1987)

2.3.2.2 *The relationship of the Ogee curve as approximated by the UASCE (1970)*

The U.S. Army Corps of Engineers (USACE, 1970, revised 1987) suggested a revised compound circular curve to describe the upstream quadrant of the Ogee curve. The upstream quadrant originally defined in **Figure 2-14** and **Figure 2-15** by the USBR (1987), resulted in a surface discontinuity at the vertical spillway face. Model studies at the U.S. Army Waterways Experiment Station indicated that the incorporation of a small arc with radius = $0.04H_d$ improved pressure conditions, reduced possible cavitation of the spillway crest and increased the discharge coefficients for heads exceeding the design head (USACE (a), 1987). The coordinates for the origins of curvature and transition points of the improved design is schematically indicated in **Figure 2-18** together with a table that reflect the numerical values of the origins.

Recent model studies have verified the use of an elliptical upstream quadrant design that was also discussed by the USACE (1992) and reflected in section 2.3.2.3 of this dissertation. The USACE suggest that the method, depicted by the elliptical curve should be used for future spillway design and that the Standard Shape Criteria as presented in this section, must **only be retained for reference purposes**.

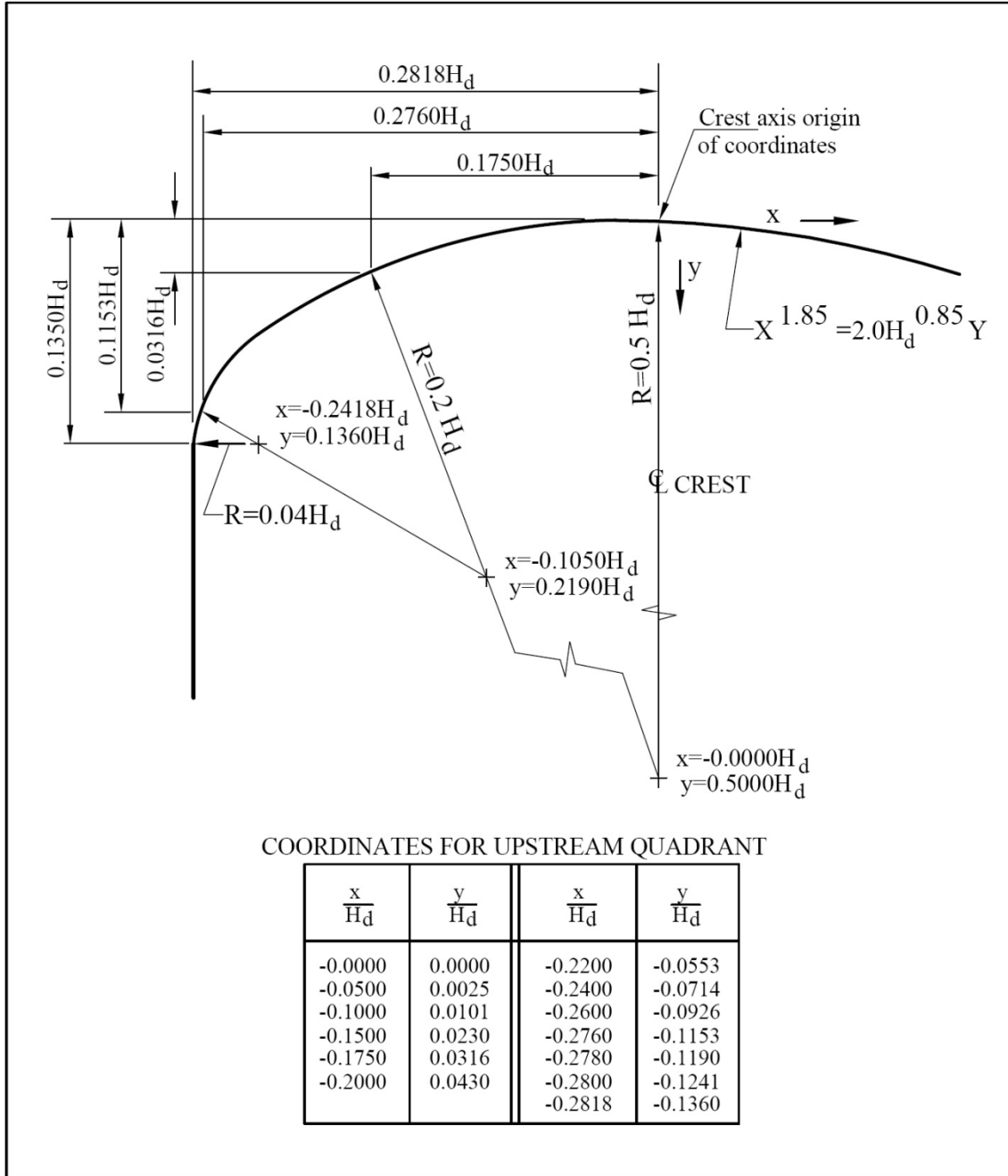


Figure 2-18: The coordinates for the upstream quadrant of the Ogee curve as defined by the USACE (1987)

The downstream quadrant of the Ogee curve is defined by a power function (**Equation 2-19**) similarly to the description used by the USBR (1987). The USACE (1987) define the K and n coefficients in the equation as 0.5 and 1.85, respectively. Therefore is the downstream quadrant of the USACE Ogee curve in **Figure 2-18** the same as the downstream quadrant defined by the USBR in **Figure 2-14**.

$$\frac{y}{H_d} = -K \cdot \left(\frac{x}{H_d} \right)^n$$

Equation 2-19

Where:

H_d - water depth measured upstream of the crest (m)

2.3.2.3 *The relationship of the Ogee curve as approximated by USACE (b) (1987)*

The Bureau of Indian Standards (IS: 6934-1998) has adapted this design procedure for Ogee spillways in the national standards (Anon., 2006).

The USACE (1987) found that their earlier attempts to fit circular arcs to the profile of the lower nappe of the flow over a sharp-crested weir produced surface discontinuities at the weir's crest. Even with adding the short-radius arc tangent to the vertical face, the intermediate-radius arc discontinuities still existed at the weir's crest although this ascertained to be an improvement of the original design. The U. S. Army Engineer Waterways Experiment Station (WES) conducted physical model studies to compare the hydraulic performance of the most commonly used upstream quadrant design procedures and concluded that the short-radius arc method (section 2.3.2.2) and an elliptical curve method appeared to yield the most acceptable results, although only considering 2-dimensional flow parameters (USACE (b), 1987). For the upstream quadrant Murphy (1973) found that, by systematically varying the axes of an ellipse with depth of approach, it was possible to approximate the lower nappe surfaces similar to that estimated by the USBR (1987). Murphy also indicated that any sloping upstream of the spillway face could be used with little loss of accuracy if the slope became tangent to the ellipse calculated for a vertical upstream face.

In 1973 WES published results of preliminary studies done to verify a design procedure incorporating an elliptical upstream quadrant developed from the USBR data (USACE (b), 1987). The procedure was verified for high spillways during these tests and a comprehensive test program with a wide range of approach velocities, upstream face slopes, and head ratios was conducted at WES from 1977 to 1982.

Murphy (1973) indicated that the quadrant of an ellipse in which the axes systematically varied with depth of the approach channel would fit the measured data, except that the ellipse quadrants would extend upstream of the position of the sharp-crested weir used to generate the nappe form to become tangent to the vertical of the spillway wall. This extension is more pronounced when P/H_d is relatively small.

Translating the origin of the elliptical curve of the upstream quadrant to the crest of the Ogee profile and referencing the positive y-direction downwards (**Figure 2-19**), the elliptical curve can be mathematically expressed by **Equation 2-20** (USACE (b), 1987).

$$Y=B \left(1- \sqrt{1- \frac{X^2}{A^2}} \right)$$

Equation 2-20

Where:

- A - coefficient to be solved from normalizing by the design head H_d **Figure 2-19**
- B - coefficient to be solved from normalizing by the design head H_d **Figure 2-19**
- X - horizontal co-ordinate of Ogee profile
- Y - vertical co-ordinate of Ogee profile

In the case of the downstream quadrant of the Ogee curve the general power function as proposed by the USBR (1987) is still valid (**Equation 2-18**). For high spillways where the ratio of velocity head (H_a) to the design head (H_d) is less than 0.06, K and n coefficients of 0.5 and 1.85 are suggested, respectively. As the depth of the approach channel decreases, the approach velocities increase proportionally and the Ogee profile will in essence become flatter to match the partially suppressed vertical contraction of the nappe. Experimental data by WES for sharp-crested weirs found that the downstream quadrant of the spillway can be estimated by maintaining the form of **Equation 2-18** with $n = 1.85$ and varying K with approach depth. The K value can be determined from **Figure 2-19**.

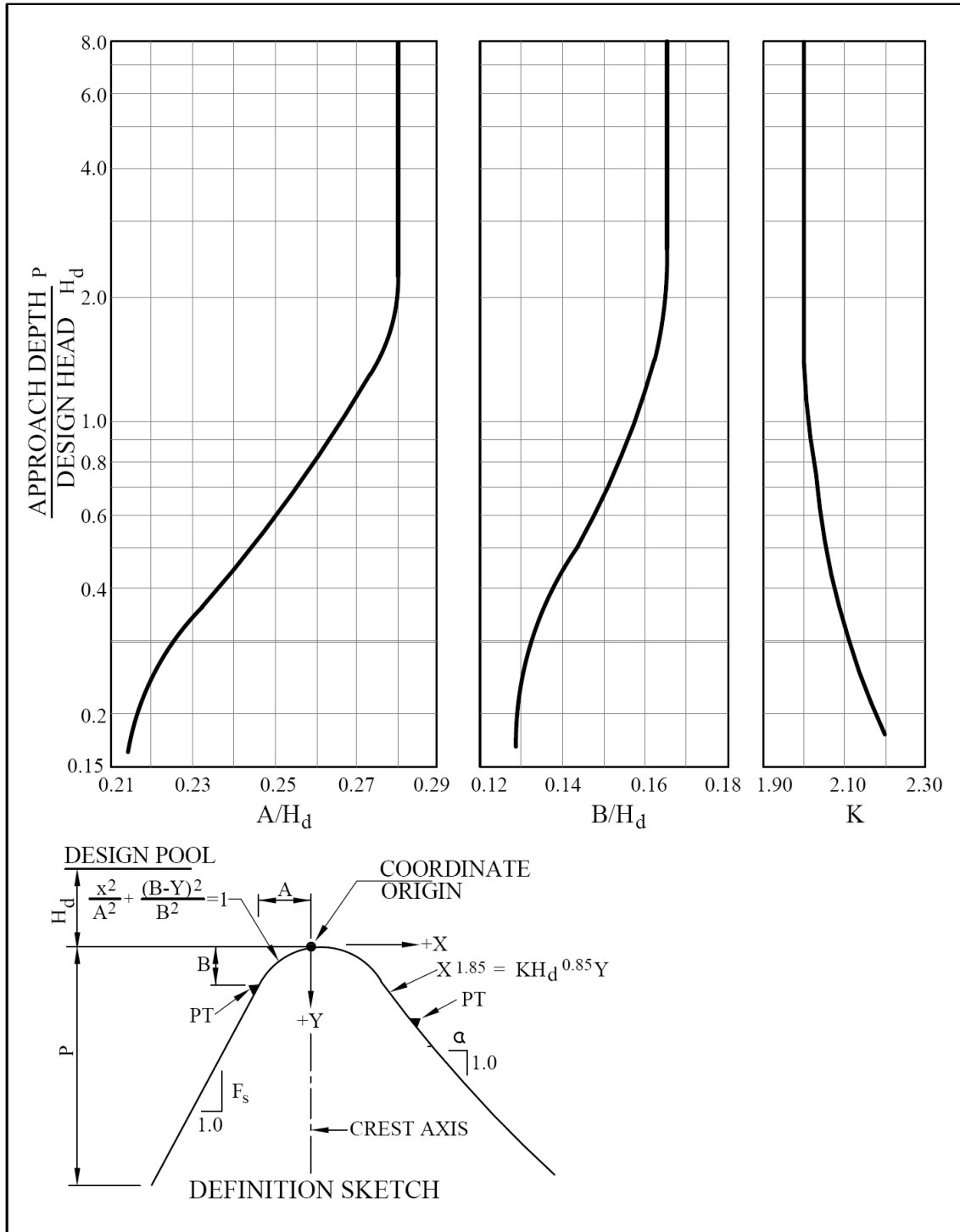


Figure 2-19: Elliptical curve method for determining the Ogee curve (USACE (b), 1987)

2.3.2.4 *The relationship of the Ogee curve as approximated by Hager (1987)*

Vischer & Hager (1999) noted that the Ogee curve approximated by the USBR (1987) and USACE (1987) was made up of multiple compound circular curves. This was disadvantageous as there are sudden discontinuities on the Ogee profile that occur at each of the transition points where the arcs intersect. The concern with this was explained by pointing out the shortcomings of the geometry with regards to:

- Computational solutions of the approach geometry was not possible due to the discontinuity of curvature at the transition points between arcs; and
- Cavitation problems arising at the discontinuities of the arcs during high flow.

Hager (1987), approximated the Ogee curve by an alternative smooth curve determined by transposing the co-ordinates given by the USACE (1987) onto a transposed co-ordinate system. Hager (1987) has transferred the origin of the co-ordinate system used by the USACE (1987) located at the highest point of the Ogee's crest to the minimum horizontal distance value. The Ogee curve suggested by Hager (1987) can be mathematically calculated by means of **Equation 2-21**.

$$Z^* = -X^* \ln X^*, \text{ for } X^* > -0.2818$$

Equation 2-21

Where:

X^* and Z^* are transformed coordinates based on the three arc compound circular curve of USACE (1987)

and

$$X^* = 1.3055 \cdot (X + 0.2818)$$

$$Z^* = 2.7050 \cdot (Z + 0.1360)$$

With

$$X = \frac{x}{H_d}$$

$$Z = \frac{z}{H_d}$$

Where:

- | | | |
|-------|---|--|
| H_d | - | water depth measured upstream of the crest (m) |
| x | - | horizontal co-ordinate of Ogee profile |
| y | - | vertical co-ordinate of Ogee profile |

In 1991, Hager has simplified the transformed coordinates of X^* and Z^* to obtain an equation for the same Ogee curve in Cartesian format equations by making use of **Equation 2-22**

$$\frac{Y}{H_{des}-\Delta z} = 0.136 + 0.482625 \left(\frac{X}{H_{des}-\Delta z} + 0.2818 \right) \cdot \ln \left[1.3055 \left(\frac{X}{H_{des}-\Delta z} + 0.2818 \right) \right]$$

Equation 2-22

Valid for:

$$-0.498 < \frac{X}{H_{des}-\Delta z} < 0.484$$

Where:

H_{des} and Δz are defined in **Figure 2-20**

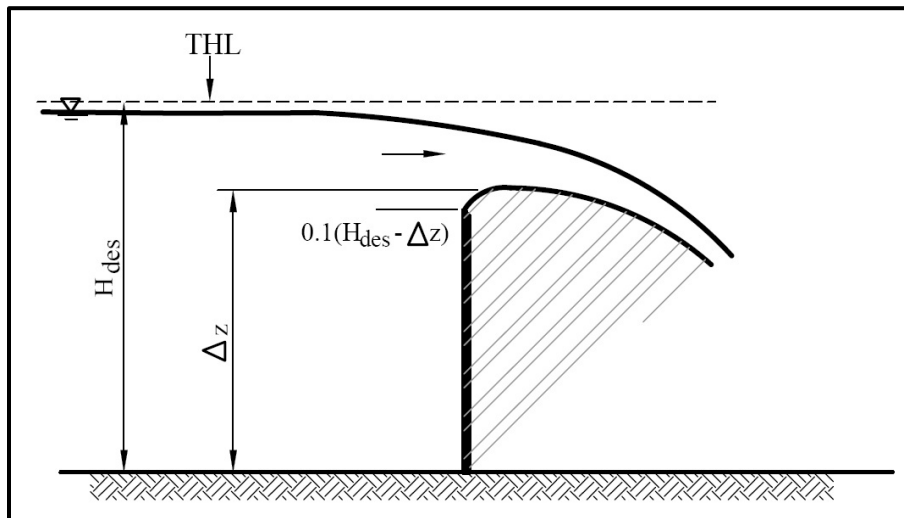


Figure 2-20: Definition sketch of parameters for Ogee Profile (Chanson, 2004)

A comparison of the USACE (1987) and Hager (1987) Ogee curves are depicted below in **Figure 2-21**. For design purposes the difference between the two profiles are usually negligible and differences only exists on the downstream quadrant of the Ogee curve.

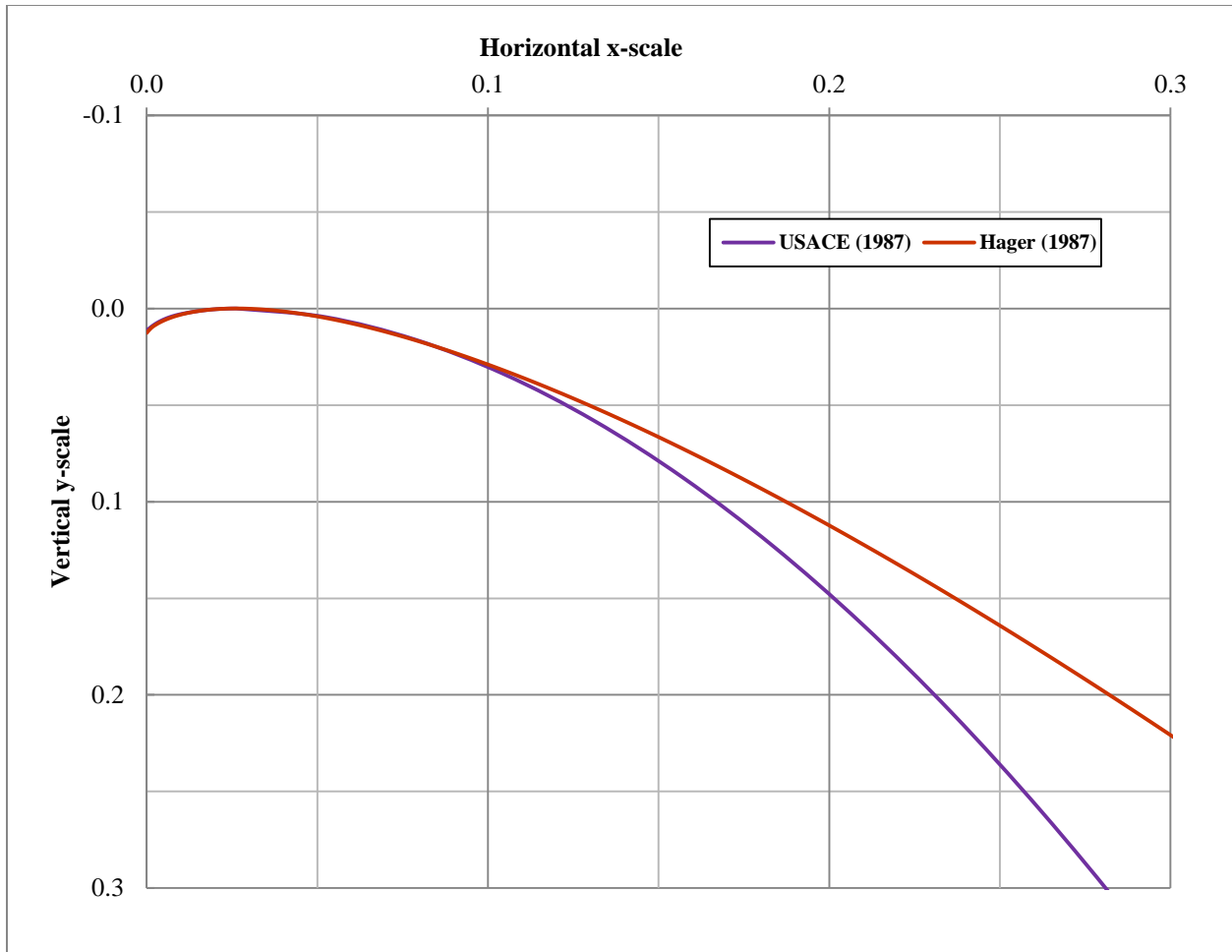


Figure 2-21: The Ogee curve as defined by Hager (1987) and USACE (1987)

In the following sections a summary (section 2.3.2.5 to section 2.3.2.8) of some of the longstanding Ogee curve relationships are given by Hubert Chanson (2004). These relationships can be in many ways be regarded as the origin of the mathematical relationship of the Ogee curve and date as far back as 1888 from which Creager in 1917 has used the original data of Bazin in 1886-1888 to develop one of the first mathematical extension of the Ogee curve.

The most common profiles were the U. S. Army Engineer Waterways Experiment Station (WES) by Scimemi in 1930 and the Creager profile (Chanson, 2004). These relationships however still only considered the 2-dimensional flow parameters.

2.3.2.5 The relationship of the Ogee curve as approximated by Creager, 1917 (Chanson, 2004)

$$Y=0.47 \cdot \frac{X^{1.8}}{(H_{des}-\Delta z)^{0.8}} \text{ valid for } X \geq 0;$$

Where:

H_{des} and Δz are defined in **Figure 2-20**

2.3.2.6 The relationship of the Ogee curve as approximated by Scimeni, 1930 (Chanson, 2004)

The WES standard Ogee curve is based upon detailed observations of the lower nappe of sharp-crested weir flows.

$$Y=0.50 \cdot \frac{X^{1.85}}{(H_{des}-\Delta z)^{0.85}} \text{ valid for } X \geq 0;$$

Where:

H_{des} and Δz are defined in **Figure 2-20**

2.3.2.7 The relationship of the Ogee curve as approximated by Montes, 1992 (Chanson, 2004)

In 1992, Montes developed a continuous spillway profile with continuous curvature radius on curvilinear co-ordinate system that acts along the crest shape. The lower asymptote of the relationship: i.e. for small values of $s/(H_{des} - \Delta z)$ was approximated by **Equation 2-23**; with a smooth variation between the asymptotes by **Equation 2-24** and the upper asymptote: i.e. for large values of $s/(H_{des} - \Delta z)$ estimated by **Equation 2-25**.

$$\frac{R_1}{H_{des}-\Delta z} = 0.05 + 1.47 \cdot \frac{s}{H_{des}-\Delta z}$$

Equation 2-23

$$\frac{R}{H_{des}-\Delta z} = \frac{R_1}{H_{des}-\Delta z} \left[1 + \left(\frac{R_u}{R_1} \right)^{2.625} \right]^{\frac{1}{2.625}}$$

Equation 2-24

$$\frac{R_u}{H_{des}-\Delta z} = 1.68 \cdot \left(\frac{s}{H_{des}-\Delta z} \right)^{1.625}$$

Equation 2-25

Where:

H_{des} and Δz are defined in **Figure 2-20**

- s** - curvilinear co-ordinate along the crest shape
- R** - radius of curvature of the crest (m)

A comparative plot of Creager's, Scimemi's and Montes' Ogee profiles are reflected in **Figure 2-22**. Similar results is obtained by Scimemi's and Montes' with Creager estimating a greater Ogee profile for similar conditions. The axes of the plot was normalized by deviding the X and Y co-orinates by ($H_{des} - \Delta z$) respectively (Chanson, 2004).

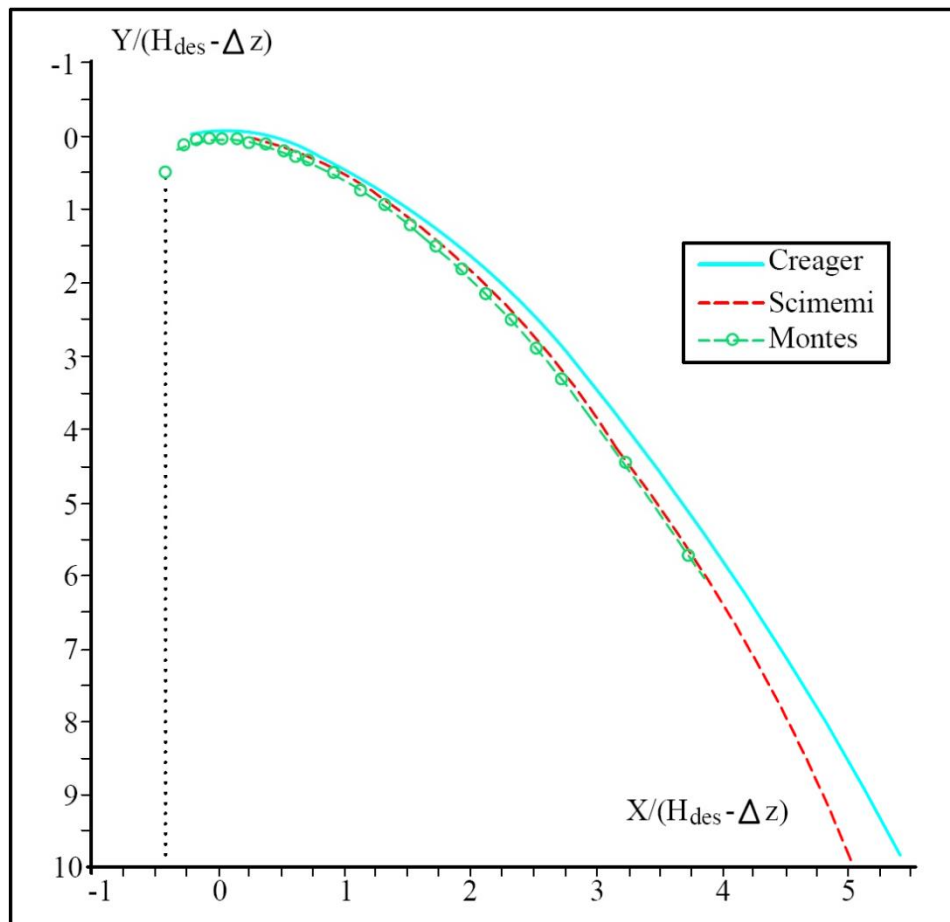


Figure 2-22: Comparative normalized plot of Creager's, Scimemi's and Montes' Ogee profiles (Chanson, 2004)

2.3.2.8 The relationship of the Ogee curve as approximated by Knapp, 1960 (Chanson, 2004)

In 1960, Knapp approximated the crest of the Ogee profile by **Equation 2-26**. A comparative plot of Creager's, Knapp's, Hager's and Montes' Ogee profiles for the crest region only are reflected in **Figure 2-23**.

$$\frac{Y}{H_{des}-\Delta z} = \frac{X}{H_{des}-\Delta z} - \ln \left(1 + \frac{X}{0.689(H_{des}-\Delta z)} \right)$$

Equation 2-26

Where:

H_{des} and Δz are defined in **Figure 2-20**

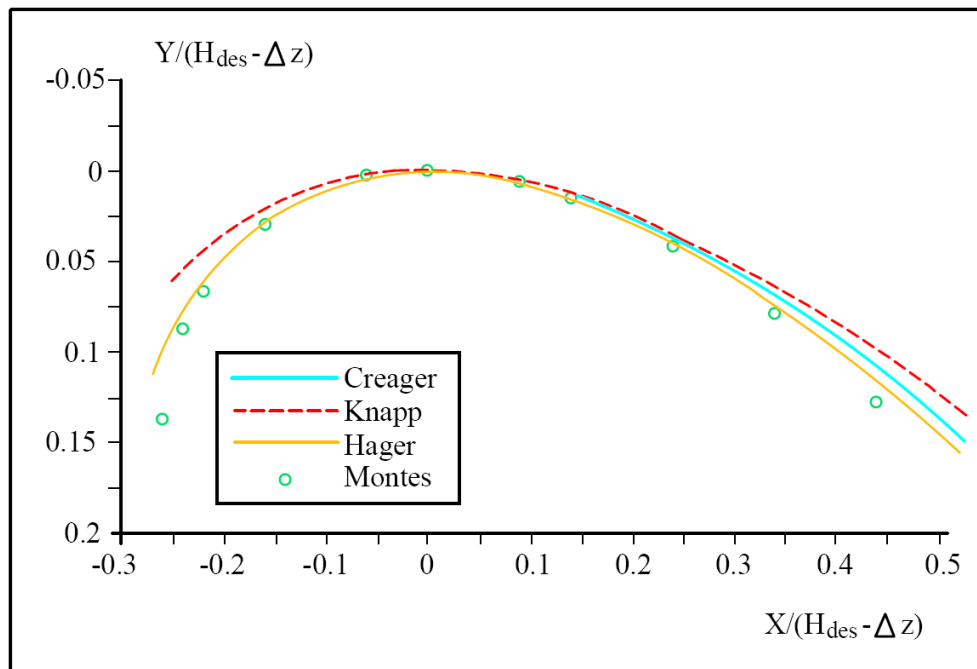


Figure 2-23: Comparative normalized plot of Creager's, Knapp's, Hager's and Montes' Ogee profiles for the crest region only (Chanson, 2004)

2.3.2.9 The relationship of the Ogee curve as approximated by CE-05016 (Ministry of Science and Technology, 2007)

In the document published by the Ministry of Science and Technology (2007): CE-05016, the upstream quadrant of the Ogee profile is approximated by **Equation 2-27**. CE-05016 stipulates that the vertical face of the spillway should be tangential to the approximated Ogee curve and should have a zero slope at the crest axis to ensure that there is no discontinuity along the upstream and downstream quadrants of the Ogee curve.

$$Y = \frac{0.724(X + 0.270H_d)^{1.85}}{H_d^{0.85}} + 0.126H_d - 0.4315H_d^{0.375} \cdot (X - 0.270H_d)^{0.625}$$

Equation 2-27

Where:

- H_d - water depth measured upstream of the crest (m)
- X - horizontal co-ordinate of Ogee profile
- Y - vertical co-ordinate of Ogee profile

The maximum absolute value of X is $0.270H_d$, corresponding to a y -value equal to $0.126H_d$ when the upstream face of the spillway is vertical as depicted in **Figure 2-24**.

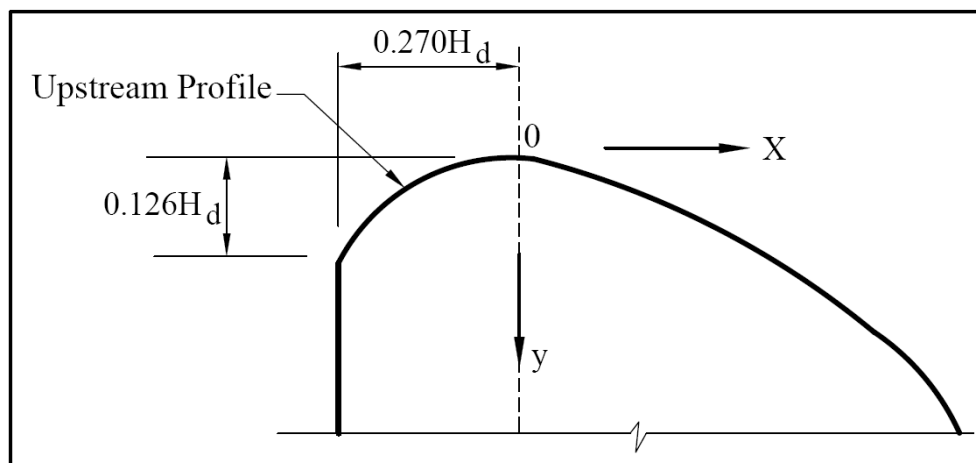


Figure 2-24: Definition sketch of parameters for Ogee Profile (Ministry of Science and Technology, 2007)

The downstream quadrant of the Ogee curve is represented by the same general power curve function as described by the USBR (1987) (**Equation 2-19**). However, the K - and n -values are constants, which

depend upon the inclination of the upstream face of the spillway and can be obtained for a variety of upstream face spillway configurations, with the tangent β as the angle which the upstream face makes with the vertical.

$$\frac{y}{H_d} = -K \cdot \left(\frac{x}{H_d}\right)^n$$

Equation 2-28

Where:

H_d - water depth measured upstream of the crest (m)

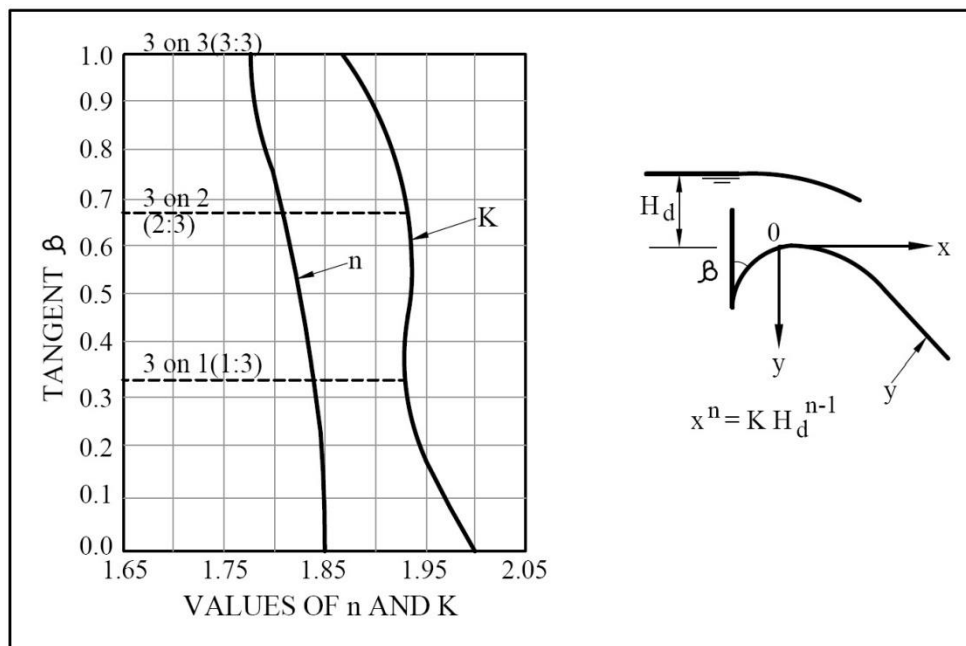


Figure 2-25: K and n constants for the approximation of the downstream quadrant of the Ogee curve (Ministry of Science and Technology, 2007)

2.3.3 Summary and comparison of Ogee profile formulae

The upstream quadrants of the aforementioned methods for defining the Ogee curve have nuances which can be seen in **Figure 2-26**. **Figure 2-26** displays the approximations of the upstream quadrant of the Ogee curves on one axis. In order to compare all the approximated Ogee curves, it was necessary to select a typical scenario for which an Ogee curve needs to be designed for. Such a scenario with all its 2-dimensional flow parameters is portrayed in **Table 2-4**. From the plot of the Ogee curves the USBR (2 circular compound curve), USBR (insignificant approach velocity), USACE (3 circular compound curve), Hager, and CE-05016 plot on more or less the same position with negligible differences. The results for

Knapp, 1960 reflects only the profile for the crest region. The USACE (elliptical curve) seems to differ also from the other approximations, this will be verified during the experimental setup undertaken as described in Chapter 3 of this dissertation.

Table 2-4: 2-dimensional flow parameters required to approximate Ogee curve

2-Dimensional flow parameter	Value	Unit
Total head (H_e)	2.0	m
θ	7.0	degrees
Gravitational acceleration (g)	9.81	m/s^2
Average approach velocity (v_o)	3.617	m/s
Velocity Head (h_v)	0.667	m
Flow depth over weir (H_d)	1.33	m
Upstream depth (H_{des})	7.0	m
Spillway height (P)	5.0	m
$(\Delta z - P)/H$	0.20	m
Height to crest (Δz)	5.20	m
Unit flow rate (q)	4.82	$m^3/s/m$

Note: Notation as described in **Figure 2-20**

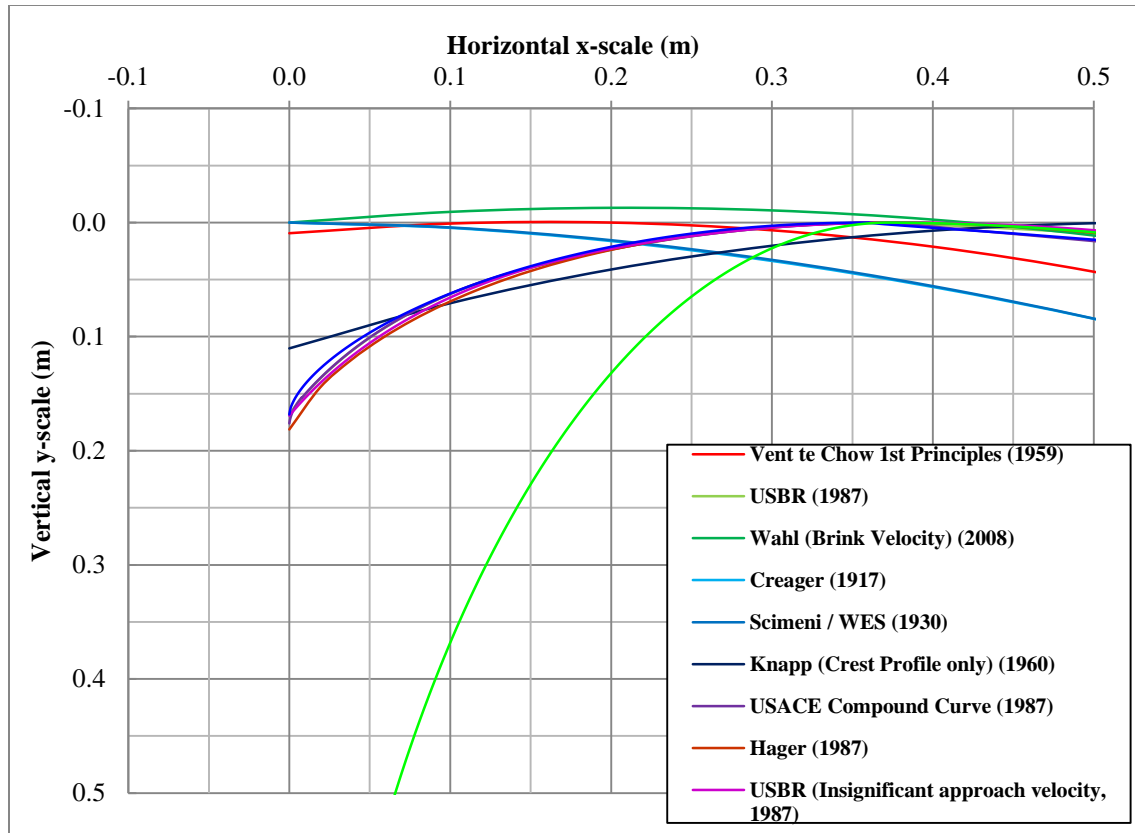


Figure 2-26: The upstream quadrant as defined by the aforementioned methods for defining the Ogee curve

The downstream quadrants of the aforementioned methods for defining the Ogee curve have discrepancies indicated in **Figure 2-27**. All the approximations of the downstream quadrant of the Ogee curve are within reasonable range of each other with Hager seeming to overestimate the downstream quadrant the most, while the Vent to Chow derivation from 1st Principles actually underestimate the Ogee downstream quadrant. These will be verified during the experimental setup undertaken as described in Chapter 3 of this dissertation.

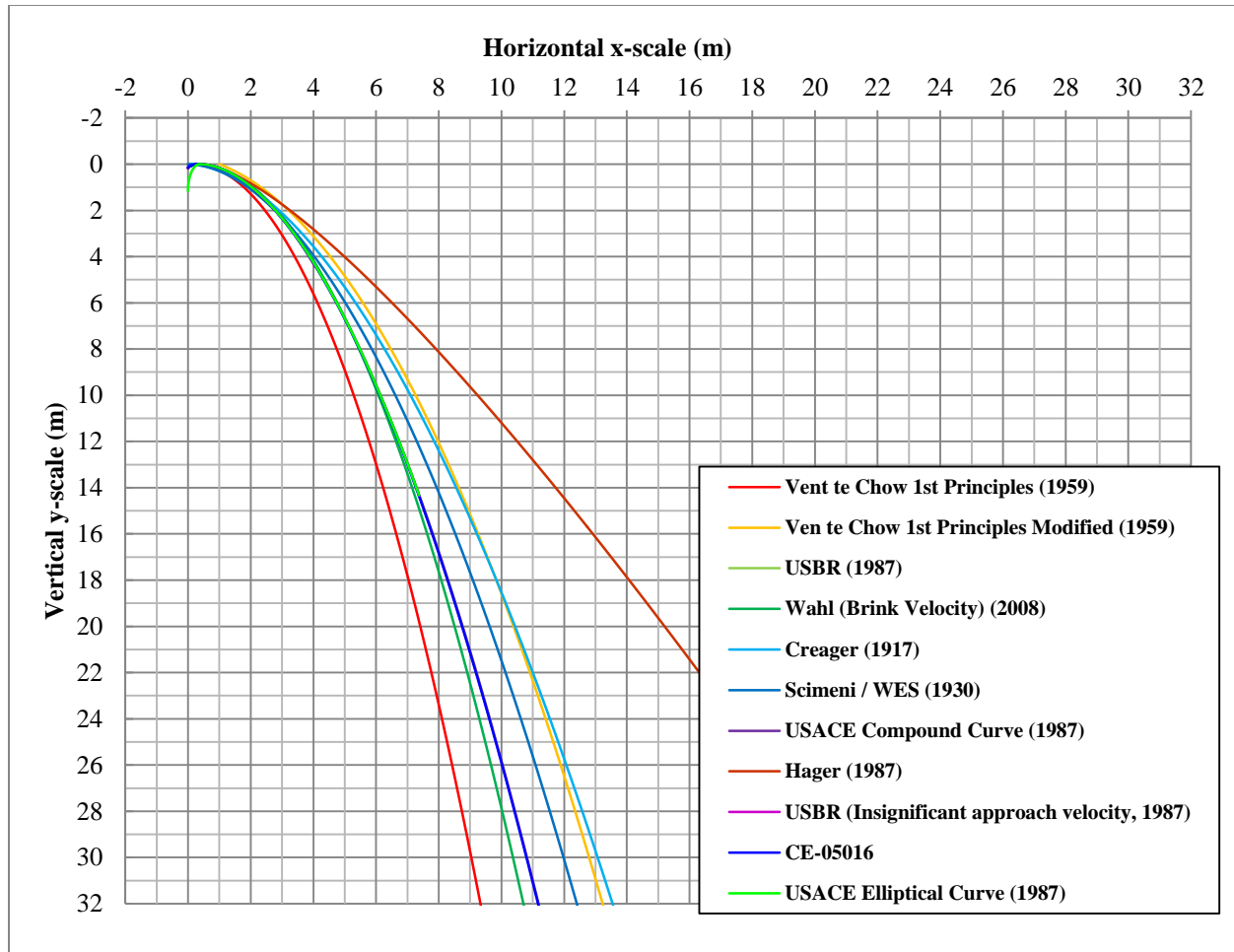


Figure 2-27: The downstream quadrant as defined by the aforementioned methods for defining the Ogee curve

As can be seen in these approximations and the literature surrounding them, there are certain characteristics of the dam and spillway which are not taken into account when considering the shape of the Ogee curve. A discussion on the current knowledge pertaining to the effect of these unconsidered flow parameters is follow under section 2.6.

2.4 OGEE CURVE APPROXIMATIONS OF ACTUAL DAMS (Şentürk, 1994)

It is recommended that for Ogee curve spillways required for discharging large floods under high hydraulic heads the n coefficient for the downstream quadrant be selected to be less or equal to 2 (Şentürk, 1994). By selecting the n coefficient to be less or equal to 2 the hydraulic efficiency of the system will be in a stable condition and a flatter curve will be obtained. It is for this reason that the Ogee

curve of Keban Dam is a second degree parabola. If negative pressures are to be completely avoided this procedure is recommended. Other examples illustrating such cases are summarized in **Table 2-5** (Şentürk, 1994). Each one of these Ogee spillways was designed to spill large floods. Şentürk (1994), recommend that physical modulation should always be investigated for the specific design of Ogee spillways where large floods are expected. It is then possible to compare computed theoretical results using relations similar to the formulas in section 2.3 with those obtained from the model study of the Ogee spillway.

Table 2-5: Examples of Ogee spillways with second degree parabola curves to prevent sub-atmospheric conditions under high flow conditions (Şentürk, 1994)





Dam	Photo (http://www.usbr.gov/projects)	Approximate Ogee curve equation
Canyon Ferry Dam (USA)		$Y = \frac{X^2}{127} + \frac{X}{6}$
Hoover Dam (USA)		$Y = \frac{X^2}{75} + \frac{X}{5} + 1.39$

Table 2-5: Examples of Ogee spillways with second degree parabola curves to prevent sub-atmospheric conditions under high flow conditions (Şentürk, 1994) continue...

Dam	Photo (http://www.usbr.gov/projects)	Approximate Ogee curve equation
Angostura Dam (Mexico)		$Y = \frac{X^2}{120}$
Keban Dam (Turkey)		$Y = \frac{X^2}{39.3}$

2.5 TANGENT POINT ON DOWNSTREAM SLOPE OF THE OGEE CURVE

The point of tangency depends on the slope of the downstream face of the spillway and is determined by the stability requirements of the overflow section of the dam wall. To determine the tangent point of the Ogee curve mathematically, the first derivative of the downstream slope of the ogee spillway's crest must be set equal to the slope of the spillway. The first derivative of the USACE's downstream profile is given in **Equation 2-29**. The slope of the downstream crest is determined by taking moments about the toe of the dam wall and considering the hydrostatic pressures and own weight of the hydraulic structure. By doing so the unknown horizontal distance x can be determined. A factor of safety against sliding or overturning of the dam wall should also be included (**Figure 2-28**).

$$\frac{dz}{dx} = 0.5 \cdot H_d \cdot 1.85 \cdot \left(\frac{x}{H_d}\right)^{(1.85-1)} \cdot \frac{H_d}{H_d^2}$$

Equation 2-29

Where:

H_d - water depth measured upstream of the crest (m)

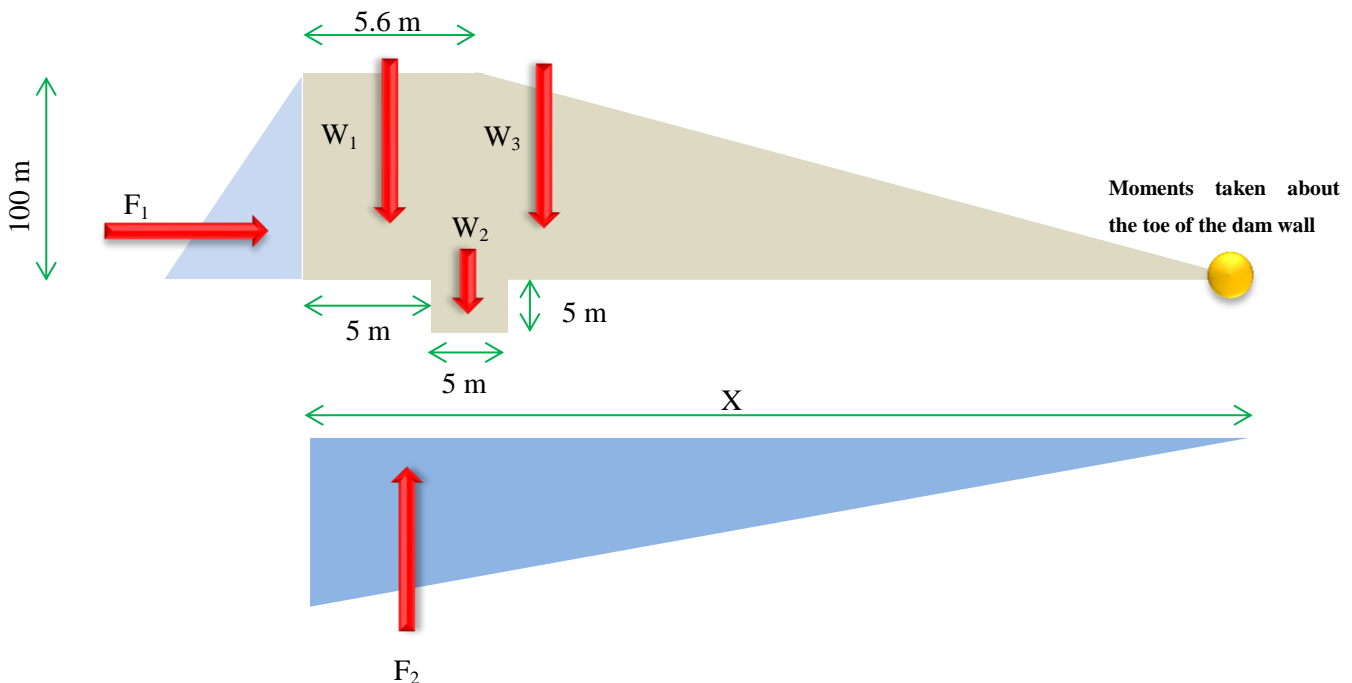


Figure 2-28: Schematic section of a dam wall used to calculate the downstream slope of the hydraulic structure

Occasionally, a reverse curve at the bottom of the spillway may also be utilized to direct the flow into the apron of a stilling basin or into a spillway discharge channel (Ministry of Science and Technology, 2007). An example of such a design is depicted in **Figure 2-29**, indicating the point of tangency with an orange dot.

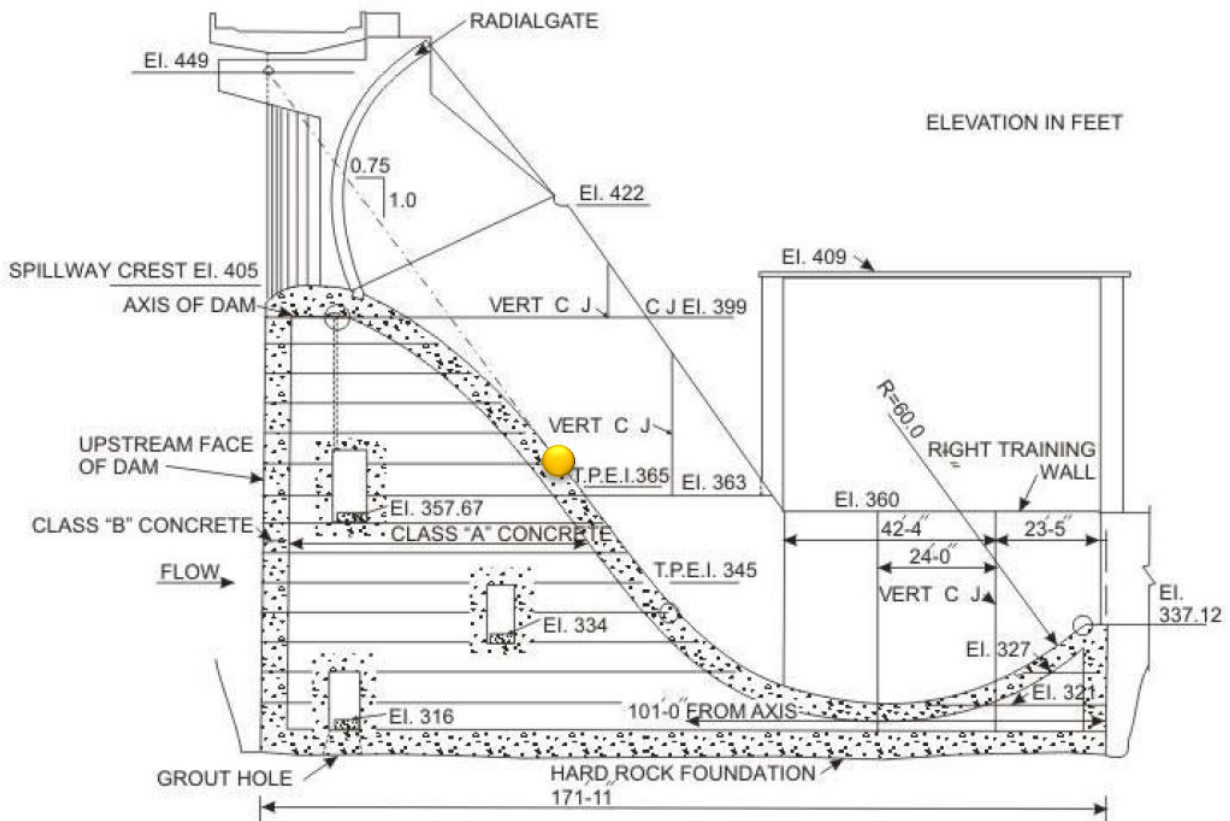


Figure 2-29: Example of an Ogee spillway with reverse curve at the bottom for dissipation of energy. The tangent point is indicated and located at the orange dot (Anon., 2006)

The USACE (a) (1987) has computed an empirical slope function graph of the tangents X and Y to the downstream quadrant for Ogee spillways that can be used to determine the location of the tangent point of the curve. This graph was setup by considering **Equation 2-30** and **Equation 2-31**. However, it should be noted that the tangent point will still, in most cases, be determined analytically for the final design by means of the method as described above. This graph can still be of value in the preliminary layouts in connection with stability analyses and cost estimates.

$$\frac{X}{H_d} = 1.096 \left(\frac{1}{a} \right)^{1.176}$$

Equation 2-30

$$\frac{Y}{H_d} = 0.592 \left(\frac{1}{a} \right)^{2.176}$$

Equation 2-31

Where:

a - vertical distance for 1 m horizontal

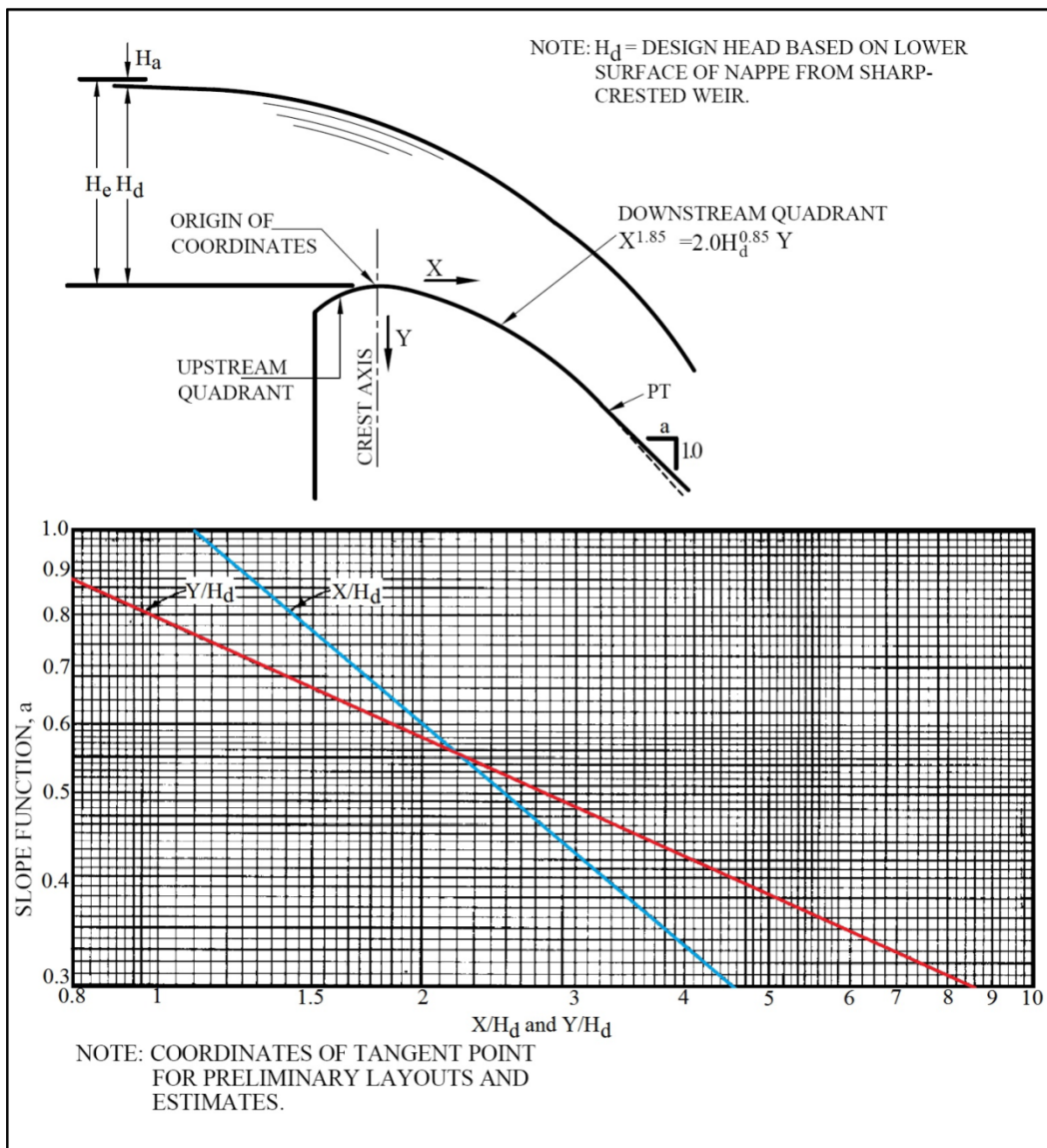


Figure 2-30: Slope function graph of the tangents X and Y to the downstream quadrant of Ogee spillways (USACE (a), 1987)

2.6 3-DIMENSIONAL FLOW PARAMETERS TO BE CONSIDERED WHEN APPROXIMATING THE OGEE CURVE

2.6.1 Introduction

The current methods for the approximation of the Ogee curve, as discussed in section 2.3 of this dissertation only considered 2-dimensional flow parameters. These parameters being the design head, the upstream inclination of the spillway and the pool depth. The latter can be related to the average approach velocity upstream of the spillway structure (in cases where the upstream pool depth is great in relation to the design head the approach velocity may actually be negligibly small), see section 2.6.2.

2-Dimensional flow parameters may be sufficient for describing the Ogee curve in cases that conform to all the criteria below:

1. the upstream approach channel is symmetrical;
2. the spillway can be regarded as a full width un-contracted weir;
3. the orientation of the approach channel relative to the spillway structure intercept the spillway at a perpendicular angle (the centerline of the spillway is parallel to the flow lines); and
4. the radius of the spillway structure tend to infinity.

However, in most cases the spillway structure does not conform to these 2-dimensional flow criteria. The upstream topography of the approach channel have an effect on the distribution of the velocity over the spillway (**Figure 2-31**) and will thus adversely alter the Ogee profile from one position on the spillway relative to another, resulting in non-uniform curvature throughout the spillway. Even with only a symmetrical approach channel the velocity distribution in the approach channel is not uniform throughout the system and a mean average velocity is normally used to compute the velocity head used in the calculations to approximate the geometry of the Ogee curve. Curvature of spillways is a common design practice for increasing the structural integrity of the dam wall and should also be considered for approximating the geometry of the Ogee curve.

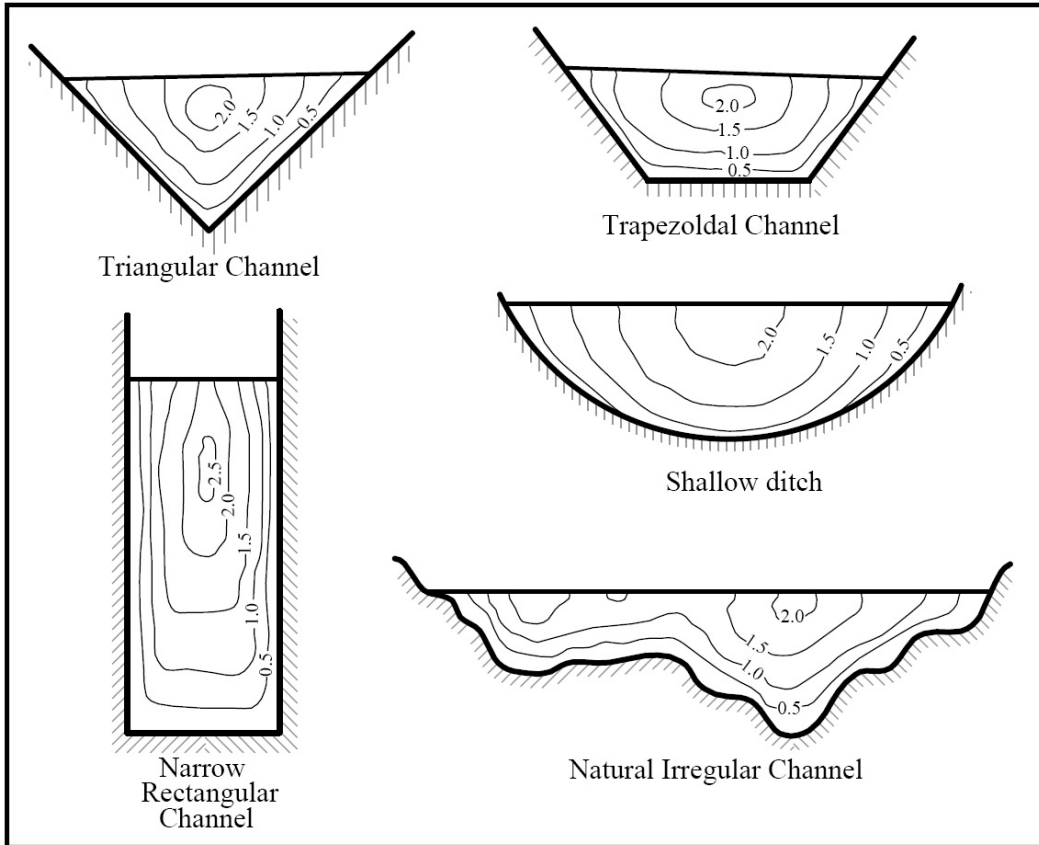


Figure 2-31: Upstream topography of approach channel influencing the velocity distribution over the spillway (Chow, 1959)

A physical model study of the Neckertal Dam in Namibia undertaken by Prof S. J. van Vuuren in 2010, University of Pretoria, has introduced the hypothesis of upstream asymmetry of the approach channel and research in this aspect was required (van Vuuren, 2010). The Neckertal Dam's approach channel is asymmetrical resulting in a non-uniform velocity distribution over the spillway structure which is further worsened by the curvature of the dam wall (**Figure 2-32**). 2-Dimensional flow parameters may thus not always be sufficient for approximating the Ogee curve of the spillway and upstream flow conditions, together with the orientation and curvature of the spillway must always be considered in order to ensure the design of the most effective spillway system. Subsequently, preventing the formation of possible sub-atmospheric pressures may lead to cavitation. The 3-dimensional parameters which are expected to most likely influence the geometry of the Ogee curve is discussed in the following sub-sections of this dissertation.

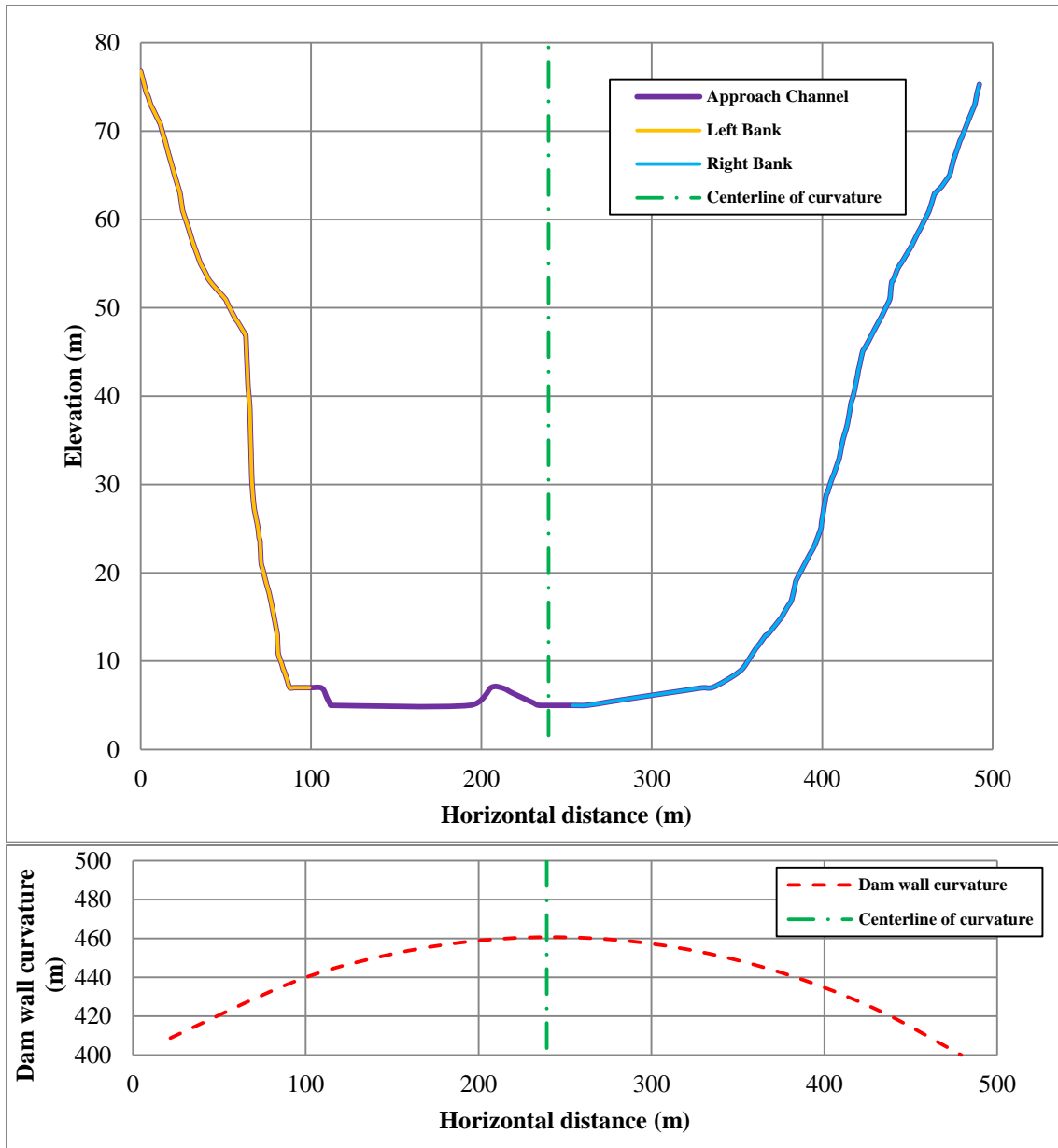


Figure 2-32: Asymmetry of approach channel for the Neckertal Dam (van Vuuren, 2010)

2.6.2 Velocity distribution of approach channel

In 1907, Horton reflected that the discharge over a weir takes place by virtue of the potential energy of the layer of water lying above the level of the weir's crest, which is rendered as kinetic energy by the act of falling over the weir. If the water approaches the weir with an initial velocity, it is evident that some part of the concurrent energy will facilitate the discharge (Horton, 1907).

According to Horton (1907) the theoretical correction formulas for estimating the discharge over any hydraulic structure does not truly represent the effect of the velocity distribution of the approach channel. Reasons for this may be explained by the following statements:

- The head loss in the leading channel adjacent to the spillway section is the source of the approach velocity, and this head loss will always be greater than that required to produce the existing velocities, due to the fact that some losses will be utilized in overcoming friction in the channel;
- The velocity distribution in the channel is seldom uniform throughout its width, thus resulting in the energy of the water effectively varies accordingly.
- It is uncertain what portion of the energy of the water in the upstream channel contributes to the increase of discharge over the spillway.

Vertical layers and horizontal sections of the approach channel upstream of a weir may thus have varying velocities. According to Horton (1907) the ratio of the actual energy of the approaching water to the energy due to the mean velocity will be greater than unity, and for this reason the correction for the approach velocity will be greater than if the energy was due to a loss through a head produced by the mean velocity. The more uniform the velocity distribution in the approach channel is, the smaller will be the need for a correction coefficient in the velocity head formula. In experimental setups, baffles and flow straighteners can be readily applied to simulate a satisfactory velocity distribution (ISO 1438, 2008). However, in actuality, this may be a difficult and economically unfeasible procedure for ensuring a uniform velocity distribution upstream of a hydraulic structure.

The vertical and horizontal velocity distribution curves in an open channel can usually be approximated by parabolas. A weir interposes an obstruction in the lower part of the channel, lessening the bottom velocities. The velocity is not, however, confined to the layers in line with the section of the discharge opening of the weir. As a result of viscosity of the liquid, the upper rapidly moving layers drag the lower layers underneath, and the velocity may extend quite near to the bottom of the channel. However, there are usually a line A B C, as depicted in **Figure 2-33**, rising as the weir is approached. Below this line there is no *forward* velocity. The line A B C is the envelope of the curve for the vertical velocity distribution in the approach channel. Similar to this envelope there can be an area defined of low velocity at each side of the channel for a contracted weir (Horton, 1907).

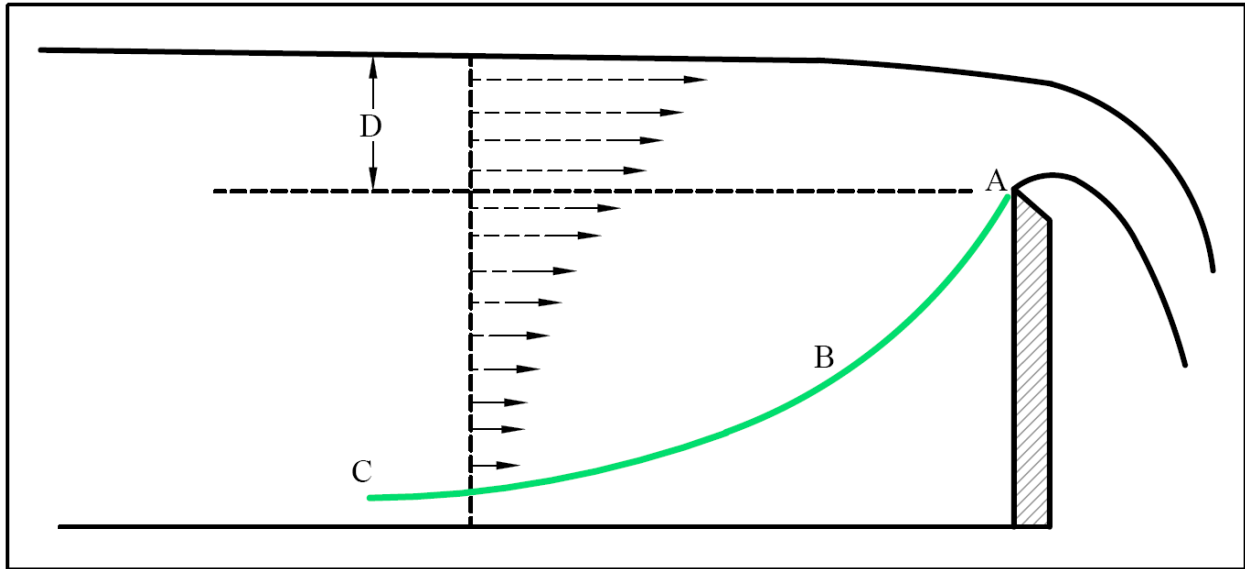


Figure 2-33: Velocity distribution upstream of a sharp-crested weir (Horton, 1907)

When considering a unit width of the approach channel, the general formula for kinetic energy can be approximated by **Equation 2-32**.

$$E_k = \frac{Wv^2}{2g}$$

Equation 2-32

Where:

- E_k - kinetic energy (J)
- v - velocity in approach channel at a specific depth (m/s)
- W - weight of the moving mass (N)

Should the assumption held as depicted in **Figure 2-33** and it is assumed that the approach velocity increases linearly from bottom to the water surface, the velocity at any depth can be approximated by **Equation 2-33**.

$$v = v_b + \frac{x}{X}(v_s - v_b)$$

Equation 2-33

Where:

- v_s - surface velocity (m/s)

- v_b - bottom velocity (m/s)
 x - depth to calculate velocity (m)
 X - pool depth upstream of the weir (m)

If the thickness of a specific water layer, one unit wide and at a depth of x can be defined by dx , the total kinetic energy for the depth can be approximated by **Equation 2-34**.

$$E_k = \int_0^X \left[v_b + \frac{x}{X} (v_s - v_b) \right]^3 \cdot \frac{w}{2g} dx$$

Equation 2-34

Where:

- w - weight of unit volume

For a uniform velocity distribution the total kinetic energy per unit width as depicted by **Equation 2-34** is found to be:

$$E_k = \frac{wXv_m^3}{2g}$$

Equation 2-35

Where:

- v_m - mean velocity (m/s)

When integrating **Equation 2-34** where the bottom velocity (v_b) is 0 m/s and the velocity increases linearly from the bottom to the surface so that the mean velocity (v_m) is half of the surface velocity (v_s) the kinetic energy is estimated by **Equation 2-36**.

$$E_k = \frac{wXv_m^3}{g}$$

Equation 2-36

Comparing **Equation 2-36** with the expression for kinetic energy of a stream flowing with the uniform velocity (v_m) (**Equation 2-35**), it is found that the mass energy of the stream with linear varying velocity to be twice that of a stream with a uniform velocity of the same measured value.

Horton (1907) indicated that by a similar integration the ratio of the total kinetic energy to the kinetic energy corresponding to the mean velocity in the approach channel can be obtained for any assumed

velocity distribution in the approach channel. The resulting ratio will depend upon the relative areas of section with low and high velocities which go to make up the mean, and in practice it will generally exceed unity.

The kinetic energy of a mass of water will remain sensibly constant while it flows through the approach channel with a uniform cross section. With a constant head, the kinetic energy can only change through a change of slope or through fluid friction. The channel slope is nearly absent and the latter only results in a slow transfer of energy. If the velocities in the vertical plane were originally unequal and become equalized in the approach channel, then there must have been an increase in the mean velocity of the mass of water, or otherwise the kinetic energy per unit mass will decrease. It follows that the mean velocity will increase, although the mean kinetic energy per unit mass remains constant, and hence the total kinetic energy of the water passing over the weir will increase in the same proportion as the velocity and discharge. Normally, two scenarios exist in cases where the mean velocity is the same, but in which the velocities in the approach channels are uniform in the first case and non-uniform in the second. When the weight of the water that is passing over the weir per second is represented by W and W^1 respectively, and the kinetic energies are presented by E_k and E_k^1 ; then, since $E_k = Wh$, where h being the head due to the mean velocity v , then (**Equation 2-37**):

$$Wh : W^1h \text{ and } E_k : E_k^1$$

Equation 2-37

Thus, according to Horton (1907) it follows that an equalization of the velocities in the approach channel by means of flow straighteners or baffles may cause an increase in the discharge, whilst the measured design head remains the same.

For a typical approach velocity distribution as given by ISO 1438 (2008) for a rectangular approach channel (**Figure 2-34**), the velocity in the channel at the surface may vary between 0,8 and 1,2 times the mean velocity. This variance will influence the Ogee profile measured along the spillway as depicted in **Table 2-6** and **Figure 2-35** for a hypothetical scenario where the Ogee curve is approximated by the USACE (a) (1987) relationship.

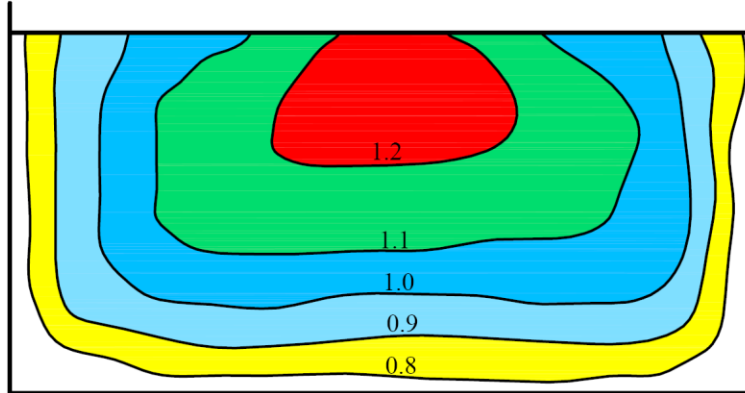


Figure 2-34: Velocity distribution of a rectangular open channel as given by ISO 1438 (2008)

Table 2-6: Hypothetical scenario where the Ogee profile is approximated by the USACE (a) (1987)

Parameter	Value for H_c/P ratio			Unit
	0.344	0.321	0.300	
Total head (H_c)	1.720	1.605	1.500	m
Gravitational acceleration (g)	9.81			m/s^2
Approach velocity (v_o)	3.758	3.445	3.132	m/s
Velocity Head (H_a)	0.720	0.605	0.500	m
Flow depth over weir (H_d)	1.0			m
Upstream depth (H_{des})	6.720	6.605	6.500	m
Spillway height (P)	5.0			m
$0.1(H_{des} - \Delta z)$	0.152	0.142	0.135	m
Height to crest (Δz)	5.200	5.180	5.150	m

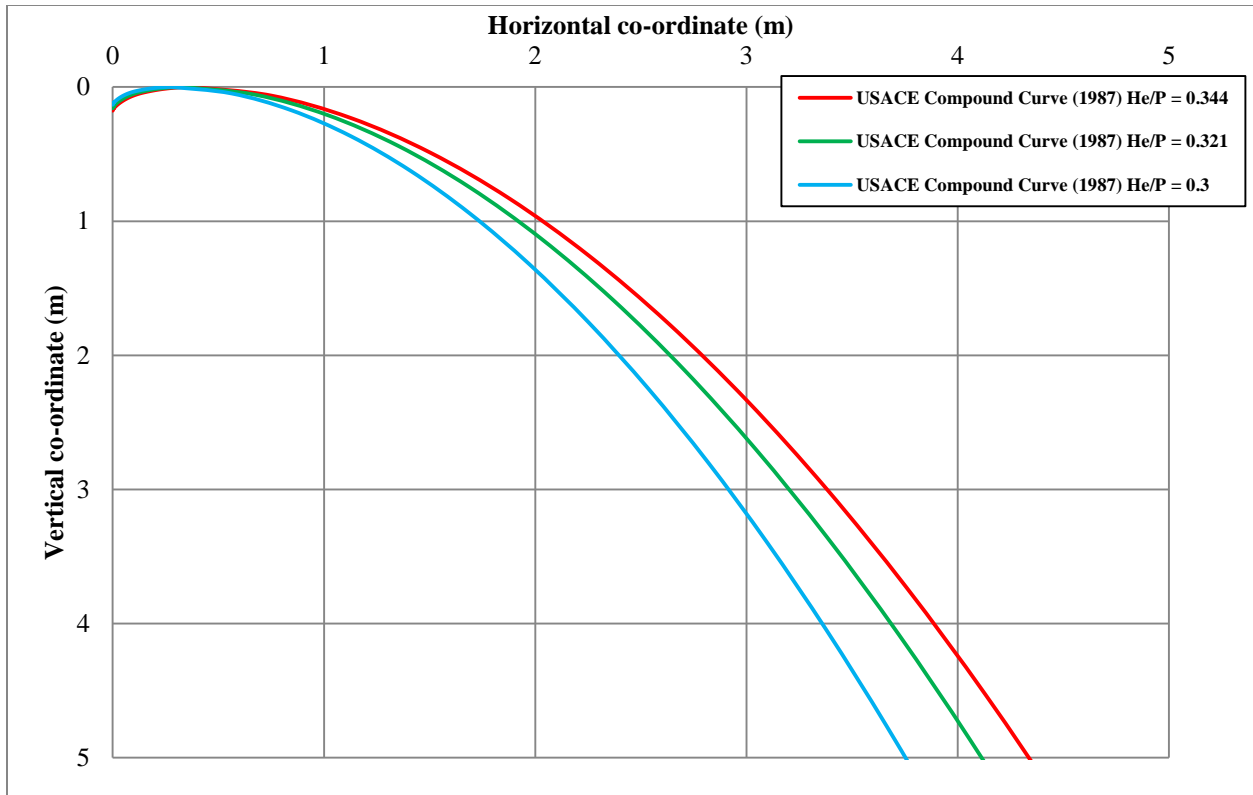


Figure 2-35: Hypothetical scenario where the Ogee curve is approximated by the USACE (a) (1987)

One factor that is closely related to the velocity distribution of the approach channel is the approach channel's depth. The USACE (1992) has indicated that the spillway approach configuration will influence the abutment contraction coefficient, the nappe profile, and possibly the flow characteristics throughout the spillway chute and stilling basin. Approach channels have been classified into three general configurations, each of which requires a different treatment at the abutments in order to provide for a satisfactory spillway design. Listed below are the three approach channels' classifications, as well as a short description of each:

1. *Deep Approach.* Firstly, there is the high spillway where approach velocities are negligible. The deep approach channel results in slow movement of the water, consequently the velocity head being negligibly small. This condition usually exists at a spillway in the main river channel flanked by concrete non-overflow sections. The P/H_d (pool depth also known as the approach channel depth relative to the design head, defined as the water depth measured above the spillway's crest height) ratio for a deep approach spillway is defined as being greater than 1,0.
2. *Shallow Approach.* Secondly, there is the broad but relatively shallow approach that results in strong lateral currents at the abutments. This condition is found at spillways in a river valley

flanked by embankment sections. The P/H_d ratio for the shallow approach spillway is defined as being equal to or less than 1,0. When a spillway includes adjacent embankment sections, and particularly where approach velocities are appreciable, the configuration of the abutments and adjoining topography, the depth of approach flow, and the angularity of approach flow all have a significant influence on abutment contraction coefficients and flow characteristics. The USACE (1992) indicated that rock dikes extending into the reservoir may be used to improve flow conditions at the abutments; however, optimum configurations are essential and can only be developed by means of a model study.

3. *Confined Approach.* The third configuration is attained when the spillway is distant from the main dam and an excavated approach channel is required. In this type of approach, velocities may be high and flow distribution may be unequal, but there will be no strong lateral currents at the abutments. When conditions require an excavated approach channel to the spillway, friction losses in the channel should be considered when determining the spillway capacity.

2.6.3 The orientation of approach velocity relative to the spillway structure

Also influencing the shape of the Ogee curve is the angle of the water flow velocity approaching the spillway. For 2-dimensional assessment of Ogee spillways, it is assumed that the angle of approach velocity is parallel to the centerline of the spillway i.e. perpendicular onto the spillway. However, this is not always the case with the design of dams as topographical limitations may restrict design engineers to construct spillways in this manner. This scenario, in which the orientation of flow onto the spillway is skew compared to a perpendicular orientation, is schematically shown in **Figure 2-36**. Although there is not significant literature available on the influence of the orientation of the approach channel, it can in many cases be included in the velocity distribution of the approach channel (USACE, 1992). The possible outcome of this effect is that the spillway's natural Ogee curve may not be uniformly constructed throughout the total length of the spillway structure, but will instead require different Ogee curves as water is making headway along the length of the spillway. These Ogee curves will be a function of the perpendicular velocity head component reaching the boundary of the spillway at the give position.

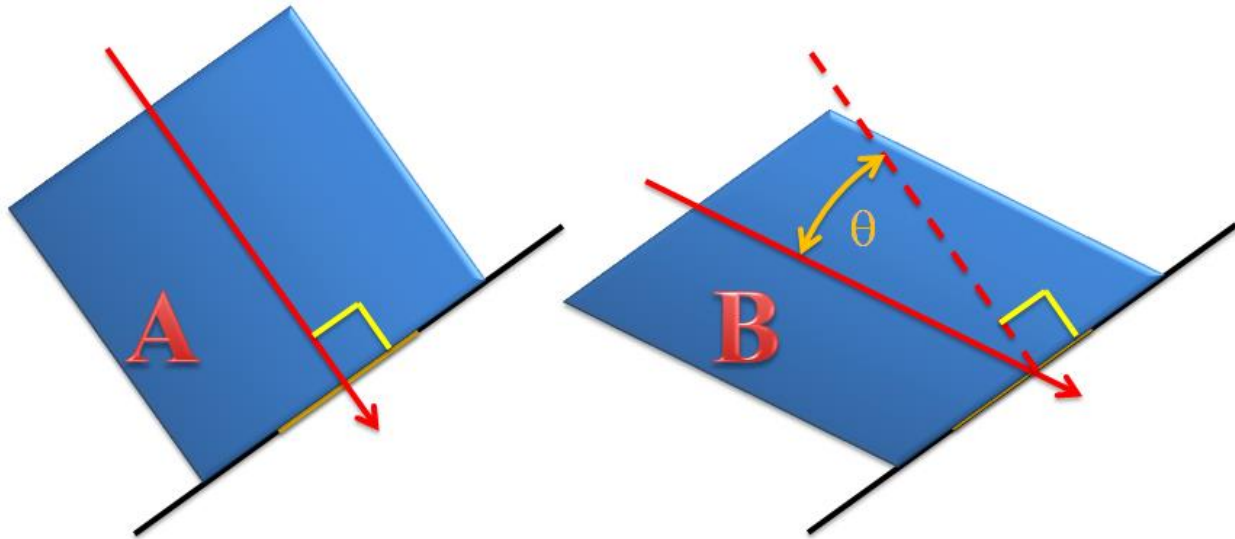






Figure 2-36: Angles of river approaching a spillway

Typical examples of South African Dams' approach channels are indicated in **Table 2-7**. **Table 2-7** is reflecting the visual differences between a so called “good” orientation where the flow lines intersect the spillway structure at a perpendicular angle enabling 2-dimensional flow parameters to be used to design a feasible spillway structure, compared with a skew orientation for the approach channel relative to the spillway structure, requiring 3-dimensional flow parameters or physical modelling for the design of a feasible spillway structure.

This aspect of relative orientation of the approach channel with regards to the spillway structure is mentioned for completeness of the dissertation, although it was not investigated during the physical modelling experiment.

Table 2-7: Examples of spillway orientation relative to the approach channel for selected South African Dams (images form Google Earth 6.2)

Perpendicular orientation of approach channel ("good")	Skew orientation of approach channel
<p style="text-align: center;">Jericho Dam</p> 	<p style="text-align: center;">Grootdraai Dam</p> 
<p style="text-align: center;">Gariiep Dam</p> 	<p style="text-align: center;">Morgenstond Dam</p> 

2.6.4 Effects of asymmetry of the upstream cross-section

Furthermore factors that are having an influence on the shape of the Ogee curve are the upstream cross-sectional shapes of the approach channels. This refers to the dimensions of the approach channel in the vicinity of the spillway structure. Features of the cross-section in the approach channel that could vary are the relative bank slopes of the approaching channel, and whether the banks are symmetrical in relation to each other or not. Also see the discussion on the Neckertal Dam in section 2.6.1 together with **Figure 2-32**. **Figure 2-37** indicates a schematic view of a typical approach channel's cross-section having a symmetrical (A) or asymmetrical (B) layout. The influence of the symmetry of the approach channel can in many cases be included in the velocity distribution of the approach channel (USACE, 1992). The possible outcome of this effect is that the spillway's natural Ogee curve may not be uniformly constructed

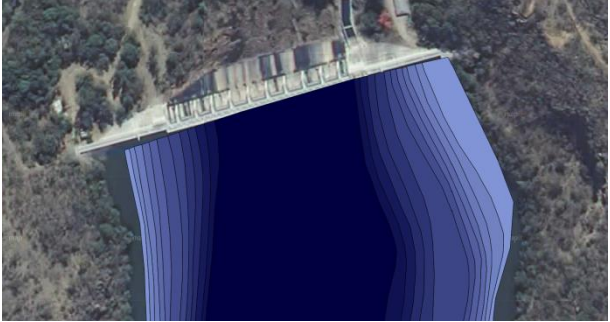
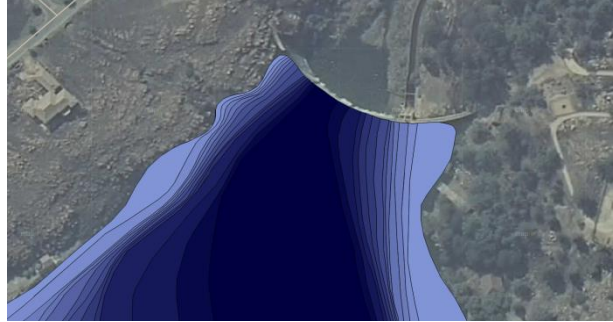
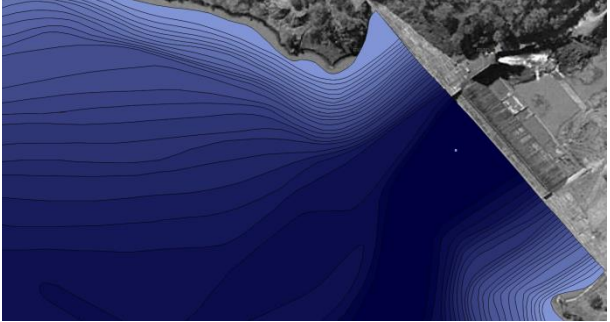
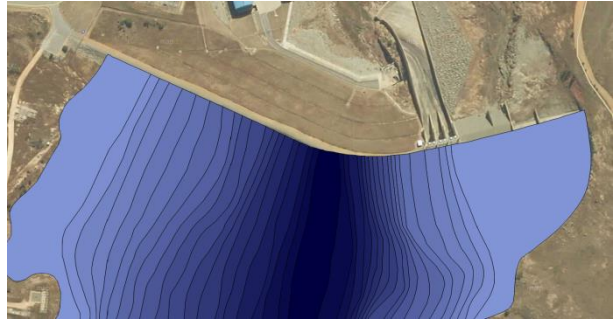
throughout the total length of the spillway structure, but will instead require different Ogee curves as progressing along the length of the spillway. These Ogee curves will be a function of the velocity magnitude at the specific location upstream of the spillway structure.



Figure 2-37: Symmetry of upstream cross-section in the approach channel

Typical examples of South African Dams' symmetry of the approach channel upstream of their spillways are indicated in **Table 2-8**. **Table 2-8** is reflecting the visual difference by means of contours between the so called symmetrical approach channels versus an asymmetrical approach channel. Notice that although the approach channel of the Morgenstond Dam is somewhat symmetrical, the spillway was constructed off-centre, which will result in asymmetrical flow over the hydraulic structure. Contours of selected South African dams are available online courtesy of Dam Contours (2010).

Table 2-8: Visual comparison of symmetrical approach channels versus asymmetrical approach channels for selected South African Dams (Dam Contours, 2010)

Symmetrical approach channel	Asymmetrical of approach channel
Doorndraai Dam 	Bronkhorstspruit Dam 
Spioenkop Dam 	Morgenstond Dam 

2.6.5 Effects of the radius of the wall

The curvature of the spillway structure influences the effective approach velocity's magnitude, breaking the velocity component into an effective perpendicular component for flow over the spillway structure. This results in the effective velocity over the spillway's crest to be the greatest at the center of the spillway, and to reduce towards the sides (**Figure 2-38**). An effective, perpendicular component for flow over the spillway structure implies that the unit flow rate at the mid position of the crest will be greater than that compared with the sides of the spillway. The influence of the curvature of the spillway also affects the spillway's natural Ogee curve and will result in the Ogee curve not being uniform throughout the total length of the spillway structure, but will instead require a larger Ogee curve at the spillway's mid position and reduce progressively towards the sides of the spillway. During high flow conditions, the lower nappe of the water flowing over the Ogee curve may cause cavitation of the spillway's surface if proper aeration of the water is not allowed.

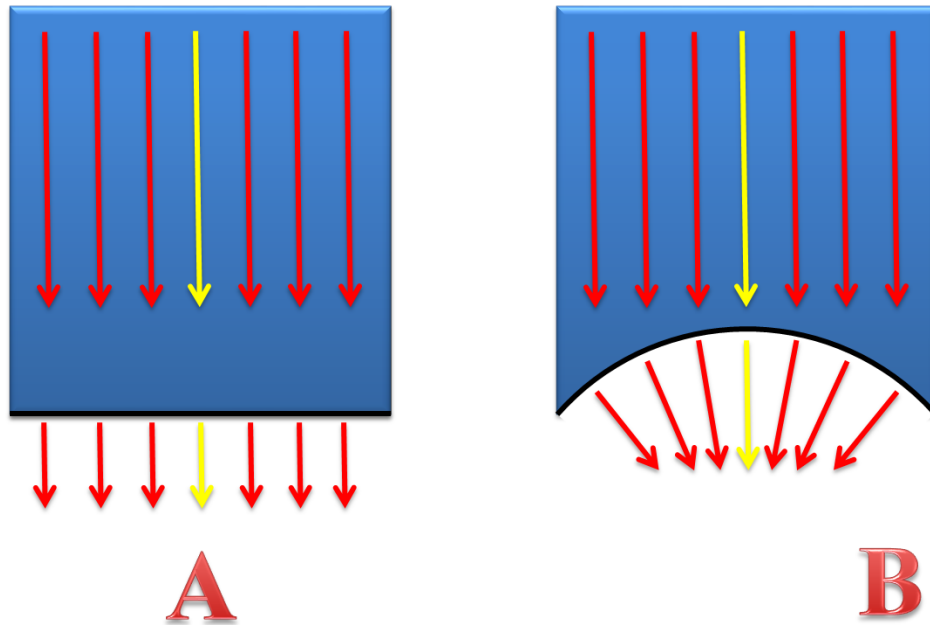


Figure 2-38: Velocity distribution of a straight spillway compared to a curved spillway

This phenomena of the influence of a curved Ogee spillway flowing can be appreciated in a photo (**Figure 2-39**), taken by Prof S.J. van Vuuren (University of Pretoria) of the Blyderiverpoort Dam, South Africa (2010). As indicated in the photo, it is clear that the trajectory of water flowing over the mid-position of the structure is greater than that of the water flowing at the sides of the structure, directly implying that the effective velocity must be greater in the center than that at the sides of the spillway.

This aspect of curvature of the spillway is mentioned for completeness of the dissertation, although it was not investigated during the physical modelling experiment.



Figure 2-39: Influence of curvature visible at the Blydepoortriver Dam indicating a larger trajectory of water flowing over the center of the spillway compared to the sides.

2.6.6 Comparison of opinions of 3-D effects

A great deal of the current literature pertaining to the issue of 3-dimensional and 2-dimensional flow deals with the reliability of numerical and physical modelling, particularly with regards to them being a viable means of analysing a hydraulic system. The use of numerical modelling in order to solve problems involving 3-dimensional flow is considered by many as a plausible solution if boundary conditions can be applied correctly. *Savage et al.* (2001), stated that there was a “good agreement between the physical and numerical models for both pressures and discharges”. The fact that the numerical modelling is similar to that of physical modelling shows that it is possible to be applied, as physical modelling is well regarded as a trustworthy means of testing a system, as noted by *Savage et al.* (2001) and supported by *Chatila & Tabbara* (2004). However, *Chatila & Tabbara* also noted that researchers have reduced the 3-dimensional flow effects to being sufficiently described by 1-dimensional (1-D) or 2-dimensional flow, indicating that the 3-dimensional shape of the Ogee curve may have been overlooked (*Chatila & Tabbara*, 2004).

According to Martinerie *et al.* (2005), who conducted physical model studies on a spillway experiencing non-uniform approach velocity, approach velocity has an effect on the uniformity of the flow downstream of the spillway. Although there are differences between the system analysed by Martinerie *et al.* (2005), and an Ogee curve, comparisons can be made and assumptions drawn that similar outcomes would occur on an Ogee curve when it experiences an approach velocity not parallel to the spillway centerline. In the 3-dimensional numerical and physical analyses undertaken by Olsen & Kjellesvig (2010) on a spillway indicated an encouraging correspondence between the two with regards to water surface and discharge coefficient, however the pressure distribution is only considered as a 2-dimensional problem.

Other physical model testing was undertaken by van Vuuren (2010), whose results provided strong evidence for the fact that the 3-dimensional flow parameters mentioned in this current study need to be considered when approximating the shape of the Ogee curve. The model study conducted actually focussed on the spillway section of the Neckartal Dam, and it was discovered that sub-atmospheric pressure regions were definitely present. This was unexpected, as it opposed the well-known relationship for the profile of the Ogee spillway. In addition, it was proposed that further research be conducted on this topic.

Taking into account that several of the aforementioned studies did not concentrate on the effect of specific 3-dimensional flow alterations on the pressures on the crest, and that physical modelling is necessary to supplement numerical analysis. It can therefore be concluded that further physical modelling research is needed into the effect that 3-dimensional flow has on the shape of the Ogee curve.

2.7 SEPARATION FROM SPILLWAY

Ogee spillways are designed for a specific design head at a given discharge. During the hydraulic structure's life span, the spillway will have to operate at heads lower than its design head but possibly also at heads higher than its design head. The former will result in pressures on the spillway's crest being higher than atmospheric pressure, together with a reduced discharge coefficient due to friction losses that need to be overcome by the flowing water. *Visa versa*, the latter behaves in exactly the opposite manner: namely sub-atmospheric pressure is experienced on the spillway together with an increase in the discharge coefficient (USACE, 1992). This is known as under-designing of an Ogee spillway, and may result in cavitation if the pressure on the spillway's crest is lowered to vapour pressure. From experimental investigations by Rouse and Reid it was found that the actual head (H) may exceed the design head (H_d) by up to 50% with a 10% increase in the discharge coefficient subjected that the local crest pressures do not fall below vapour pressure to prevent cavitation (Thandaveswara, 2006). Thandaveswara (2006) indicated that this pressure reduction is normally not a serious problem, unless the actual head exceeds the design head by a factor of 1.5. Separation of the water nappe flowing over the spillway will only occur once the actual head exceeds the design head by a factor of 3. The acceptable range is 1,5 to 3,0 for the design head. **Figure 2-40** is a graphical presentation of this design criteria when designing an Ogee spillway.

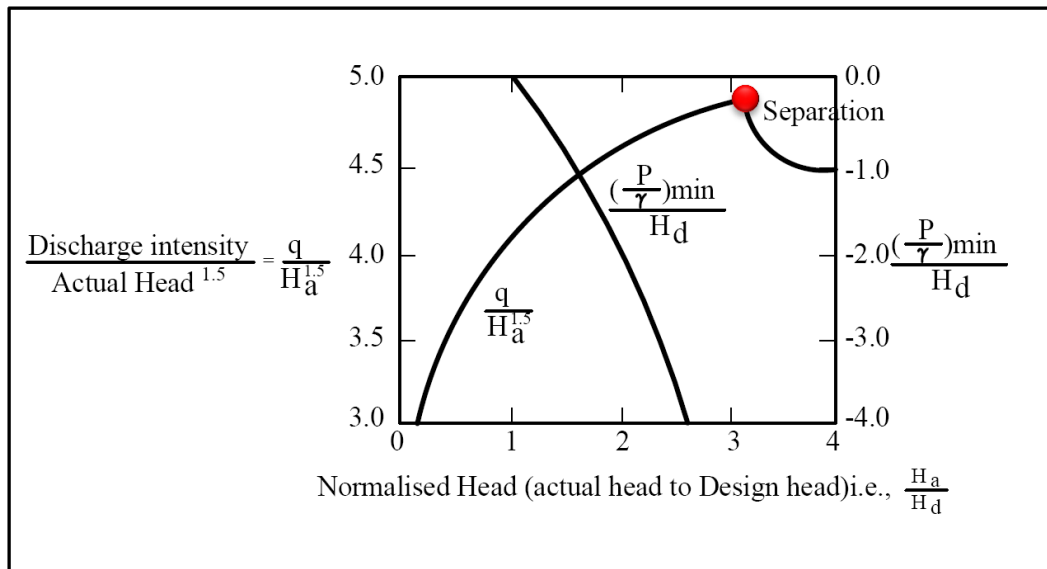


Figure 2-40: Nappe separation for spillway at heads exceeding 3 times the design head (Thandaveswara, 2006)

2.8 CREST PRESSURES (Melsheimer & Murphy, 1970)

According to the USACE (1992), the free discharge over a spillway crest will develop pressures on the concrete boundary that is inversely proportional to the ratio of Total Head (H_e) to the Design Head (H_d). When the ratio of H_e/H_d approaches unity, the pressures on the spillway crest are essentially atmospheric. With an increase in the ratio of H_e/H_d , the crest pressures tend to reach conditions that are lower than atmospheric pressure. These sub-atmospheric pressures are the reason for the increase in the discharge coefficient compared with that of a ventilated sharp-crested weir. The USACE (1992) suggests that reasonable approximations of the crest pressures are necessary in order to ensure a reliable design of a structural stable spillway structure. More importantly, crest pressure calculations will also provide for the hydraulic design guidance on the limiting pressures that the crest under designing yields prior to reaching pressures where cavitation damage may occur that could ultimately cause failure of the structure.

In 1965, Cassidy used potential flow theory and mapping into the complex potential plane to obtain the solution for the free surface and crest pressures on spillways and the results were in good agreement with experimental data (Thandaveswara, 2006). In a report published by the USACE (1992), Bauer and Beck (1969) and Abecasis (1970), indicated that minimum pressure fluctuation levels in relation to local atmospheric pressure is what leads to cavitation. It was indicated that cavitation on the crest would be incipient at an average pressure of about -7.62 m. However, it was the fluctuations and duration of the actual pressures at or near absolute, and not the average pressure on the crest boundary that caused cavitation damage on the spillway crest. The USACE (1992) recommend that a spillway crest should be designed so that the maximum expected head will result in an average pressure on the crest of not lower than -4.5 m of water at sea level measured at 4°C. Melsheimer & Murphy (1970) had done extensive research to evaluate the crest pressures on spillways. **Figure 2-41** depicts a relationship between the horizontal distance on the spillway relative to the design head of the crest to evaluate the corresponding crest pressure (USACE, 1992).

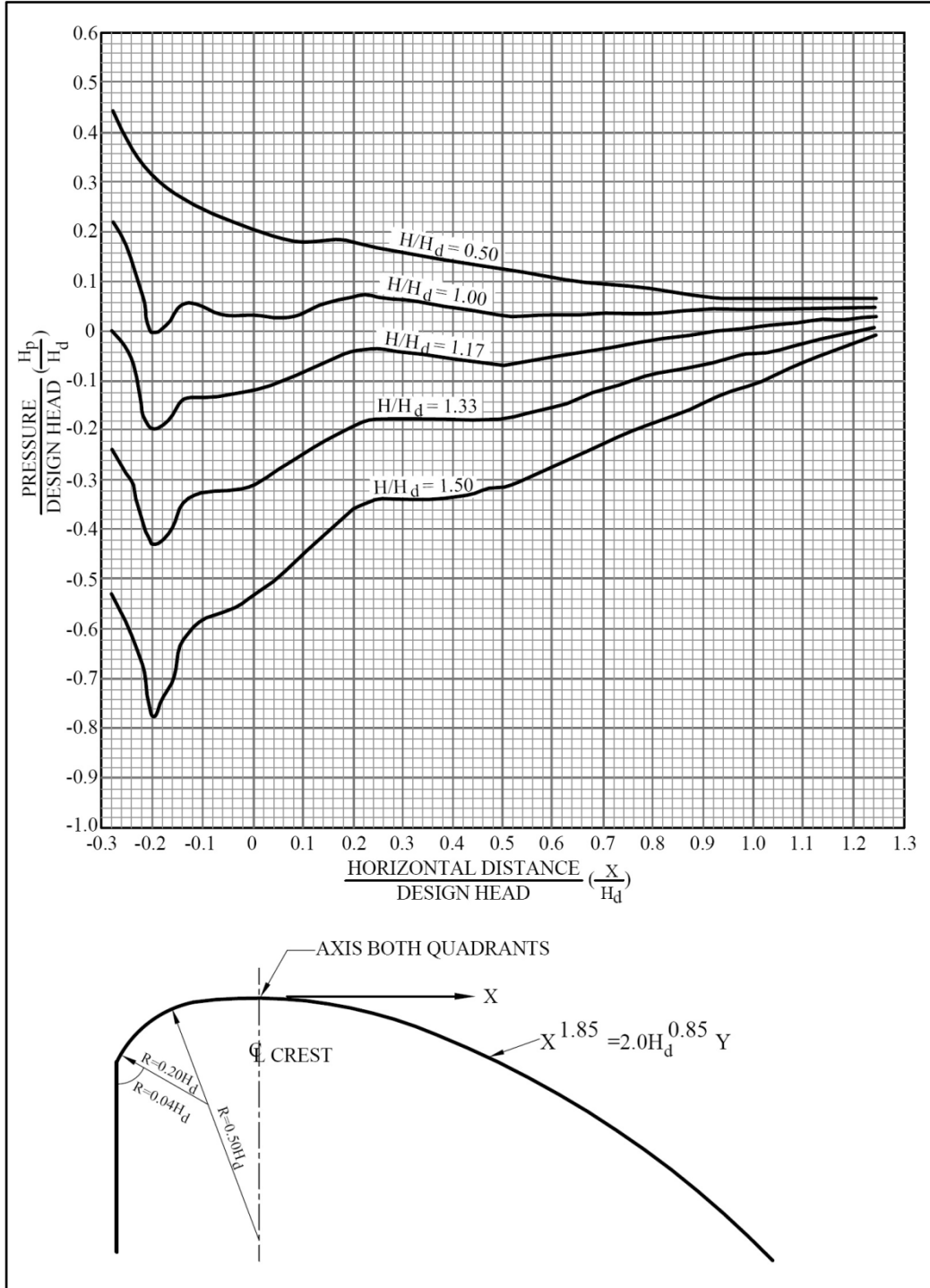


Figure 2-41: Crest pressures on Ogee spillways evaluated by Melsheimer & Murphy (1970)

2.9 CAVITATION

Cavitation is a microscopic phenomenon that is capable of producing destructive results on a significant scale. It is brought about when the pressure of water, at a specific temperature, lowers to the vapour pressure of the water at that specific temperature. This decrease in pressure causes unstable voids to form within the water particles. If pure H₂O is being dealt with then the water vapour would remain evenly distributed throughout the liquid and would be harmless in a dissolved state, however, all water in nature contains nuclei around which the water vapour will begin to accumulate. These can come in the form of impurities or even in the form of microscopic voids (Brennen, 1995). When these particles come to be in a region of higher pressure, they “implode violently”, possibly leading to what is known as cavitation erosion (Koivula, 2000). Fan *et al.* (n.d.) is in agreement with Koivula (2000) and stipulated that the exact cause of cavitation erosion is still unknown, however, the most likely two phenomenon of causing the damage is the creation of a shock wave (**Figure 2-42**), or high velocity micro-jets being emitted from a collapsed particle **Figure 2-43**.

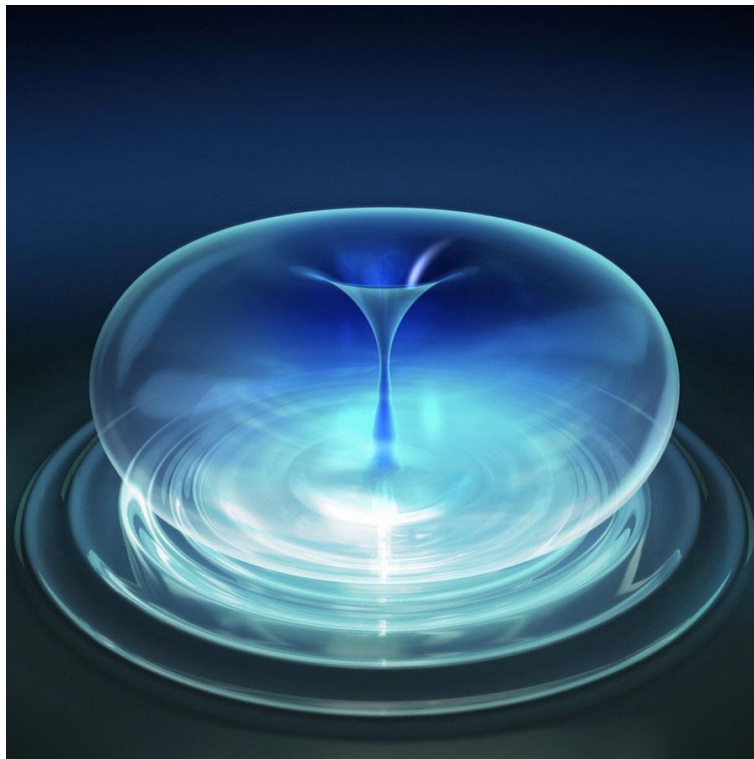


Figure 2-42: Shock-wave formation during collapse of an air void particle

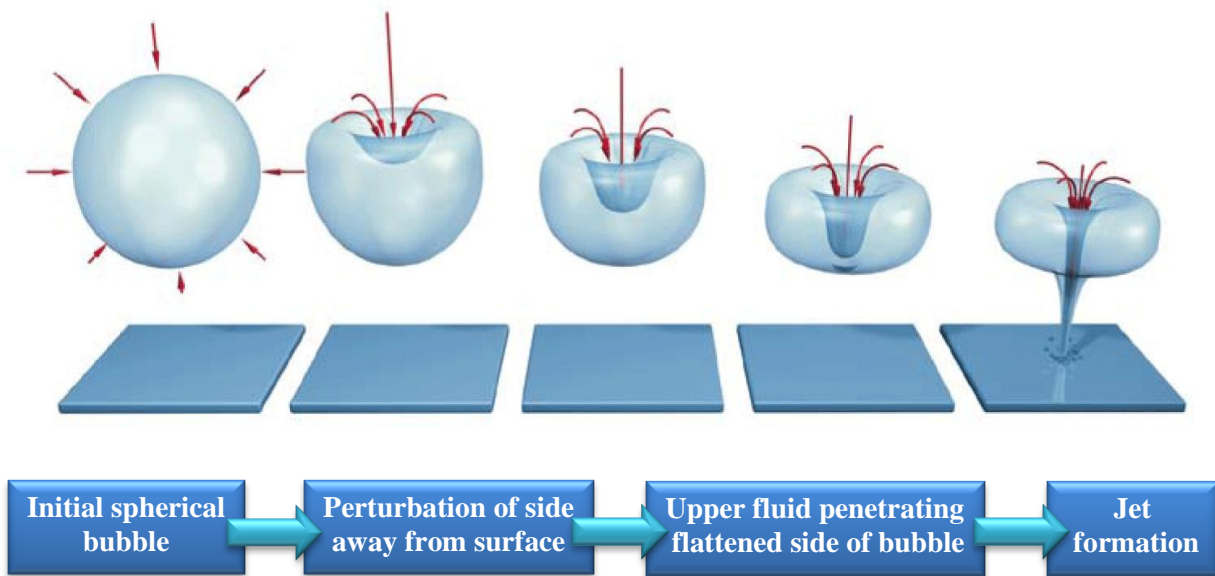


Figure 2-43: Micro-jet collapse edited from Knapp *et al.* (1970)

Cavitation occurs on hydraulic structures due to the fact that surface roughness's of a spillway causes separation of the boundary layer from the surface of the spillway, thereby forming a lower pressure region immediately downstream of the roughness. This fact was confirmed by the USBR (1987), Asawa (2008) and Vischer & Hager (1999), who stated that abrupt offsets, depressions, or projections will amplify the sub-atmospheric pressures to a magnitude where cavitation conditions can develop. Asawa (2008) continued that if the pressure in the wake region of the abrupt offset falls to the vapour pressure of water, vapour bubbles are formed and are carried downstream. When these bubbles reach a high pressure region, they suddenly collapse giving rise to extremely localized high pressures. This is particularly relevant to the shape of spillways, as high velocities are attained and cavitation risk is likely to occur. An example of an extreme incident is shown in **Figure 2-44** where cavitation have resulted in an 11 m deep hole caused by releasing water from the Glen Canyon Dam (Falvey, 1990).



Figure 2-44: Damage in a spillway tunnel at Glen Canyon Dam as a result of cavitation (Morris, 2012)

Asawa (2008) indicated that cavitation-resistant materials can be used to minimize the effect of cavitation; however, more effectively would be the adoption of specification surface finishing criteria that limits surface roughness on spillways. More recently, new methods have been developed to protect spillway surfaces that are known as aeration devices. This method is based on the fact that the presence of air bubbles prevents the formation of cavitation (Vischer & Hager, 1999).

For high-speed flow, as occurring on spillways, security concepts against cavitation damage have significant relevance. Kramer (2009) indicated that should the bottom air concentration in the lower nappe of flow over the spillway decreases to the order of between 6 to 10%, cavitation may cause large scale damage of concrete due to a process known as fracturing, as is illustrated in **Figure 2-46** for the Karun dam in Iran. Given that a spillway is a major safety element for a dam, its loss may cause major

structural instability, and ultimately result in major inundations in the downstream valley should the structure fail. It is therefore imperative to aerate spillways adequately to prevent any uncontrolled flow conditions of flow (Kramer, 2009). Hence, the present-day design of spillways with high velocities envisages the provision of aeration devices, also known as spillway aerators across the spillway face. Three basic types of aerators are: grooves, deflector, and offsets. These aerators may also be used in combination of one other. Examples of aeration devices are given in **Figure 2-45** (Asawa, 2008).

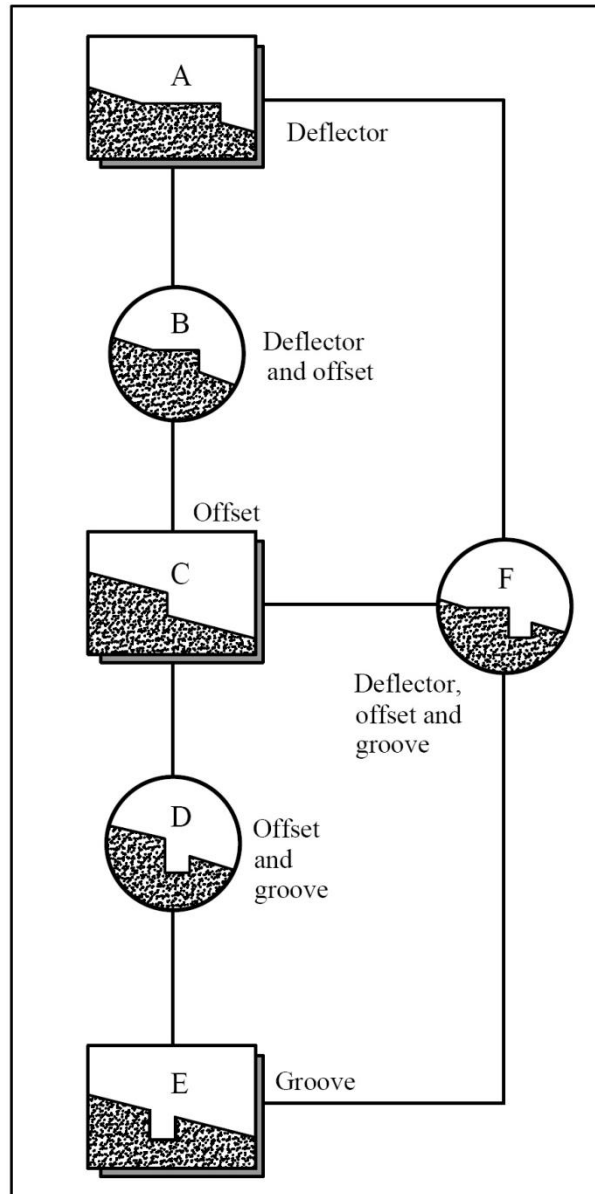


Figure 2-45: Examples of basic aeration devices as given by Asawa (2008)

Aerators are relatively cheap to include in the design of spillways, especially when considering the financial implications of restoration that is required for spillways should cavitation have occurred. Aerators produce a local pressure drop which causes the flow to suck in air. The compressibility of the air-water mixture reduces the collapsing pressure of vapour bubbles and thus protects the concrete surface from cavitation erosion.



Figure 2-46: Cavitation damage on the Karun dam, Iran (Kramer, 2009)

An extract from the 2011/2012 Dam Safety Office Report of South Africa (**Figure 2-47**) indicates that 80 cases of cavitation damage to spillways has been reported in 2011/2012 financial year, further emphasizing the need for an effective and more efficient design of dam spillways (DWA, 2012). This was also the case for the Dam Safety Office Reports of South Africa from 2009/2010 to 2010/2011 with cavitation deficiencies being identified at South African Dams averaging at 80 incidences annually (DWA, 2010; DWA, 2011).

APPENDIX B: DEFICIENCIES AT DAMS WITH A SAFETY RISK					
Code	Description	Previous year		This Year	
		Number	Rectified	Number	Rectified
H01	Spillway capacity less than requirements of current criteria	442	86	456	94
H02	Erosion of toe of dam or downstream thereof	46	8	46	8
H03	Damage to spillway lining (e.g. erosion or cavitation)	81	22	80	22
H04	Damage to outlet works (e.g. cavitation)	16	4	15	4

Figure 2-47: Extract form the 2011/2012 Dam Safety Office Report of South Africa indicate the 80 cases of cavitation damage to spillways (DWA, 2012)

2.9.1 CAVITATION INDEX

The possibility of cavitation to occur in the outlet conduit can be determined by calculating the cavitation index at all the positions where pressure losses are likely to occur. It is most likely for cavitation to occur at positions where secondary pressure losses occur because of the disruption in the surface boundary at that specific position. According to Vischer & Hager (1999) the cavitation index is defined by **Equation 2-38**, where cavitation is expected to occur if the cavitation index is less than 1.8. Joseph (1997) and Brennen (1995) stipulates that there are many factors influencing the possibility for cavitation to occur. These factors include: the fluid temperature and degree of oxygen saturation of the fluid. Factors previously mentioned have a great influence especially in the design of an outlet structure, as stratification of water layers in the reservoir is to be expected, thus reducing the oxygen content in the lower levels of the reservoir where the fluid's density is increased due to its lower temperature. Joseph (1997) suggests that the cavitation index should be calculated by **Equation 2-39** where values exceeding 2 are free from cavitation.

$$\sigma = \frac{P - P_o}{\frac{\rho V_o^2}{2}}$$

Equation 2-38

$$\sigma = \frac{P_2 - P_v}{P_1 - P_2}$$

Equation 2-39

Where

σ	-	cavitation index
P	-	local pressure (m)
P_o	-	reference pressure (m)
ρ	-	fluid's density (kg/m^3)
V_o	-	reference velocity (m/s)
P_1	-	inlet pressure (m)
P_2	-	outlet pressure (m)
P_v	-	vapour pressure at specific temperature (m)

The vapour pressure of water can be calculated by making use of the following **Equation 2-40**. **Equation 2-40** is schematically presented in **Figure 2-48**.

$$P=e^{20.386 - \frac{5132}{T}}$$

Equation 2-40

Where

P	=	vapour pressure of water (mmHg)
T	=	temperature (Kelvin)

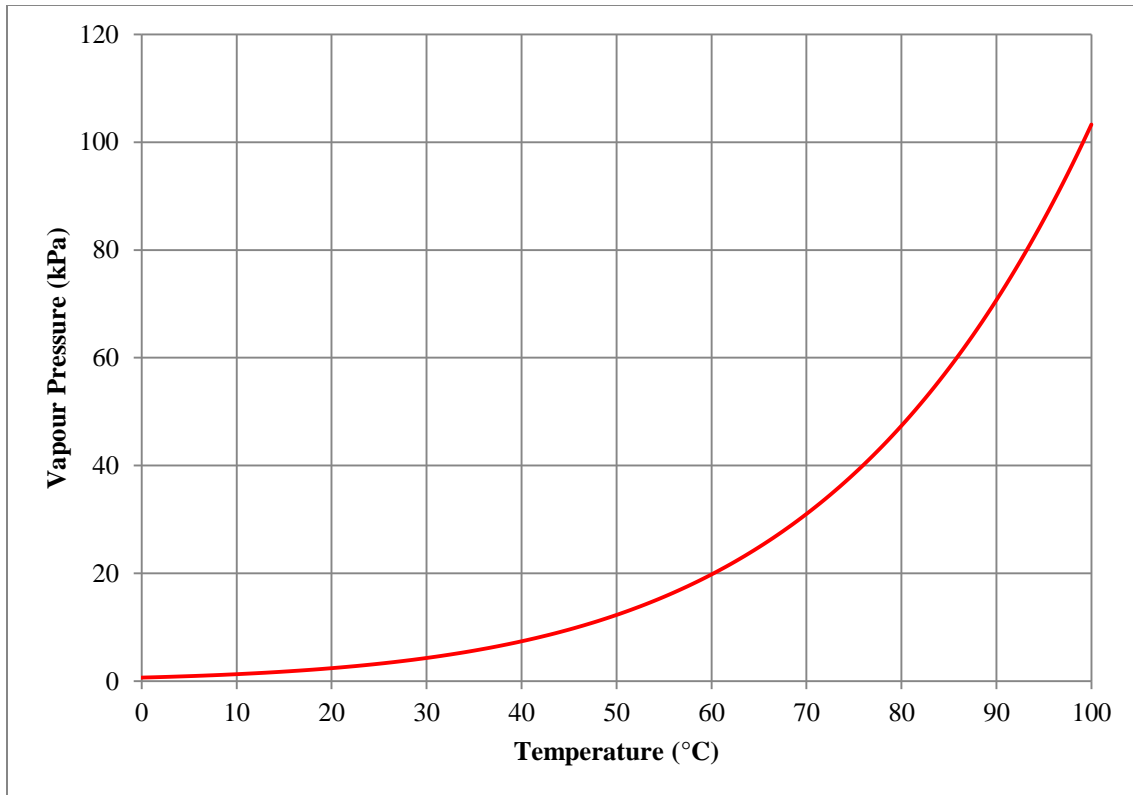


Figure 2-48: Vapour pressure as a function of temperature

2.10 INTERNATIONAL DESIGN STANDARDS OF SHARP-CRESTED WEIRS

Sharp-crested weirs are commonly used where highly accurate discharge measurements are needed to determine the discharge in hydraulic laboratories, industrial applications and irrigation systems (Bagheri & Heidarpour, 2010). The lower nappe of water flowing over a sharp-crested weir was used to derive the geometric profile of an Ogee curve as was discussed in section 2.3.

Some of the most common advantages and disadvantages in using a weir as a discharge measuring device are listed below (Merkley, 1995):

Advantages:

- Weirs can accurately measure a wide range of flows. ASTM International (2001) indicated that sharp-crested weirs can be utilized in accurately measuring the discharge varying between $0,00023 \text{ m}^3/\text{s}$ and $1,4 \text{ m}^3/\text{s}$;
- Merkley (1995), suggests that weirs can provide more accurate discharge measurements than flumes and orifices;
- Weirs are simple and easy to construct;
- Weirs can be used in combination with turnout and division hydraulic structures;
- Weirs can be designed so that it can be adjustable and calibrated infield.

Disadvantages:

- Weirs can require a relatively large head as difficulty lies in the fact that very low heads are difficult to measure accurately, particularly for free flow conditions. For this reason weirs are disqualified for the practical use of flow measurement in flat areas (Merkley, 1995).
- The upstream pool must be maintained clean of sediment and kept free of debris and weeds, otherwise the calibration will shift and the measurement accuracy will be compromised

Sharp-crested weirs are applied throughout industry and relied upon for the accurate measurement of a fluid's discharge. For this reason international design standards are available to ensure that a standard of conformance is achieved throughout the world. In order to ensure that this conformance is achieved, specific critical design parameters must be met when making use of a sharp-crested weir (ASTM International, 2001; ISO 1438, 2008).

For the design of a fully contracted weir (nappe unaffected by boundary conditions) the geometric parameters of the channel and head must fall within the limits as depicted below (**Figure 2-49**), otherwise the weir is known as a partially contracted weir:

- $h/p \leq 0.5$
- $h/b \leq 0.5$
- $0.08 \text{ m} \leq h \leq 0.6 \text{ m}$
- $b \geq 0.3 \text{ m}$

- $p \geq 0.3 \text{ m}$
- $(B - b)/2 \geq 2h$

Where:

- h - measured head (m)
P - crest height above the bottom of the channel (m)
b - crest length (m)
B - channel width (m)

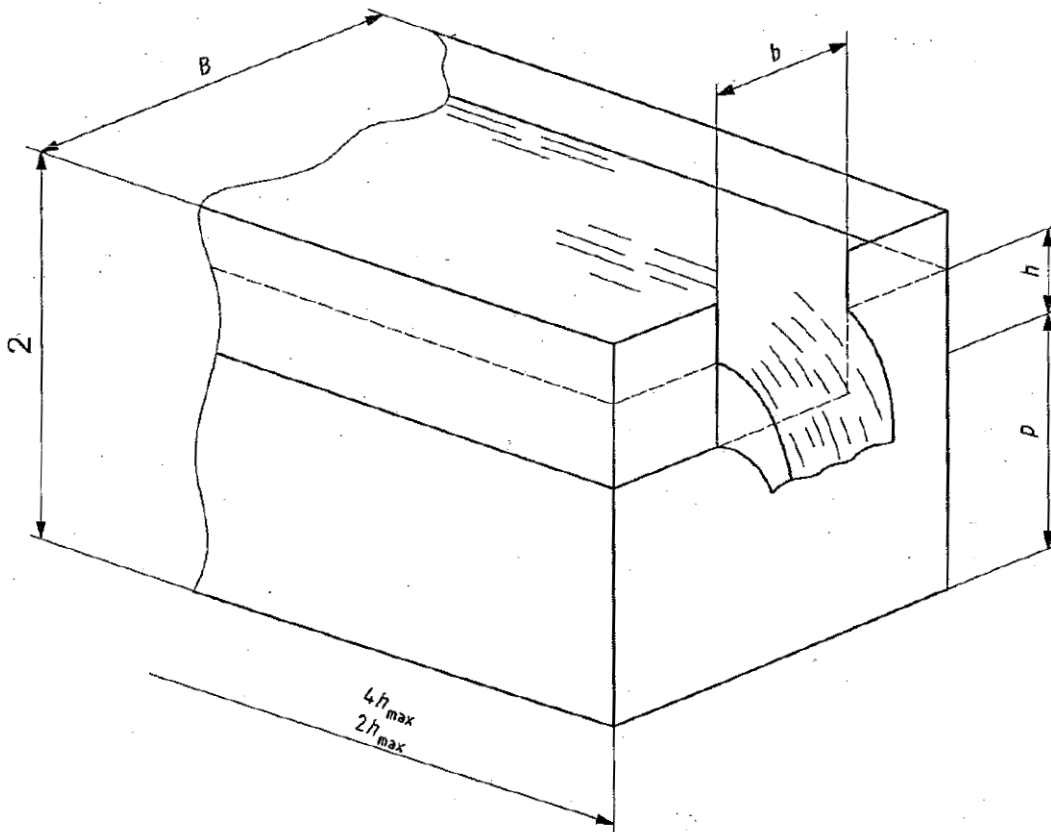


Figure 2-49: Approach channel requirements for designing a fully contracted sharp-crested weir (ISO 1438, 2008)

ISO 1438 (2008), recommends that for an experimental setup the channel length should be equal to 10 times the width of the nappe at the maximum head. The flow in the approach channel should be uniform, with a velocity distribution that can develop satisfactory flow with smooth and straight flow lines. Baffles and flow straighteners can be placed in the approach channel in order to achieve this requirement.

The head on the weir is known as the measured depth above the elevation of the crest of the weir. This measurement should be made at a distance upstream of the weir between $4H_{\max}$ to $5H_{\max}$, where H_{\max} is the maximum head expected on the weir. Both ASTM International (2001) and ISO 1438 (2008) suggests that a stilling well connected to the approach channel by means of a piezometer may be used for the accurate measurement of the head on the weir.

The plate thickness in the direction of flow of a sharp-crested weir must be between 1 to 2 mm. It is required that the plate be manufacture of smooth metal. The upstream edge of the overflow section must be sharp and burr-free, and the edges must be flat, smooth, and perpendicular to the weir face (**Figure 2-50**). The plane of the weir plate must be vertical and perpendicular to the channel walls. The overflow section must be laterally symmetrical and its bisector must be vertical and located at the lateral mid-point of the approach channel (ASTM International, 2001).

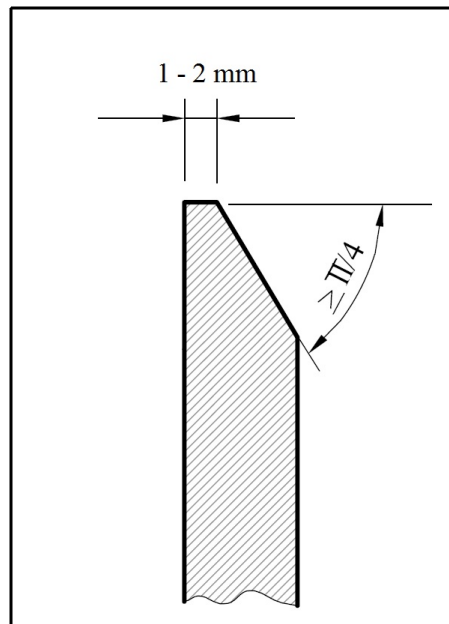


Figure 2-50: Plate requirements for a sharp-crested weir (ASTM International, 2001; ISO 1438, 2008)

To prevent the lower nappe of the water flowing over the weir from clinging onto the weir or oscillating, proper aeration of the nappe is required (Vischer & Hager, 1999). Should the lower nappe not be adequately ventilated, then sub-atmospheric pressure may occur on the lower side of the nappe. This is most common at un-contracted weirs were the water clings to the side walls creating an air tight seal of

the area below the lower nappe. Aeration in fully contracted weirs can be achieved by averting the tailwater level to rise above 0.06 m below the crest of the weir.

The discharge over the weir can be approximated by making use of the Kindsvater-Cater equation. The equation was derived from the conservation of energy by considering the Bernoulli equation. In its basic form the Kindsvater-Cater formula can be expressed by **Equation 2-41**:

$$Q = \frac{2}{3} C_d b_e \sqrt{2g} h_e^{\frac{3}{2}}$$

Equation 2-41

Where:

- C_d - the discharge coefficient
- g - gravitational acceleration (m/s²)
- b_e - effective weir width (m)
- h_e - effective head above the crest of the weir

The effective weir width and effective head above the weir can be calculated from **Equation 2-42** and **Equation 2-43** respectively. k_L can be determined by **Figure 2-51** for different ratios of b/B , whereas k_h is recommended to be taken as a constant 0,001 m by ISO 1438 (2008).

$$b_e = b + k_L$$

Equation 2-42

$$h_e = h + k_h$$

Equation 2-43

Kindsvater-Cater have determined the discharge coefficient for different ratios of h/p and are depicted in **Figure 2-52**.

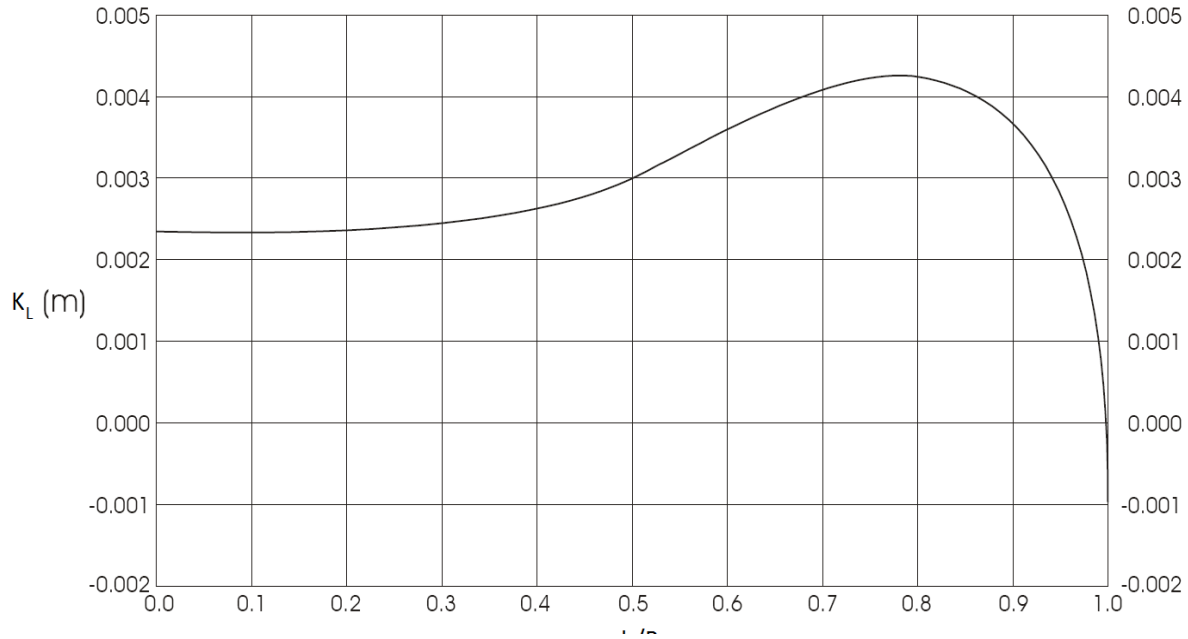


Figure 2-51: Estimation of effective weir widths for ratios of b/B (ISO 1438, 2008)

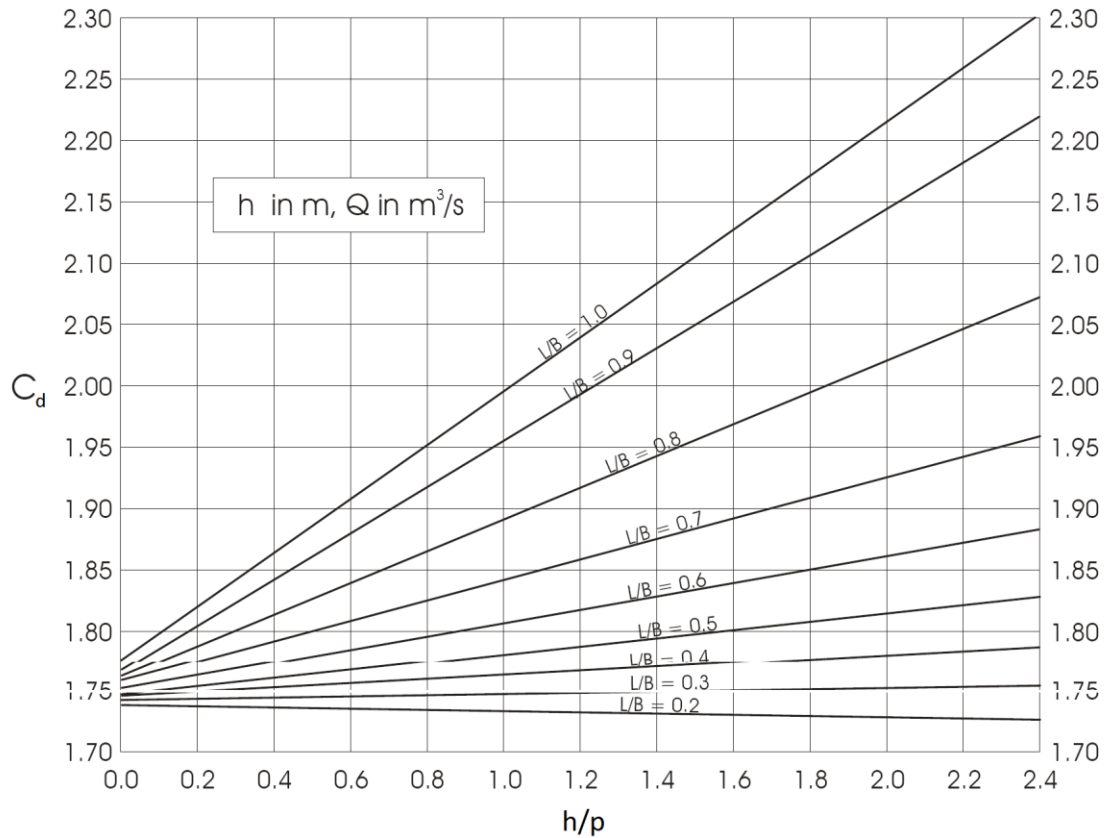


Figure 2-52: Estimation of discharge coefficient for ratios of h/p (ISO 1438, 2008)

2.10.1 MORE DISCHARGE COEFFICIENTS OF SHARP-CRESTED WEIRS

Since both the sharp-crested weir is such a highly studied hydraulic structure, it is no surprise that considerable research has gone into the determination of its discharge coefficient. The discharge coefficient is a number that ties the theoretical ideal flow conditions to the actual flow conditions by means of a single factor that has to consider for the 3-dimensional flow parameters in the approach channel. Due to the empirical nature of the coefficient and the complexity of the system, that is the flow transitions from sub-critical to super-critical, the effects of viscosity, weir contraction, 3-dimensional flow conditions and surface tension, a single solution is in most cases not possible. Discharge over a sharp-crested weir may in controlled conditions be accurately predicted within 1.5% of the actual flow rate. However, it is difficult to achieve this accuracy levels in full scale weirs constructed in rivers (Aydin, *et al.*, 2011). Reflected in **Table 2-9** and **Table 2-10** is the discharge coefficient form various researchers both for contracted and un-contracted sharp-crested weirs.

Table 2-9: Discharge coefficient for un-contracted (full width) weirs (Bagheri & Heidarpour, 2010; ISO 1438, 2008)

Reference	Discharge Coefficient (C_d)	Valid Range
Rehbock (1929)	$0.602 + 0.083 \frac{h_{1e}}{p}$ $h_{1e} = h_1 + 0.0012$	$\frac{h_1}{p} < 4$ $0.03\text{m} < h_1 < 1\text{m}$ $b > 0.3\text{m}$ $p > 0.06\text{m}$
Rouse (1936)	$1.06 \left(1 + \frac{p}{h} \right)^{1.5}$	$\frac{h}{p} \geq 15$

Table 2-10: Discharge coefficient for contracted weirs

Reference	Discharge Coefficient (C _d)	Valid Range
Swamee, 1988 in Bagheri & Heidarpour (2010)	$1.06 \left[\left(\frac{14.14p}{8.15p+h} \right)^{10} + \left(\frac{h}{h+p} \right) \right]^{-0.1}$	Full range
Aydin, <i>et al.</i> (2011)	$0.562 + \frac{10 \left[1 - e^{-\left(\frac{2h}{b} \right)^2} \right]^{-1}}{Re^{0.45}}$	Slit Weir
Bagheri & Heidarpour (2010)	$0.79 \ln \left[2.206 + 0.242 \frac{h}{p} \cdot \left(\frac{B}{b} \right)^{0.0615} \right]$	$0.15 < \frac{h_1}{p} < 1$

2.11 CALIBRATION OF SHARP-CRESTED WEIR

The calibration of flow measuring structures (i.e. weirs) still remains a problem in the design and operation of any hydraulic structure today. Described in this section of the dissertation is the calibration method based on the *Principle of the Pondage Drawdown Method* as describe by Johnson & Green (1977). This method allows the design engineer to calibrate a hydraulic structure for flows greater than that which are available at the time of calibration by means of blocking the outlet of the weir and to raise the water level higher than the design head.

Analysing the drawdown curve produced when the blockage is removed, it is possible to calculate values of outflow for successive head values. The concept is based on the principle that the storage at any time is the difference between the inflow and outflow, which in turn is equal to the rate of change of storage volume **Equation 2-44**.

$$(Q_i - Q_o)_h = A_h \left(\frac{dh}{dt} \right)_h$$

Equation 2-44

Where:

- Q_i - inflow (m³/s)
- Q_o - outflow (m³/s)
- A - plan area of channel at corresponding head (m²)
- h - head value (m)
- dh/dt - is the slope of the drawdown curve at a head h (m/s)

Equation 2-44 can be used for variable inflows and variable plan area, provided that the depth to area relationship is known. Should it be possible to stop the inflow during the calibration process the equation can be further simplified as for a channel with a constant plan area as given in **Equation 2-45**.

$$(Q_o)_h = -A \left(\frac{dh}{dt} \right)_h$$

Equation 2-45

Johnson & Green (1977) described five possible methods for calibrating sharp-crested weirs. These methods are graphically shown in **Figure 2-53** together with the conditions required and the range of calibration head for each method summarized in **Table 2-11**.

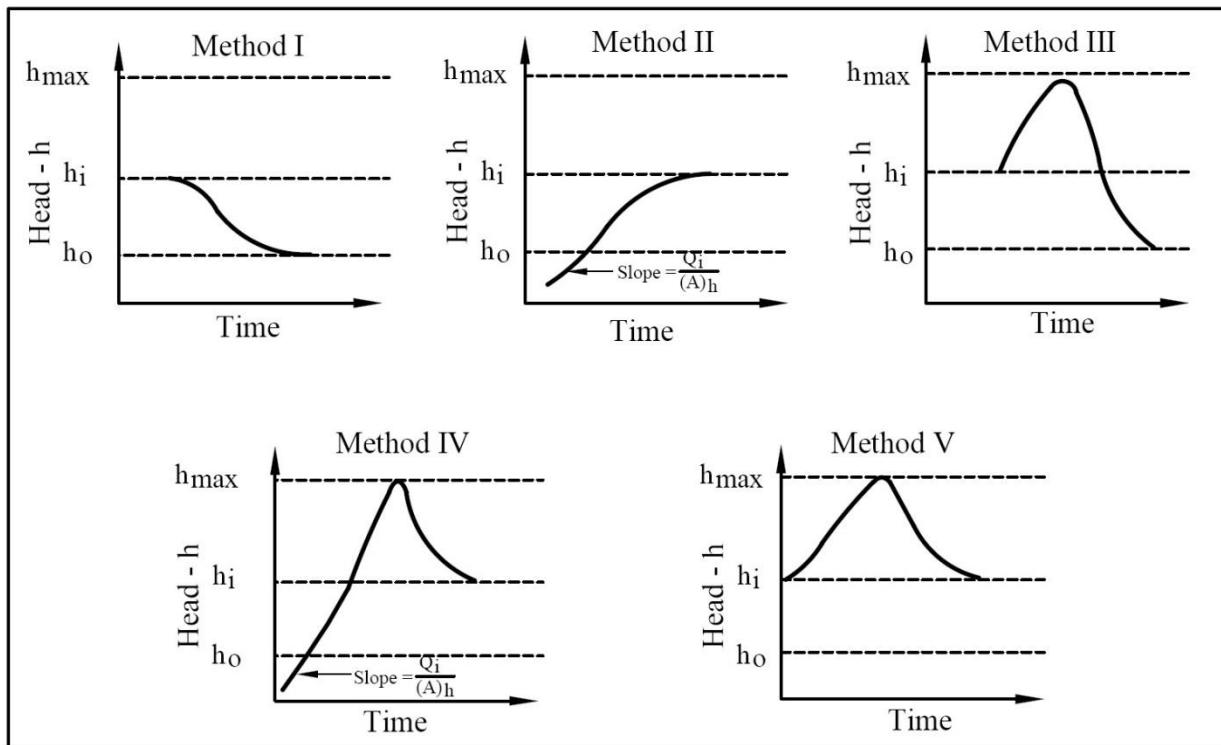


Figure 2-53: Calibration methods for sharp-crested weirs by Johnson & Green (1977)

Table 2-11: Conditions required and range of calibration head for different calibration methods by Johnson & Green (1977)

Method	Condition	Calibration Range	Calibration
I	1. Stop inflow	$h_i \rightarrow h_o$	$(Q_o)_h = -A \left(\frac{dh}{dt} \right)_h$
II	1. Stop inflow 2. Drain pond below h_o 3. Start inflow	$h_o \rightarrow h_i$	$(Q_o)_h = Q_i - A \left(\frac{dh}{dt} \right)_h$
III	1. Block structure increase h_i to h_{max} 2. Stop inflow 3. Remove blockage	$h_{max} \rightarrow h_o$	$(Q_o)_h = -A \left(\frac{dh}{dt} \right)_h$
IV	1. Stop inflow 2. Drain pond below h_o 3. Block structure 4. Start inflow, increase head to h_{max} 5. Remove blockage	$h_{max} \rightarrow h_i$	$(Q_o)_h = Q_i - A \left(\frac{dh}{dt} \right)_h$
V	1. Block structure, increase head h_i to h_{max} 2. Remove blockage	$h_{max} \rightarrow h_i$	$(Q_o)_h = Q_i - A \left(\frac{dh}{dt} \right)_h$

In order to solve any of the equations given in **Table 2-11** it is necessary to determine the rate of change of the depth of water with time at specific head values, i.e: the slope of the drawdown curve. Johnson & Green (1977) indicated that this could be best achieved by fitting a polynomial to the drawdown curve and differentiating the function to obtain values for dh/dt .

2.12 CASE STUDIES

In the *Compendium of Case Histories on Repair of Erosion-Damaged Concrete in Hydraulic Structures* by Tatro, *et al.* (1994), a series of case studies on hydraulic structures that have been damaged by erosion from various physical, mechanical and chemical actions have been summarized. These case histories cover the damage being caused to the hydraulic surfaces due to the action of water, waterborne material or chemical attack of concrete from fluids conveyed along the hydraulic passages.

In **Table 2-12** is an extract of spillways that has been damaged due to cavitation, where the highlighted rows refers specifically to Ogee spillways that have been damaged due to this phenomenon. The reader is referred to the report by Tatro, *et al.* (1994) included in the appendix of this dissertation for more detail on each case study.

Table 2-12: Spillways that has damaged due to cavitation damage (Tatro, et al., 1994)

Project name	Year completed	Type	Location	Owner	Problem	Repair type
Lucky Peak Dam	1956	Outlet structure	Idaho	Corps of Engineers	Cavitation	various
Terzaghi Dam	1960	Outlet structure	British Columbia	B.C. Hydro Authority	Cavitation	Hydraulic redesign
Glen Canyon Dam	1964	Arch dam	Arizona	Bureau of Reclamation	Cavitation	Aeration
Yellowtail Afterbay Dam	1966	Stilling basin	Montana	Bureau of Reclamation	Cavitation	Various overlays
Yellowtail Dam	1966	Stilling basin	Montana	Bureau of Reclamation	Cavitation	Aeration and overlays
Keenleyside Dam	1968	Outlet structure	British Columbia	B.C. Hydro	Cavitation	High-strength concrete
Red Rock Dam	1969	Stilling basin	Iowa	Corps of Engineers	Abrasion	Underwater concrete
Lower Dam Monumental	1969	Navigation lock	Washington	Corps of Engineers	Cavitation	Epoxy
Dworshak Dam	1974	Gravity dam	Idaho	Corps of Engineers	Cavitation	Polymer impregnation

Cavitation damage at the Keenleyside Dam sluiceway crest near the gate slots has occurred on all four bays of the sluices. The damage on the spillway had extended from inside the upstream portion of the gate slot over a distance of 1.2m downstream, extending at an angle of 30° to the direction of flow.

Depicted in **Figure 2-54** is an overview of the damage being caused by cavitation on the sluiceway crest of Keenleyside Dam.



Figure 2-54: Keenleyside Dam cavitation damage on the sluiceway crest near the gate slots (Tatro, et al., 1994)

2.13 SCALED MODELS

“When dealing with water, first experiment then use judgement”

Leonardo da Vinci

Da Vinci was one of the first researchers who described and sketched several flow profiles of free jets and velocity patterns for the flow of water by making use of visual observations of scaled experimental setups (Hughes, 1993). Chanson (2004), has defined a physical model as a scaled representation of a hydraulic flow situation where both the boundary conditions of the system are included and scaled in an appropriate manner.

Physical hydraulic models may be used during the feasibility study of a project, during the design stages of a project to optimize a structure and also to ensure safe operation of the structure under all flow conditions or to rectify intriguing 3-dimensional hydraulic flow conditions that may be problematic in an existing system. Scaled models can also help to assist non-engineering people during the 'decision-making' process of a hydraulic project. This may help the decision-makers to visualize the flow that will occur in the system, before deciding on the final design criteria. In hydraulic applications, a physical hydraulic model is usually a smaller-sized representation of the prototype and the model is investigated in a laboratory under controlled conditions (Chanson, 2004).

Some of the basic scale ratios that should be considered when making use of physical modelling of a hydraulic structure are the geometric, kinematic and dynamic similarities. These similarities refer to the prototype characteristic length versus that of the model, the prototype velocity versus that of the model and the forces exerted or generated in the prototype versus that of the model's.

Chanson (2004) indicated that for free surface flow the gravitational effects are important and should be considered. This implies that the Froude number will always be the predominant factor to consider when designing a free surface flow physical model and secondary scale ratios should thus be derived from the constancy of the Froude number. These scale ratios was describe by Henderson (1966) as the discharge, force and pressure and, can be calculated by **Equation 2-46** to **Equation 2-48** respectively (Chanson, 2004, Hughes, 1993 and Henderson, 1966).

$$Q_r = V_r L_r = L_r^{\frac{5}{2}}$$

Equation 2-46

$$F_r = \frac{M_r L_r}{T_r} = \rho_r L_r^3$$

Equation 2-47

$$P_r = \frac{F_r}{L_r^2} = \rho_r L_r$$

Equation 2-48

Where:

r	-	ratio of prototype to model
Q_r	-	discharge ratio (m ³ /s)
V_r	-	velocity ratio (m/s)
L_r	-	length ratio (m)
F_r	-	force ratio (N)
M_r	-	mass ratio (kg)
ρ_r	-	density ratio (kg/m ³)
P_r	-	pressure ratio (N/m ²)

In order to achieve dynamic similarity in a geometric similar physical model, it is required that the Froude, Euler, Reynolds, Weber and Sarrau-Mach numbers must be the same for both the prototype and the model. Should this not be achieved, then differences between the flow characteristics of the prototype and the model will exist. These differences are known as scale effects and can be defined as distortions that will occur due to the viscosity and surface tension of the water and may be more dominant than the gravitational parameters. Chanson (2004) indicated that scale effects may often be small but should not be neglected altogether. Chanson further indicated that dynamic similarity for geometric similar physical models can only be achieved if a different fluid is used in the model than that of the prototype, as the Reynolds number cannot be the same in both cases if the density of the fluid stays constant.

For more information on the modelling of free-surface flow the reader is referred to see Chanson (2004): *The Hydraulics of Open Channel Flow: an Introduction*.

Physical modelling of flow over an Ogee spillway was researched to a great extent in the 1980's by governmental organizations like the USBR (1987) and USACE (1987). However, because most of the

studies investigated unknowingly, only the 2-dimensional flow parameters of flow over the spillway gaps in the knowledge and design of Ogee spillways currently exists (Chatila & Tabbara, 2004).

Recently, technological development in the field of Computational Fluid Dynamics (CFD) has enabled numerous modern researchers to move away from the physical modelling of flow over Ogee spillways to a more numerical and graphical evaluation of the system. Although close agreement with measured free surface flow profiles are obtained in many of these investigations (Chatila & Tabbara, 2004 and Savage & Johnson, 2001) flow characteristics are still considered to be symmetrical as Ferrari (2010) refers: *The side contractions in the overtopping flow has been neglected (Figure 2-55)*. This indicates that boundary conditions when considering CBD analysis may still be problematic, thus neglecting the true 3-dimensionality and asymmetry of actual spillways. Physical modelling is therefore, in a great sense, still required to assess the true 3-dimensional complexity that exists at actual Ogee spillways.

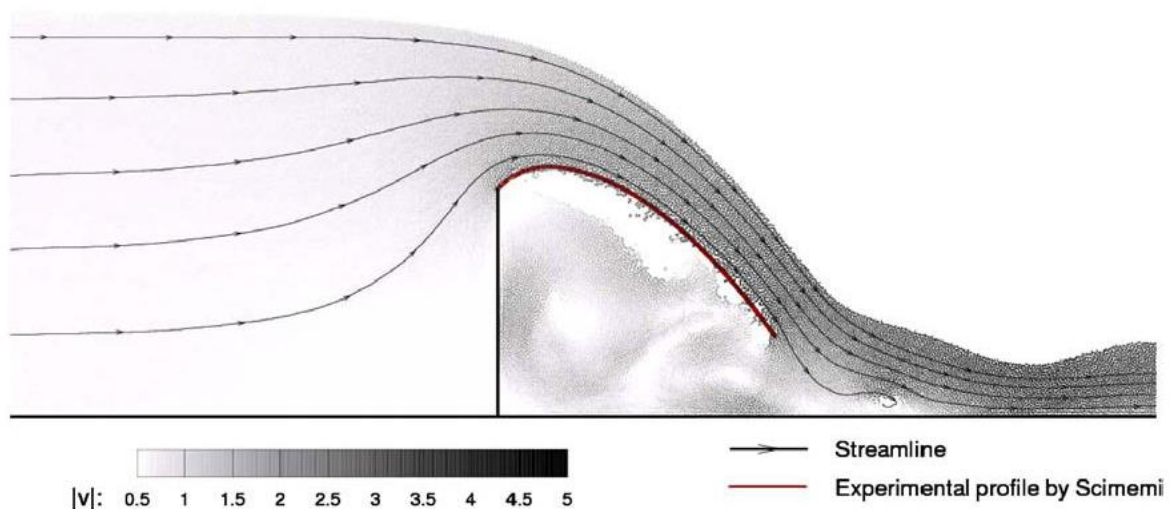


Figure 2-55: Neglecting the 3-dimensional effect being caused by the contraction of side walls at a sharp-crested weir, a relative good approximation of the Ogee curve is obtained by means of a CFD analysis (Ferrari, 2010)

In this chapter different contributions by numerous authors highlighted the characteristics and theoretical approaches used to estimate the geometric profile of an Ogee spillway. This background and knowledge has been used in the design of an experimental setup with the extension to measure the bottom nappe of the flow across a sharp-crested weir. The discussion of the methodology and experimental setup were discussed in chapter 3 of this dissertation report.

3 METHOD

3.1 EXPERIMENTAL SETUP AT THE DEPARTMENT OF WATER AFFAIRS HYDRAULIC LABORATORY

3.1.1 Introduction

A physical scaled down experimental setup of a sharp-crested weir was constructed at the Department of Water Affairs Hydraulic Laboratory located in Pretoria-West. In order to complete the purpose of this research topic the main functions of the setup were:

- Measure the profile of the underlying nappe of water flowing over the sharp-crested weir;
- Provide an undisturbed, uniform approach flow pattern across the weir, and vary the flow rate to enable the investigation of different stage versus flow rate scenarios. Also accurately measure the stage of the approach flow;
- Provide the model with the correct dimensions and specifications in order to ensure that equations provided by the current literature are valid and that international credibility is achieved (ISO 1438, 2008; ASTM International, 2001); and
- Allow for the adjustment of the upstream cross-section layout of the channel approaching the sharp-crested weir (which is one of the defined 3-dimensional flow behaviour parameters).

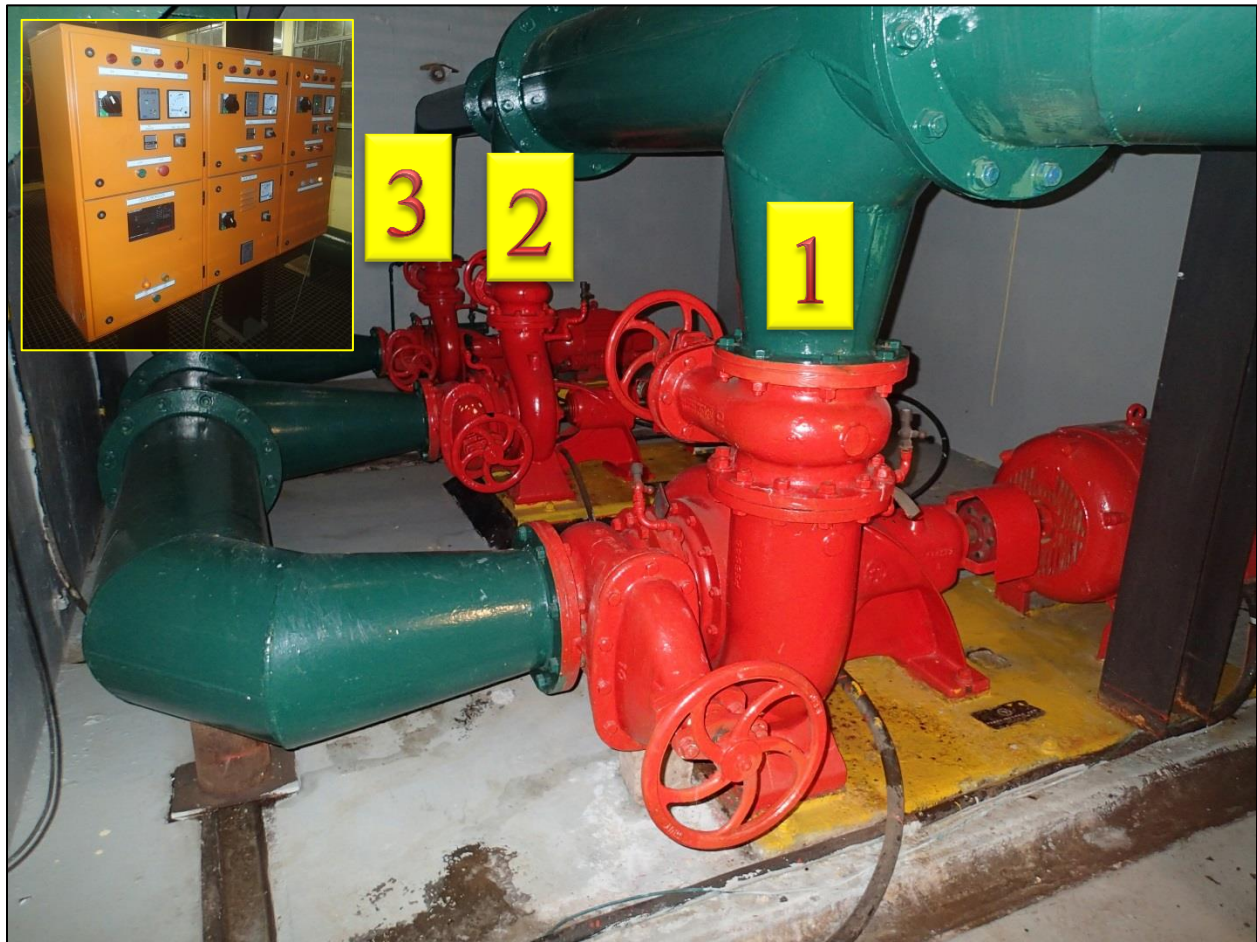
With these parameters in mind, the following paragraphs describe the process undertaken to meet these needs, as well as the difficulties faced when satisfying these parameters and the actions taken to resolve these difficulties.

3.1.2 Existing layout at the Department of Water Affairs Hydraulic Laboratory

The Department of Water Affairs (DWA) situated in Pretoria-West has a $\pm 100 \text{ m}^3$ underground sump serving as a reservoir to conduct fluid physical modelling. Three centrifugal pumps in parallel, pump water to a constant head tank at an elevation of six meters to deliver a maximum constant flow rate of $\pm 260 \text{ l/s}$. The constant-head tank is fitted with a 300 mm steel discharge pipe that diverts the excess water from the constant-head tank to the underground sump. Water to the physical model is supplied via a 250 mm steel pipeline that gravity feeds from the constant-head tank to the model. The flow rate to the model

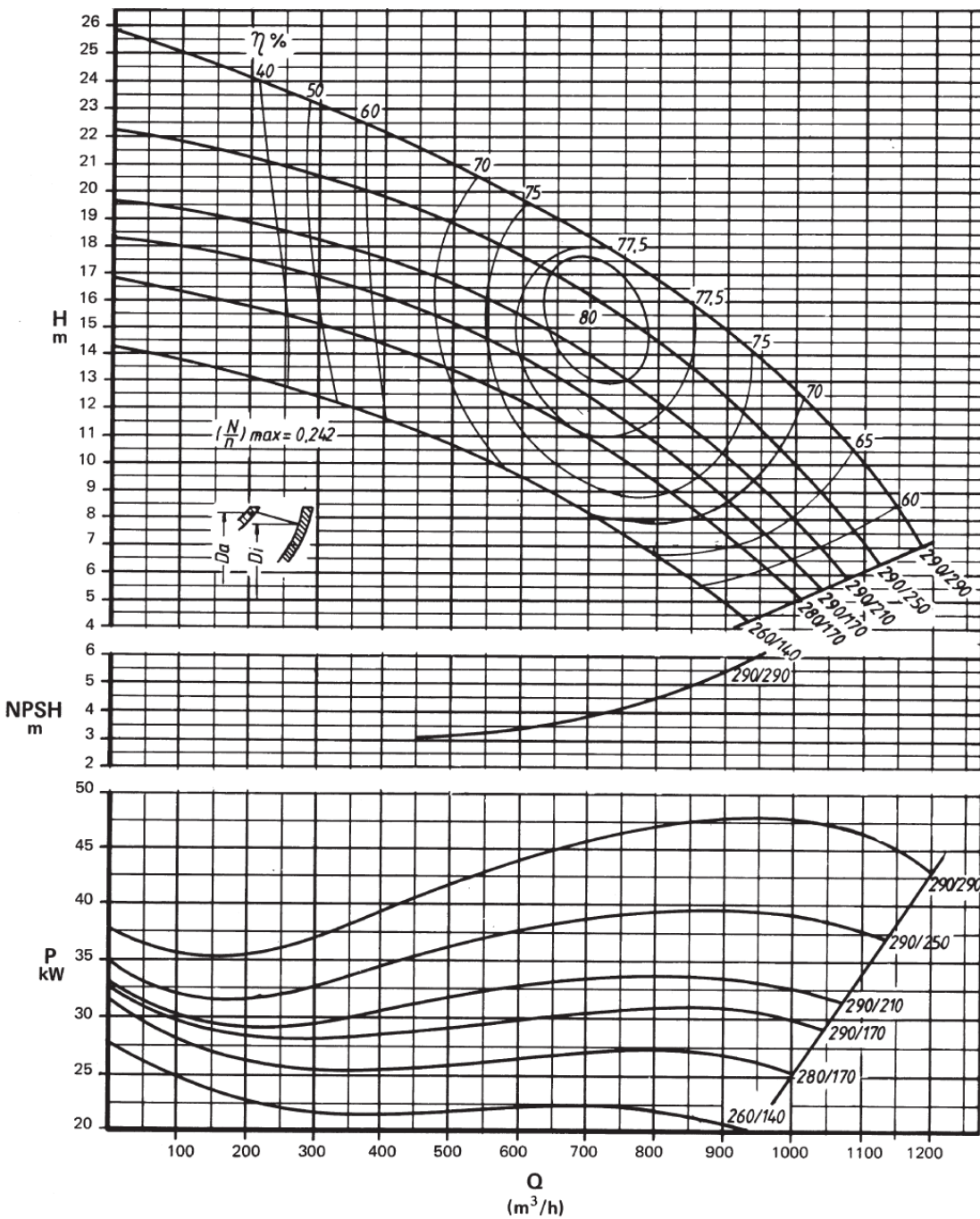
was regulated by making use of a full-bore butterfly valve and verified with the installed magnetic flow meter that is fitted inside the pump station.

For the purpose of the study, the Ogee profile was measured for flow rate increments of 60, 80, 115 and 130 l/s (as given by the magnetic flow meter) and discussed in Chapter 4. Only one centrifugal pump was utilized, (the KSB ETA 250-29) capable of delivering a constant flow rate of 160 l/s in the system. The centrifugal pump (no. 1), system control panel and pump curve is reflected in **Figure 3-1** and **Figure 3-2** respectively.



**Figure 3-1: Three centrifugal pumps installed at DWA Hydraulic Laboratory
(Pump no. 1, KSB ETA250/29 was utilized for the experimental setup)**

ETA 250-29



Impeller 290/290 - 260/140 mm \varnothing Impeller outlet width 80 mm **1450 R.P.M.**

57

Figure 3-2: Pump curve of pump no. 1, KSB ETA250/29 (KSB Pumps, 2005)

The butterfly valve utilized to adjust the flow rate to the required discharge is indicated in **Figure 3-3** by the yellow circle together with an insert of the magnetic flow meter. The direction of flow in die pipe is indicated by the arrows. The accuracy of the magnetic flow meter was calibrated against a volumetric tank with a known depth/area relationship. The discharge from the volumetric tank is also verified by making use of an installed crump weir and measuring the stage for different flow rates. The calibration process was repeated six times and the 2nd degree polynomial trend line was used to estimate the required correction factor for a specific flow rate. Calibration of the magnetic flow meter is indicated in **Figure 3-4**.

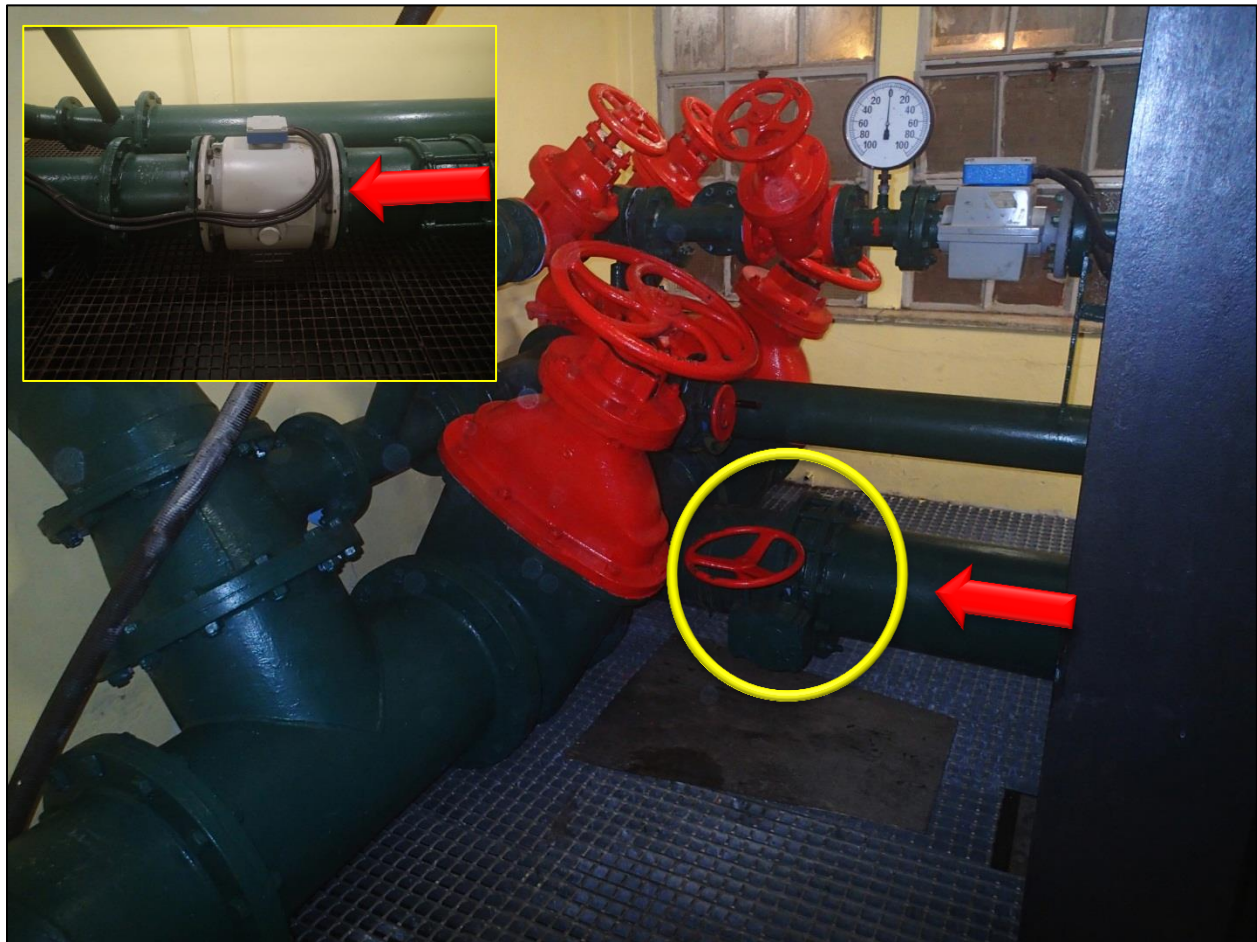


Figure 3-3: Flow regulated to physical model by adjusting the full-bore butterfly valve

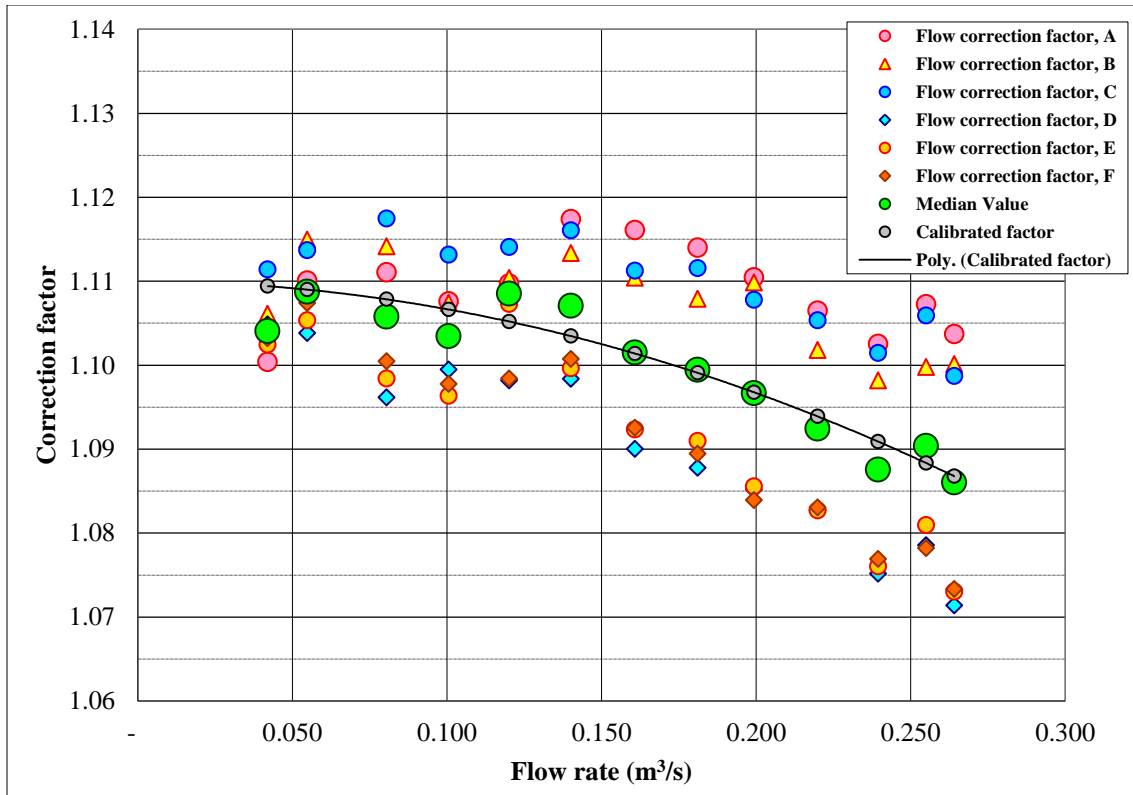


Figure 3-4: Calibration of the magnetic flow meter by making use of the provided crump weir and volumetric tank

The layout of the constant-head tank that gravity feeds to the physical model as well as the excess discharge pipe that transfers the excess water to the underground sump is reflected in **Figure 3-5**. The direction of flow in the pipe is indicated by the fitting arrows. The magnetic flow meter is installed on the supply line from the constant head tank.

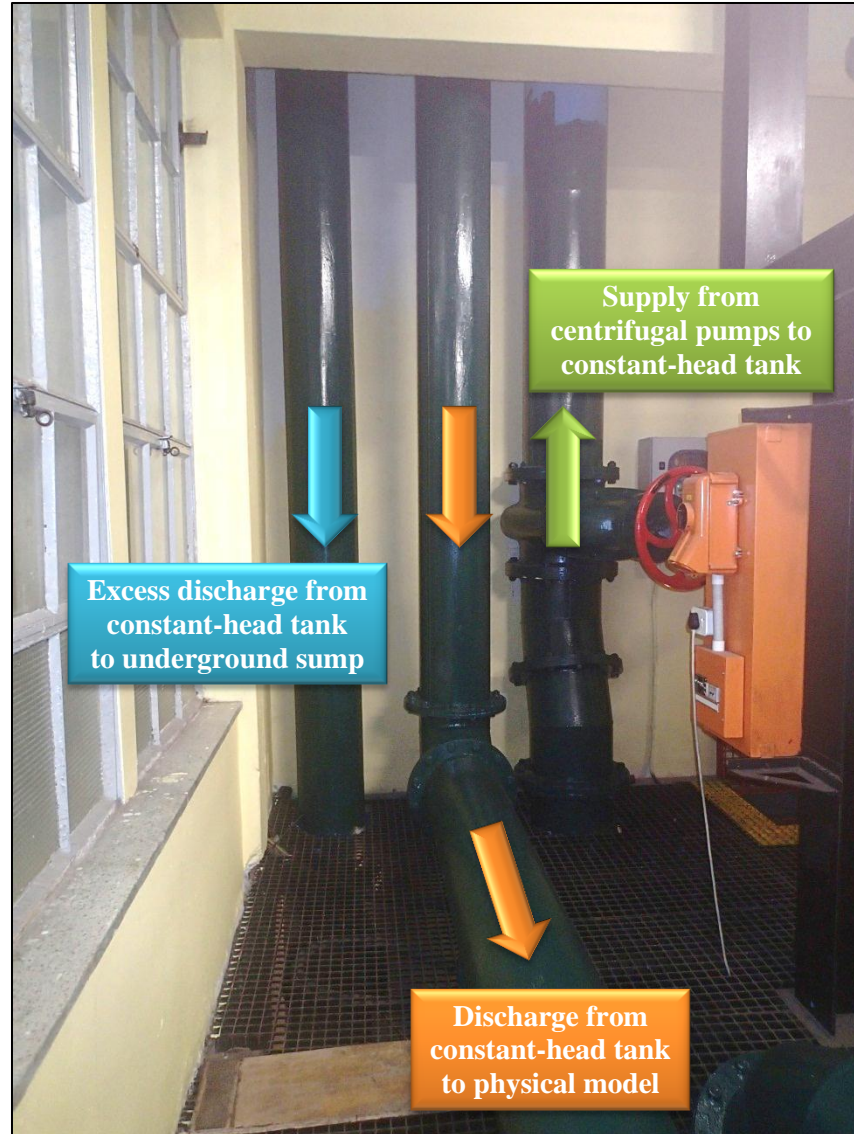


Figure 3-5: Configuration of the constant-head tank layout

The DWA Hydraulic Laboratory allocates a specific site within the laboratory according to the requirements of the physical model. For the construction of the physical model of the sharp-crested weir utilized in this research project, a site of $\pm 60 \text{ m}^2$ was allocated (15 m x 4 m). The preliminary design and construction of the physical model follow in the subsequent sections of this chapter.

3.1.3 Preliminary design of the model

During the early stage of the research project it was required to investigate the design of a physical model that could allow for the accurate measurement of an Ogee profile. Since the low nappe of water flowing

over a sharp-crested weir follows the same geometric profile of an Ogee curve, it was decided to construct a sharp-crested weir both large enough to measure the lower profile of the water flowing over the weir, but also that conforms to international standards. The model was maximized in terms of the available allocated area space of 60 m². A model with an approach channel of 10 m in length and 3 m in width (long wide channel to ensure uniform undisturbed flow approaching the weir), and a crest height of 800 mm were proposed. In order to ensure that the sharp-crested weir conform to the international standards' specifications of a fully contracted weir as specified by ISO 1438 (2008) in **section 2.10** the ratios of the geometric layout of the proposed system compared with ISO 1438 (2008) is given in **Table 3-1**.

Table 3-1: Comparison of proposed models geometric ratios to ISO 1438 (2008)

International Organization for Standardization (ISO 1438, 2008) specification for a fully contracted weir	Proposed value for the construction of the physical model at a flow rate of 110 l/s	Values of proposed physical model used for the calculation of ratio parameters
$h/p \leq 0.5$	0.125	(100/800)
$h/b \leq 0.5$	0.085	(100/1175)
$0.08 \text{ m} \leq h \leq 0.6 \text{ m}$	0.1 m	-
$b \geq 0.3 \text{ m}$	1.175 m	-
$p \geq 0.3 \text{ m}$	0.8 m	-
$(B - b)/2 \geq 2h$	$0.9125 > 200$	$(3000-1175)/2 \geq 100 \cdot 2$

The weir's crest was proposed to be manufactured from 2 mm thick stainless steel laser cut to form a precise 90° angle. The stainless steel crest would be reinforced by a 5 mm thick mild steel plate to prevent any deformation of the weir due to the hydrostatic pressure exerted onto the structure under normal operational conditions. The total width of the weir was proposed to be 1800 mm and can be reduced to a lesser value of 1175 mm by the addition of removable plates fitted to the weir's crest in order to alter the approaching flow conditions. The plan layout of the sharp-crested weir is reflected in **Figure 3-6** and the downstream view of the proposed sharp-crested weir is indicated in **Figure 3-7**.

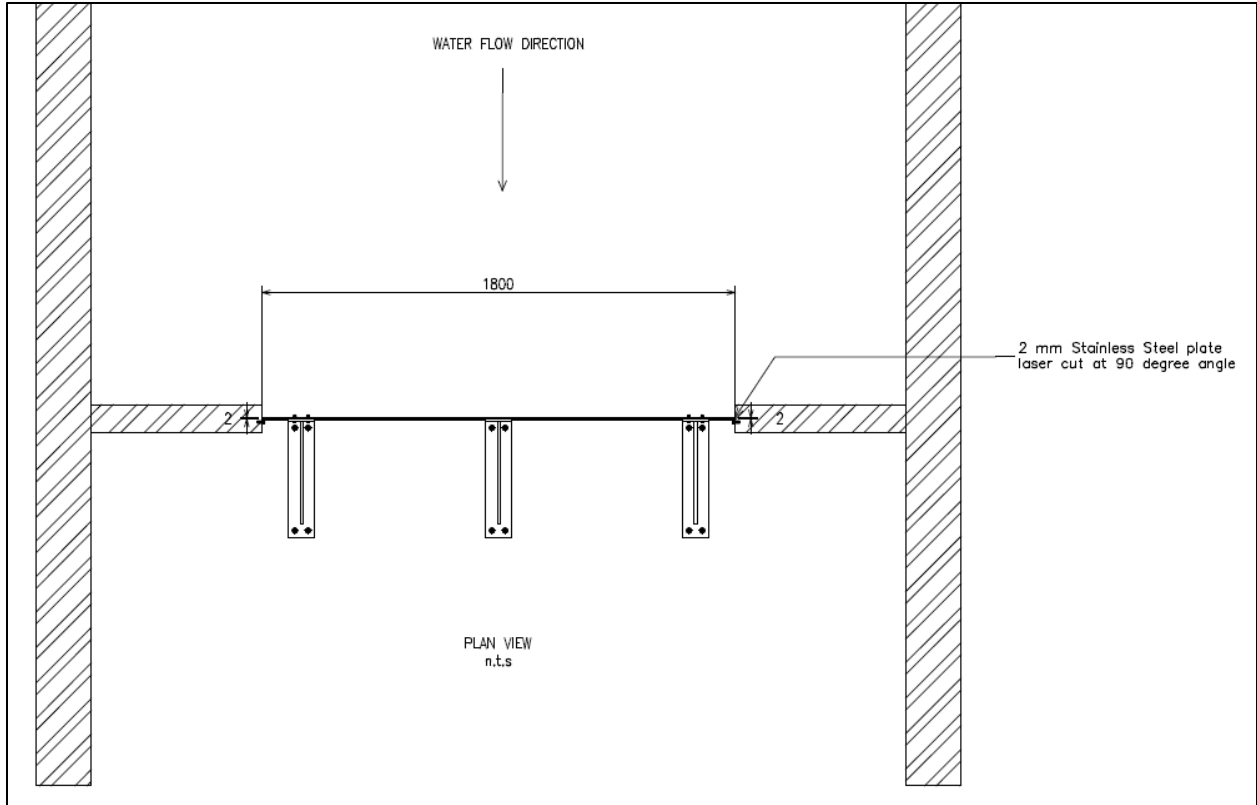


Figure 3-6: Plan view of proposed sharp-crested weir

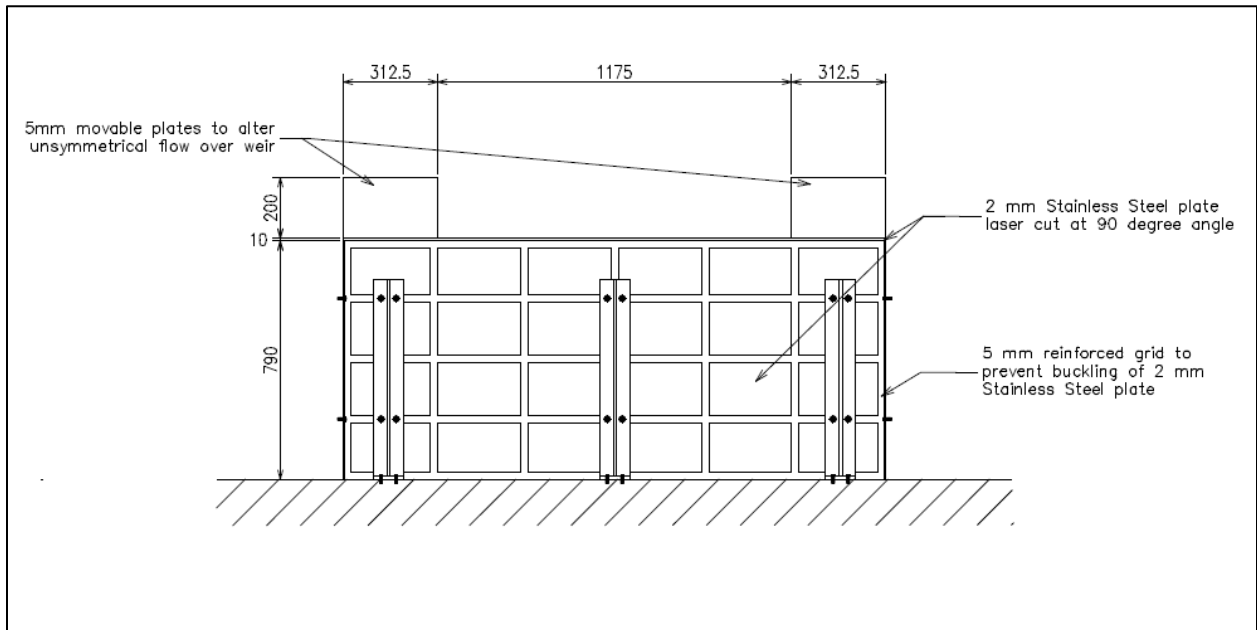


Figure 3-7: Downstream view of the proposed sharp-crested weir

The side view of the proposed sharp-crested weir model is indicated in **Figure 3-8**. Details of the crest-configuration i.e. the 2 mm stainless steel plate laser cut at an angle of 90° together with the 5 mm mild steel used to reinforce the stainless steel plate and the 5 mm movable plates installed to alter the flow conditions upstream of the weir are indicated in the insert of **Figure 3-8** titled: *DETAIL A*.

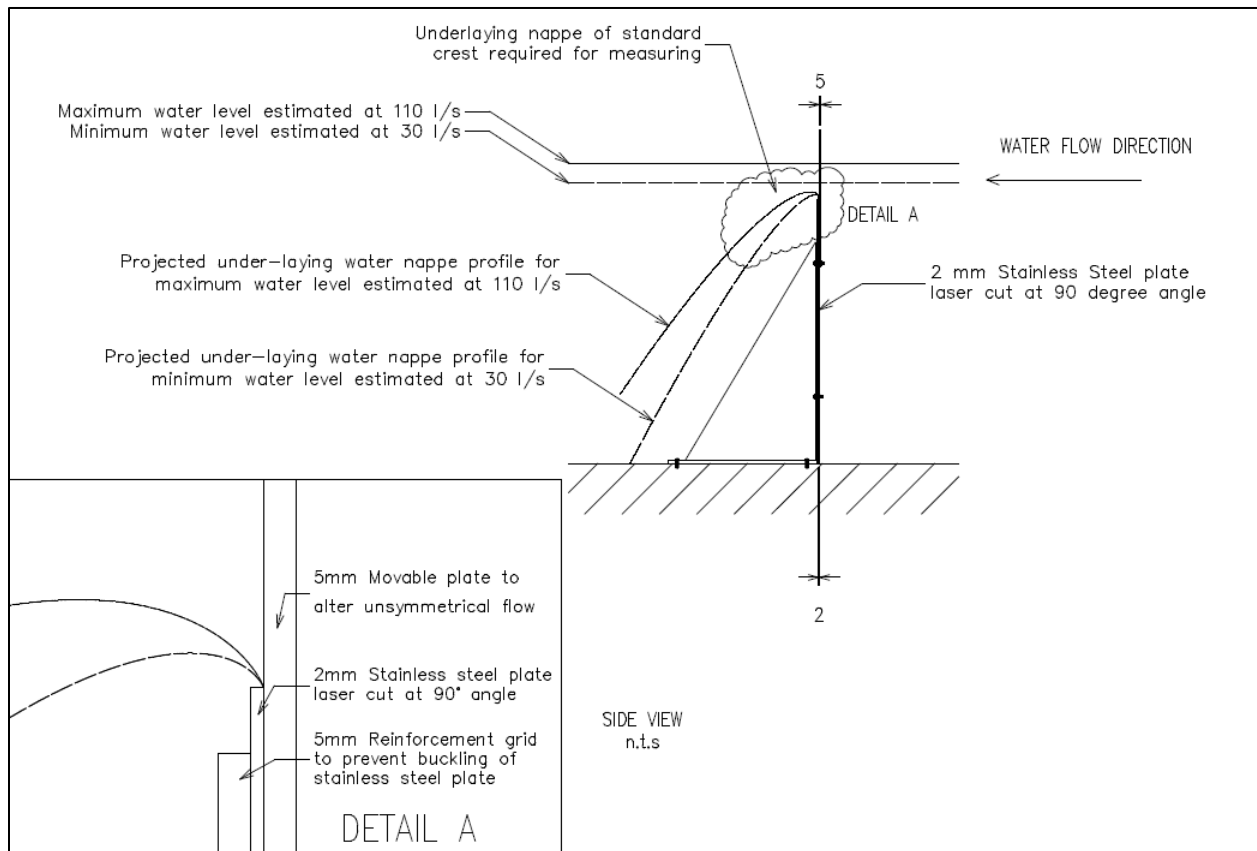


Figure 3-8: Side view of the proposed sharp-crested weir model and detail of the crest-configuration

3.2 CONSTRUCTION OF THE PHYSICAL MODEL

The construction process of the physical model at the Department of Water Affairs Hydraulic Laboratory is depicted in the following paragraphs by means of a step-by-step pictorial. Although slight variations exist from the proposed model discussed in **section 3.1.3** the essence of the physical model is still the same. The changes were incorporated for the ease of construction of the model and are discussed together with each sequel picture.

3.2.1 Construction of the outer boundary of the physical model

The outer boundary of the physical model was constructed by means of plastered brickwork to a height of 1135 mm. The width of the layout was 3106 mm and total length was ± 15 m. In order to prevent failure of the sides due to the hydrostatic pressure exerted onto the structure during filling of the channel upstream of the weir, the boundary walls were reinforced with a brickwork column every ± 1500 mm.

Water was fed from the constant head tank to the model by means of a perforated tapered steel pipe. This configuration was used to enhance an even distribution of uniform flow upstream of the sharp-crested weir. In **Table 3-2** is the pictorial sequel of the construction of the outer boundary of the physical model.

Table 3-2: Construction of the outer boundary of the physical model



a. Overview of approach channel.	b. Reinforcement of side walls.
 <p style="text-align: right; color: orange; font-size: small;">08 02 2012</p>	 <p style="text-align: right; color: orange; font-size: small;">08 02 2012</p>

Table 3-2: Construction of the outer boundary of the physical model continue

<p>c. Plastered left channel wall.</p>	<p>d. Plastered right channel wall.</p>
	
<p>e. Inlet from constant head tank to model.</p>	<p>f. Distribution of discharge flow rate from the perforated tapering pipe.</p>
	
<p>g. Downstream view of circulation back to the ground sump via a grid inlet.</p>	
	

3.2.2 Installation of the wall structure utilized to dam the water

The wall structure utilized to dam the water in the channel was made of 5 mm thick mild steel with dimensions 1800 mm x 800 mm. The plate was predrilled with staggered 7 mm holes spaced 150 mm apart. This was done in order to fit the laser cut stainless steel crest of the sharp-crested weir effortlessly and accurately onto the wall structure. The plate was reinforced by 6 x 50 mm x 3.5 mm angles welded back to back to increase the plate's inertia in the direction of flow. Chalk lines, together with semi-circles were used to accurately determine the mid-line of the channel. The structure was held in position, perpendicular by 3 lipped channels welded to the plate and 2 x 50 mm x 3.5 mm angles. The structure was bolted to the concrete surface with 6 x M8 Fischer roll bolts and could be precisely adjusted to ensure the structure is both level and perpendicular to the direction of water flow in the channel. The structure was first coated with red oxide paint and a second coat of *Plascon*[®] light grey enamel to prevent corrosion during immersion of the structure. In **Table 3-3** is the pictorial sequel of the installation of the wall structure being utilized to dam the water.

Table 3-3: Installation of the wall structure utilized to dam the water



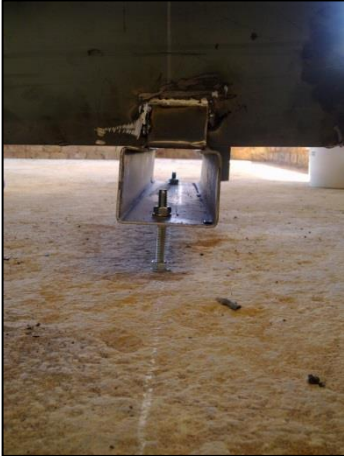

a. Wall structure utilized to dam the water in the channel.	b. Wall structure reinforced by 6 x 50 mm x 3.5 mm angles welded back to back.
	

Table 3-3: Installation of the wall structure utilized to dam the water continue

c. M8 Fischer roll bolts used to tweak the level of the structure.	d. Wall structure coated with Plascon light grey enamel to prevent corrosion.
	

3.2.3 Levelling the wall structure of the sharp-crested weir

With most spirit levels having an accuracy of only 1mm/meter, a more accurate procedure was required to level the wall structure of the sharp-crested weir. A dumpy level was setup ± 15 m away from the structure and was used to level of the wall structure of the sharp-crested weir. By fine-tuning the M8 Fischer bolts connected to the structure, a final configured level was arranged with a level difference of less than 0.5 mm over the total width of 1800 mm. The levelled structure was verified with an automated *Bosch* laser spirit level and indicated that an accurate setup was obtained. In **Table 3-4** is the pictorial sequel of levelling the wall structure of the sharp-crested weir.

Table 3-4: Levelling the wall structure of the sharp-crested weir

<p>a. Measuring tape used to determine the level of the wall structure.</p>	<p>b. Level setup of the dumpy level.</p>
 <p>A close-up photograph showing a person's hands holding a yellow spirit level against a brick wall. A measuring tape is also visible, extending vertically along the wall. The date '02 07 2012' is printed in orange at the bottom right of the image.</p>	 <p>A close-up photograph of a dumpy level instrument mounted on a tripod. The instrument is white and black, with a blue lens cap. The date '02 07 2012' is printed in orange at the bottom right of the image.</p>
<p>c. View through the dumpy level to the wall structure ± 15 away.</p>	<p>d. Levelled structure verified with an automated <i>Bosch</i> laser spirit level.</p>
 <p>A photograph of a person in a dark vest and blue jeans looking through the eyepiece of a dumpy level mounted on a yellow tripod. The date '02 07 2012' is printed in orange at the bottom right of the image.</p>	 <p>A photograph showing a yellow Bosch laser spirit level mounted vertically on a grey wall structure. The date '02 07 2012' is printed in orange at the bottom right of the image.</p>

3.2.4 Waterproofing and sealing of the wall structure of the sharp-crested weir

In order to prevent water from seeping through the boundaries of the wall structure, the lipped channel onto which the wall structure was mounted was covered in polystyrene. The polystyrene was held in position with duct tape. The footing was then covered by brickwork and plastered to create a water tight seal. This reduced the upstream depth of the weir and required that the channel upstream of the wall structure had to be filled to the level of the step to prevent any discontinuities in flow. This procedure can be viewed under **section 3.2.11**. In **Table 3-5** is the pictorial sequel of waterproofing and sealing of the wall structure of the sharp-crested weir.

Table 3-5: Waterproofing and sealing of the wall structure of the sharp-crested weir



a. Polystyrene used to cover the lipped channel footings of the wall structure.	b. Polystyrene covered in duct tape.
	

Table 3-5: Waterproofing and sealing of the wall structure of the sharp-crested weir continue

<p>c. Downstream view of polystyrene and duct tape fitted to the wall structure footings.</p>	<p>d. Upstream view of polystyrene and duct tape fitted to the wall structure footings.</p>
	
<p>e. Downstream footings covered in brickwork.</p>	<p>f. Upstream footings covered in brickwork.</p>
	

3.2.5 Construction and plastering of fill-in walls

The fill-in wall constructed between the boundary of the channel and the wall structure of the sharp-crest weir was build flush to the upstream side of the weir’s wall structure. This is slightly different from the proposed design where the wall structure was proposed to be at the center of the fill-in walls (**section 3.1.3**). It was built in this manner to prevent any side flow effects and to ensure that the flow in the approach channel was undisturbed when reaching the weir. The surface of the fill-in walls, as well as the brickwork step at the footing of the weir’s wall structure were plastered and finished on the upstream

side of the weir with a trowel and cement mixture to ensure that an as smooth as possible finish was obtained. In **Table 3-6** is the pictorial sequel of construction and plastering of fill-in walls.

Table 3-6: Construction and plastering of fill-in walls




<p>a. Construction of the fill-in walls flush to the upstream side of the wall structure of the weir.</p>	<p>b. Plastering of the footing step on the upstream side of the weir.</p>
	
<p>c. Plastering of the fill-in walls on the downstream side of the weir.</p>	<p>d. Trowel finished of the plastered walls on the downstream side of the weir.</p>
	

Table 3-6: Construction and plastering of fill-in walls continue...





e. Smooth trowel and cement finished of the plastered walls on the upstream side of the weir.



3.2.6 Attachment of the stainless steel sharp-crested weir's crest

The laser cut stainless steel sharp-crested weir's crest was installed onto the wall structure plate by means of staggered M6 stainless steel bolts spaced 150 mm apart. The holes were predrilled into the wall structure plate and the M6 bolts were welded onto the stainless steel plate to ensure that a tight fit of the setup was possible. The crest level of the sharp-crested weir was verified again with the dumpy level to ensure that a precise assembly was obtained. The stainless steel staggered M6 bolts were tightened and sealed with silicon to ensure a water tight setup was achieved. The sharp-crested weir was installed flush with the upstream side of the approach channel's fill-in walls. In **Table 3-7** is the pictorial sequel of the attachment of the stainless steel sharp-crested weir's crest.

Table 3-7: Attachment of the stainless steel sharp-crested weir’s crest

<p>a. Upstream view of the installation of the sharp-crested weir’s crest.</p>	<p>b. Downstream view of the installation of the sharp-crested weir’s crest.</p>
	
<p>c. Installation of the sharp-crested weir’s crest flush to the upstream side of the fill-in walls.</p>	<p>d. M6 stainless steel bolts sealed with silicon after which they were grinded flush with the nuts.</p>
	

3.2.7 Assembly of the aluminium frame for the Ogee profile measuring apparatus

In order to measure the Ogee nappe accurately it was required to fix a structure onto which a measuring apparatus could be mounted to measure the Ogee profile without interfering with the natural flow of the water over the sharp-crested weir. An aluminium frame was made from extruded *FlexiLine* aluminium profiles manufactured by *PRO-VEY* (Pty) Ltd. It was erected downstream of the sharp-crested weir and positioned in such a fashion that the water would not interfere with the structure during the normal flow conditions.

The hollow extruded aluminium sections used for the frame was 44 mm x 44 mm support beams and 63 mm x 63 mm angle support brackets were used to fix beams together. Dimensions of these extruded aluminium sections are given in **Figure 3-9** and **Figure 3-10** respectively (PRO-VEY (Pty) Ltd., 2012).

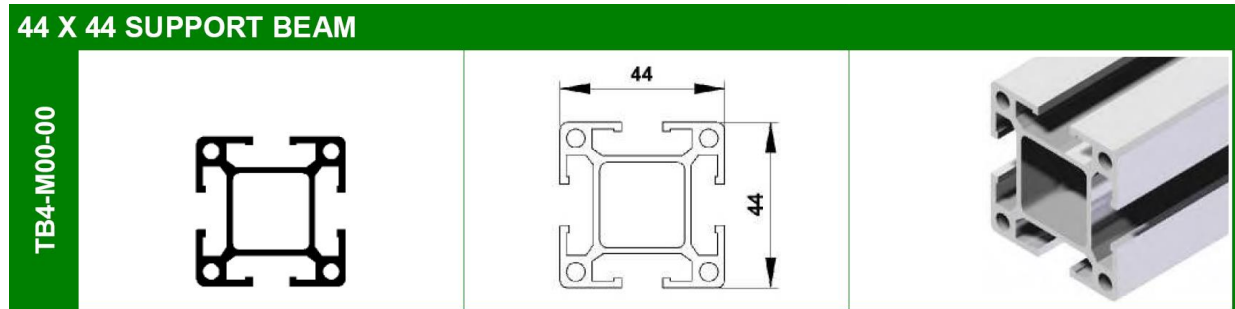


Figure 3-9: 44 mm x 44 mm aluminium support beams (PRO-VEY (Pty) Ltd., 2012)

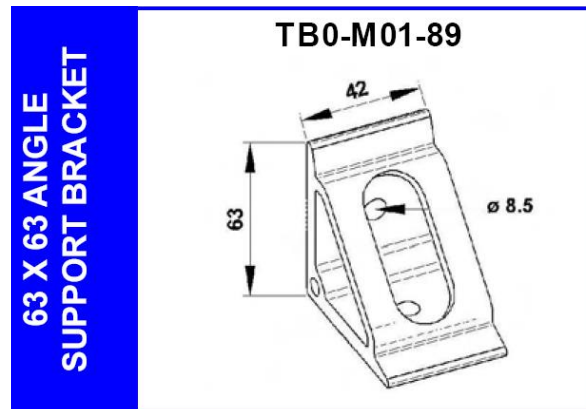


Figure 3-10: 63 mm x 63 mm aluminium angle support brackets (PRO-VEY (Pty) Ltd., 2012)

The aluminium frame consisted of four column sections fixed to the concrete ground with M12 Fischer bolts to ensure that the structure was firmly held in place, ridged and that no movement was possible during the experimental runs. The positions of the four columns were accurately set out by making use of a Bosch Laser spirit level, chalk lines and semi-circles to determine the mid-line of the structure. The columns were braced at the bottom and top with rectangles that were held in position with three 63 mm x 63 mm aluminium angle support brackets at each corner. This ensured that the structure was ridged and firmly intact. Finally, the preliminary rails on which the measuring apparatus could move were connected (this was discussed in more detail under **section 3.2.14**). Dimensions of the structure and its position relative to the sharp-crested weir are given in **Figure 3-11**.

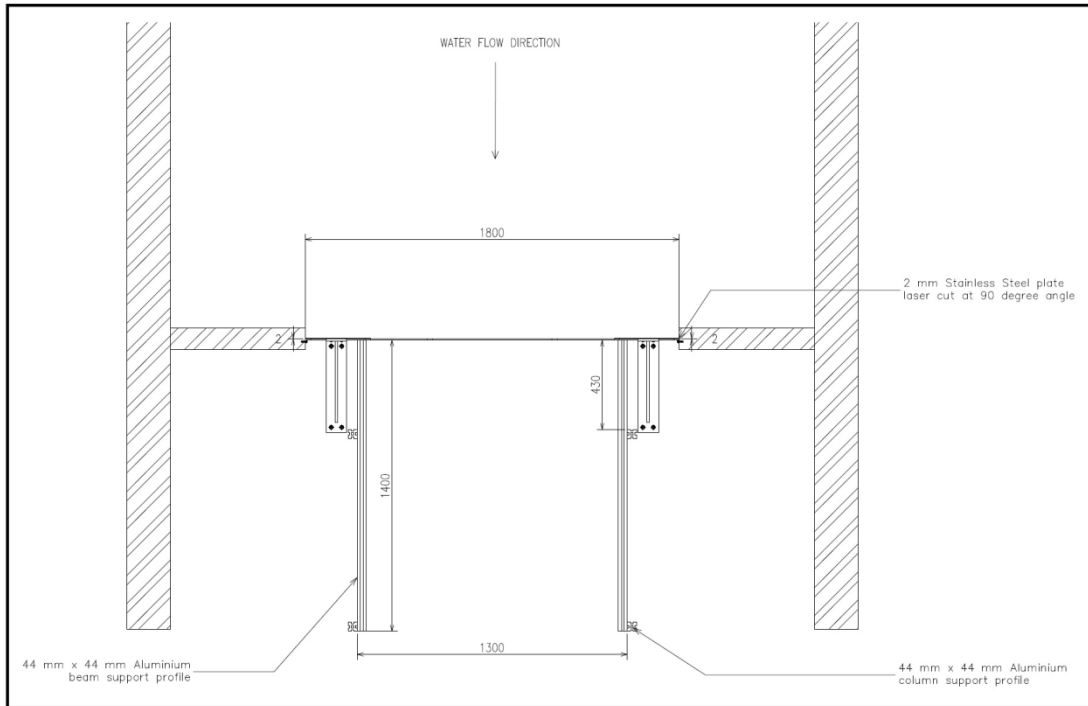


Figure 3-11: Plan view with dimensions of the aluminium frame and its position relative to the sharp-crested weir

In **Table 3-8** is the pictorial sequel of the assembly of the aluminium frame for the Ogee profile measuring apparatus.

Table 3-8: Assembly of the aluminium frame for the Ogee profile measuring apparatus

<p>a. A Bosch laser spirit level used to determine the relative position and alignment of the aluminum frame</p>	<p>b. View of horizontal and vertical laser projection onto the wall structure of the sharp-crested weir.</p>

Table 3-8: Assembly of the aluminium frame for the Ogee profile measuring apparatus continue





<p>c. Drilling of pilot holes at the intersection of the chalk lines used to set out the position of the aluminium frame.</p>	<p>d. M12 Fischer Bolt used to fix the aluminium column to the concrete ground.</p>
	
<p>e. Assembly of the unbraced columns (view of position relative to the sharp-crested weir).</p>	<p>f. Ensuring that the beams are level before bracing of the structure at the bottom and top.</p>
	

Table 3-8: Assembly of the aluminium frame for the Ogee profile measuring apparatus continue





<p>g. Ensuring that the columns are level before bracing of the structure at the bottom and top.</p>	<p>h. Bracing of the structure at the bottom.</p>
	
<p>i. Three 63 mm x 63 mm aluminium angle support brackets at each corner.</p>	<p>j. Assembly of preliminary rails on which the measuring apparatus would move.</p>
	

Table 3-8: Assembly of the aluminium frame for the Ogee profile measuring apparatus continue



3.2.8 Painting and measuring position markers on the sharp-crested weir

The Ogee profile was measured at 7 locations along the crest of the sharp-crested weir. With the total length of the crest being 1201 mm, the profile was measured at locations of 100 mm, 200 mm, 400 mm, 600 mm, 800 mm, 1000 mm and 1100 mm respectively. The locations were accurately determined by making use of the Bosch Laser Level. The locations were colour coded as given in **Table 3-9**. The Yellow locations (100 mm from the sides of the crest) were included in the measurement of the Ogee profile to include the boundary effects existing in the system due to the effect of flow contraction occurring at the sides of the crest.

Table 3-9: Colour coded locations where the Ogee curve was measured along the crest of the sharp-crested weir

Position	Location along the crest of the sharp-crested weir
Yellow 1	100 mm
Purple 1	200 mm
White	400 mm
Red	600 mm
Blue	800 mm
Purple 2	1000 mm
Yellow 2	1100 mm

Note: * *measured from left to right, when viewed from upstream of the physical model*

In **Table 3-10** is the pictorial sequel of the painted measuring position markers on the sharp-crested weir.

Table 3-10: Painting measuring position markers on the sharp-crested weir

<p>a. Bosch Laser Level setup to determine the locations of measuring positions.</p>	<p>b. Masking tape template used to paint position markers on the sharp-crested weir.</p>
	
<p>c. Seven locations where the Ogee profile was measured along the crest of the sharp-crested weir.</p>	
	

3.2.9 Installation of Plexiglas contractions sheets on the crest of the sharp-crested weir

In order to increase the unit flow rate across the sharp-crested weir, removable Plexiglas contraction pieces were installed to reduce the width of the sharp-crested weir's crest. These contraction pieces can also be used to alter the symmetry of flow over the hydraulic structure. This reduced the crest width from 1795 mm to 1201 mm. The Plexiglas contraction pieces were cut to fit the crest of the structure closely to ensure that a water tight fit was possible. Each contraction side was made up from a series of sheets cut to specific dimensions, laminated together and reinforced by a 30 mm x 250 mm x 12 mm strip. A schematic cross-section of the laminated Plexiglas contraction attached to the crest of the sharp-crested weir is given in **Figure 3-12**.

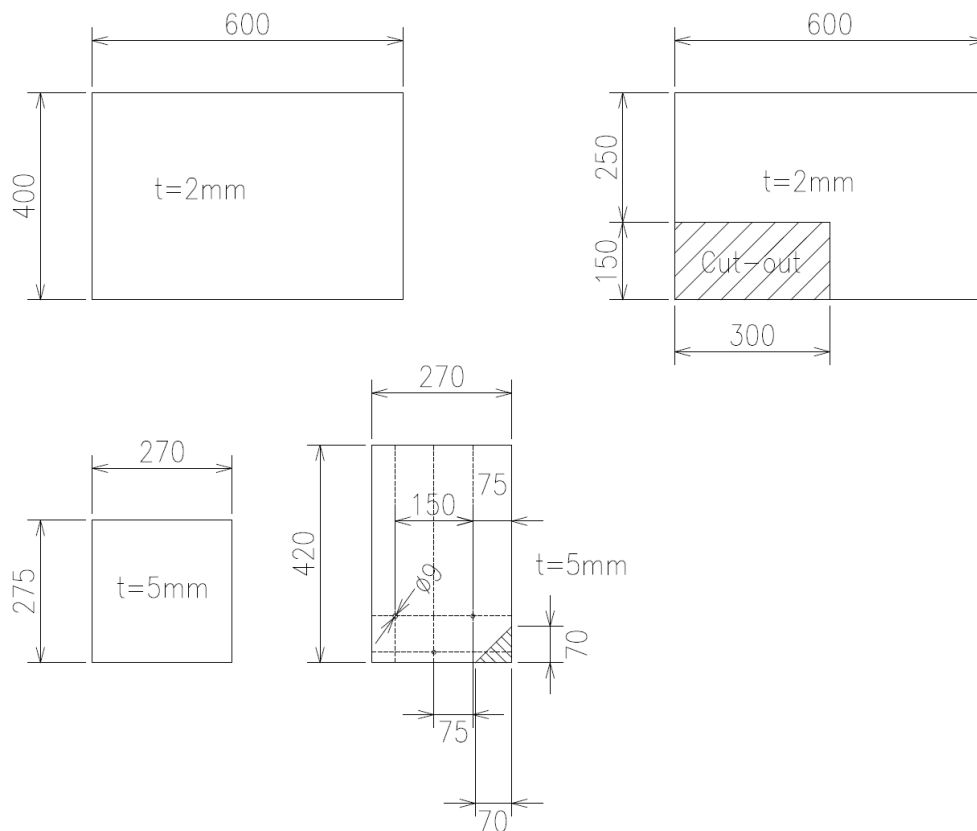




Figure 3-12: Cross-section of the laminated Plexiglas contraction attached to the crest of the sharp-crested weir

In **Table 3-11** is the pictorial sequel of the installation of Plexiglas contractions on crest of sharp-crested weir.

Table 3-11: Installation of the Plexiglas contraction sheets on the crest of the sharp-crested weir

<p>a. Installation of Plexiglas contraction sheets at the upstream side of the sharp-crested weir.</p>	<p>b. Plexiglas sheets laminated together and held in place with crocodile clamps.</p>
 <p>18 08 2012</p>	 <p>18 08 2012</p>
<p>c. Downstream view of the laminated Plexiglas contraction sheets attached on the left side of the crest.</p>	<p>d. Upstream view of the laminated Plexiglas contraction sheets attached on the right side of the crest.</p>
 <p>18 08 2012</p>	 <p>18 08 2012</p>

**Table 3-11: Installation of the Plexiglas contraction sheets on the crest of the sharp-crested weir
continue...**

<p>e. Reinforcement of laminated Plexiglas sheets with a 30 mm x 250 mm x 12 mm strip on the left side of the crest.</p>	<p>f. Installation of Plexiglas contraction sheet completed (downstream view, right side of the crest).</p>
	

3.2.10 Installation of flow straighteners in the approach channel of the physical model

The perforated steel pipe discharging water from the constant head tank to the model was enclosed with 2 halves of a steel drum and rubber flaps attached to reduce the effect of prominent stream lines in the system. Other than this amendment to the discharge pipe, were 2 rows of flow straighteners installed. The flow straighteners were made up from 50 mm asbestos cement cylinders, \pm 300 mm in length staggered on top of one other to form a honeycomb to a height of 1.1 m. Upstream of the flow straighteners was a 50 % HDPE shade net installed to allow for an even distribution of flow into the flow straighteners. The flow straighteners were located 8 m upstream of the sharp-crested weir.

In **Table 3-12** is the pictorial sequel of the installation of flow straighteners in the approach channel of the physical model.

Table 3-12: Installation of flow straighteners in the approach channel of the physical model

<p>a. 2 halves of a steel drum and rubber flaps were attached to the perforated steel discharge pipe.</p>	<p>b. Water discharging into the model via the perforated steel discharge pipe.</p>
 <p style="text-align: right; color: orange; font-size: small;">17 10 2012</p>	 <p style="text-align: right; color: orange; font-size: small;">10 07 2012</p>
<p>c. 2 rows of flow straighteners and 50 % HDPE shade net positioned upstream of flow straighteners.</p>	<p>d. Flow straighteners staggered in a honeycomb configuration.</p>
 <p style="text-align: right; color: orange; font-size: small;">17 10 2012</p>	 <p style="text-align: right; color: orange; font-size: small;">18 08 2012</p>

**Table 3-12: Installation of flow straighteners in the approach channel of the physical model
continue...**





3.2.11 Levelling of the upstream pool

In order to ensure a water tight seal of between the boundary walls, floor surface and sharp-crested weir, a small brick step was constructed upstream of the hydraulic structure (**section 3.2.4**). This however, effectively reduced the pool depth in the upstream channel and had to be levelled out to reduce any possible disturbance that might influence the hydraulic characteristics of the flow in the approach channel of the model. The approach channel was levelled at a depth measured from the crest to the floor of the channel a 666 mm. Six galvanized steel plates were installed supported on 54 columns of staggered bricks.

In **Table 3-13** is the pictorial sequel of the levelling of upstream pool depth.

Table 3-13: Levelling of the upstream pool depth

a. Galvanized steel plates supported by brick columns.	b. Six galvanized steel plates placed in approach channel of physical model.
	

3.2.12 Fitment of the wooden slope at the toe of the sharp-crested weir

In an attempt to prevent the excessive splashing of water, which may result in vibration of the aluminium frame when water is discharged from the sharp-crested weir, a wooden slope has been fitted at the toe of the hydraulic structure. The wooden slope, made from 12 mm plywood was installed to extend over the supporting brace of the aluminium frame. The water that is discharged from the sharp-crested weir is guided downstream from the toe of the model to the underground sump to be pumped again to the constant head tank.

The initial slope fitted to the downstream toe of the model had to be modified to accommodate the measuring apparatus. The initial slope restricted the movement of the apparatus and was modified to a lower gradient and shorter chute length. In **Table 3-14** is the pictorial sequel of the fitment of the wooden slope at the toe of the sharp-crested weir.

Table 3-14: Fitment of the wooden slope at the toe of the sharp-crested weir

<p>a. Initial slope selected at downstream toe of the sharp-crested weir.</p>	<p>b. Initial slope fitted at downstream toe of the sharp-crested weir and over the aluminum bracing.</p>
	
<p>c. Movement of Ogee profile measuring apparatus was restricted, thus requiring the amending of the downstream slope.</p>	<p>d. Downstream slope-support made to support the wooden slope.</p>
	

Table 3-14: Fitment of the wooden slope at the toe of the sharp-crested weir continue...

<p>e. Side view of amended wooden slope.</p>	<p>f. Frontal view of amended wooden slope.</p>
 <p style="text-align: right; color: orange; font-size: small;">21 09 2012</p>	 <p style="text-align: right; color: orange; font-size: small;">21 09 2012</p>
<p>g. View from the back of the wooden slope indicating no contact between the aluminum beam and the wooden slope.</p>	<p>h. View of discharge from model being guided downstream to the underground sump via the wooden slope.</p>
 <p style="text-align: right; color: orange; font-size: small;">21 09 2012</p>	 <p style="text-align: right; color: orange; font-size: small;">19 09 2012</p>

3.2.13 Construction of the variable side angle walls used to alter the symmetry of the approach channel

The study focuses on the influence is of an asymmetrical approach channel on the geometric variation of the theoretical Ogee profile. In order to facilitate this asymmetrical approach channel it was required to fit the existing symmetrical approach channel with some sort of element that would allow for the altering of the symmetry of the channel. This was achieved by fitting the channel with sheets of plywood whose inclination relative to the base of the channel can be easily adjusted. Steel frames made from 25 mm square tubing was made with dimensions as given in **Figure 3-13**. These steel frames allowed for the relative movement of the plywood to be easily adjusted between 45° and 60°.

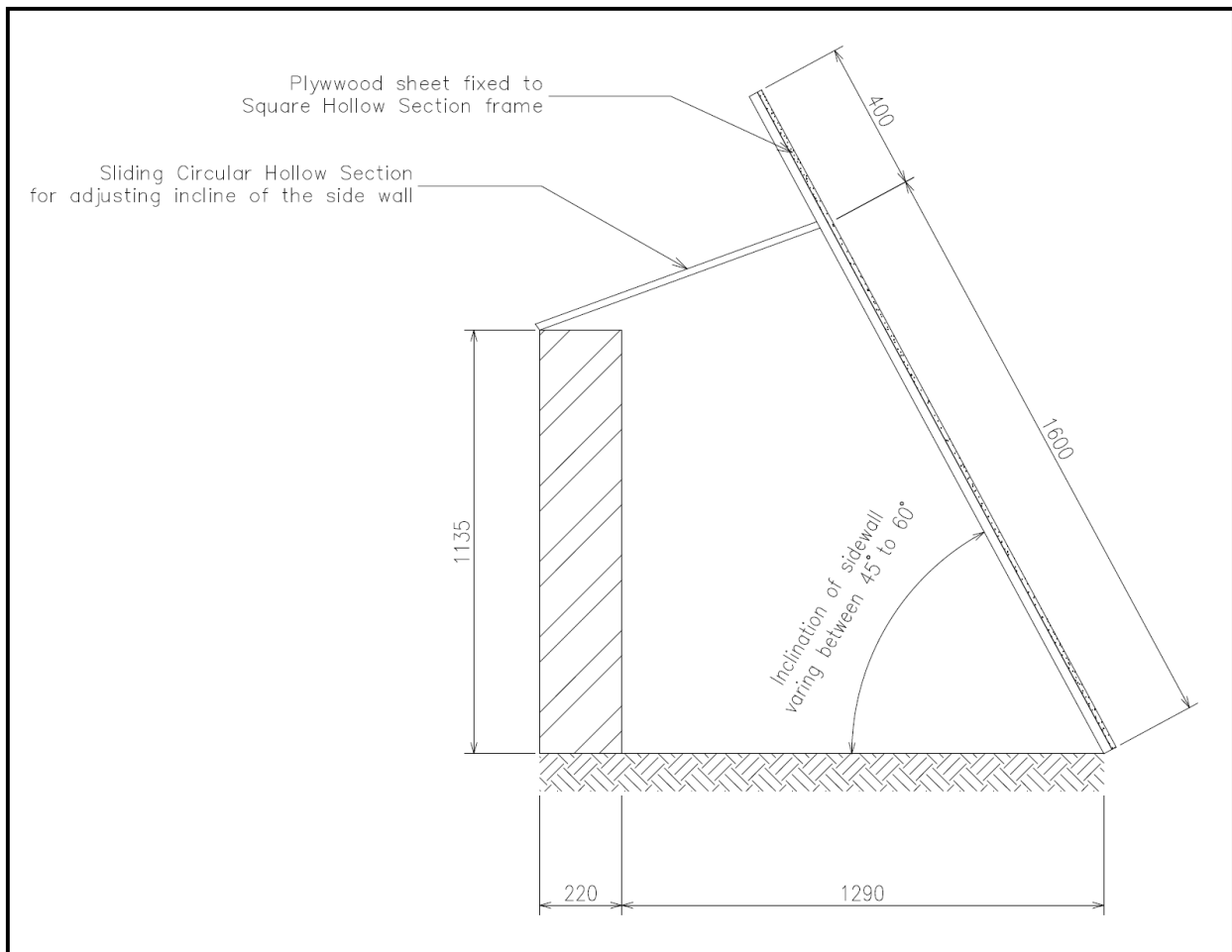


Figure 3-13: Upstream view of approach channel with steel frame made from 25 mm square tubing used to alter the symmetry of the approach channel

Two setups were made, connecting three sheets of plywood with three steel frames. Lowering the two setups in series to each other into the right side of the approach channel the symmetry was changed to an asymmetrical approach channel with the right bank either being at 45° or 60° . The total length of the asymmetrical right bank measured 7.2 m. The cross-sectional view of these two configurations is portrayed in **Figure 3-14**.

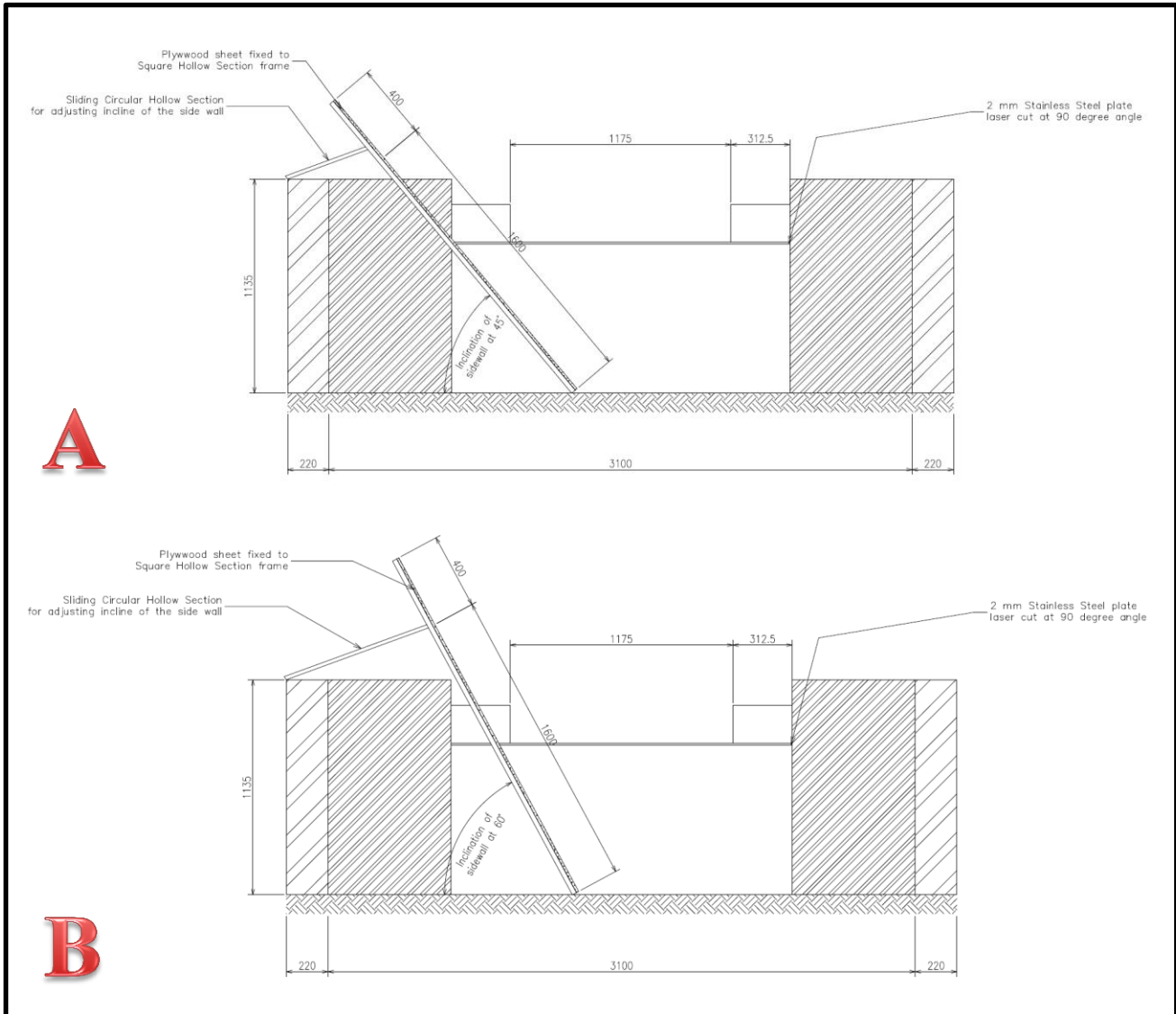


Figure 3-14: The upstream cross-sectional view of the asymmetrical approach channel with side wall inclined at 45° (A) and 60° (B) respectively

In **Table 3-15** is the pictorial sequel of the construction of the variable angle side walls used to alter the symmetry of the approach channel.

Table 3-15: Construction of the variable angle side walls used to alter the symmetry of the approach channel





<p>a. Steel frame made from 25 mm square tubing reflecting possible variation in the inclination of the side slope of the approach channel.</p>	
	
<p>b. Multiple steel frames made at the University of Pretoria's steel laboratory (Proefplaas) with footings to increase stability.</p>	<p>c. Steel frames at DWA Hydraulic Lab painted with red oxide to improve corrosion resistance.</p>
 <p style="text-align: right; color: orange;">18-08-2012</p>	

Table 3-15: Construction of the variable angle side walls used to alter the symmetry of the approach channel continue...









<p>d. Plywood sheets (1.2 m x 2 m) painted with Plascon light blue enamel paint.</p>	<p>e. Preparing a setup of 3 plywood sheets connected to each other and attaching the steel frames.</p>
	
<p>f. View of assembled plywood setup supported by the three steel frames.</p>	<p>g. Black parallel lines drawn 50 mm apart on plywood setup to visualize change in the water level during the research.</p>
	

Table 3-15: Construction of the variable angle side walls used to alter the symmetry of the approach channel continue...

<p>h. Assembly of steel supports for plywood setup on boundary wall of approach channel.</p>	<p>i. Plywood setup ready to be lifted into the approach channel.</p>
	
<p>j. Assembled plywood setup in approach channel at 60° inclination (upstream view).</p>	<p>k. Assembled plywood setup in approach channel at 60° inclination (downstream view).</p>
	

3.2.14 Sliding mechanism for Ogee profile measuring instrument (OPMI)

The OPMI required movement of the instrument along the three Cartesian axes's as defined in **section 3.2.17**. In order to allow for the in-plane movement of the OPMI small aluminium rails where machined to fit the aluminium beam profiles exactly. These small aluminium rails where held in position on the aluminium extruded beams by means of square nuts and hexagon socket countersunk head screws. The small aluminium rails functioned as guide rails to allow only for lateral movement of the OPMI (i.e. movement in the X-direction). Movement of the OPMI in the Y-direction was achieved by sliding the OPMI on two extruded aluminium beams by means of a machined engineering plastic slide mechanism (**section 3.2.15**).

In **Table 3-16** is the pictorial sequel of the installation of the sliding mechanism for Ogee profile measuring instrument.

Table 3-16: Sliding mechanism for Ogee profile measuring instrument (OPMI)



a. Small aluminium rails machined to fit the extruded aluminium beam profiles	b. Side and bottom view of the small machined aluminium rails with square nuts and hexagon socket countersunk head screws
	

Table 3-16: Sliding mechanism for Ogee profile measuring instrument (OPMI) continue...

<p>c. Small aluminium rail fitted to the extruded aluminium beam profiles.</p>	<p>d. Precision made, the aluminium extruded profile fits snugly onto the small aluminium machined rail.</p>
	
<p>e. Extruded aluminium profile secured onto small aluminium machined rail.</p>	<p>f. Guide rails positioned level before assembling the small aluminium machined rails.</p>
	

Table 3-16: Sliding mechanism for Ogee profile measuring instrument (OPMI) continue...

g. Lateral movement on the aluminium guide rails achieved by making use of the small machined aluminum rails.

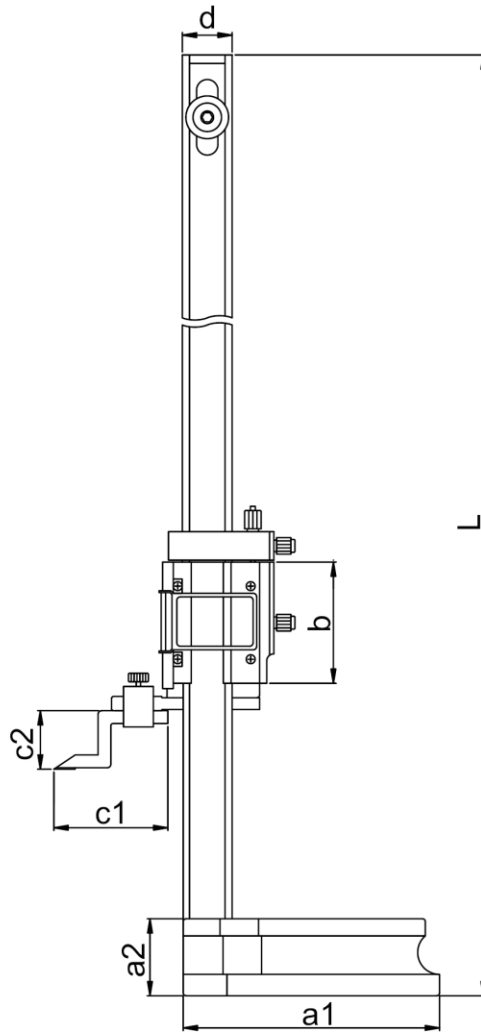


3.2.15 Construction of the Ogee profile measuring instrument (OPMI)

The OPMI was built around an Insize vernier height gauge (IVHG) (**Figure 3-15**). The inkling behind this was that the height gauge can function in a similar manner as a point gauge used to measure the water level, except that in this case it will be measuring the water surface of the Ogee nappe. If a XYZ-coordinate can be assigned to a specific location on the nappe, multiple measurements would allow one to create a surface resembling the nappe of the water flowing over the sharp-crested weir. The IVHG was manufactured from hardened stainless steel making it corrosion resistant and thus suitable for reliable and accurate measurements. The height gauge comprises of an adjustable main scale, fitted onto a sturdy cast iron footing. The main scale is fitted with a movable mechanism for the measurement of elements with different heights and has a fine adjustment screw for precision measurement. The vernier scale has a gradation of 0.02 mm.

To build the OPMI a 450 mm IVHG was dismantled. The movable mechanism of the height gauge was fitted to a machined block of aluminium together with the adjustable main scale. This assembly was fitted onto 2 pieces of engineering plastic, mounted between a small piece of extruded aluminium beam. Assembling this onto the 2 aluminium guide rails (**section 3.2.14**), this allowed for the sliding movement of the apparatus in the Y-direction of the Cartesian axis as defined in **section 3.2.17**.

A 12 mm hole was machined into the block of aluminium mounted onto the engineering plastic, similarly a small piece of aluminium was machined and a 12 mm hole drilled into it. This small piece of aluminium block was fitted to the top of the height gauge. This allowed for the fitment of a HBM linear variable differential transducer (LVDT) to enable the recording of measurements automatically.



**Figure 3-15: Insize vernier height gauge with fine adjustment
(accuracy ± 0.05 mm, model no. 1250-450)**

At the top of the IVHG was a stainless steel tip, isolated with a rectangular piece of Plexiglas. A circuit allowing current to flow from the water to the tip of the height gauge will close the instance the tip of the height gauge touches the water, similar to a water level sensor. A 12 volt light emitting diode (LED) connected to a relay switch will illuminate, indicating that the tip of the height gauge has made contact with the water surface as soon as the tip of the IVHG touches the lower nappe of the water flow over the sharp-crested weir. This enables one to make very precise measurements repetitively without penetrating

the nappe of the Ogee. (Section 3.2.16 describes the circuit used for the OPMI water sensor). The stainless steel tip was replaced with a copper tip to reduce the resistance of the electrical current in the tip.

In Table 3-17 is the pictorial sequel of the construction of the Ogee profile measuring instrument.

Table 3-17: Construction of the Ogee profile measuring instrument (OPMI)


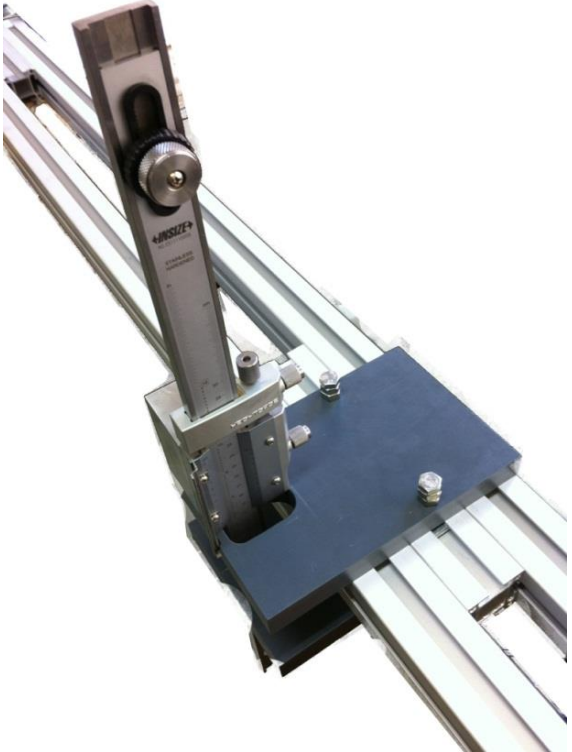




a. IVHG with fine adjustment.	b. IVHG moving mechanism fitted onto machined block of aluminium. Engineering plastic sliding mechanism allowing lateral movement in the Y-direction.
	

Table 3-17: Construction of the Ogee profile measuring instrument (OPMI) continue

<p>c. HBM LVDT allowing for automated recordings of measurements.</p>	<p>d. Assembled OPMI with stainless steel tip and LVDT attached.</p>
	
<p>e. Stainless steel tip, isolated by rectangular Plexiglass block, attached to OPMI</p>	<p>f. Stainless steel tip replaced with copper tip isolated by rectangular Plexiglass block.</p>
	

3.2.16 Installation of the water level sensor to the OPMI

The OPMI was fitted to a KEMO® *M158 Waterswitch* that functioned in the same manner as a water level sensor. The KEMO® *M158 Waterswitch* with geometric dimensions is given in **Figure 3-16**. The approach channel was fitted with a 75 mm x 150 mm x 2 mm copper plate and connected to the *Waterswitch* to function of one of the electrodes/sensors. The copper plate was submersed during normal operation. Providing a direct current of 500 mA via the 12V power supply, the instance the copper tip of the OPMI touch the lower nappe of the water flowing over the sharp-crested weir, the resistance in the circuit of the *Waterswitch* is more than the resistance for the current to flow via the water, at this instance the relay switch is triggered and the LED illuminate. A schematic layout of the circuit for the *Waterswitch* is given below in **Figure 3-17**.

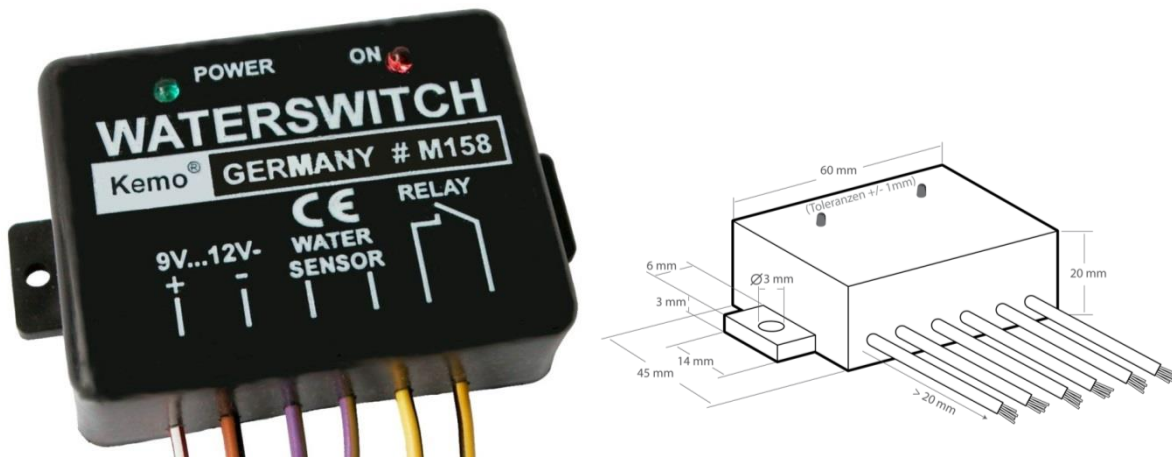


Figure 3-16: KEMO® *M158 Waterswitch* with geometric dimensions (KEMO®, 2012 (a))

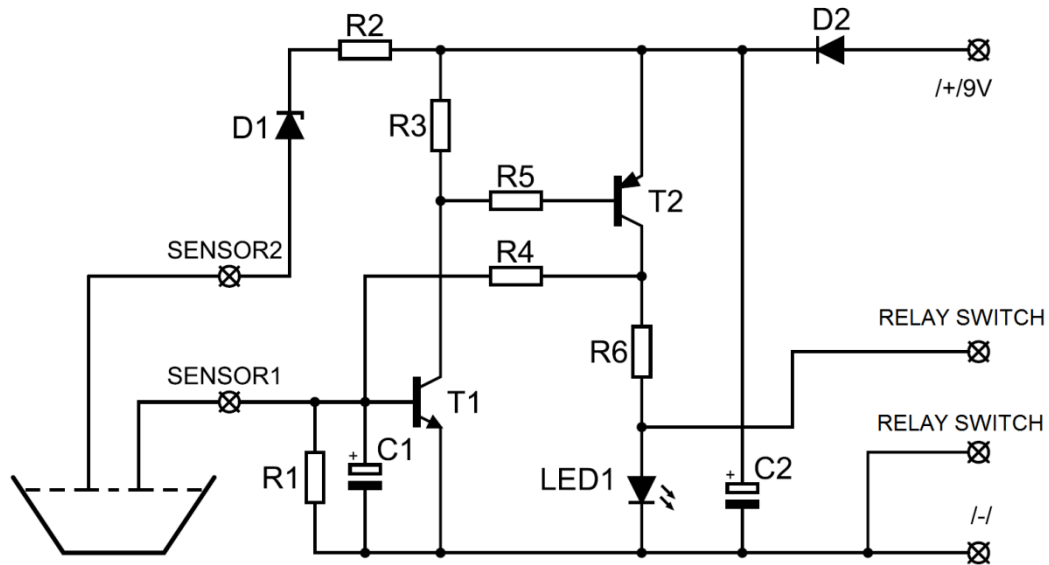


Figure 3-17: Water level sensor circuit (KEMO®, 2011)

To increase the conductivity of the copper tip fitted to the OPMI, the tip was coated with liquid conducting silver from KEMO®. The silver has a resistance of approx. $0.02 \Omega - 0.1 \Omega / \text{cm}^2$ (KEMO®, 2012 (b)).





Figure 3-18: Conducting Silver used to coat the copper tip of the OPMI (KEMO®, 2012 (b))

The complete assembly of the *Waterswitch* and 12V LED was fitted into a 150 mm x 300 mm x 150 mm plywood box with Plexiglas cover to prevent any possible short-circuit of the assembly due to the splashing of water in the near vicinity.

In **Table 3-18** is the pictorial sequel of the installation of the water level sensor to the OPMI.

Table 3-18: Installation of the water level sensor to the OPMI

<p>a. Approach channel fitted with a 75 mm x 150 mm x 2 mm copper plate and connected to the Waterswitch to function of one of the electrodes.</p>	<p>b. Complete assembly of the Waterswitch and 12V LED fitted into a 150 mm x 300 mm x 150 mm plywood box with Plexiglas cover</p>
 <p style="text-align: right; color: orange; font-size: small;">11 10 2012</p>	 <p style="text-align: right; color: orange; font-size: small;">11 10 2012</p>

3.2.17 Definition of Cartesian co-ordinate system

A right-handed Cartesian axis co-ordinate system was applied to the physical model to enable one to define each measuring position on the lower nappe to a unique XYZ-co-ordinate. All the measurements were made relative to the crest of the weir, thus requiring for each setup to calibrate and record zero position measurements. Measurements were taken at 10 mm intervals in the X-axis direction and at the 7 pre-determined positions along the crest of the sharp-crested weir as discussed in **section 3.2.8**. The copper point fixed to the OPMI was orientated in two positions during measurements. At a 90°/vertical orientation for the initial measurements and then rotated at an angle as the OPMI approaches the lower nappe of the flowing water over the sharp-crested weir and space became limited.

In **Table 3-19** is the pictorial sequel of the definition of Cartesian co-ordinate system.

Table 3-19: Definition of Cartesian co-ordinate system






<p>a. Mastercraft 1000 mm rulers fixed to extruded aluminium profiles. Intersection of X and Y axes.</p>	<p>b. OPMI slide mechanism fixed to the Y-axis.</p>
	
<p>c. XYZ-axis as defined for the physical model.</p>	
	

Table 3-19: Definition of Cartesian co-ordinate system continue...

<p>d. Calibration of OPMI taking zero measurements with vertical copper point at each measuring position along the crest of the weir.</p>	<p>e. Calibration of OPMI taking zero measurements with rotated copper point at each measuring position along the crest of the weir.</p>
	
<p>f. Taking measurements of lower nappe with vertical copper point.</p>	<p>g. Taking measurements of lower nappe with rotated copper point.</p>
	


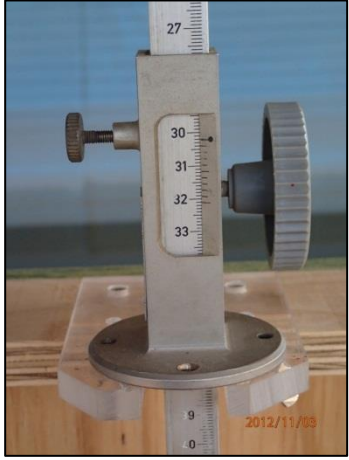


3.2.18 Installation of the stage depth meters with OTT-point gauges in stilling columns

Measuring the stage depth accurately is critical for calculating the discharge from the weir, and more so in relating the design head of the corresponding Ogee profile. The stage depth for a sharp-crested weir is defined as the level above the vertex notch of the crest. ISO 1438 (2008) recommends that the stage depth in the approach channel should be measured at least a distance upstream of 4 times the anticipated maximum stage. However, a more accurate assessment can be made by making use of stilling columns. Two stilling columns were installed and connected to the approach channel of the model via a 12 mm tube. The tubes were cleaned after the installation with Sunlight Liquid to reduce the effect of surface tension in the tubes. Fitting OTT-point gauges to the stilling columns, and ensuring that the point gauges are precisely vertical in 2 directions, it was possible to measure the stage depth accurately. In **Table 3-20** is the pictorial sequel of the definition of the OTT-point gauges used as water level meters in the stilling columns.

Table 3-20: Installation of water level meters in stilling columns

<p>a. Ensuring the OTT-point gauge are precisely vertical in 2 directions.</p>	<p>b. Two stilling columns and OTT-point gauge fitted to the approach channel of the model.</p>
	

Table 3-20: Installation of water level meters in stilling columns continue...

<p>c. Measuring the stage depth during 80 l/s flow scenario.</p>	<p>d. OTT-point gauge with vernier scale and fine adjustment screw.</p>
 <p>Two OTT-point gauges are shown installed in stilling columns. The columns are made of brick and have a wooden frame around the gauge. The gauges are connected to a data logger or computer system.</p>	 <p>A close-up view of the OTT-point gauge. The gauge has a vernier scale and a fine adjustment screw. The scale is marked with numbers 27, 30, 31, 32, and 33. The fine adjustment screw is on the right side. The gauge is mounted on a wooden base.</p>
<p>e. View of point gauge tip at the surface of the water in the stilling column.</p>	
 <p>A view of the point gauge tip at the surface of the water in the stilling column. The gauge is a vertical rod with a sharp point at the bottom. The water surface is visible, and the gauge is positioned vertically.</p>	 <p>A close-up view of the point gauge tip touching the water surface. The tip is a sharp, conical point. The water surface is visible, and the gauge is positioned vertically. A date stamp '2012/10/17' is visible in the bottom right corner.</p>

3.3 OTHER OGEE PROFILE MEASURING TECHNIQUES INVESTIGATED

Measuring the profile of the lower nappe when water is flowing over a sharp-crested weir can be both a time consuming and very difficult task. Measurements must be accurate, precise but even more so it should be repeatable. To measure the profile of the lower nappe various techniques and apparatus has been experimented with in the early stages of the study ranging from laser reflection on the water surface of the lower nappe, laser triangulation devices, laser profile devices, ultra-sonic displacement sensors, 3-dimensional photography and finally mechanical measurements.

At the end a mechanical measuring apparatus (the OPMI as discussed in **section 3.2.15**) was used to measure the nappe profile, both for its simplistic design, robustness, reliability and ability to give repeatable results. It does however not mean that the other methods/measuring instrumentation used for measuring the nappe profile can be discarded. Measuring the profile mechanically is both time consuming and the “human factor” cannot be excluded as the apparatus must be physically moved to each of the 7 locations along the crest of the sharp-crested weir. By measuring the Ogee profile at for example a discharge rate of 80 l/s at the assigned 7 positions along the crest of the sharp-crested weir can take up to 12 hours of physical measuring. Some of the laser and ultra-sonic apparatus can speed up the measuring procedure but are very costly and there is a risk of water damage.

3.3.1 Laser measuring apparatus

Some laser devices do not interfere with the normal flow of the water, thus making use of them may be a valuable method for measuring the Ogee profile. The crux of laser measurements are however the possible penetration of the laser beam into the layer of water, causing a false reading due to the reflection of the penetrated light wave on the opposing surface. It is however possible to overcome this problem by implementing a proper layout of the light source and accounting for the secondary reflected light waves, a high quality laser apparatus is also essential. In the following two sub-paragraphs the use of two laser apparatuses are briefly discussed namely a commercial *Laser Pointer* and a laser triangulation device, known as the *optoNCDT 2300* manufactured by Micro-Epsilon.

Laser Pointer

A commercial Laser Pointer was fitted to the lower side of the nappe of water flowing over a sharp-crested weir in view of making use of this apparatus to measure the profile of the Ogee curve. In theory by shining the laser beam at an angle greater than the refraction angle of water, the beam will be reflected from the surface of the water. Should the angle at which the beam is shined from be known, by making use of trigonometry, it is possible to calculate the position where it reflects from the water surface. Should the surface however be curved, as in the case of the Ogee profile the position of reflection would be more difficult to calculate, but still possible. By making use of a known reference position i.e. reflecting the laser beam at a mirror level with the crest of the sharp-crested weir and comparing it with the laser beam reflected from the same angle when reflecting from the surface of the lower nappe, the difference in the opposing co-ordinate can be used to calculate the curvature of the Ogee curve at that specific location. The curvature can then be transposed and used to calculate the position of reflection of the surface of the lower nappe.

A setup as describe was test at the Department of Water Affairs Hydraulic Lab on an existing physical model of a free falling weir, **Figure 3-19**. Results however, was difficult to interpolate since a small movement/instability of the nappe was dramatically emphasized on the opposing side where the beam position was measured resulting in unreliable results. A schematic layout of making use of this method is portrayed in **Figure 3-20**.



Figure 3-19: Existing physical model of free falling weir at the Department of Water Affairs Hydraulic Laboratory

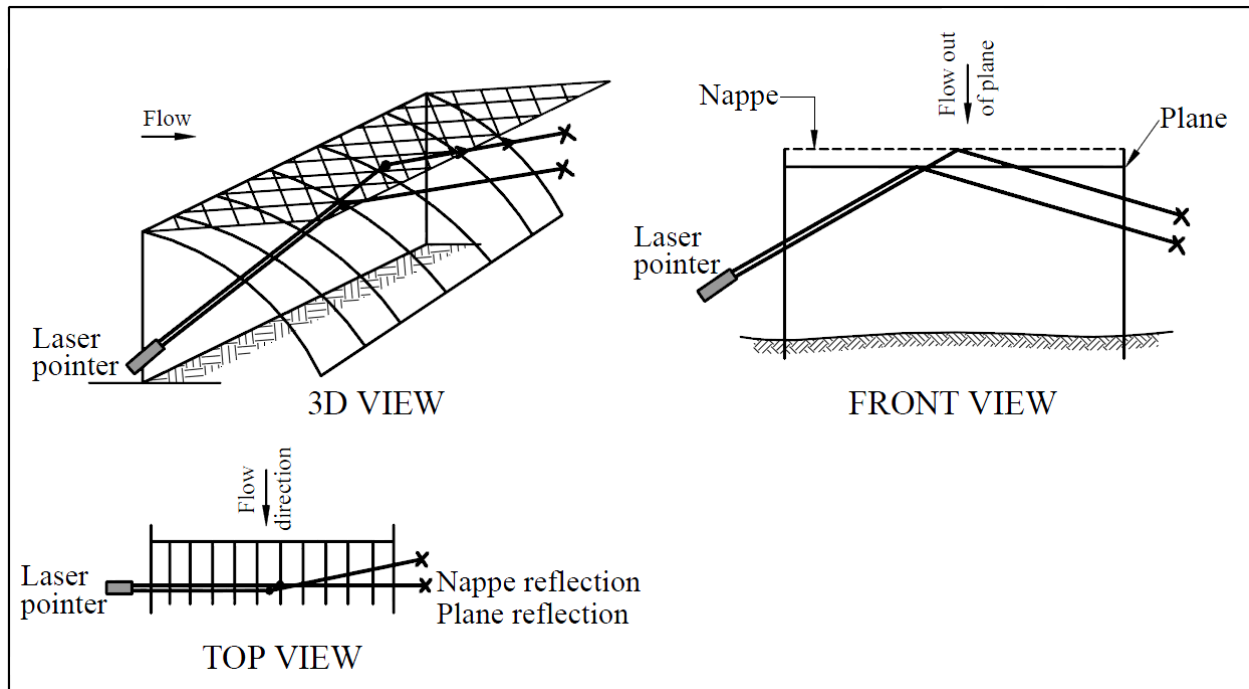


Figure 3-20: Schematic layout of making use of a Laser Pointer to measure the Ogee profile

Laser triangulation sensor: optoNCDT 2300 by Mirco-Epsilon

The optoNCDT 2300 is one of the latest high-end laser triangulation sensors from Micro-Epsilon and make use of the reflection of the red 1 mW semi-conductor laser installed to determine the distance between the apparatus and the measured surface. The optoNCDT 2300 is specially designed for fast measuring states with challenging surfaces, thus making it an ideal candidate for measuring the Ogee profile. The optoNCDT 2300 is schematically portrayed in **Figure 3-21**.



Figure 3-21: Laser triangulation sensor: optoNCDT 2300 by Mirco-Epsilon

ESTEIQ Group (Pty) Ltd provided a demonstration model of the optoNCDT 2300-100 laser triangulation sensor. This device had a measuring range of 100 mm and started measuring at a distance of 70 mm from the surface. The apparatus must be positioned at such an angle that the reflected laser beam from the surface is reflected to the “eye” of the sensor. When the device is positioned at this specific angle a green LED will indicate that measurements are being recorded.

A sharp-crested weir was constructed at the University of Pretoria’s Hydraulic Laboratory located on the Proefplaas. The weir was constructed to assess possible measuring techniques of the Ogee profile. The optoNCDT 2300-100 has the ability of measuring the surface of the lower nappe of the water flowing over the sharp-crested weir from the upper side of the water surface as indicated in **Figure 3-22**. The optoNCDT 2300-100 gave accurate and repeatable measurements. However, the device required to be positioned a specific angle where the laser beam is reflected back to the “eye” of the apparatus (i.e. a sweet spot) before measurements are made. This angle change constantly as one moves downstream of the nappe thus making it very time consuming to setup the apparatus. The relative position of the apparatus in reference with the weir’s crest also needs to be accurately defined before multiple measurements can be of any use. The cost of the optoNCDT 2300-100 without the Universal Controller

is over R50 000, and with long setup times the optoNCDT 2300-100 may not be the best alternative for measuring the Ogee profile.

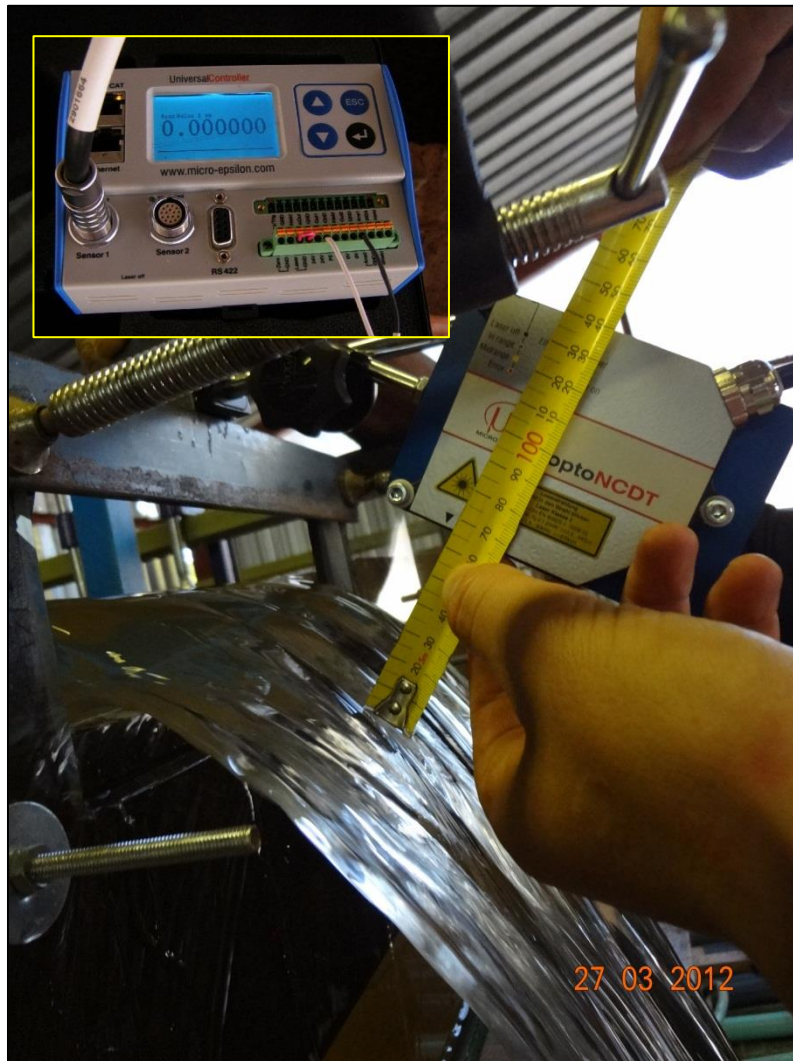


Figure 3-22: The optoNCDT 2300-100 measuring a co-ordinate on the Ogee profile from above the water surface at a sharp-crested weir

Other Laser displacement devices

The optoNCDT 2410 by Micro-Epsilon is a confocal displacement measuring device specially developed for measuring transparent materials and liquids. The optoNCDT 2410 by Micro-Epsilon can also measure the thickness of the material. Unfortunately ESTEQ Group (Pty) Ltd had no demonstration model in stock for testing the effectiveness of the apparatus. The relative location of the device needs to be determined before measurements can be undertaken. The cost of the device is over R100 000 and effectiveness of measurements is recommended before investing in such an instrument.

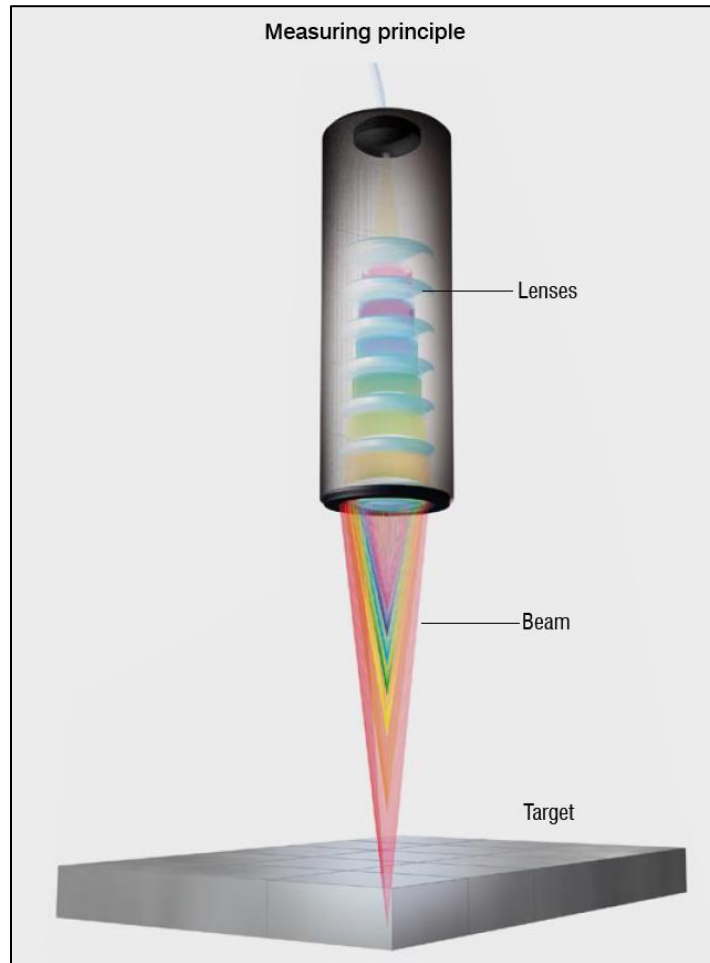


Figure 3-23: Confocal displacement measurement system: optoNCDT 2410 by Micro-Epsilon

The ultimate Ogee profile measuring apparatus would be a device that has the ability of processing 3-dimensional measured co-ordinates in a surface-like model. The CC3100 by Cross Check is a laser profile sensor that has this ability. Measuring a surface to an accuracy of 0,1 mm the possibilities of such an apparatus would make measurements fast, accurate and precise. Unfortunately cost of such an instrument or similar can easily exceed R500 000 making it impossible to use without adequate funding. A demonstration model is recommended before investing in such an apparatus to ensure measuring of moving water is possible and accurate.



Figure 3-24: Laser Profile Sensor (CC3100) by Cross Check

3.3.2 PhotoModeler® Scanner

PhotoModeler® Scanner (**Figure 3-25**) is a Windows software package that can be used to generate high resolution 3-dimensional models and accurate scaled measurements from photographs using ordinary digital cameras (PhotoModeler®, 2012). The software has the capability of generating dense point clouds of the surface of the models similar to a 3-dimensional laser scan, as discussed above.

PhotoModeler® Scanner's new feature called *SmartMatch*, allows you to generate photorealistic 3-dimensional models with high accuracy from digital photographs entirely automatically. The *SmartMatch* feature detects and matches natural features in images - giving automated project setup and 3-dimensional intelligence to the photo without the using additional targets on the model.

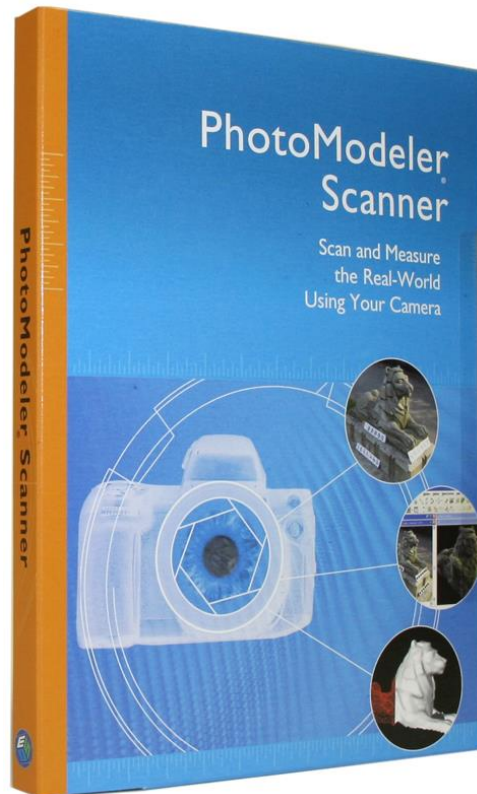


Figure 3-25: PhotoModeler® Scanner software package (PhotoModeler®, 2012)

The photographic software package was used in an attempt to generate a 3-dimensional surface of the lower nappe of water flowing over the sharp-crested weir. A guide channel in which the camera was secured (**Figure 3-27**) and lowered behind the nappe was constructed. A view of the lower nappe is indicated in **Figure 3-26**. In theory by recording a high definition AVI video clip, the frame images will be overlapping each other and can be used to generate a 3-dimensional model with the SmartMatch feature of the PhotoModeler® Scanner software.

Unfortunately a problem occurred in this measuring attempt. The transparency of the water caused instability in the software thus being not able to generate the 3-dimensional surface. Because a random pattern at the surface of the model is required to link the pixels of the various photos taken at different angles to the same object a solution to this problem might be by fixing a lightweight silk pattern sheet to the crest of the sharp-crest weir and allowing water to flow over the structure. This might be a solution in the rendering problem of the program. However, the possible influence of the flow pattern has to be investigated when attempting this. Unfortunately time was limited in the application of the PhotoModeler® Scanner software and further research in this topic is required.

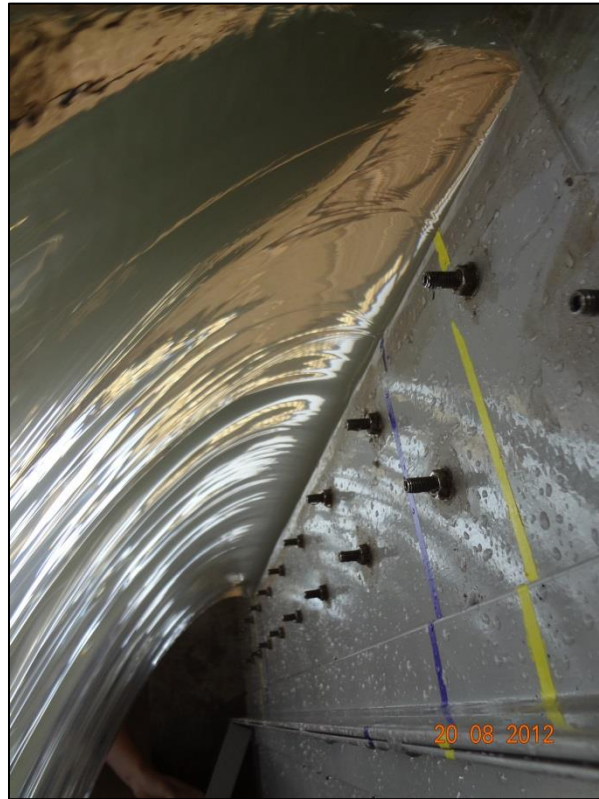


Figure 3-26: View of lower nappe from guide channel in which the camera was secured

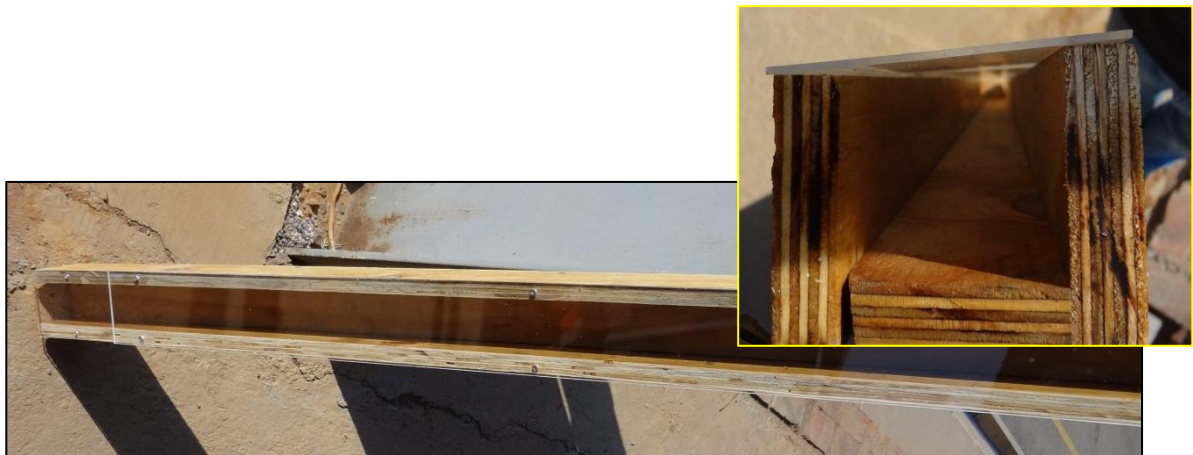


Figure 3-27: Guide channel in which the camera was secured constructed from plywood and Plexiglas

3.3.3 Ultra-sonic sensors

Various ultra-sonic sensors were briefly investigated to view its application in measuring the Ogee profile. One of the most promising sensors being the UC 500-30GM-IU-V1 by Pepperl + Fuchs GmbH, however suppliers were sceptical that the moving water might influence the signal strength sent by the sensor resulting in unreliable recordings (**Figure 3-28**). Accuracy of some ultra-sonic sensors may be much lower at 5 mm making it not suitable for measuring on a scaled physical model. Ultra-sonic sensors are therefore not recommended for measuring the Ogee-profile.

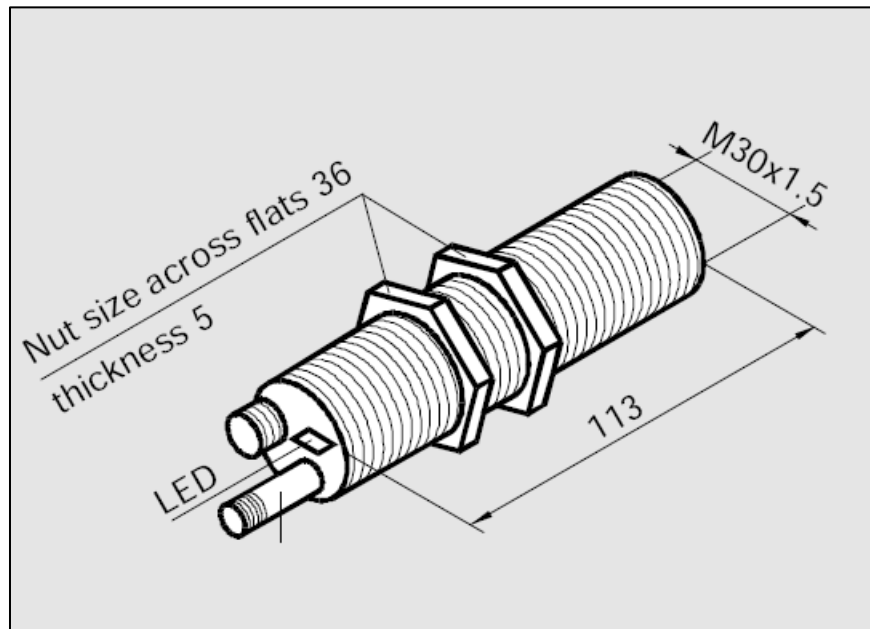


Figure 3-28: Ultra-sonic displacement sensor (UC 500-30GM-IU-V1) by Pepperl + Fuchs GmbH

3.4 PROCEDURE FOLLOWED DURING THE EXECUTION OF MEASURING THE OGEE PROFILE

In determining the effect that an asymmetrical approach channel has on the geometric shape of the Ogee profile it was required to be able to alter the properties affecting the nature of the flow and measure its influence. Dimensions of the approach channel, sharp-crested weir, as well as other properties with regards to the OPMI etc. were noted in **section 3.2**. Considering the characteristics of the physical model and the layout it was possible to design a plan for the execution of the experiment. This execution plan is described in more detail in the following paragraphs.

In order to make an analysis of any sort it is required to measure the baseline Ogee profile in a symmetrical approach channel and to compare the effects of an asymmetrical approach channel with it. However, before any measurements of the Ogee profile could be performed it was required to have an accurate, calibrated measuring apparatus. The OPMI was calibrated to record displacement measurements of the lower nappe of water flowing over the sharp-crested weir relative to the crest of the weir. By doing so, the effect of sagging caused by the slenderness of the extruded aluminium beam profiles, as well as the offset of the aluminium frame relative to the crest of the sharp-crested weir can be disregarded.

The OPMI was calibrated before measuring the Ogee profile for each scenario. Calibrating the OPMI required one to measure the relative offset of the copper tip attached to the top of the OPMI relative to the crest of the weir, as well as measuring the vertical displacement of the copper tip to the crest of the weir. The offset and the vertical displacement were measured when the copper tip was level and orientated vertical with the crest of the sharp-crested weir and the measurement was repeated for the case when the copper tip was level and rotated relative to the crest of the sharp-crested weir.

Measuring the offset of the copper tip of the OPMI relative to the crest of the weir for both the vertical and rotated orientation settings was made with an electronic vernier ruler and is indicated in **Figure 3-29**.

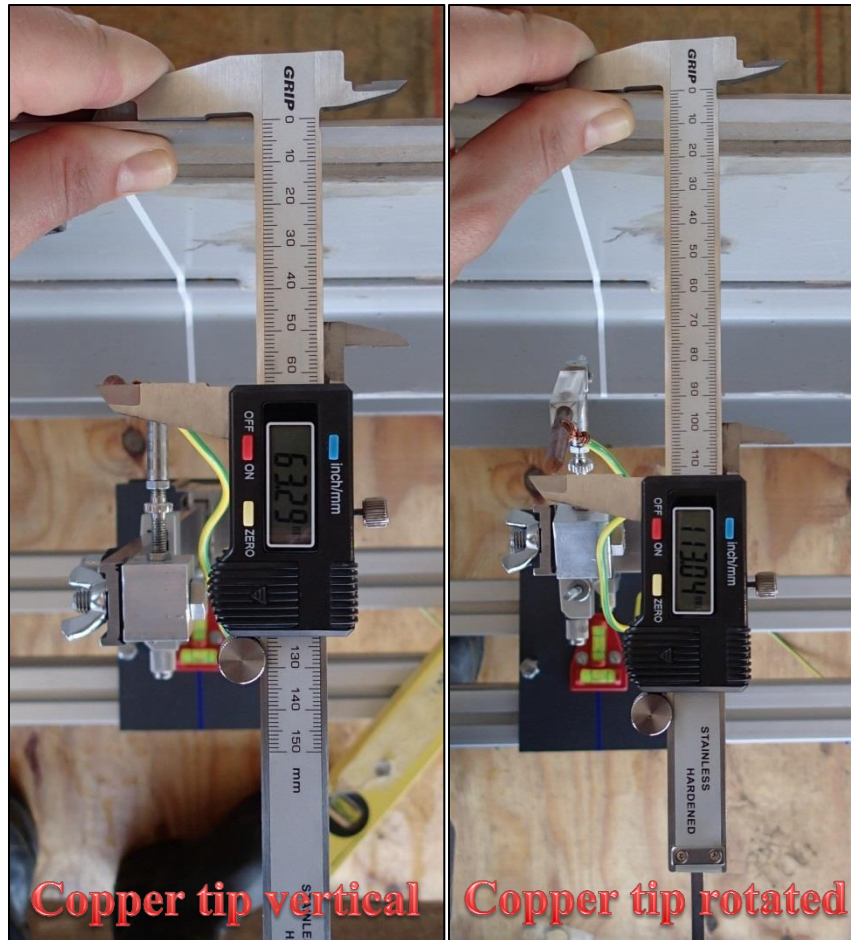


Figure 3-29: Offset of the copper tip of the OPMI relative to the crest of the weir (vertical - left, rotated - right)

Measuring the vertical displacement of the copper tip of the OPMI relative to the crest of the weir for both the vertical and rotated orientation settings was made with the vernier scale installed on the OPMI and is indicated in **Figure 3-29**.



Figure 3-30: Vertical displacement of the copper tip of the OPMI relative to the crest of the weir (vertical - left, rotated - right)

The offset measurements were defined as X_0 readings and the vertical displacement measurements were defined as Z_0 readings. By recording these measurements at the 7 locations where the Ogee profile was measured along the crest of the sharp-crested weir one has a “reference surface” onto which all measurements were made. Thus by subtracting the “reference surface” from the measured displacements of the Ogee profile one obtains the actual geometric dimensions of the Ogee profile.

A typical reference surface is indicated in **Figure 3-31** for the case when the copper point tip was vertical as well as when the copper tip was rotated.

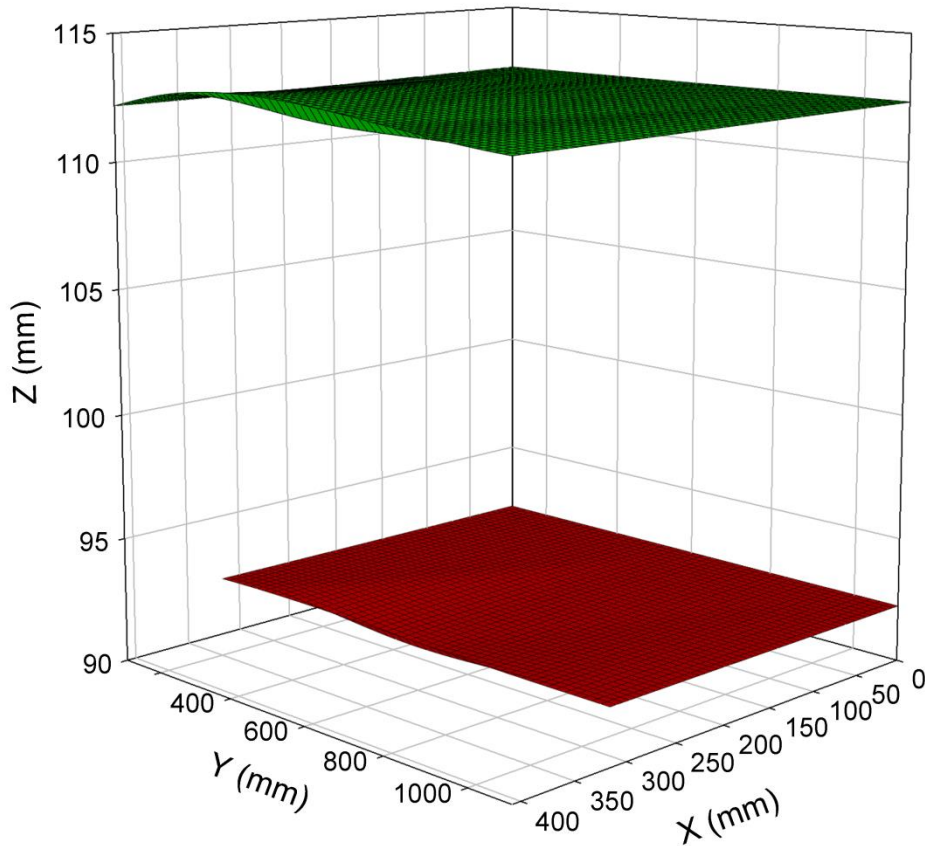


Figure 3-31: “Reference surface” for scenario 2 with the green surface reflecting the case of the rotated copper tip and the red surface that of the case of the vertical copper tip

Once the OPMI was setup and calibrated, baseline recordings of the Ogee profile was undertaken. These baseline recordings refer to a symmetrical approach channel layout and were conducted at a flow rate of 60 l/s and 80 l/s. Symmetrical approach channel refer to the case when no additions were made to the geometric cross-section of the approach channel. The graphical presentation of all the measured Ogee curves are discussed and given in **Chapter 4** of this dissertation. Measurements of the Ogee profile was recorded at intervals of 10 mm measured on the *Mastercraft* steel rulers attached to the extruded aluminium profile beams supporting the slide mechanism of the OPMI. These intervals were measured along the X-axis of the system and are graphically portrayed in **Figure 3-32**. As the flow rate increase the Ogee profile increase and profile measurements was extended up to 190 mm measured from the crest for the flow rate of 130 l/s.

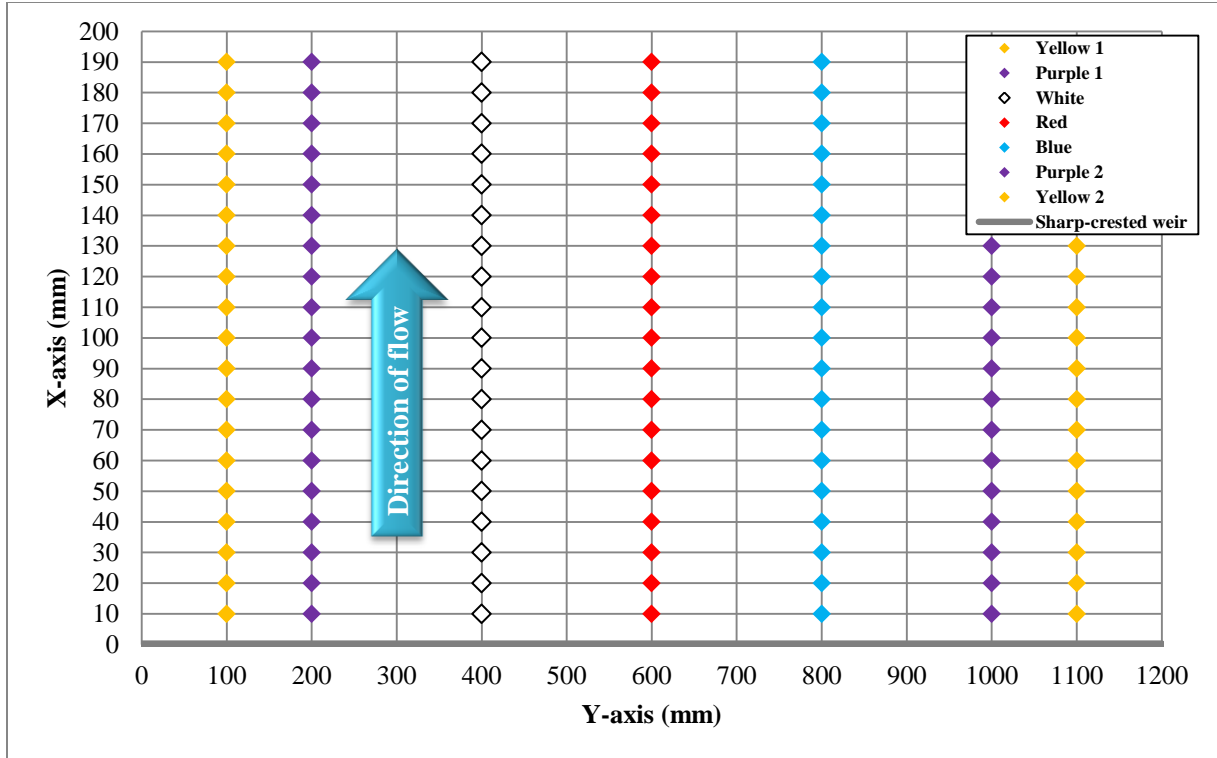


Figure 3-32: Measurements of the Ogee profile was recorded at 10 mm intervals

The schematic layout of the symmetrical approach channel is given in **Figure 3-33**.

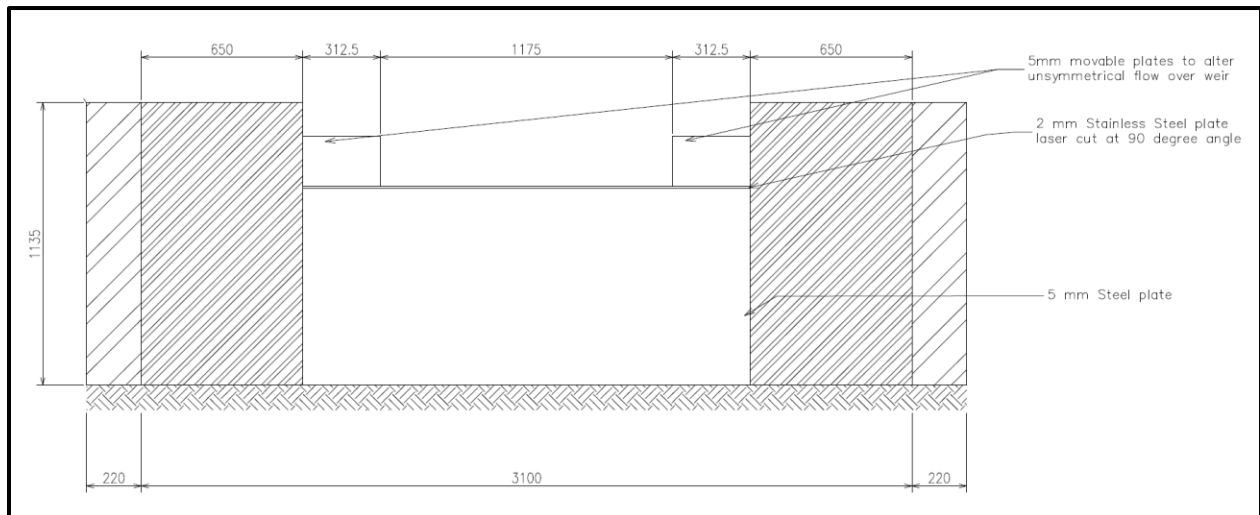


Figure 3-33: Upstream view of the layout for the symmetrical approach channel

The symmetrical approach channel baseline scenarios were compared with asymmetrical approach layouts that were conducted at various flow rates. The flow rate ranges from 80 l/s to 130 l/s as given by

the installed magnetic flow meter at the Department of Water Affairs Hydraulic Laboratory. The asymmetry of the approach channel was achieved by changing the inclination of the installed plywood sidewall as discussed in **section 3.2.13**. The inclination of the plywood sidewall was set at 45° and 60° respectively and was verified mathematically by trigonometry. In **Figure 3-34** was a protractor indicating the inclination of the installed plywood sidewall.

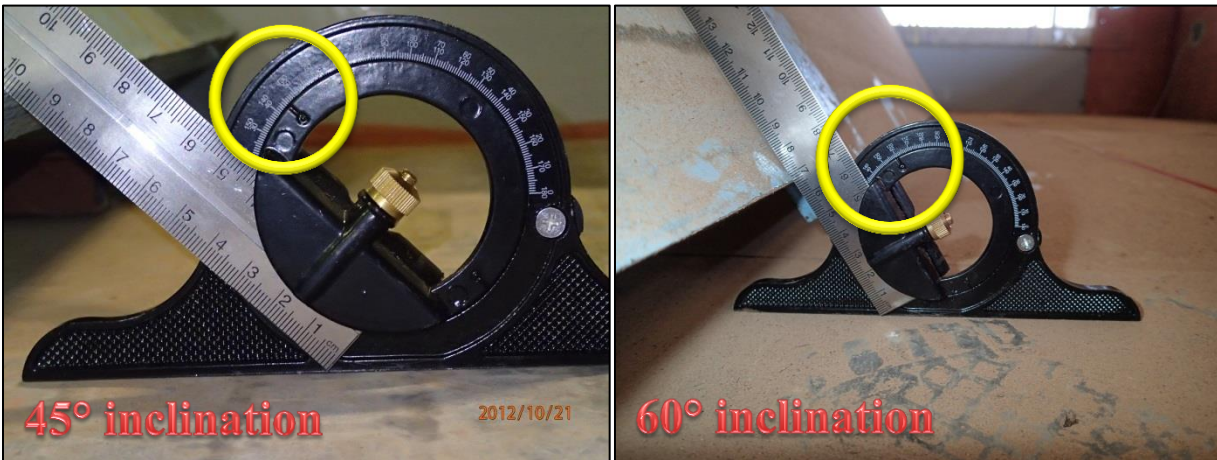


Figure 3-34: Protractor indicating the inclination of the installed plywood sidewall at 45° and 60° respectively

The various scenarios executed were labelled as in **Table 3-21** and were referred to in the rest of the dissertation by the notation given in the table.

Table 3-21: Various scenarios executed with allocated notation

Label/Notation	Description of approach channel	Flow rate as given by the magnetic flow meter	Section in the dissertation
Scenario 1	Symmetrical (Baseline)	60 l/s	4.1.1
Scenario 2A	Symmetrical (Baseline)	80 l/s	4.1.2
Scenario 2B	Asymmetrical; sidewall inclined at 45°	80 l/s	4.1.3
Scenario 2C	Asymmetrical; sidewall inclined at 60°	80 l/s	4.1.4
Scenario 3A	Asymmetrical; sidewall inclined at 45°	130 l/s	4.1.5
Scenario 3B	Asymmetrical; sidewall inclined at 60°	115 l/s	4.1.6

For each of the scenarios conducted, a datasheet was setup in Microsoft® Excel was populated to record all the required measurements. An example of such a data sheet is given in **Figure 3-35** (Afrikaans version). These populated data sheets are attached in **Appendix A on the supporting CD** of the dissertation.

<u>Datum:</u>		<u>Beskrywing:</u>					
		<u>Vloei tempo:</u>					
	Punt regop	Punt skuins		Kruin Hoogte			
	X=150	X=150		Punt regop	Punt skuins	A (Roes)	B
Posisie	X ₀	X ₀ '	Kruin afstand	Z ₀	Z ₀ '	Guage Redings at No Flow	
Geel 1			Y ₀			Guage Redings at Max Flow	
Pers 1							
Wit							
Rooi							
Blou							
Pers 2							
Geel 2							

<u>Lesing 1 @ X = 100 mm</u>		<u>Lesing 2 @ X = 110 mm</u>	
Posisie	Z-lesings	Vloei tempo	
Geel 1		Tyd	
Pers 1			
Wit			
Rooi			
Blou			
Pers 2			
Geel 2			

<u>Lesing 3 @ X = 120 mm</u>		<u>Lesing 4 @ X = 130 mm</u>	
Posisie	Z-lesings	Vloei tempo	
Geel 1		Tyd	
Pers 1			
Wit			
Rooi			
Blou			
Pers 2			
Geel 2			

Figure 3-35: Datasheet complete for each scenario conducted (Afrikaans version)

The stage depth measured in the stilling columns by the two OTT-point gauges were averaged and converted to the design head of an equivalent Ogee structure. This was achieved by making use of **Equation 2-7** as defined by Rajaratnam *et al.* (1968) that stipulates:

$$C' = 0.112 \cdot H_d \cdot \frac{0.4v_o^2}{2g}$$

Equation 2-7

Where:

- H_d - water depth on the crest (m)
- C' - the vertical displacement of the particle at x = 0 m (m)
- v_o - the initial velocity of the water particle (m/s)

g - gravitational acceleration acting onto the water particle (m/s^2)

The measured Ogee profile for each of the scenarios was plotted by means of *SigmaPlot* version 12.3 in a 3-dimensional XYZ surface plot together with the theoretical equivalent Ogee profile as defined by the USACE (1970). These 3-dimensional XYZ surface plots are discussed in **Chapter 4**.

The calibrated flow rate was determined by making use of the calibration factors determined in **Figure 3-4**. These calibrated flow rates were used to estimate the unit flow rate per meter width.

3.5 MOTIVATION FOR THE EXPERIMENTAL METHOD USED

Many open channel flow problems, like this one are unique and have complex boundary conditions due to their site specific geometric design. The boundaries can be equivalent to the 3-dimensional flow parameters that are discussed earlier in this dissertation and may be in a sense insolvable by theory or by reference to standard empirical data. In such a case the solution to these parameters is found either by physical hydraulic modeling or, more recently, by numerical modelling (CFD analysis). There is extensive examples in physical scale modeling which allows for the Froude model results to be interpreted by engineers to aid in the prediction of prototype behaviours (USACE (a), 1987; USACE, 1970). However, more recently computing power has increased dramatically and more numerical models and software packages may be offered as a feasible alternative. Large integrated systems may still be problematic and before numerical output results can be accepted, they must be validated with real life scenarios and experience by engineers. Constraints due to time, computing power, input boundary conditions and model limitations, can cause approximations by numerical models to result in flow patterns to be incorrectly modeled. A physical model is a feasible alternative to solve difficult boundary conditions in complex and integrated systems where 3-dimensional flow is prominent and this was thus also the reason for the selection of a physical model as premises for this research study.

From the outset of the project, the experimental setup was planned to be conducted at the Department of Water Affairs (DWA) Hydraulic Laboratory in Pretoria West instead of at the University of Pretoria's Hydraulic Laboratory (Proefplaas). The Department of Water Affairs (DWA) Hydraulic Laboratory has an extended capacity to provide a constant flow rate in excess of 130 l/s unlike the University of Pretoria. The larger capacity allowed the construction of a larger scaled physical model, permitting one to neglect the scale effects that may be caused by the viscosity and surface tension of the water that may distort the

results in a small scale application. Increasing the model's size allows for more realistic and accurate results that can be applied readily to real life situations.

A physical model constructed of this size allows one to obtain repeatable and accurate measurements of the Ogee profile that might not always be possible when conducted on a smaller scale.

The precision construction of the sharp-crested weir was being handled by a third party (Interlock Systems) due to the instrumentation needed to construct such a weir. There were delays in the production of the weir, which limited the amount of time available for testing. Nevertheless, this was not detrimental as the Department of Water Affairs (DWA) Hydraulic Laboratory provided access to the premises to work after-hours.

The major concern with the experimental setup was selecting the correct instrumentation to measure the profile of the nappe. The following options were considered, among a few other less significant ones (**Section 3.2** and **Section 3.3**):

- Laser sensor by reflection;
- Laser sensor by triangulation;
- Confocal sensor;
- Laser Profile Sensor;
- Photographic modelling;
- Ultrasonic sensor; and
- Mechanical gauge instrumentation (OPMI).

The last option was selected for the following reasons:

- The confocal sensor and the laser sensor which uses triangulation, although having an immensely high accuracy, had a cost far beyond the budget of the research project.
- Tests were conducted to see whether a laser could be reflected off the nappe onto a specific spot. The tests showed that it produced a reflected line which experienced large movement. Another concern was whether the laser reflected off the upper or lower surface of the nappe.
- The accuracy of the ultrasonic sensor when measuring water was not as high as the experiment required.

- It was discovered that the photographic modelling software was unable to model transparent objects, rendering the same problem with water although further research in this aspect is recommended.

The mechanical measuring apparatus (OMPI) was used as it had sufficient accuracy (± 0.1 mm), was robust to the effect of water and constructing the OPMI was within the project budget. The OPMI achieved reliable, repeatable and within reason accurate measurements of the Ogee profile.

3.6 OBSTACLES FACED DURING THE PROJECT

The outcome of the research project reflected what the influence was of an asymmetrical approach channel on the geometric shape of the free surface bottom nappe for water flowing over a sharp-crested weir. There were some issues that arose during the course of the study which did not impair the outcome but merely redirected the planning of the experiment. These issues required alternative solutions to be made, which did produce meaningful results able to provide insight into the postulated hypothesis. The obstacles were as follows:

- Instrumentation Cost: As was previously mentioned, the cost of some of the preferred measurement instrumentation was extremely expensive. The cost of the confocal sensor was quoted at approximately €14 000, which at the time was just below R150 000. The laser sensor was initially quoted at approximately R30 000, but was increased to R50 000. A great advantage of these instruments is their ability to continuously log data measurements electronically.
- Time to Measure: The measurement of the nappe mechanically is a time consuming experiment. The location where the physical model was constructed was located in a large steel shed together with 4 other models. Sudden as well as gradual variations in the nappe shape might have occurred from time to time as the shed's sides were open and only the slightest gust of wind would cause movement of the water in the approach channel because of its large surface area. If the recordings were able to be logged continuously, this would not have been too much of a problem as the statistical mean would be able to be used. The fluctuation of the nappe was the most prominent at the side boundaries as can be seen in **Figure 3-36** where a sequence of photos has been taken during a gust of wind at the Yellow1 measuring location. However, the solution was that great care was taken in the reading of each measurement and allowing the nappe to soothe should a gust of wind have occurred. The interaction of the OPMI with the nappe was

monitored until the copper tip was at the peak height that maintained interaction, and this was done consistently for all measurements.

The Ogee profile for different scenarios was measured with the OPMI. These profiles were analysed and compared with that of the 2-dimensional approximations by Hager, (1987); Ministry of Science and Technology (2007); USACE (1987); and the USBR (1987). The 7 positions along the crest where the Ogee profile was measured were combined to form the surface of the lower nappe for the water flowing over the sharp-crested weir. These surface plots were recorded with XYZ-coordinates and are reflected in the following chapter. The analyses of the experimental data en discussion of the results are reflected in Chapter 4 of this dissertation.

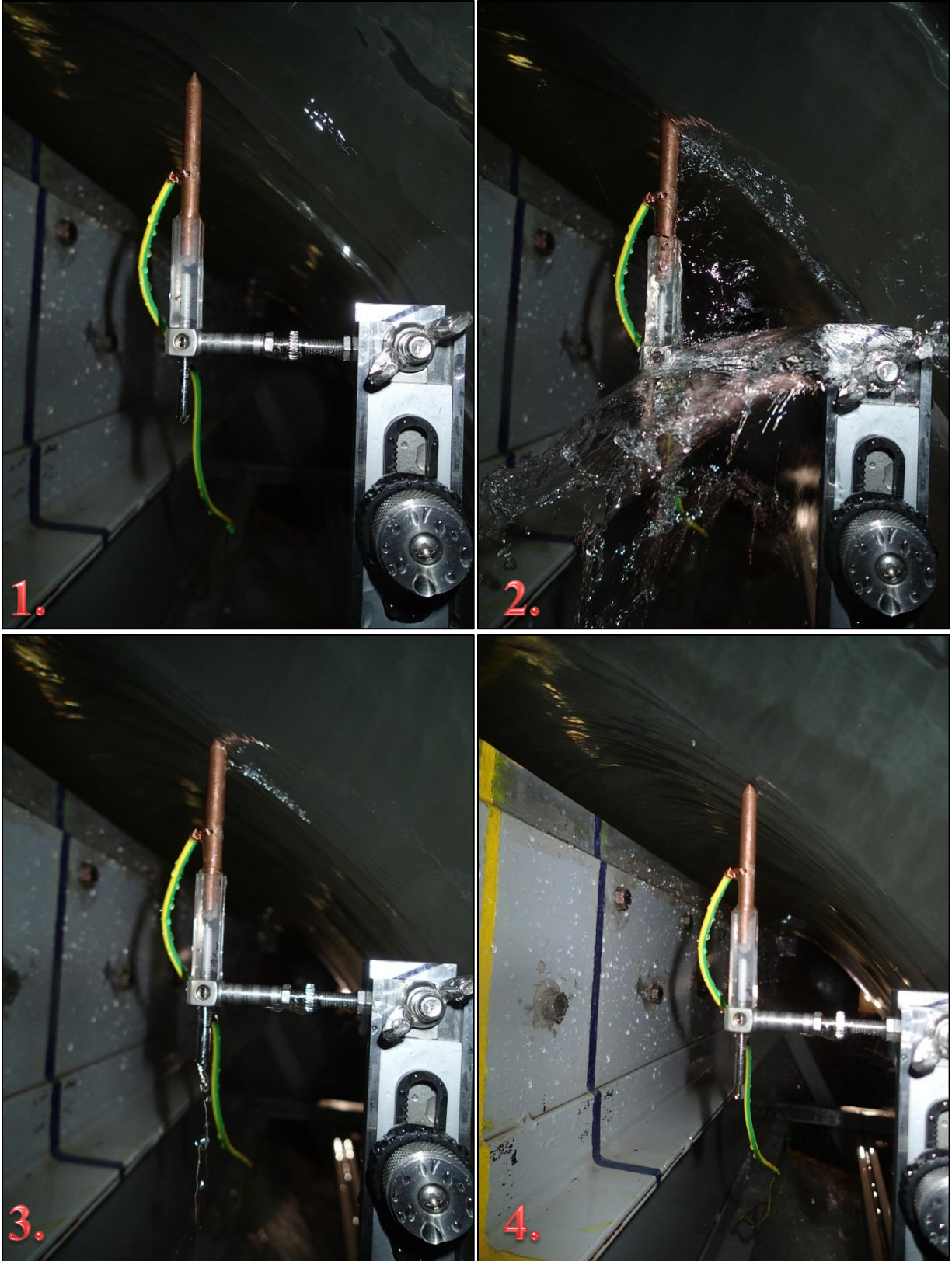


Figure 3-36: Gust of wind causing fluctuation in the Ogee profile at measuring location Yellow 1

4 ANALYSIS OF EXPERIMENTAL RESULTS AND COMPARISON WITH THEORY

The experimental results produced by the asymmetrical approach channel generated 7 Ogee curves for each channel configuration, representing the 3-dimensional shape of the asymmetrical bottom nappe. In the case of the symmetrical base line recordings, the Ogee curve was measured at 5 increments along the crest of the sharp-crested weir, representing the 3-dimensional shape of the symmetrical bottom nappe. These measured curves were the shape of the nappe that extends from the left boundary, centre, and up to the right boundary of the nappe. The positions of the curves were chosen so that all the scenarios would be able to be analysed individually and compared with the other configurations. Each point that was measured was recorded as a 3-dimensional XYZ coordinate. These coordinates were logged in a spreadsheet and then graphically depicted using Microsoft® Excel and Sigma Plot v. 12.3.

4.1 DISCUSSION OF RESULTS

The measured Ogee profiles obtained for each of the scenarios are discussed in more detail in this section of the dissertation. The Ogee profile was measured along the crest of the sharp-crested weir at 7 locations except for the case of the baseline measurements (scenario 1 and scenario 2A), which was measured only at 5 locations (Yellow 1, Purple 1, Red, Purple 2 and Yellow 2). The baseline measurements were only recorded at 5 locations as the approach channel was symmetrical for these scenarios and increasing the density of measurements would not affect the outcome of the analysis. The distances along the crest where the recordings were conducted are reflected in **Table 3-9** and is repeated below:

Table 3-9: Colour coded locations where the Ogee curve was measured along the crest of the sharp-crested weir *repeated*

Position	Location along the crest of the sharp-crested weir
Yellow 1	100 mm
Purple 1	200 mm
White	400 mm
Red	600 mm
Blue	800 mm
Purple 2	1000 mm
Yellow 2	1100 mm

Note: * *measured from left to right, when viewed from upstream of the physical model*

The scenarios that were analysed as depicted in **Table 3-21** are repeated below:

Table 3-21: Various scenarios executed with allocated notation (*Table repeated*)

Label/Notation	Description of approach channel	Flow rate as given by the magnetic flow meter	Section in the dissertation
Scenario 1	Symmetrical (Baseline)	60 l/s	4.1.1
Scenario 2A	Symmetrical (Baseline)	80 l/s	4.1.2
Scenario 2B	Asymmetrical; sidewall inclined at 45°	80 l/s	4.1.3
Scenario 2C	Asymmetrical; sidewall inclined at 60°	80 l/s	4.1.4
Scenario 3A	Asymmetrical; sidewall inclined at 45°	130 l/s	4.1.5
Scenario 3B	Asymmetrical; sidewall inclined at 60°	115 l/s	4.1.6

The discussion of each scenario comprises of the 2-dimensional XZ-plot of the measured profile, as well as a 3-dimensional XYZ-plot and comparison with the theoretical Ogee profile as recommended by the USACE with upstream 3 compound circular curve layout and downstream power function (USACE, 1970).

4.1.1 Scenario 1: Symmetrical Approach Channel with flow rate at 60 l/s

The flow rate was set to 60 l/s by adjusting the full bore butterfly valve as discussed in **section 3.1.2**. The constant flow rate yielded a stage depth of 88,3 mm measured from the crest of the sharp-crested weir to the water surface in the stilling column. This stage depth is equivalent to a design head (H_d) of 78,58 mm for an Ogee crest spillway, calculated by making use of **Equation 2-7**. The recorded flow rate of 59,59 l/s (measured by the installed magnetic flow meter) was calibrated by making use of the calibration factors as given in **Figure 3-4**. The actual discharge from the sharp-crested weir was equivalent to 53,78 l/s ($q = 44.779$ l/s/m).

The Ogee profile was measured at 5 locations along the crest of the weir. 35 measurements were made at increments of 10 mm in the direction of the X-axis. These measurements are depicted in a 2-dimensional XZ-plot in **Figure 4-1**, and are being compared with the theoretical Ogee profile for a design head of 78,58 mm as estimated by the USBR (1987), USACE (1970), Hager (1987) and Ministry of Science and Technology (CE-05016) (2007). The populated datasheet containing the measurements of the Ogee profile can be view in Appendix A on the supporting CD of this dissertation.

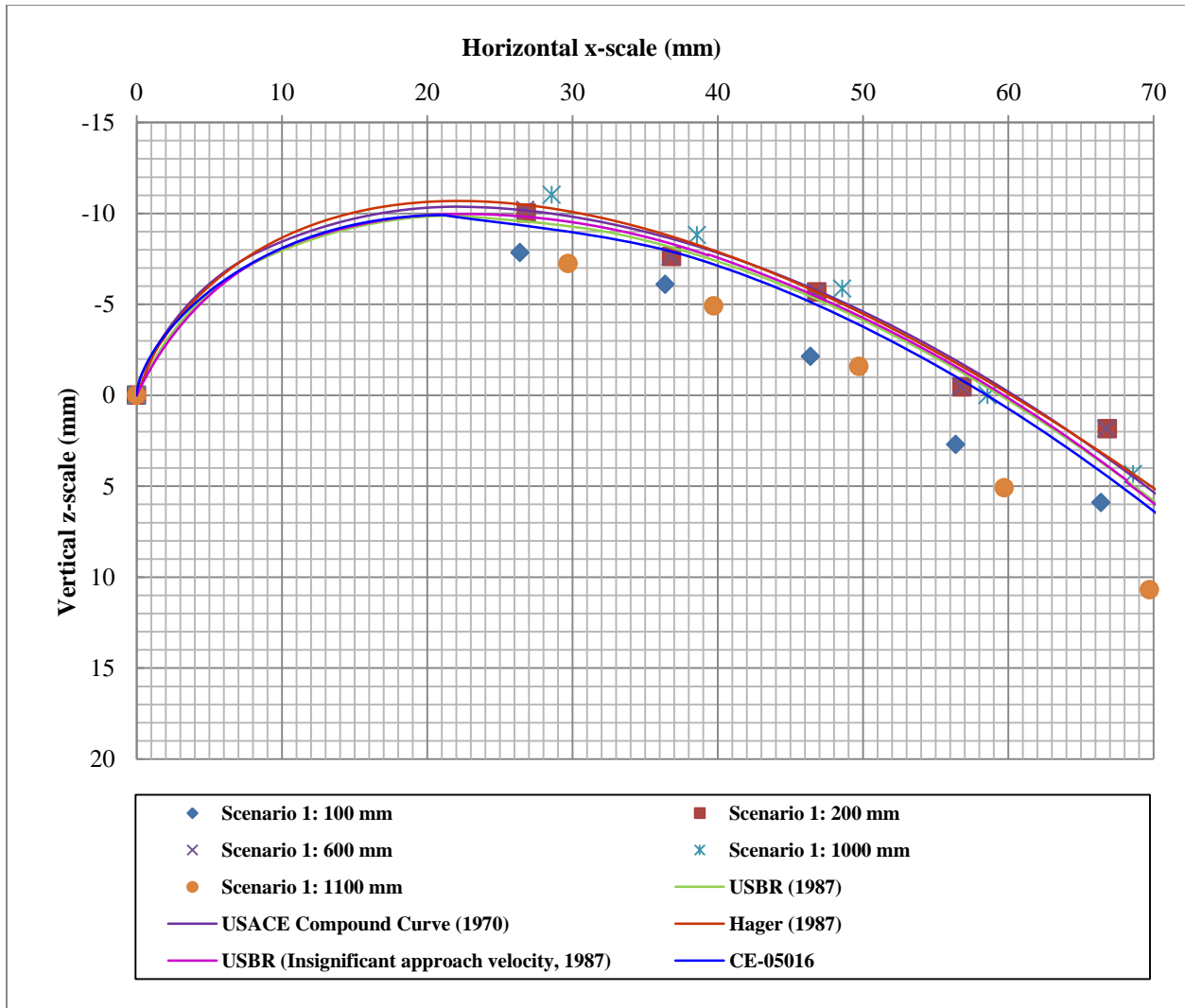


Figure 4-1: 2-dimensional plot of measured Ogee profile for scenario 1

Noticed in the 2-dimensional plot of scenario 1 that the Ogee profile in the centre of the nappe was greater than those measured at the outer boundary. This trend was also noticed in the final results where the surface plot of the measured nappe was depicted in a XYZ-plot (**Figure 4-5**). This phenomenon was visible in all of the scenarios and therefore is not ascribed to inaccurate measurements. However, there are two possible reasons to which this phenomenon could be attributed:

- The velocity of the water at the centre of the weir has a velocity vector component directed only perpendicular to the crest of the weir; whereas the water further from the centre of the weir may have small velocity components at an angle to the weir, due to the fact that the weir is a fully-contracted sharp-crested weir. The contraction means that the water flowing over the weir nearer

to the edges will have approached the channel at an angle, even if this angle is slight. This was also visible in photos taken during the experiment of the contracted flow at the boundary of the crest indicating the redirected flow lines (**Figure 4-2**).

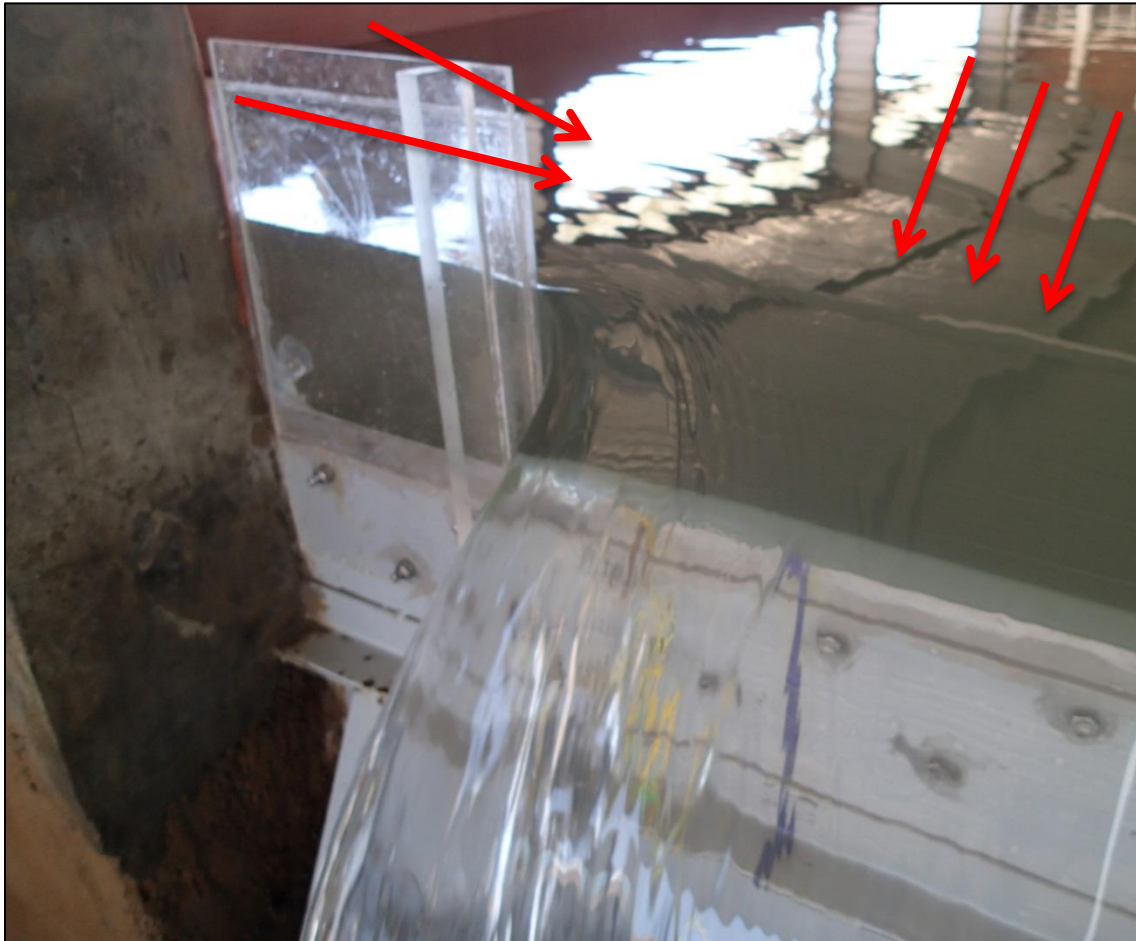


Figure 4-2: Prominent flow pattern visible at boundaries due to change in flow direction caused by contraction of the weir

- The irregular flow patterns in the approach channel were not completely avoided where water is being discharged upstream of the flow straighteners. However, this might only been the case if the physical model's approach channel was relatively small in relation to the crest structure. In this case the approach channel's volume capacity of $\pm 30 \text{ m}^3$ meant that the approach velocity in the channel approaches $0,026 \text{ m/s}$ which is unlikely to cause prominent flow patterns at the crest of the weir. The smooth water surface in **Figure 4-3** is evidence of no significant flow patterns occurring in the approach channel.



Figure 4-3: Smooth water surface of the approach channel evidence of no prominent flow patterns existing in the channel

It is thus concluded that the velocity in the centre of the crest has less resistance and is directed perpendicular to the crest. This indicates that the theoretical approximations of the Ogee profile tend to under-estimate the measured Ogee profile at the centre of the weir.

The maximum variance of the measured Ogee profile versus the theoretical Ogee profile by the USACE (1970) for each of the measuring positions along the crest of the weir is given in **Table 4-1**.

Table 4-1: Maximum variance of the measured Ogee profile during scenario 1 at the different measuring locations

In-plane X-coordinate of measurement (mm)	Theoretical Ogee Z-coordinate (mm)	Measured Ogee Z-coordinate (mm)	Difference (+/-mm)
At 100 mm (Yellow1)			
0.0	0.0	0.0	0.0
26.4	-10.3	-7.8	-2.5
36.4	-8.9	-6.1	-2.8
46.4	-6.6	-2.1	-4.5
56.4	-2.4	2.7	-5.1
66.4	2.0	5.9	-3.9
Maximum variance within crest region (X < 60 mm)			5.1
At 200 mm (Purple1)			
0.0	0.0	0.0	0.0
26.8	-10.2	-10.0	-0.2
36.8	-8.9	-7.6	-1.3
46.8	-5.9	-5.7	-0.2
56.8	-2.4	-0.5	-1.9
66.8	3.2	1.8	1.4
Maximum variance within crest region (X < 60 mm)			1.9
At 600 mm (Red)			
0.0	0.0	0.0	0.0
26.8	-10.2	-10.2	0.0
36.8	-8.9	-7.6	-1.3
46.8	-5.9	-5.7	-0.2
56.8	-2.4	-0.5	-1.9
66.8	3.2	1.8	1.4
Maximum variance within crest region (X < 60 mm)			1.9
At 1000 mm (Purple2)			
0.0	0.0	0.0	0.0
28.6	-10.2	-11.0	0.8
38.6	-8.4	-8.8	0.4
48.6	-5.9	-5.9	0.0
58.6	-1.4	0.0	-1.4
68.6	3.2	4.3	-1.1
Maximum variance within crest region (X < 60 mm)			1.4
At 1100 mm (Yellow2)			
0.0	0.0	0.0	0.0
29.7	-10.0	-7.2	-2.7
39.7	-8.4	-4.9	-3.5
49.7	-5.1	-1.6	-3.5
59.7	-1.4	5.1	-6.5
69.7	4.5	10.7	-6.2
Maximum variance within crest region (X < 60 mm)			6.5

Note: * *Recordings where an under estimation of the Ogee nappe was recorded are highlighted in red. These are the critical positions on the Ogee profile*

The measured Ogee profile is plotted as a red surface in a 3-dimansional XYZ-plot in **Figure 4-4**. Overlapping the measured Ogee surface plot in **Figure 4-5** is the theoretical Ogee profile by the USACE (1970) depicted by the green surface.

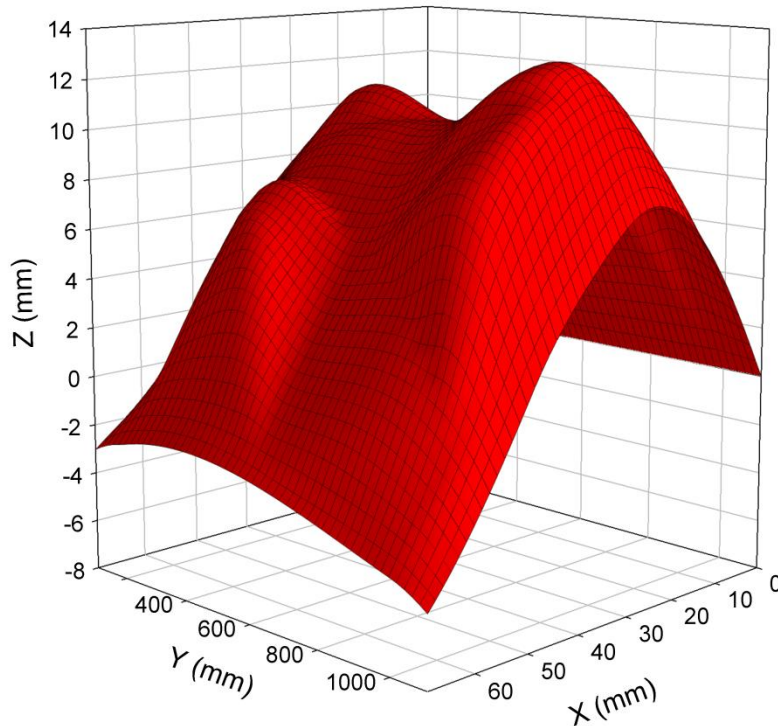


Figure 4-4: Measured Ogee surface for scenario 1

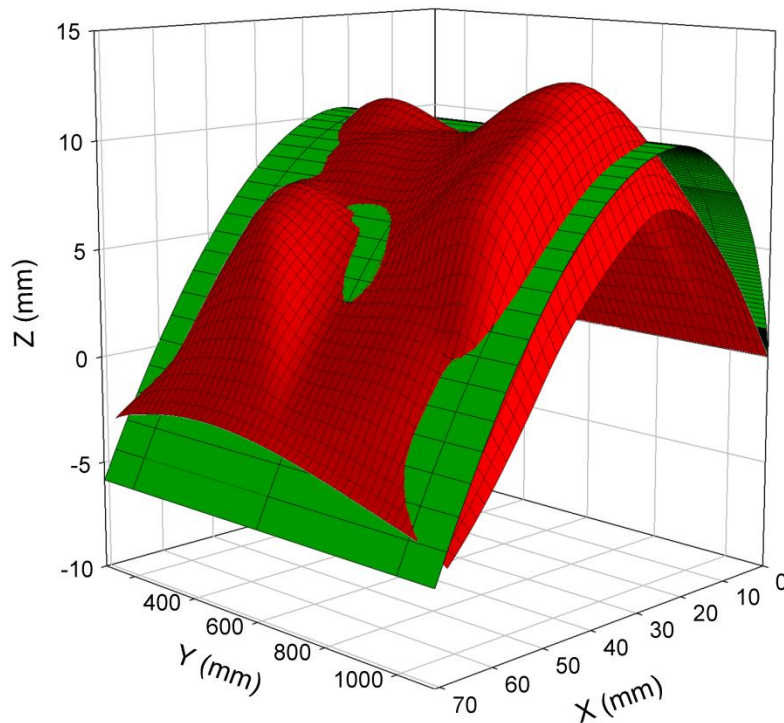


Figure 4-5: Measured Ogee surface for scenario 1 compared with theoretical Ogee profile as given by the USACE (1970)

4.1.2 Scenario 2A: Symmetrical Approach Channel with flow rate at 80 l/s

The flow rate was set to 80 l/s by adjusting the full bore butterfly valve as discussed in **section 3.1.2**. The constant flow rate yielded a stage depth of 105,1 mm measured from the crest of the sharp-crested weir to the water surface in the stilling column. This stage depth is equivalent to a design head (H_d) of 93,35 mm for an Ogee crest spillway, calculated by making use of **Equation 2-7**. The recorded flow rate of 79,544 l/s (measured by the installed magnetic flow meter) was calibrated by making use of the calibration factors as given in **Figure 3-4**. The actual discharge from the sharp-crested weir was equivalent to 71,929 l/s ($q = 59,890$ l/s/m).

The Ogee profile was measured at 5 locations along the crest of the weir. 50 measurements were made at increments of 10 mm in the direction of the X-axis. These measurements are depicted in a 2-dimensional XZ-plot in **Figure 4-5**, and are being compared with the theoretical Ogee profile for a design head of 93,35 mm as estimated by the USBR (1987), USACE (1970), Hager (1987) and Ministry of Science and Technology (CE-05016) (2007). The populated datasheet containing the measurements of the Ogee profile can be view in Appendix A on the supporting CD of this dissertation.

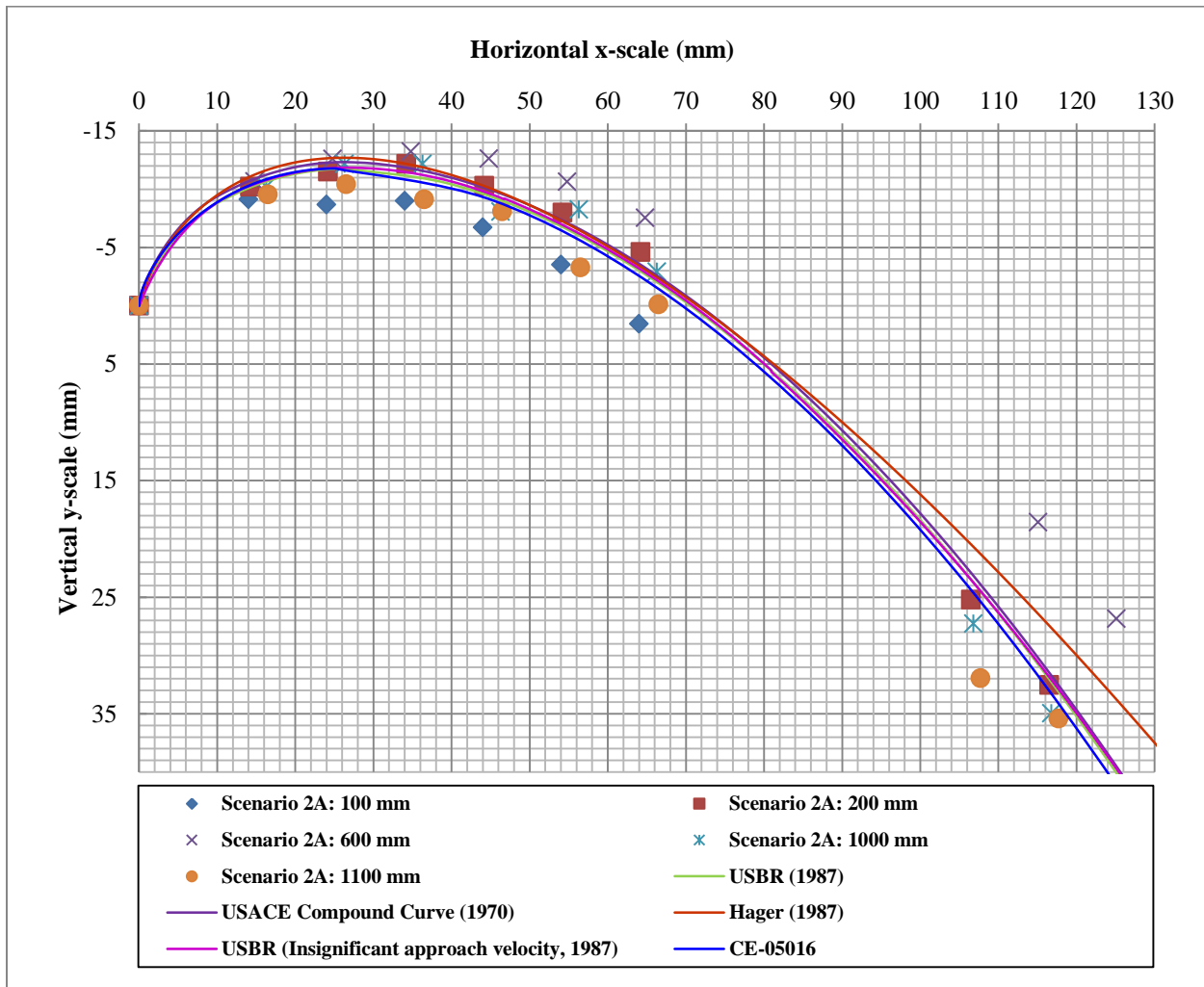


Figure 4-6: 2-dimensional plot of measured Ogee profile for scenario 2A

It was noticed from the 2-dimensional plot of scenario 2A (similar to that of scenario 1) that the Ogee profile in the centre of the nappe was greater than those measured at the outer boundaries. This trend was also noticed in the final results where the surface plot of the measured nappe was depicted in a XYZ-plot (**Figure 4-8**). The discussion of this phenomena is the same as given under scenario 1, **section 4.1.1**. The reason for this was that both the Ogee profiles (scenario 1 and scenario 2A) were measured for the same symmetrical approach channel and other than the increase in flow rate no other parameters were changed.

This indicate that the theoretical approximations of the Ogee profile tend to under-estimate the measured Ogee profile at the centre of the weir and over-estimate the Ogee profile at the boundaries. Over-

estimation of the Ogee profile is not as critical as under-estimation of the Ogee profile. The over-estimation of the Ogee profile at the boundaries will simply imply that a positive hydrostatic pressure is being experienced in these regions on the spillway. However, under-estimating the Ogee profile may cause a more detrimental effect causing cavitation of the boundary surface of the spillway as a result of the sub-atmospheric pressures being experienced. Long term exposure to these sub-atmospheric conditions may cause failure of the spillway structure.

The maximum variance of the measured Ogee profile versus the theoretical Ogee profile by the USACE (1970) for each of the measuring positions along the crest of the weir is given in **Table 4-2**.

Table 4-2: Maximum variance of the measured Ogee profile during scenario 2A at the different measuring locations

In-plane X-coordinate of measurement (mm)	Theoretical Ogee Z-coordinate (mm)	Measured Ogee Z-coordinate (mm)	Difference (+/- mm)
At 100 mm (Yellow1)			
0.0	0.0	0.0	0.0
14.0	-10.6	-9.1	-1.5
24.0	-12.2	-8.7	-3.6
34.0	-12.1	-9.0	-3.1
44.0	-10.6	-6.7	-3.9
54.0	-7.8	-3.5	-4.3
64.0	-4.0	1.6	-5.5
106.1	21.9	27.6	-5.8
116.1	30.8	29.5	1.3
Maximum variance within crest region (X < 70 mm)			5.5
At 200 mm (Purple1)			
0.0	0.0	0.0	0.0
14.2	-10.6	-10.2	-0.4
24.2	-12.3	-11.5	-0.7
34.2	-11.8	-12.2	0.3
44.2	-10.6	-10.3	-0.3
54.2	-7.8	-8.0	0.1
64.2	-4.0	-4.6	0.6
106.5	21.9	25.2	-3.3
116.5	30.8	32.5	-1.7
Maximum variance within crest region (X < 70 mm)			0.7
At 600 mm (Red)			
0.0	0.0	0.0	0.0
14.8	-10.8	-10.7	-0.2
24.8	-12.3	-12.6	0.3
34.8	-11.8	-13.2	1.4

In-plane X-coordinate of measurement (mm)	Theoretical Ogee Z-coordinate (mm)	Measured Ogee Z-coordinate (mm)	Difference (+/- mm)
44.8	-10.0	-12.6	2.6
54.8	-7.8	-10.6	2.8
64.8	-4.0	-7.5	3.6
105.1	19.8	-	-
115.1	28.5	18.6	9.9
Maximum variance within crest region (X < 70 mm)			0.2
At 1000 mm (Purple2)			
0.0	0.0	0.0	0.0
16.3	-11.2	-10.2	-1.0
26.3	-12.3	-12.2	-0.1
36.3	-11.8	-12.2	0.3
46.3	-10.0	-8.1	-1.9
56.3	-7.0	-8.3	1.3
66.3	-2.8	-2.9	0.1
106.8	21.9	27.3	-5.4
116.8	30.8	35.0	-4.2
Maximum variance within crest region (X < 70 mm)			1.9
At 1100 mm (Yellow2)			
0.0	0.0	0.0	0.0
16.5	-11.2	-9.6	-1.7
26.5	-12.3	-10.4	-1.9
36.5	-11.8	-9.1	-2.7
46.5	-10.0	-8.1	-1.9
56.5	-7.0	-3.3	-3.7
66.5	-2.8	-0.1	-2.7
107.7	21.9	31.9	-10.1
117.7	30.8	35.4	-4.6
Maximum variance within crest region (X < 70 mm)			3.7

Note: * Recordings where an under estimation of the Ogee nappe was recorded are highlighted in red. These are the critical positions on the Ogee profile

The measured Ogee profile is plotted as a red surface in a 3-dimensional XYZ-plot in **Figure 4-7**. Overlapping the measured Ogee surface plot in **Figure 4-8** is the theoretical Ogee profile by the USACE (1970) depicted by the green surface.

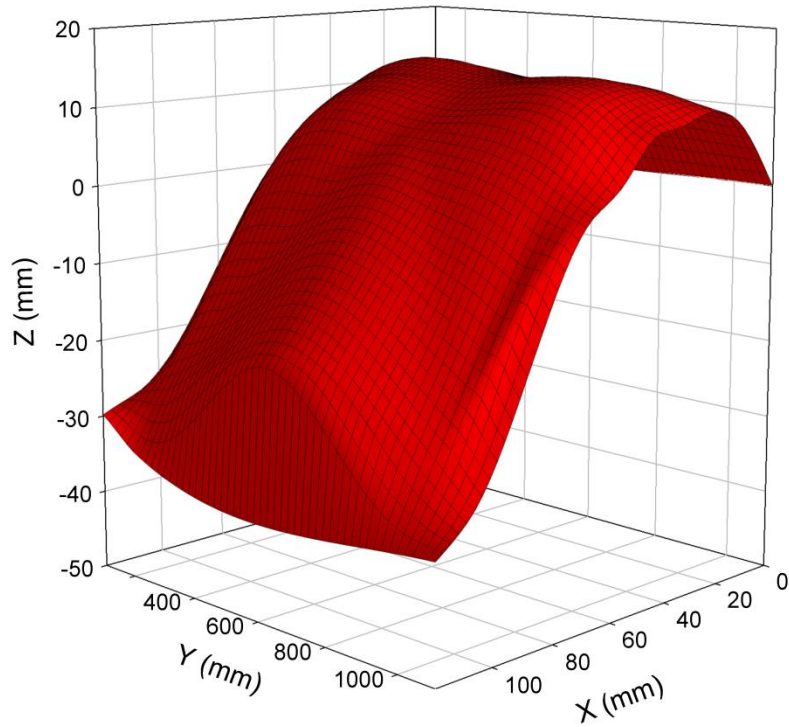


Figure 4-7: Measured Ogee surface for scenario 2A

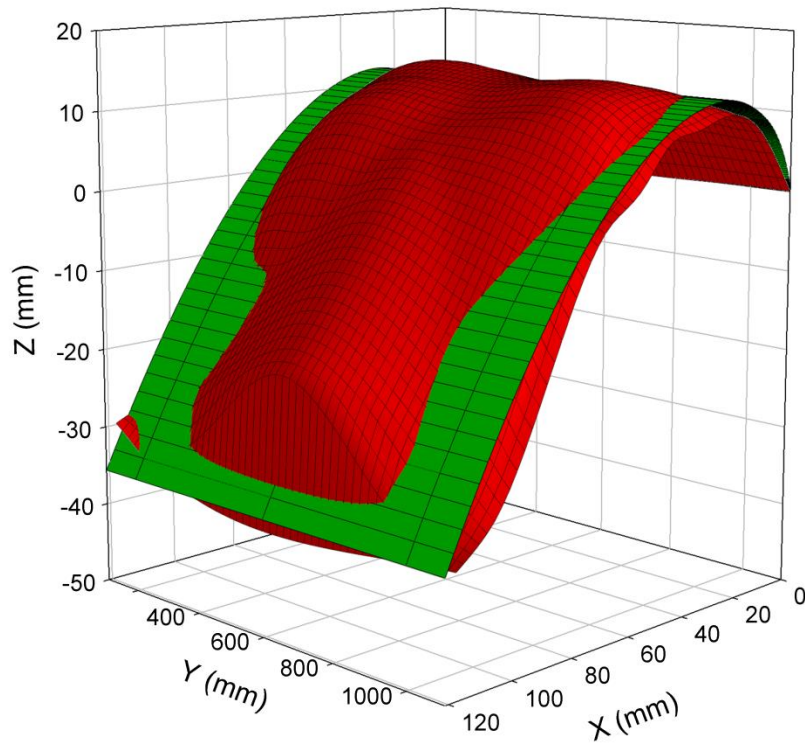


Figure 4-8: Measured Ogee surface for scenario 2A compared with theoretical Ogee profile as given by the USACE (1970)

4.1.3 Scenario 2B: Asymmetrical Approach Channel with side wall inclined at 45° with flow rate at 80 l/s

The flow rate was set to 80 l/s by adjusting the full bore butterfly valve as discussed in **section 3.1.2**. The side wall installed in the approach channel was inclined at an angle of 45° measured from the base of the channel. The constant flow rate yielded a stage depth of 116,65 mm measured from the crest of the sharp-crested weir to the water surface in the stilling column. This stage depth was greater than that measured for the baseline scenario 2A since the cross-section of the approach channel was effectively reduced by the inclined side wall. The measured stage depth is equivalent to a design head (H_d) of 105,28 mm for an Ogee crest spillway, calculated by making use of **Equation 2-7**. The recorded flow rate of 80,366 l/s (measured by the installed magnetic flow meter) was calibrated by making use of the calibration factors as given in **Figure 3-4**. The actual discharge from the sharp-crested weir was equivalent to 72,678 l/s ($q = 60,514$ l/s/m).

The Ogee profile was measured at 7 locations along the crest of the weir. 105 measurements were made at increments of 10 mm in the direction of the X-axis. These measurements are depicted in a 2-dimensional XZ-plot in **Figure 4-9**, and are being compared with the theoretical Ogee profile for a design head of 105,28 mm as estimated by the USBR (1987), USACE (1970), Hager (1987) and Ministry of Science and Technology (CE-05016) (2007). The populated datasheet containing the measurements of the Ogee profile can be view in Appendix A on the supporting CD of this dissertation.

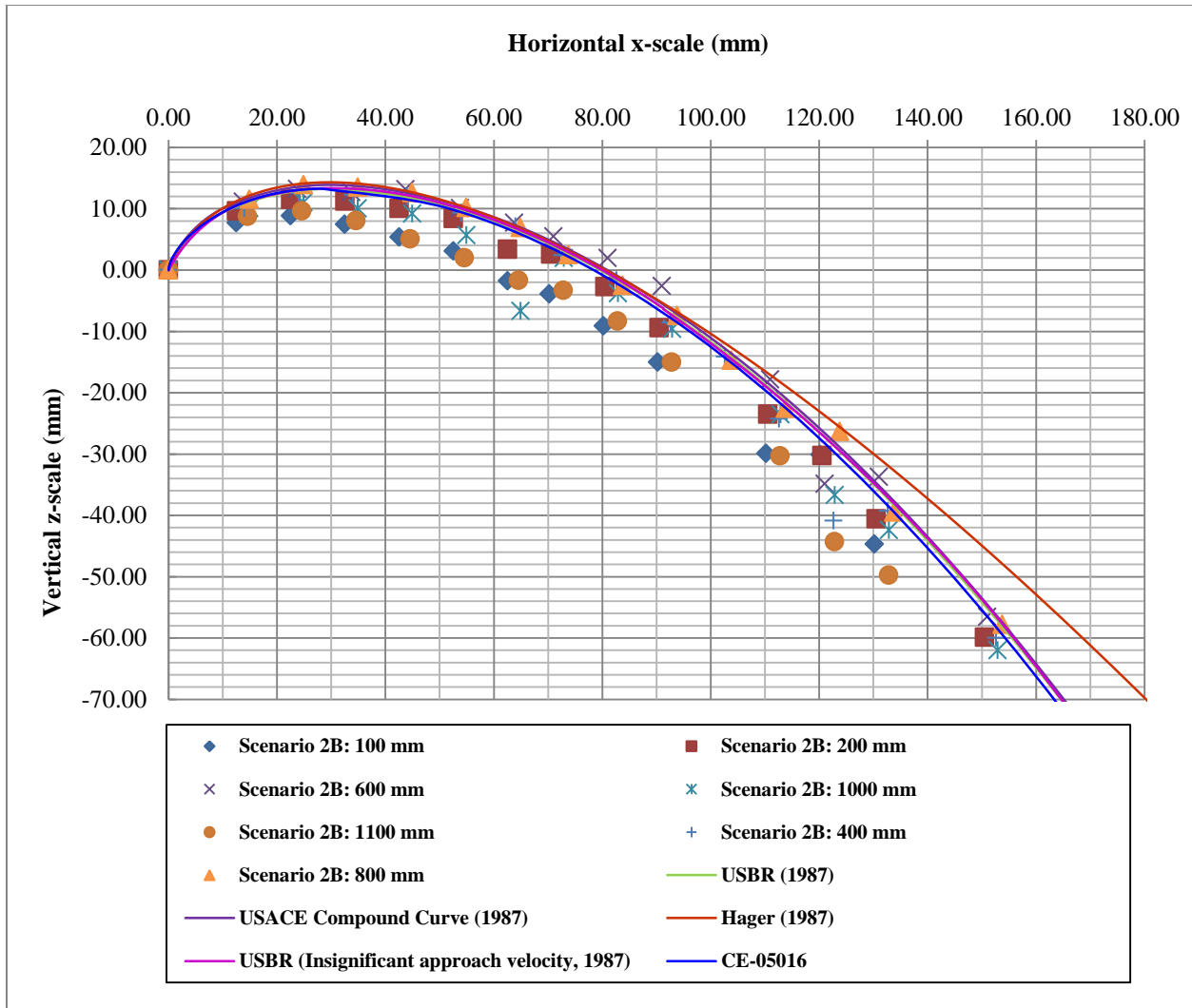


Figure 4-9: 2-dimensional plot of measured Ogee profile for scenario 2B

Indicated by the 2-dimensional plot of scenario 2B was that the Ogee profile was greater at some locations along the crest of the sharp-crested weir than the theoretical estimated Ogee profile. Unlike in scenario 2A where the greatest Ogee profile occurred in the centre, due to the symmetry of the approach channel, the greatest Ogee profile tend to lie between the 600 mm and 800 mm measuring location. The inclined side wall was installed to the right of the approach channel i.e. measuring location Yellow2 (or the 1200 mm mark on the sharp-crested weir). This emphasizes the hypothesis that an asymmetrical approach channel influences not only the geometric shape of the Ogee profile, but also the symmetry of flow across the hydraulic structure. The centreline tends to be moved off-centre in the direction where the inclined side wall has been installed. This trend was also noticed in the final results where the surface plot of the measured nappe was depicted in a XYZ-plot (**Figure 4-12**). Outliers in the

surface plot were excluded, since it is known that the Ogee nappe must follow a smooth profile. These outlier measurements were probably a result of some environmental influence causing a slight instability of the nappe while the measurement was being recorded (section 3.6) (7 measurements were excluded). The 3-dimensional surface plot of the measured Ogee nappe (including and excluding) the outlier measurements are depicted in **Figure 4-10** and **Figure 4-11** respectively.

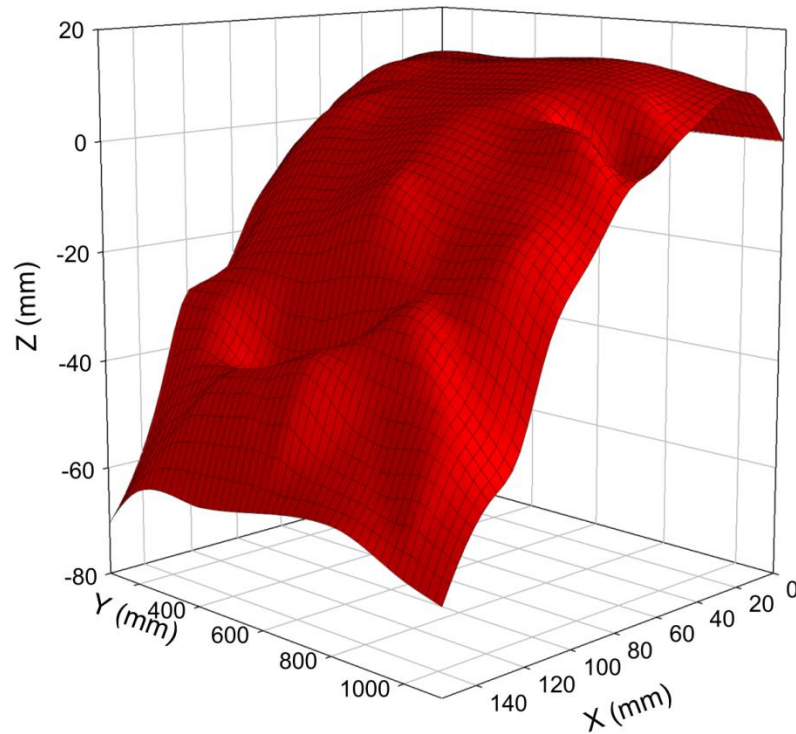


Figure 4-10: Measured Ogee surface for scenario 2B (including outlier measurements)

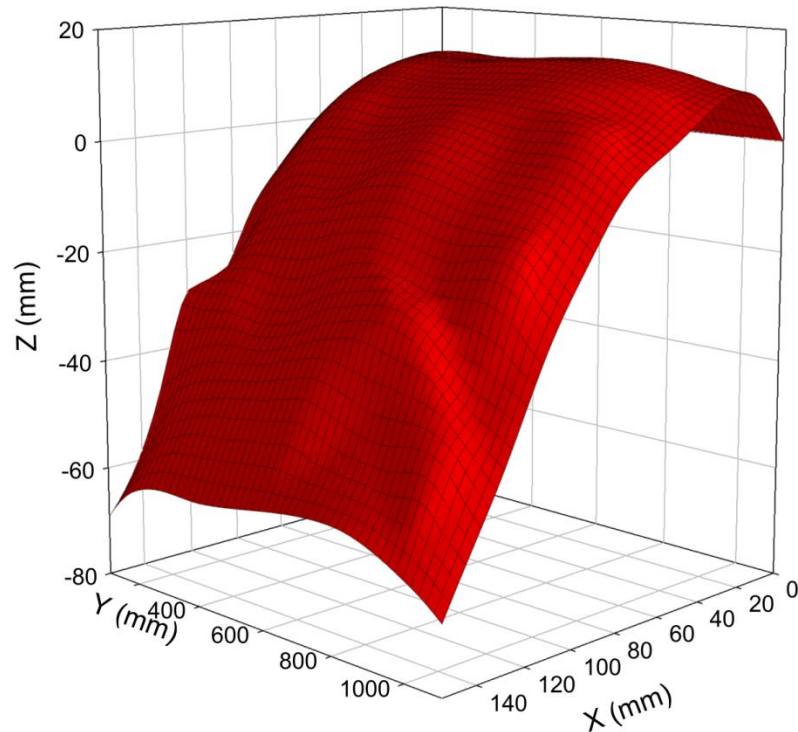


Figure 4-11: Measured Ogee surface for scenario 2B (excluding outlier measurements)

The result was that the theoretical approximations of the Ogee profile tend to under-estimate the measured Ogee profile between the 600 mm and 800 mm mark measured along the crest and again over-estimate the Ogee profile at the boundaries similar to the symmetrical approach channel layout. The discussion on over-estimation and under estimation of the Ogee profile is similar to that given in **section 4.1.2**.

The maximum variance of the measured Ogee profile versus the theoretical Ogee profile by the USACE (1970) for each of the measuring positions along the crest of the weir is given in **Table 4-3**.

Table 4-3: Maximum variance of the measured Ogee profile during scenario 2B at the different measuring locations (excluding outlier measurements)

In-plane X-coordinate of measurement (mm)	Theoretical Ogee Z-coordinate (mm)	Measured Ogee Z-coordinate (mm)	Difference (+/- mm)*
At 100 mm (Yellow1)			
0.0	0.0	0.0	0.0
12.5	11.0	7.7	3.2
22.5	13.4	8.9	4.5
32.5	13.9	7.5	6.4
42.5	13.0	5.4	7.6
52.5	11.3	3.1	8.2
62.5	7.9	-1.7	9.6
70.2	5.7	-3.9	9.6
80.2	0.4	-9.1	9.5
90.2	-4.3	-15.0	10.7
100.2	-9.7	-	-
110.2	-17.9	-29.9	12.0
120.2	-24.7	-30.1	5.4
130.2	-32.1	-44.7	12.6
150.2	-51.8	-	-
Maximum variance within crest region (X < 80 mm)			9.6
At 200 mm (Purple1)			
0.0	0.0	0.0	0.0
12.5	11.0	9.7	1.3
22.5	13.4	11.6	1.8
32.5	13.9	11.2	2.7
42.5	13.0	10.1	2.9
52.5	11.3	8.4	2.9
62.5	7.9	3.4	4.5
70.5	5.7	2.6	3.1
80.5	0.4	-2.7	3.1
90.5	-4.3	-9.4	5.1
100.5	-9.7	-	-
110.5	-17.9	-23.5	5.7
120.5	-24.7	-30.2	5.6
130.5	-32.1	-40.6	8.4
150.5	-51.8	-59.9	8.1
Maximum variance within crest region (X < 80 mm)			4.5
At 400 mm (White)			
0.0	0.0	0.0	0.0
14.0	11.5	10.1	1.4
24.0	13.6	12.6	1.0
34.0	13.8	12.3	1.5
44.0	13.0	12.0	1.0

In-plane X-coordinate of measurement (mm)	Theoretical Ogee Z-coordinate (mm)	Measured Ogee Z-coordinate (mm)	Difference (+/- mm)*
54.0	10.6	9.4	1.2
64.0	7.9	7.1	0.8
72.6	4.5	2.4	2.1
82.6	0.4	-1.6	2.0
92.6	-6.0	-8.6	2.5
102.6	-11.6	-14.1	2.5
112.6	-17.9	-24.2	6.4
122.6	-27.1	-40.9	13.8
132.6	-34.7	-39.3	4.5
152.6	-54.9	-60.0	5.1
Maximum variance within crest region (X < 80 mm)			2.1
At 600 mm (Red)			
0.0	0.0	0.0	0.0
13.7	11.3	11.1	0.2
23.7	13.5	13.2	0.3
33.7	13.8	12.7	1.1
43.7	13.0	13.2	-0.2
53.7	10.6	10.1	0.5
63.7	7.9	7.7	0.1
71.0	5.7	5.5	0.2
81.0	0.4	2.0	-1.6
91.0	-4.3	-2.6	-1.7
101.0	-11.6	-	-
111.0	-17.9	-17.9	0.0
121.0	-24.7	-34.9	10.2
131.0	-34.7	-33.7	-1.0
151.0	-51.8	-56.5	4.7
Maximum variance within crest region (X < 80 mm)			1.1
At 800 mm (Blue)			
0.0	0.0	0.0	0.0
14.9	11.7	11.5	0.2
24.9	13.7	13.9	-0.2
34.9	13.8	13.5	0.3
44.9	12.5	12.6	-0.1
54.9	10.6	10.2	0.4
64.9	7.9	6.9	0.9
73.8	4.5	2.5	2.0
83.8	-1.1	-2.5	1.4
93.8	-6.0	-7.4	1.4
103.8	-11.6	-14.7	3.1
113.8	-20.1	-22.6	2.5
123.8	-27.1	-26.3	-0.8
133.8	-37.4	-39.5	2.0

In-plane X-coordinate of measurement (mm)	Theoretical Ogee Z-coordinate (mm)	Measured Ogee Z-coordinate (mm)	Difference (+/- mm)*
153.8	-54.9	-57.8	2.9
Maximum variance within crest region (X < 80 mm)			2.0
At 1000 mm (Purple2)			
0.0	0.0	0.0	0.0
14.9	11.7	10.1	1.6
24.9	13.7	11.1	2.6
34.9	13.8	10.0	3.8
44.9	12.5	9.2	3.3
54.9	10.6	5.7	4.9
64.9	7.9	-6.7	14.5
72.9	4.5	1.9	2.5
82.9	0.4	-3.8	4.2
92.9	-6.0	-9.6	3.5
102.9	-11.6	-	-
112.9	-20.1	-23.5	3.5
122.9	-27.1	-36.7	9.6
132.9	-34.7	-42.4	7.7
152.9	-54.9	-62.0	7.1
Maximum variance within crest region (X < 80 mm)			14.5
At 1100 mm (Yellow2)			
0.0	0.0	0.0	0.0
14.6	11.6	8.8	2.8
24.6	13.6	9.6	4.0
34.6	13.8	8.0	5.8
44.6	12.5	5.1	7.4
54.6	10.6	2.0	8.6
64.6	7.9	-1.6	9.5
72.8	4.5	-3.3	7.8
82.8	0.4	-8.3	8.7
92.8	-6.0	-15.0	9.0
102.8	-11.6	-	-
112.8	-20.1	-30.3	10.2
122.8	-27.1	-44.3	17.2
132.8	-34.7	-49.8	15.0
152.8	-54.9	-	-
Maximum variance within crest region (X < 80 mm)			9.5

Note: * Recordings where an under estimation of the Ogee nappe was recorded are highlighted in red. These are the critical positions on the Ogee profile

Overlapping the measured Ogee surface (red) plot in **Figure 4-12** is the theoretical Ogee profile by the USACE (1970) depicted by the green surface.

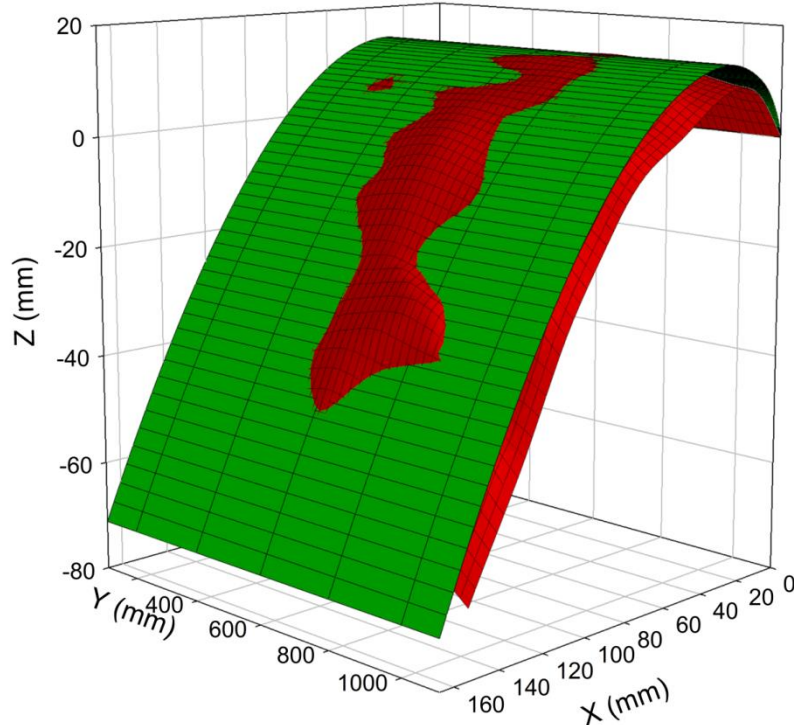


Figure 4-12: Measured Ogee surface for scenario 2B compared with theoretical Ogee profile as given by the USACE (1970)

4.1.4 Scenario 2C: Asymmetrical Approach Channel with side wall inclined at 60° with flow rate at 80 l/s

The flow rate was set to 80 l/s by adjusting the full bore butterfly valve as discussed in **section 3.1.2**. The side wall installed in the approach channel was inclined at an angle of 60° measured from the base of the channel. The constant flow rate yielded a stage depth of 116,05 mm measured from the crest of the sharp-crested weir to the water surface in the stilling column. This stage depth was greater than that measured for the baseline scenario 2A since the cross-section of the approach channel was effectively reduced by the inclined side wall. The measured stage depth is equivalent to a design head (H_d) of 104,74 mm for an Ogee crest spillway, calculated by making use of **Equation 2-7**. The recorded flow rate of 80,290 l/s (measured by the installed magnetic flow meter) was calibrated by making use of the calibration factors as given in **Figure 3-4**. The actual discharge from the sharp-crested weir was equivalent to 72,609 l/s ($q = 60,457$ l/s/m).

The Ogee profile was measured at 7 locations along the crest of the weir. 105 measurements were made at increments of 10 mm in the direction of the X-axis. These measurements are depicted in a 2-dimensional XZ-plot in **Figure 4-13**, and are being compared with the theoretical Ogee profile for a design head of 104,74 mm as estimated by the USBR (1987), USACE (1970), Hager (1987) and Ministry of Science and Technology (CE-05016) (2007). The populated datasheet containing the measurements of the Ogee profile can be view in Appendix A on the supporting CD of this dissertation.

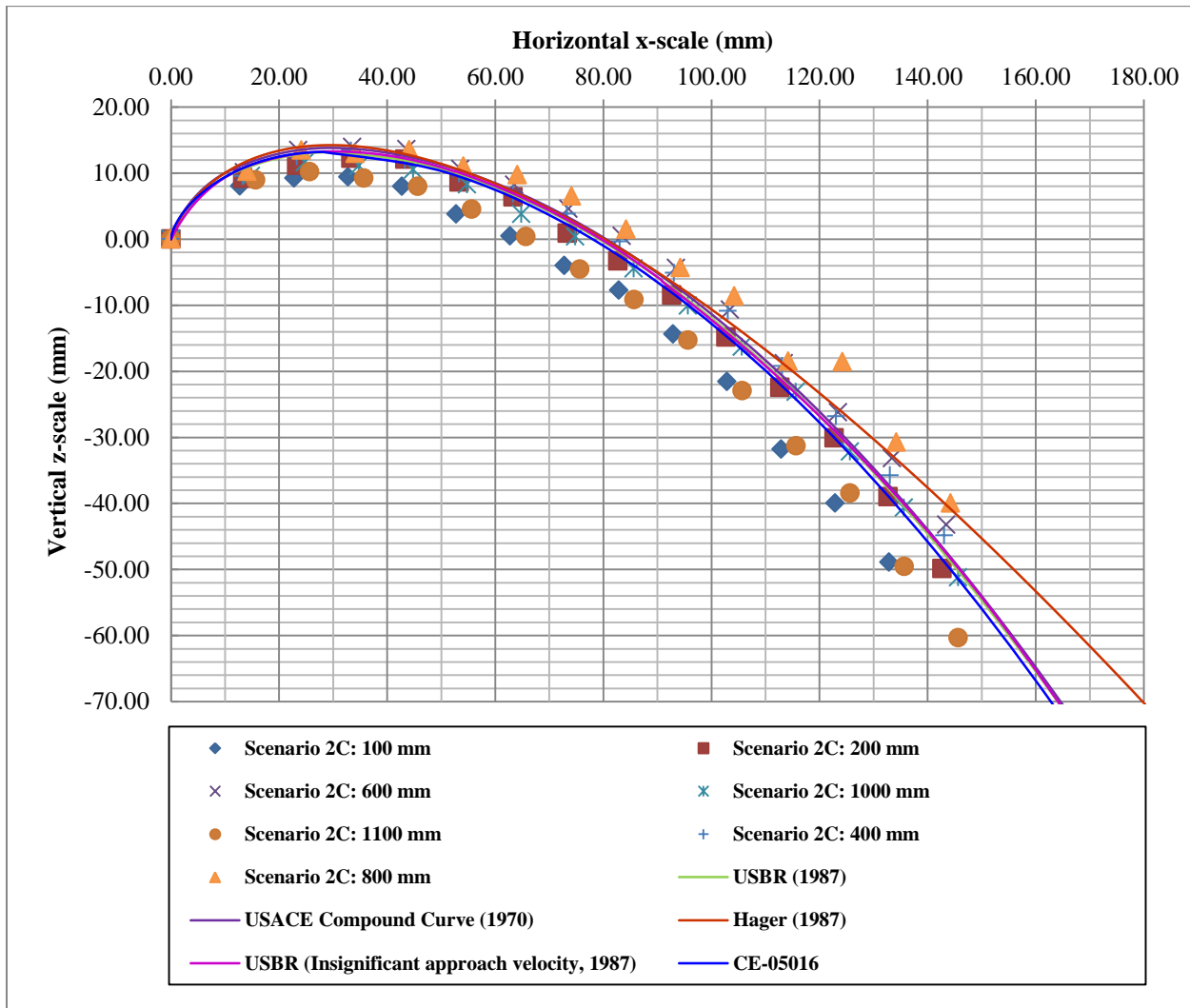


Figure 4-13: 2-dimensional plot of measured Ogee profile for scenario 2C

The 2-dimensional plot of scenario 2C indicates that the Ogee profile was greater at some locations along the crest of the sharp-crested weir than the theoretical estimated Ogee profile. Unlike in scenario 2A where the greatest Ogee profile occurred in the centre, due to the symmetry of the approach channel,

the greatest Ogee profile tend to lie at the 800 mm measuring location. The inclined side wall was installed to the right of the approach channel i.e. measuring location Yellow2 (or the 1200 mm mark on the sharp-crested weir). This indicates that the Ogee nappe was moved off-centre even more than the case when the inclination of the side wall was only 45°. This 60° angle side wall is so steep and extended closely to the boundary of the 1200 mm mark of the sharp-crested weir. This may cause the sharp-crested weir to function not as a fully-contracted weir anymore and be the reason for the higher velocities present in this region (less flow resistance), thus resulting in the Ogee profile to be the greatest in this region. High flow velocities present in this region can be noticed in **Figure 4-14** where the flow pattern can be clearly visualized.



Figure 4-14: High flow velocities experienced at boundary of sharp-crested weir's crest caused by the steep inclination of the 60° side wall

This emphasizes the hypothesis that an asymmetrical approach channel influences not only the geometric shape of the Ogee profile, but also the symmetry of flow across the hydraulic structure. The centreline tends to be moved off-centre in the direction where the inclined side wall has been installed, and even more so the greater the inclination. This trend was also noticed in the final results where the surface plot of the measured nappe was depicted in a XYZ-plot (**Figure 4-17**). Outliers in the surface plot were

excluded, since it is known that the Ogee nappe must follow a smooth profile. These outlier measurements were probably a result of some environmental influence causing a slight instability of the nappe while the measurement was being recorded (**section 3.6**) (3 measurements were excluded). The 3-dimensional surface plot of the measured Ogee nappe (including and excluding) the outlier measurements are depicted in **Figure 4-15** and **Figure 4-16** respectively.

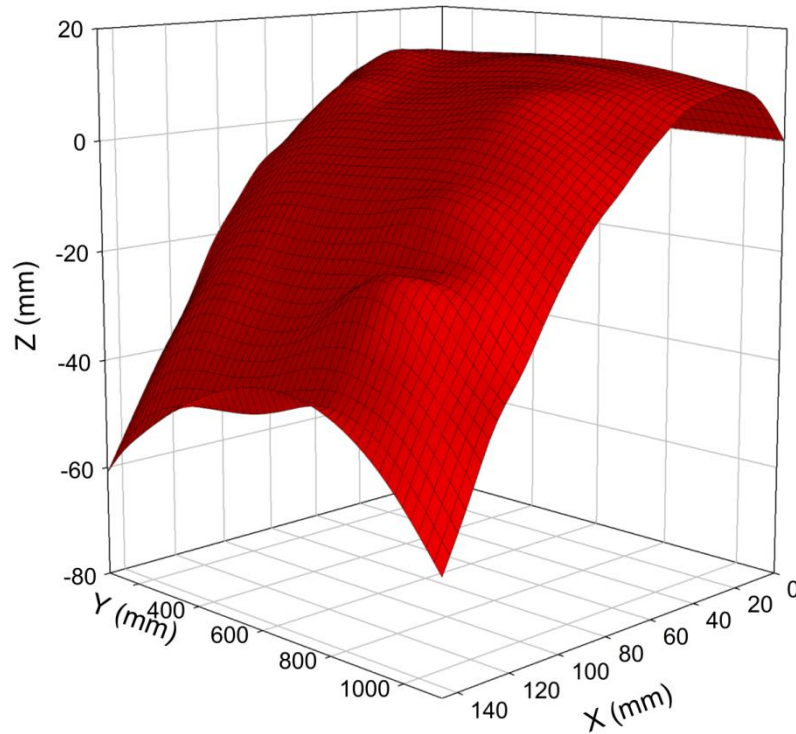


Figure 4-15: Measured Ogee surface for scenario 2C (including outlier measurements)

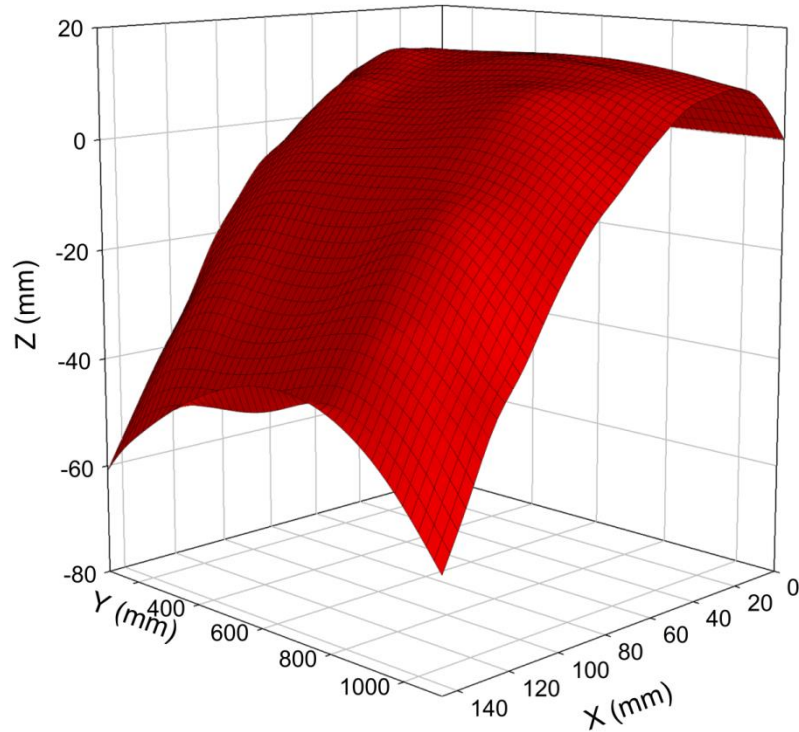


Figure 4-16: Measured Ogee surface for scenario 2C (excluding outlier measurements)

The result was that the theoretical approximations of the Ogee profile tend to under-estimate the measured Ogee profile between the 400 mm and 1000 mm mark measured along the crest and again over-estimate the Ogee profile at the boundaries similar to the symmetrical approach channel layout. The discussion on over-estimation and under estimation of the Ogee profile is similar to that given in **section 4.1.2**.

The maximum variance of the measured Ogee profile versus the theoretical Ogee profile by the USACE (1970) for each of the measuring positions along the crest of the weir is given in **Table 4-4**.

Table 4-4: Maximum variance of the measured Ogee profile during scenario 2C at the different measuring locations (excluding outlier measurements)

In-plane X-coordinate of measurement (mm)	Theoretical Ogee Z-coordinate (mm)	Measured Ogee Z-coordinate (mm)	Difference (+/- mm)
At 100 mm (Yellow1)			
0.0	0.0	0.0	0.0
12.7	11.0	8.1	3.0
22.7	13.4	9.3	4.1
32.7	13.8	9.4	4.3
42.7	12.9	8.0	4.9
52.7	11.2	3.8	7.4
62.7	7.8	0.5	7.3
72.7	4.5	-4.0	8.5
82.9	-1.1	-7.7	6.6
92.9	-6.0	-14.4	8.3
102.9	-11.6	-21.5	10.0
112.9	-20.0	-31.8	11.8
122.9	-27.0	-40.0	13.0
132.9	-37.2	-48.9	11.7
142.9	-45.6	-	-
Maximum variance within crest region (X < 80 mm)			8.5
At 200 mm (Purple1)			
0.0	0.0	0.0	0.0
13.3	11.2	9.2	2.0
23.3	13.5	11.2	2.3
33.3	13.8	12.3	1.5
43.3	12.9	12.1	0.8
53.3	10.5	8.6	1.9
63.3	7.8	6.4	1.4
73.3	4.5	0.9	3.6
82.7	-1.1	-3.3	2.2
92.7	-6.0	-8.5	2.5
102.7	-11.6	-14.8	3.2
112.7	-20.0	-22.4	2.5
122.7	-27.0	-30.1	3.1
132.7	-34.6	-39.0	4.4
142.7	-45.6	-49.9	4.2
Maximum variance within crest region (X < 80 mm)			3.6
At 400 mm (White)			
0.0	0.0	0.0	0.0
13.3	11.2	9.6	1.6
23.3	13.5	12.5	0.9
33.3	13.8	13.4	0.4
43.3	12.9	12.0	0.9

In-plane X-coordinate of measurement (mm)	Theoretical Ogee Z-coordinate (mm)	Measured Ogee Z-coordinate (mm)	Difference (+/- mm)
53.3	10.5	9.9	0.6
63.3	7.8	6.9	1.0
73.3	4.5	3.9	0.6
83.0	-1.1	-0.3	-0.8
93.0	-6.0	-5.1	-0.9
103.0	-11.6	-10.9	-0.7
113.0	-20.0	-19.2	-0.8
123.0	-27.0	-26.8	-0.1
133.0	-37.2	-35.7	-1.5
143.0	-45.6	-44.9	-0.8
Maximum variance within crest region (X < 80 mm)			1.6
At 600 mm (Red)			
0.0	0.0	0.0	0.0
13.5	11.3	10.1	1.2
23.5	13.5	13.5	0.0
33.5	13.8	14.0	-0.2
43.5	12.9	13.6	-0.7
53.5	10.5	10.6	-0.1
63.5	7.8	8.2	-0.4
73.5	4.5	4.6	-0.1
83.4	-1.1	0.5	-1.6
93.4	-6.0	-4.4	-1.7
103.4	-13.6	-10.7	-2.9
113.4	-20.0	-18.8	-1.2
123.4	-27.0	-26.2	-0.8
133.4	-37.2	-33.2	-4.0
143.4	-45.6	-43.2	-2.4
Maximum variance within crest region (X < 80 mm)			1.2
At 800 mm (Blue)			
0.0	0.0	0.0	0.0
14.1	11.4	10.3	1.1
24.1	13.5	13.5	0.1
34.1	13.8	13.0	0.8
44.1	12.9	13.5	-0.6
54.1	10.5	11.0	-0.5
64.1	7.8	9.7	-1.9
74.1	3.2	6.5	-3.3
84.2	-1.1	1.5	-2.6
94.2	-6.0	-4.3	-1.7
104.2	-13.6	-8.6	-4.9
114.2	-20.0	-18.5	-1.5
124.2	-29.4	-	-
134.2	-37.2	-30.7	-6.5

In-plane X-coordinate of measurement (mm)	Theoretical Ogee Z-coordinate (mm)	Measured Ogee Z-coordinate (mm)	Difference (+/- mm)
144.2	-45.6	-40.0	-5.7
Maximum variance within crest region (X < 80 mm)			1.1
At 1000 mm (Purple2)			
0.0	0.0	0.0	0.0
14.8	11.6	9.6	2.1
24.8	13.6	11.6	2.0
34.8	13.8	11.1	2.7
44.8	12.4	10.5	1.9
54.8	10.5	8.3	2.2
64.8	7.8	3.8	4.0
74.8	3.2	0.4	2.8
85.6	-2.7	-4.4	1.8
95.6	-7.8	-10.1	2.3
105.6	-13.6	-16.3	2.7
115.6	-22.2	-23.1	0.9
125.6	-29.4	-32.2	2.8
135.6	-37.2	-40.7	3.4
145.6	-48.5	-51.2	2.7
Maximum variance within crest region (X < 80 mm)			4.0
At 1100 mm (Yellow2)			
0.0	0.0	0.0	0.0
15.7	11.9	9.0	3.0
25.7	13.7	10.2	3.5
35.7	13.6	9.3	4.3
45.7	12.4	8.0	4.4
55.7	10.5	4.5	6.0
65.7	6.8	0.4	6.4
75.7	3.2	-4.5	7.7
85.7	-2.7	-9.1	6.5
95.7	-7.8	-15.3	7.5
105.7	-13.6	-22.9	9.4
115.7	-22.2	-31.3	9.1
125.7	-29.4	-38.4	9.0
135.7	-37.2	-49.5	12.3
145.7	-48.5	-60.3	11.8
Maximum variance within crest region (X < 80 mm)			7.7

Overlapping the measured Ogee surface (red) plot in **Figure 4-17** is the theoretical Ogee profile by the USACE (1970) depicted by the green surface.

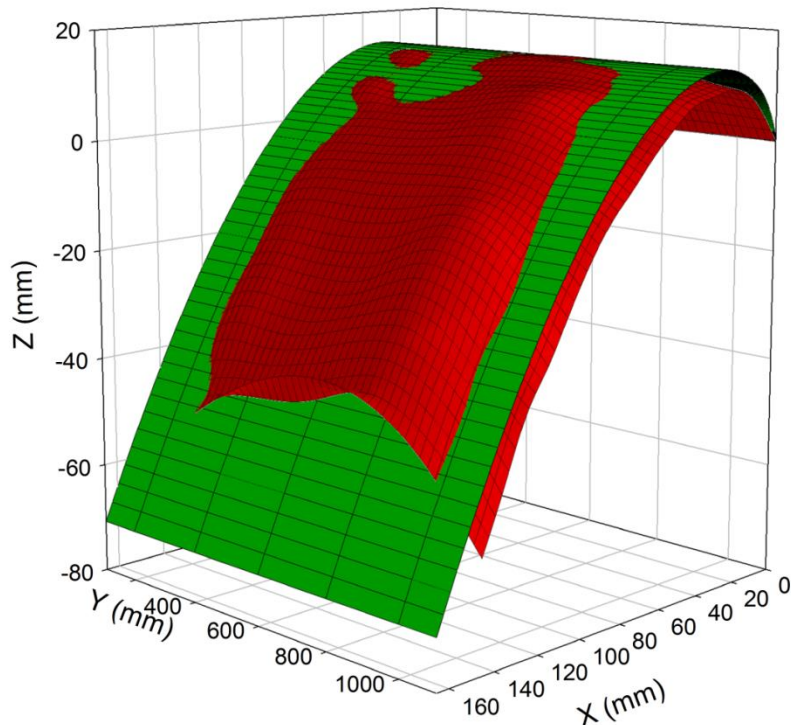


Figure 4-17: Measured Ogee surface for scenario 2C compared with theoretical Ogee profile as given by the USACE (1970)

4.1.5 Scenario 3A: Asymmetrical Approach Channel with side wall inclined at 45° with flow rate at 130 l/s

The flow rate was set to 130 l/s by adjusting the full bore butterfly valve as discussed in **section 3.1.2**. The side wall installed in the approach channel was inclined at an angle of 45° measured from the base of the channel. The constant flow rate yielded a stage depth of 158,60 mm measured from the crest of the sharp-crested weir to the water surface in the stilling column. This stage depth was greater than that measured for the baseline scenario 2B since the flow rate was increased for the same effective cross-section of the approach channel. The measured stage depth was equivalent to a design head (H_d) of 144,84 mm for an Ogee crest spillway, calculated by making use of **Equation 2-7**. The recorded flow rate of 130,396 l/s (measured by the installed magnetic flow meter) was calibrated by making use of the calibration factors as given in **Figure 3-4**. The actual discharge from the sharp-crested weir was equivalent to 117,711 l/s ($q = 98,010$ l/s/m).

The Ogee profile was measured at 7 locations along the crest of the weir. 105 measurements were made at increments of 10 mm in the direction of the X-axis. These measurements are depicted in a 2-

dimensional XZ-plot in **Figure 4-18**, and are being compared with the theoretical Ogee profile for a design head of 144,84 mm as estimated by the USBR (1987), USACE (1970), Hager (1987) and Ministry of Science and Technology (CE-05016) (2007). The populated datasheet containing the measurements of the Ogee profile can be view in Appendix A on the supporting CD of this dissertation.

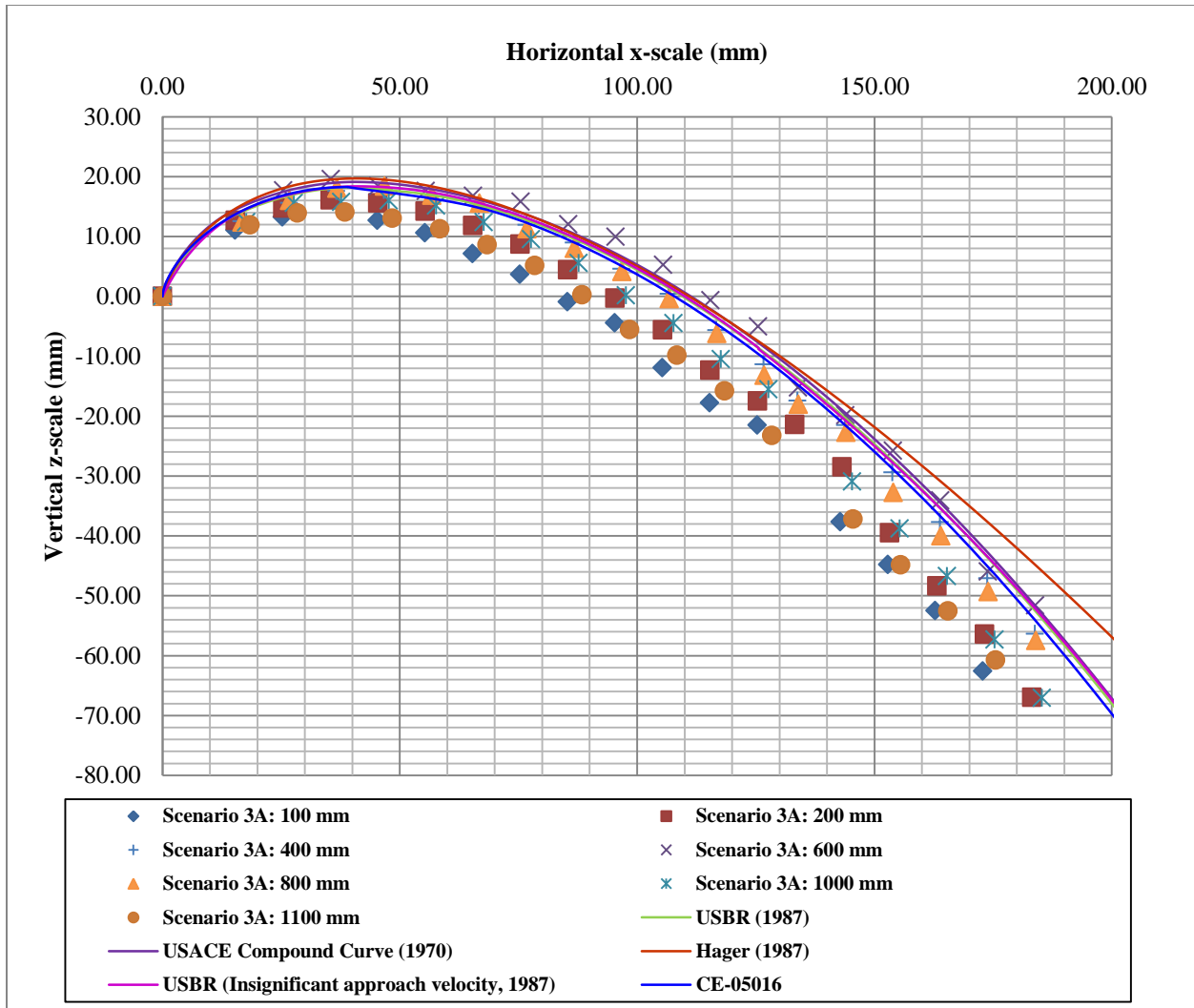


Figure 4-18: 2-dimensional plot of measured Ogee profile for scenario 3A

It can be noticed in the 2-dimensional plot of scenario 3A that the Ogee profile was greater at the centre of the crest of the sharp-crested weir than the theoretical estimated Ogee profile. Unlike in scenario 2B where the greatest Ogee profile occurred prominently between the 600 mm and 800 mm measuring location, the Ogee profile for scenario 3A tend to be only slightly off-centre to the right of the 600 mm mark. This was almost as if having a symmetrical approach channel as in the case of scenario 1 and

scenario 2A and can be explained by the fact that the approach velocity in the channel has dramatically increased from the case of the 80 l/s scenarios. This reduces the effect of contraction caused by the side wall as the water was simply forced over the crest and the ratio between the side flows at the boundaries, to the flow perpendicular to the crest was reduced. The inclined side wall was installed to the right of the approach channel i.e. measuring location Yellow2 (or the 1200 mm mark on the sharp-crested weir). This phenomenon indicate that there might be a critical flow rate at which the effect of an asymmetrical approach may be the same as a symmetrical approach channel if the flow rate exceeds a specific limit for the unique geometric conditions of the approach channel.

This trend was also noticed in the final results where the surface plot of the measured nappe was depicted in a XYZ-plot (**Figure 4-21**). Outliers in the surface plot were excluded, since it is known that the Ogee nappe must follow a smooth profile. These outlier measurements were probably a result of some environmental influence causing a slight instability of the nappe while the measurement was being recorded (**section 3.6**) (7 measurements were excluded). The 3-dimensional surface plot of the measured Ogee nappe (including and excluding) the outlier measurements are depicted in **Figure 4-19** and **Figure 4-20** respectively.

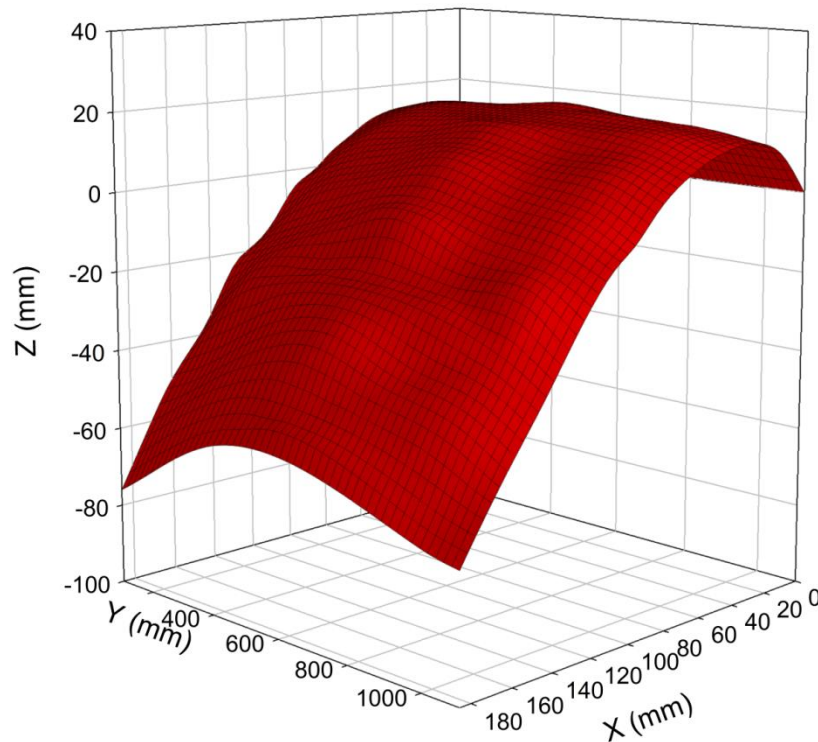


Figure 4-19: Measured Ogee surface for scenario 3A (including outlier measurements)

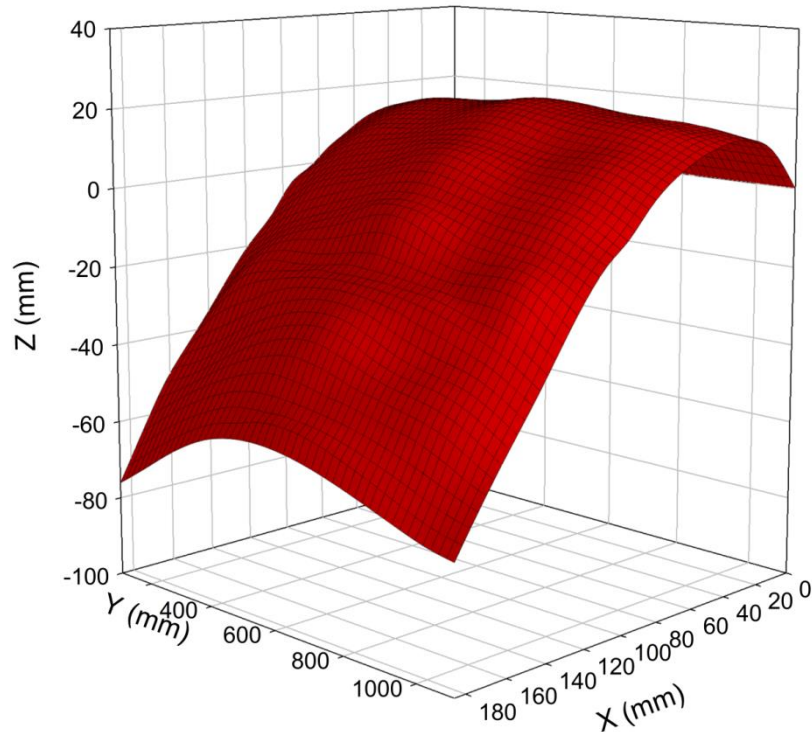


Figure 4-20: Measured Ogee surface for scenario 3A (excluding outlier measurements)

The result was that the theoretical approximations of the Ogee profile tend to under-estimate the measured Ogee profile between the 600 mm and 800 mm mark measured along the crest and again over-estimate the Ogee profile at the boundaries similar to the symmetrical approach channel layout. The discussion on over-estimation and under estimation of the Ogee profile is similar to that given in **section 4.1.2**.

The maximum variance of the measured Ogee profile versus the theoretical Ogee profile by the USACE (1970) for each of the measuring positions along the crest of the weir is given in **Table 4-5**.

Table 4-5: Maximum variance of the measured Ogee profile during scenario 3A at the different measuring locations (excluding outlier measurements)

In-plane X-coordinate of measurement (mm)	Theoretical Ogee Z-coordinate (mm)	Measured Ogee Z-coordinate (mm)	Difference (+/- mm)
At 100 mm (Yellow1)			
0.0	0.0	0.0	0.0
15.3	14.4	11.0	3.4
25.3	17.4	13.2	4.2
35.3	18.9	-	-
45.3	19.0	12.7	6.3
55.3	18.4	10.6	7.8
65.3	17.2	7.1	10.1
75.3	14.5	3.6	10.9
85.3	12.2	-0.9	13.1
95.3	7.8	-4.5	12.3
105.3	4.4	-11.9	16.3
115.3	-1.5	-17.8	16.3
125.3	-6.0	-21.5	15.6
132.8	-10.8	-	-
142.8	-16.0	-37.7	21.7
152.8	-24.6	-44.8	20.3
162.8	-30.7	-52.5	21.8
172.8	-40.7	-62.6	21.9
182.8	-47.8	-	-
Maximum variance within crest region (X < 110 mm)			16.3
At 200 mm (Purple1)			
0.0	0.0	0.0	0.0
15.4	14.4	12.7	1.7
25.4	17.4	14.7	2.7
35.4	18.9	16.1	2.8
45.4	19.0	15.6	3.4
55.4	18.4	14.2	4.2
65.4	16.4	11.8	4.6
75.4	14.5	8.7	5.8
85.4	12.2	4.4	7.8
95.4	7.8	-0.3	8.2
105.4	4.4	-5.6	10.0
115.4	-1.5	-12.4	10.8
125.4	-6.0	-17.5	11.5
133.2	-10.8	-21.4	10.6
143.2	-18.8	-28.5	9.7
153.2	-24.6	-39.5	15.0
163.2	-30.7	-48.4	17.6
173.2	-40.7	-56.4	15.7

In-plane X-coordinate of measurement (mm)	Theoretical Ogee Z-coordinate (mm)	Measured Ogee Z-coordinate (mm)	Difference (+/- mm)
183.2	-47.8	-67.0	19.2
Maximum variance within crest region (X < 110 mm)			10.0
At 400 mm (White)			
0.0	0.0	0.0	0.0
16.7	14.9	12.5	2.4
26.7	17.7	15.6	2.1
36.7	19.0	17.6	1.4
46.7	19.0	17.7	1.3
56.7	18.4	16.6	1.7
66.7	16.4	15.1	1.3
76.7	14.5	11.9	2.6
86.7	10.8	9.0	1.8
96.7	7.8	4.6	3.2
106.7	2.5	0.4	2.1
116.7	-1.5	-5.7	4.1
126.7	-8.3	-11.4	3.1
133.8	-10.8	-17.5	6.7
143.8	-18.8	-21.5	2.8
153.8	-24.6	-29.4	4.8
163.8	-34.0	-37.7	3.8
173.8	-40.7	-47.1	6.4
183.8	-51.5	-56.4	4.9
Maximum variance within crest region (X < 110 mm)			3.2
At 600 mm (Red)			
0.0	0.0	0.0	0.0
15.5	14.5	-	-
25.5	17.4	17.7	-0.3
35.5	18.9	19.6	-0.7
45.5	19.0	18.4	0.6
55.5	18.4	17.6	0.8
65.5	16.4	16.8	-0.3
75.5	14.5	15.8	-1.3
85.5	12.2	12.0	0.1
95.5	7.8	9.9	-2.1
105.5	4.4	5.2	-0.8
115.5	-1.5	-0.7	-0.8
125.5	-6.0	-5.1	-0.9
133.9	-10.8	-15.3	4.5
143.9	-18.8	-19.9	1.1
153.9	-24.6	-25.8	1.3
163.9	-34.0	-34.1	0.1
173.9	-40.7	-46.0	5.3
183.9	-51.5	-51.7	0.2

In-plane X-coordinate of measurement (mm)	Theoretical Ogee Z-coordinate (mm)	Measured Ogee Z-coordinate (mm)	Difference (+/- mm)
Maximum variance within crest region (X < 110 mm)			2.1
At 800 mm (Blue)			
0.0	0.0	0.0	0.0
16.8	14.9	12.4	2.5
26.8	17.7	16.0	1.7
36.8	19.0	18.0	1.0
46.8	19.0	18.4	0.6
56.8	18.4	16.9	1.5
66.8	16.4	15.5	0.9
76.8	14.5	11.2	3.3
86.8	10.8	8.0	2.8
96.8	7.8	4.1	3.7
106.8	2.5	-0.4	3.0
116.8	-1.5	-6.2	4.7
126.8	-8.3	-13.2	4.9
134.0	-10.8	-18.1	7.3
144.0	-18.8	-22.8	4.0
154.0	-24.6	-32.8	8.2
164.0	-34.0	-40.0	6.1
174.0	-40.7	-49.4	8.7
184.0	-51.5	-57.5	6.0
Maximum variance within crest region (X < 110 mm)			3.7
At 1000 mm (Purple2)			
0.0	0.0	0.0	0.0
17.7	15.3	12.4	2.9
27.7	17.9	15.6	2.3
37.7	19.0	15.8	3.3
47.7	19.0	16.0	3.0
57.7	17.8	15.1	2.7
67.7	16.4	12.4	4.0
77.7	13.4	9.5	3.9
87.7	10.8	5.5	5.3
97.7	7.8	0.1	7.7
107.7	2.5	-4.5	7.0
117.7	-1.5	-10.5	9.0
127.7	-8.3	-15.5	7.2
135.3	-13.3	-	-
145.3	-18.8	-30.9	12.2
155.3	-27.6	-38.8	11.2
165.3	-34.0	-46.8	12.8
175.3	-40.7	-57.4	16.7
185.3	-51.5	-67.1	15.6
Maximum variance within crest region (X < 110 mm)			7.7

In-plane X-coordinate of measurement (mm)	Theoretical Ogee Z-coordinate (mm)	Measured Ogee Z-coordinate (mm)	Difference (+/- mm)
At 1100 mm (Yellow2)			
0.0	0.0	0.0	0.0
18.4	15.4	11.9	3.5
28.4	18.0	13.9	4.1
38.4	19.1	14.1	5.0
48.4	19.0	13.0	6.0
58.4	17.8	11.3	6.6
68.4	16.4	8.6	7.8
78.4	13.4	5.1	8.3
88.4	10.8	0.2	10.6
98.4	6.2	-5.6	11.7
108.4	2.5	-9.8	12.4
118.4	-3.7	-15.8	12.1
128.4	-8.3	-23.2	14.9
135.5	-13.3	-	-
145.5	-18.8	-37.2	18.5
155.5	-27.6	-44.8	17.2
165.5	-34.0	-52.5	18.6
175.5	-40.7	-60.7	20.1
185.5	-51.5	-	-
Maximum variance within crest region (X < 110 mm)			12.4

Overlapping the measured Ogee surface (red) plot in **Figure 4-21** is the theoretical Ogee profile by the USACE (1970) depicted by the green surface.

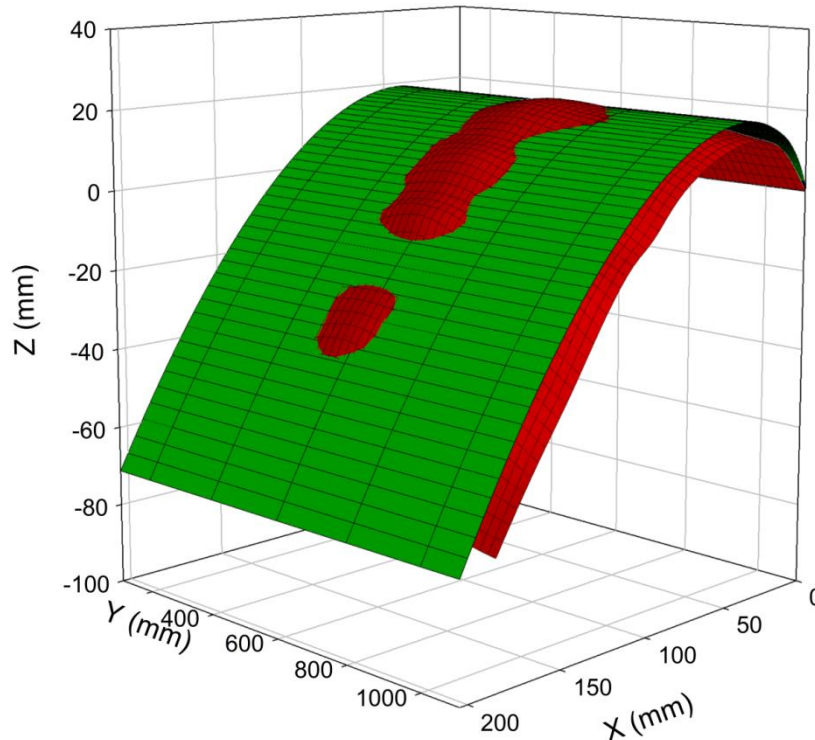


Figure 4-21: Measured Ogee surface for scenario 3A compared with theoretical Ogee profile as given by the USACE (1970)

4.1.6 Scenario 3B: Asymmetrical Approach Channel with side wall inclined at 60° with flow rate at 115 l/s

The flow rate was set to 115 l/s by adjusting the full bore butterfly valve as discussed in **section 3.1.2**. The side wall installed in the approach channel was inclined at an angle of 60° measured from the base of the channel. The constant flow rate yielded a stage depth of 147,95 mm measured from the crest of the sharp-crested weir to the water surface in the stilling column. This stage depth was greater than that measured for the baseline scenario 2C since the flow rate was increased for the same effective cross-section of the approach channel. The measured stage depth was equivalent to a design head (H_d) of 134,56 mm for an Ogee crest spillway, calculated by making use of **Equation 2-7**. The recorded flow rate of 114,767 l/s (measured by the installed magnetic flow meter) was calibrated by making use of the calibration factors as given in **Figure 3-4**. The actual discharge from the sharp-crested weir was equivalent to 103,662 l/s ($q = 86,313$ l/s/m).

The Ogee profile was measured at 7 locations along the crest of the weir. 126 measurements were made at increments of 10 mm in the direction of the X-axis. These measurements are depicted in a 2-

dimensional XZ-plot in **Figure 4-22**, and are being compared with the theoretical Ogee profile for a design head of 134,56 mm as estimated by the USBR (1987), USACE (1970), Hager (1987) and Ministry of Science and Technology (CE-05016) (2007). The populated datasheet containing the measurements of the Ogee profile can be view in Appendix A on the supporting CD of this dissertation.

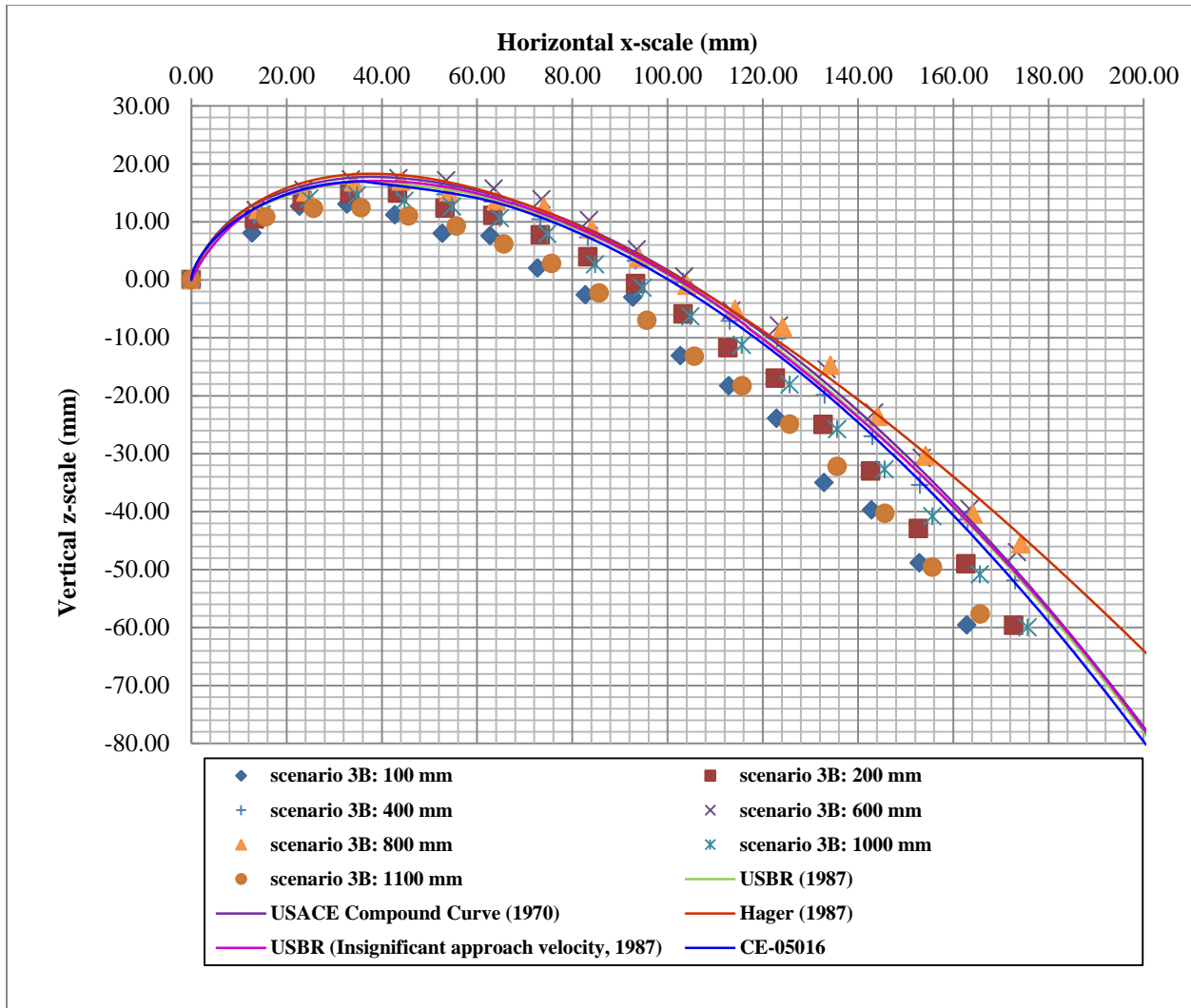


Figure 4-22: 2-dimensional plot of measured Ogee profile for scenario 3B

Similar to scenario 3A, the 2-dimensional plot of scenario 3B reflects that the Ogee profile was greater at the centre of the crest of the sharp-crested weir than the theoretical estimated Ogee profile. Unlike in scenario 2C where the greatest Ogee profile occurred prominently to the side of the weir in the region of the 1000 mm measuring location, the Ogee profile for scenario 3C, similar to 3A, tend to be only slightly off-centre to the right of the 600 mm mark. This was almost as if having a more symmetrical approach

channel as in the case of scenario 1 and scenario 2A and can be explained by the fact that the approach velocity in the channel has dramatically increased from the case of the 80 l/s scenarios. However, the Ogee profile is not as well centred as in the case of scenario 3A. The higher flow rate reduces the effect of contraction caused by the side wall as the water was simply forced over the crest and the ratio between the side flows at the boundaries, to the flow perpendicular to the crest was reduced. The inclined side wall was installed to the right of the approach channel i.e. measuring location Yellow2 (or the 1200 mm mark on the sharp-crested weir). This phenomenon indicate that there might be a critical flow rate at which the effect of an asymmetrical approach may be the same as a symmetrical approach channel if the flow rate exceeds a specific limit for the unique geometric conditions of the approach channel.

This trend was also noticed in the final results where the surface plot of the measured nappe was depicted in a XYZ-plot (**Figure 4-25**). Outliers in the surface plot were excluded, since it is known that the Ogee nappe must follow a smooth profile. These outlier measurements were probably a result of some environmental influence causing a slight instability of the nappe while the measurement was being recorded (**section 3.6**) (2 measurements were excluded). The 3-dimensional surface plot of the measured Ogee nappe (including and excluding) the outlier measurements are depicted in **Figure 4-23** and **Figure 4-24** respectively.

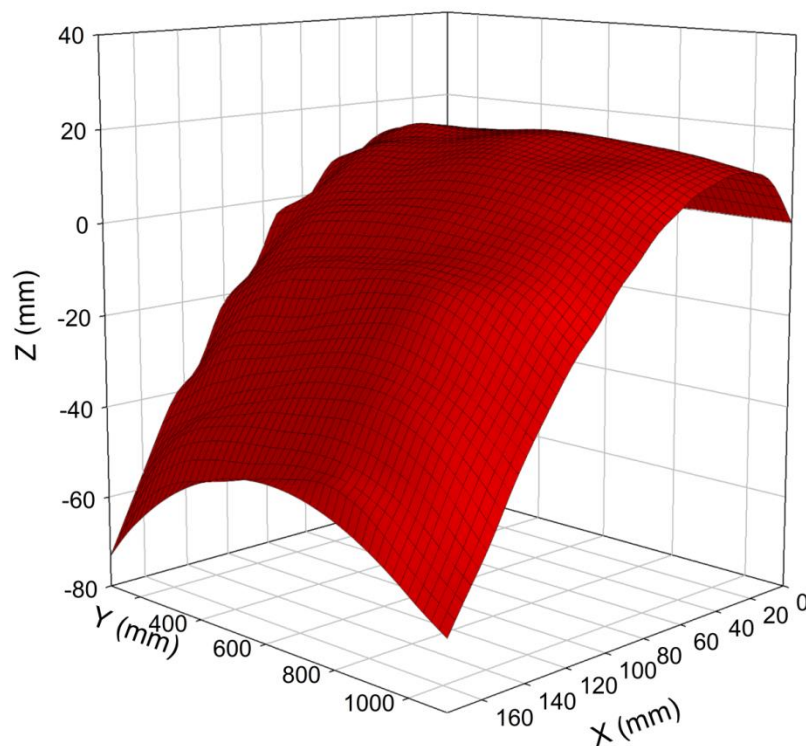


Figure 4-23: Measured Ogee surface for scenario 3B (including outlier measurements)

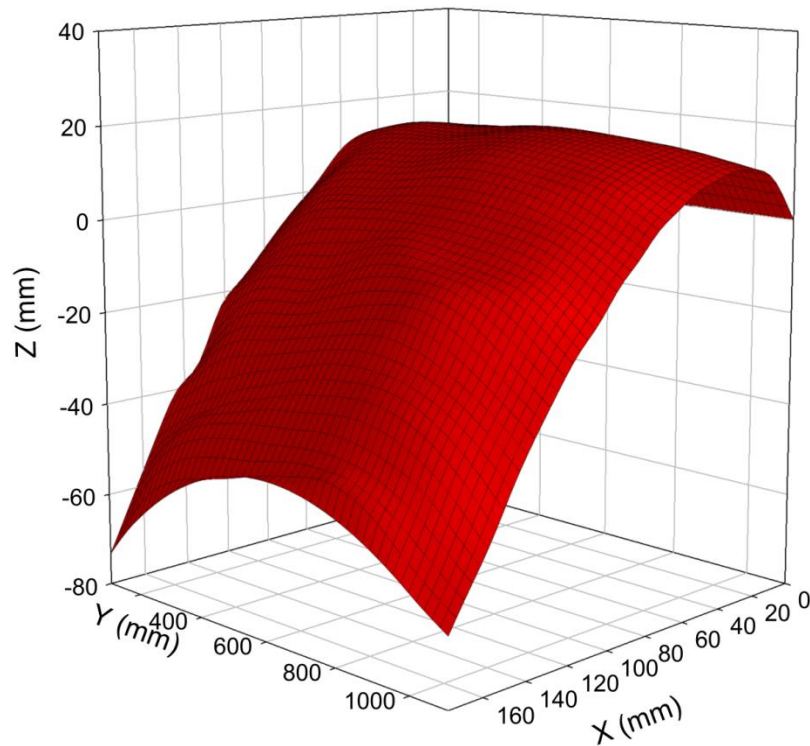


Figure 4-24: Measured Ogee surface for scenario 3B (excluding outlier measurements)

The result was that the theoretical approximations of the Ogee profile tend to under-estimate the measured Ogee profile between the 600 mm and 800 mm mark measured along the crest and again over-estimate the Ogee profile at the boundaries similar to the symmetrical approach channel layout. The discussion on over-estimation and under estimation of the Ogee profile is similar to that given in **section 4.1.2**.

The maximum variance of the measured Ogee profile versus the theoretical Ogee profile by the USACE (1970) for each of the measuring positions along the crest of the weir is given in **Table 4-6**.

Table 4-6: Maximum variance of the measured Ogee profile during scenario 3B at the different measuring locations (excluding outlier measurements)

In-plane X-coordinate of measurement (mm)	Theoretical Ogee Z-coordinate (mm)	Measured Ogee Z-coordinate (mm)	Difference (mm)
At 100 mm (Yellow1)			
0.0	0.0	0.0	0.0
12.7	12.7	8.0	4.7
22.7	15.9	12.6	3.3
32.7	17.6	13.0	4.6
42.7	17.7	11.2	6.5
52.7	17.1	8.0	9.1
62.7	15.3	7.5	7.7
72.7	12.4	2.0	10.4
82.7	10.1	-2.6	12.7
92.7	5.7	-3.0	8.7
102.7	0.5	-13.1	13.6
112.9	-3.4	-18.3	14.9
122.9	-10.0	-24.0	13.9
132.9	-17.4	-35.0	17.6
142.9	-22.8	-39.7	16.9
152.9	-31.5	-48.9	17.3
162.9	-37.8	-59.6	21.8
172.9	-47.8	-	-
Maximum variance within crest region (X < 100 mm)			12.7
At 200 mm (Purple1)			
0.0	0.0	0.0	0.0
13.3	13.1	10.4	2.6
23.3	16.1	13.6	2.5
33.3	17.6	14.8	2.8
43.3	17.7	14.9	2.7
53.3	16.6	12.3	4.3
63.3	15.3	11.1	4.2
73.3	12.4	7.7	4.7
83.3	10.1	3.9	6.1
93.3	5.7	-0.7	6.4
103.3	0.5	-5.9	6.4
112.7	-3.4	-11.8	8.3
122.7	-10.0	-17.0	7.0
132.7	-14.9	-25.0	10.1
142.7	-22.8	-33.0	10.2
152.7	-31.5	-42.9	11.4
162.7	-37.8	-49.0	11.2
172.7	-47.8	-59.7	11.8
Maximum variance within crest region (X < 100 mm)			6.4

In-plane X-coordinate of measurement (mm)	Theoretical Ogee Z-coordinate (mm)	Measured Ogee Z-coordinate (mm)	Difference (mm)
At 400 mm (White)			
0.0	0.0	0.0	0.0
13.3	13.1	11.0	2.0
23.3	16.1	14.9	1.1
33.3	17.6	15.7	1.9
43.3	17.7	15.9	1.8
53.3	16.6	14.7	1.9
63.3	15.3	13.4	1.8
73.3	12.4	10.4	2.0
83.3	10.1	7.3	2.8
93.3	5.7	3.3	2.4
103.3	0.5	-0.4	0.9
113.0	-3.4	-7.2	3.7
123.0	-10.0	-10.2	0.2
133.0	-17.4	-19.9	2.5
143.0	-22.8	-27.1	4.2
153.0	-31.5	-35.4	3.9
163.0	-37.8	-41.4	3.6
173.0	-47.8	-51.9	4.1
Maximum variance within crest region (X < 100 mm)			2.8
At 600 mm (Red)			
0.0	0.0	0.0	0.0
13.5	13.1		
23.5	16.2	15.5	0.7
33.5	17.6	17.3	0.3
43.5	17.7	17.5	0.2
53.5	16.6	17.1	-0.6
63.5	15.3	15.7	-0.5
73.5	12.4	13.9	-1.4
83.5	8.7	10.2	-1.5
93.5	5.7	5.2	0.5
103.5	0.5	0.5	0.0
113.4	-3.4	-5.4	1.9
123.4	-10.0	-7.9	-2.1
133.4	-17.4	-15.5	-2.0
143.4	-22.8	-23.0	0.1
153.4	-31.5	-30.8	-0.8
163.4	-41.1	-39.6	-1.5
173.4	-47.8	-47.0	-0.8
Maximum variance within crest region (X < 100 mm)			1.5
At 800 mm (Blue)			
0.0	0.0	0.0	0.0
14.1	13.4	12.1	1.3

In-plane X-coordinate of measurement (mm)	Theoretical Ogee Z-coordinate (mm)	Measured Ogee Z-coordinate (mm)	Difference (mm)
24.1	16.3	15.1	1.2
34.1	17.6	16.8	0.8
44.1	17.7	17.0	0.6
54.1	16.6	15.1	1.5
64.1	15.3	13.6	1.6
74.1	12.4	12.5	-0.1
84.1	8.7	8.8	-0.1
94.1	5.7	3.8	2.0
104.1	0.5	-1.0	1.5
114.2	-5.5	-5.2	-0.4
124.2	-10.0	-8.2	-1.8
134.2	-17.4	-14.8	-2.7
144.2	-25.6	-23.6	-2.0
154.2	-31.5	-30.3	-1.2
164.2	-41.1	-40.5	-0.6
174.2	-47.8	-45.6	-2.2
Maximum variance within crest region (X < 100 mm)			2.0
At 1000 mm (Purple2)			
0.0	0.0	0.0	0.0
14.8	13.5	11.3	2.2
24.8	16.5	14.0	2.5
34.8	17.7	14.5	3.1
44.8	17.7	13.6	4.1
54.8	16.6	12.6	4.0
64.8	14.4	10.6	3.8
74.8	12.4	7.9	4.6
84.8	8.7	2.6	6.1
94.8	5.7	-1.4	7.1
104.8	0.5	-6.4	6.9
115.6	-5.5	-11.3	5.7
125.6	-12.4	-18.1	5.7
135.6	-17.4	-25.8	8.4
145.6	-25.6	-32.8	7.1
155.6	-34.6	-40.9	6.2
165.6	-41.1	-50.9	9.8
175.6	-51.3	-60.0	8.7
Maximum variance within crest region (X < 100 mm)			7.1
At 1100 mm (Yellow2)			
0.0	0.0	0.0	0.0
15.7	13.9	10.8	3.0
25.7	16.6	12.3	4.3
35.7	17.7	12.4	5.3
45.7	17.4	11.0	6.5

In-plane X-coordinate of measurement (mm)	Theoretical Ogee Z-coordinate (mm)	Measured Ogee Z-coordinate (mm)	Difference (mm)
55.7	16.6	9.3	7.3
65.7	14.4	6.1	8.3
75.7	12.4	2.8	9.7
85.7	8.7	-2.3	11.0
95.7	4.1	-7.0	11.1
105.7	0.5	-13.2	13.7
115.7	-5.5	-18.3	12.8
125.7	-12.4	-24.9	12.5
135.7	-17.4	-32.2	14.8
145.7	-25.6	-40.3	14.7
155.7	-34.6	-49.6	15.0
165.7	-41.1	-57.7	16.6
175.7	-51.3	0.0	-51.3
Maximum variance within crest region (X < 100 mm)			11.1

Overlapping the measured Ogee surface (red) plot in **Figure 4-25** is the theoretical Ogee profile by the USACE (1970) depicted by the green surface.

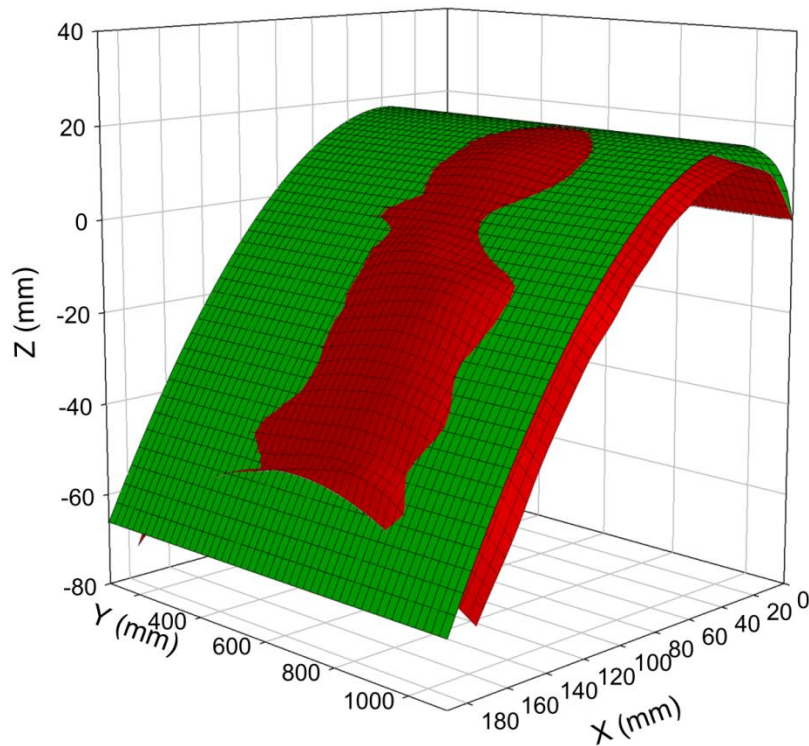


Figure 4-25: Measured Ogee surface for scenario 3B compared with theoretical Ogee profile as given by the USACE (1970)

The measured Ogee profile varied considerably with the theoretical approximations. This was to be expected since the theoretical approximations were derived from a symmetrical, uncontracted approach channel (similar to a flume). Flow lines were thus always perpendicular to the crest of the weir and were only obstructed by the vertical side wall of the hydraulic structure. Unlike in this research project, where the flow patterns were asymmetrical in the approach channel resulting in 3-dimensional flow across the sharp-crested weir. Conclusions and recommendations produced from this research study was reflected in Chapter 5.

5 CONCLUSIONS AND RECOMMENDATIONS

Based on the results of the experimental investigation, it can be concluded that the change in the symmetry of the approach channel has recognizably altered the shape of the Ogee profile. The influence of an asymmetrical approach channel on the bottom free surface nappe across a sharp-crested weir is noticeable in three ways:

1. The Ogee profile of the lower free surface nappe along the length of the weir is not uniform. From the experiments conducted it was noticed that off-centre of the weir, towards the side where the inclined side wall was positioned to alter the symmetry of the approach channel, the Ogee profile tend to be underestimated, this could potentially result in cavitation at this region;
2. When compared with the theoretical formulae (USBR 1987, USACE 1970, Hager 1987 and Ministry of Science and Technology (CE-05016) 2007) for estimating the Ogee profile, the profile of the asymmetrical cross-section configuration is greater than estimated in regions where a higher unit discharge is present; while the Ogee profile is smaller at the boundaries of the weir where more resistance against flow is being experienced;

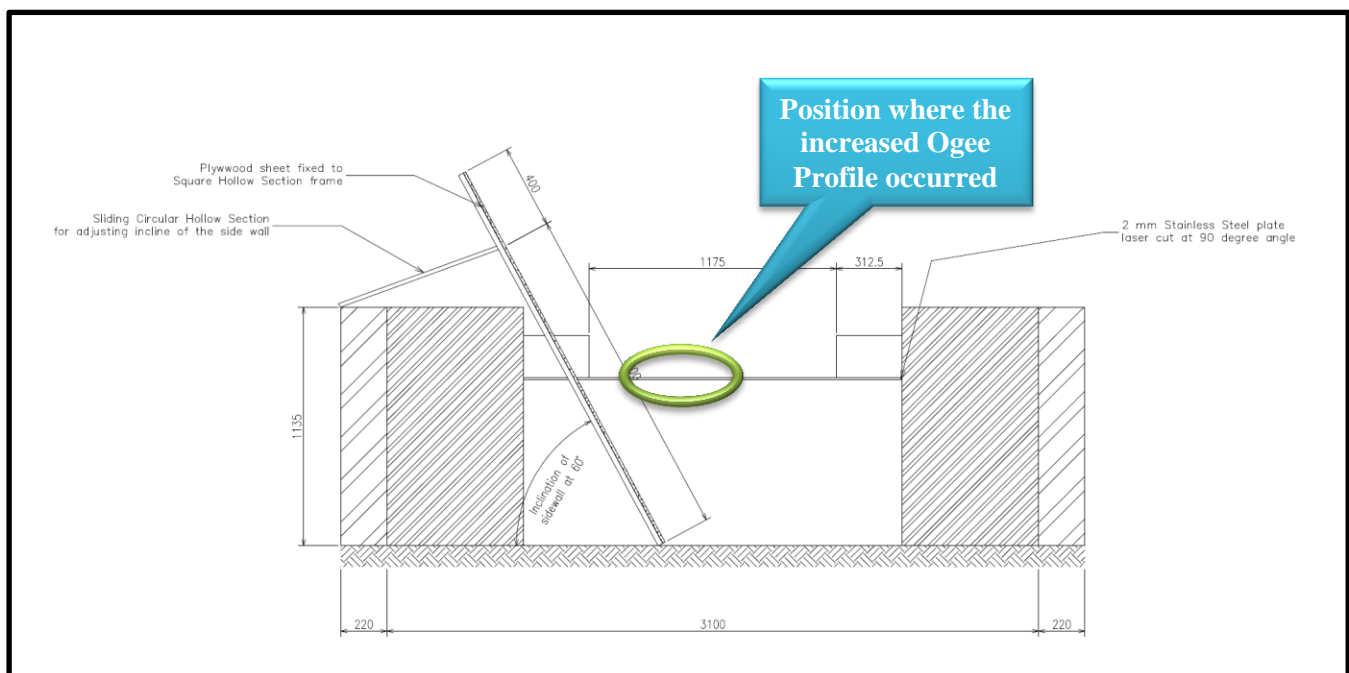


Figure 5-1: The upstream cross-sectional view of the asymmetrical approach channel reflecting the region where the increased Ogee profile is experienced

In the case that an Ogee spillway were to be designed by only considering the 2-dimensional flow parameters, problems could potentially arise if the upstream cross-section was asymmetrical. The Ogee profile would tend to be greater than expected toward the inclined side wall of the approach channel, yet lower than expected on the opposite side. This would cause the dual problem of potential separation from the spillway structure causing cavitation damage due to sub-atmospheric pressure, and sub-optimal discharge on the opposite side, respectively.

The comparison of measured Ogee profiles with the theoretically calculated Ogee profiles produced mixed results:

- The USBR (1987), USACE (1970), Hager (1987) and Ministry of Science and Technology (CE-05016) (2007) Ogee approximations corresponded well with the geometry of the measured Ogee profiles, although these curves tend to under estimate the actual Ogee profile at the position on the crest where the unit discharge is a maximum.
- Hager (1987) downstream approximation of the Ogee curve tends to over-estimate the projection of the nappe in the downstream region of the Ogee. This demonstrates that the formula is conservative and the probability of sub-atmospheric pressure occurring in the downstream region is minimized.

Based on the findings of this study it is recommended:

1. To investigate the influence of the angle of the approach channel relative to the crest of the Ogee spillway on the geometric shape of the Ogee profile and should be reviewed by means of physical modelling.
2. To investigate the influence of wall curvature of the Ogee spillway on the geometric shape of the Ogee profile by means of physical modelling.
3. Results obtained from this study, as well as the studies proposed for further investigation (1. and 2.) should be compared with a numerical simulation using a CFD analysis.

4. That the effect of 3-dimensional flow should be reviewed when designing an Ogee spillway. This is also indicative of the necessity of physical modelling during the design process, as theoretical curves do not necessarily provide optimal and safe solutions.

5. A design guideline should be developed to aid design engineers to design suitable, efficient and safe Ogee spillways.

6 REFERENCES

1. Anon., 2006. *Hydraulic Structures for Flow Diversion and Storage*, Kharagpur: National Program of Technology Enhance Learning.
2. Asawa, G., 2008. *Irrigation and Water Resource Engineering*. 1st ed. India: New Age International Publishers.
3. ASTM International, 2001. *Standard Test Method for Open-Channel Flow Measurement of Water with Thin-Plate Weirs*. United States of America, Patent No. Designation: D 5242 – 92.
4. Aydin, I., Altan-Sakarya, A. B. & Sisman, C., 2011. Discharge formula for rectangular sharp-crested weirs. *Flow Measurement and Instrumentation*, Volume 22, pp. 144-151.
5. Bagheri, S. & Heidarpour, M., 2010. Application of free vortex theory to estimating discharge coefficient for sharp-crested weirs. *Biosystems Engineering*, Volume 105, pp. 412-427.
6. Brennen, C. E., 1995. *Cavitation and Bubble Dynamics*. Illustrated ed. s.l.:Oxford University Press.
7. Chadwick, A., Morfett, J. & Borthwick, M., 2004. In: *Hydraulics in Civil and Environmental Engineering*. 4th ed. London: Spon Press, pp. 452-465.
8. Chanson, H., 2004. *The Hydraulics of Open Channel Flow: an Introduction*. 2nd ed. Oxford: Butterworth-Heinemann.
9. Chatila, J. & Tabbara, M., 2004. Computational modeling of flow over an ogee spillway. *Computers and Structures*, Volume 82, pp. 1805-1812.
10. Chow, V. T., 1959. *Open-Channel Hydraulics*. Reprint of the 1959 Edition ed. Illinois: The Blackburn Press.
11. Dam Contours, 2010. *Contour lines: South Africa Dams*. [Online]
Available at: <http://www.damcontours.co.za/>
[Accessed 26 10 2012].
12. DWA, 2010. *Dam Safety Office 2009-2010 Annual Reprt*, Pretoria: Department of Water Affairs.
13. DWA, 2011. *Dam Safety Office 2010-2011 Annual Reprt*, Pretoria: Department of Water Affairs.
14. DWA, 2012. *Dam Safety Office 2011-2012 Annual Reprt*, Pretoria: Department of Water Affairs.
15. Falvey, H., 1990. *Cavitation in Chutes and Spillways*. Denver: Bureau of Reclamation.
16. Fan, J., Mazur, J., Melicharek, N. & Schmittdiel, M., n.d. *Erosion, Cavitation, and Fretting Corrosion*. [Online]
Available at: <http://www.mse.berkeley.edu/groups/doyle/serdar/MSE112%20alias/COURSE-INFO/erosion.pdf>
[Accessed 5 February 2012].

17. Ferrari, A., 2010. SPH simulation of free surface flow over a sharp-crested weir. *Advances in Water Resources*, Volume 33, pp. 270-276.
18. Hager, W. H., 1987. Continuos crest profile for standard spillway. *Journal of Hydraulic Engineering*, 113(11), pp. 1453-1457.
19. Henderson, F. M., 1966. Open Channel Flow. *MacMillian*, pp. 191-197.
20. Horton, R. E., 1907. *Weir Experiments, Coefficients and Formulas*. Revision of Paper no. 150 ed. Washington: Government Printing Office.
21. Hughes, S. A., 1993. *Physical Models and Laboratory Techniques in Coastal Engineering*. 1st ed. Singapore: World Scientific Publishing Co. Pte. Ltd..
22. International Organization for Standardization, 2008. *Hydrometry - Open channel flow measurment using thin-plate weirs*. Switzerland, Patent No. ISO 1438.
23. International Water Power and Dam Construction, 2009. *Taking a tour of Concrete Face Rockfill Dams*, Sidcup, United Kingdom: Global Trade Media, a trading division of Progressive Media Group Ltd..
24. ISO 1438, 2008. *Hydrometry - Open channel flow measurement using thin-plate weirs*. Switzerland, Patent No. ISO 1438.
25. Johnson, F. A. & Green, C. S., 1977. The calibration of shrap-crested weirs by the pondage drawdown method. *Journal of Hydrology*, Volume 33, pp. 363-373.
26. Joseph, D., 1997. *Cavitation and the state of stress in a flowing liquid*, Minneapolis: s.n.
27. KEMO®, 2011. *BI92 - Water Level Sensor*, Beschreibung: Kemo Electronic.
28. KEMO®, 2012 (a). *M158 Waterswitch*, Beschreibung: Kemo Elecronic.
29. KEMO®, 2012 (b). *L100 Conducting Silver*, Langen: Kemo Electronic GmbH.
30. Knapp, R., Daily, W. & Hammit, F., 1970. *Cavitation*. s.l.:McGraw - Hill.
31. Koivula, T., 2000. On Cavitation in Fluid Power. *Proc. of 1st FPNI-PhD Symp.*, pp. 371-382.
32. Kramer, K., 2009. *Air detrainment of high-speed waters flows*, Zurich: Swiss Federal Institute of Technology Zurich.
33. KSB Pumps, 2005. *ETA C and D Product Catalogue*, Johannesburg: KSB Pumps.
34. LaBoon, J., Hepler, T., Lafond, R. & Pimley, L., 2011. Design Standards No. 14. In: *Appurtenant Structures for Dams (Spillways and Outlet Works) Design Standards*. s.l.:U.S. Department of Interior Bureau of Reclamation.
35. Lamb, W., 1987. *Cavitation and aeration in hydraulic systems*. Bedfordshire, UK: BHRGroup.
36. Lv, X., Zou, Q. & Reeve, D., 2011. Numerical simulation of overflow at vertical weirs using a hybrid level set/VOF method. *Advances in Water Resources*, Volume 34, pp. 1320-1334.

37. Martinerie, R. et al., 2005. Experimental study of the gated spillway of the Shahryar Dam in Iran. *Laboratory of Hydraulic Constructions*, pp. 1-10.
38. Melsheimer, E. S. & Murphy, T. E., 1970. *Hydraulic Design Criteria: Sheets 111-16 to 11-16/2*, s.l.: U.S. Army Corps of Engineers.
39. Merkley, G. P., 1995. *Lecture 7: Weirs for flow Measurement*, Utah: Utah State University.
40. Ministry of Science and Technology, 2007. *CE-05016 Design of Hydraulic Structures*, Myanmar: Department of Technical and Vocational Education.
41. Momber, A. W., 2000. Short-time cavitation erosion of concrete. *Wear*, Volume 241, pp. 47-52.
42. Morris, J. D., 2012. *Cavitation*, s.l.: Acts & Facts.
43. Murphy, T. E., 1973. *Spillway Crest Design*, Vicksburg: US Army Engineer Waterways Experiment Station.
44. Olsen, N. & Kjellesvig, H., 2010. Three-dimensional numerical flow modelling for estimation of spillway capacity. *Journal of Hydraulic Research*, 36(5), pp. 775-784.
45. PhotoModeler®, 2012. *PhotoModeler® Scanner*, Vancouver: PhotoModeler®.
46. PRO-VEY (Pty) Ltd., 2012. *FLexiLine Aluminium Profiles and Conveyor Accessories*, Pretoria: PRO-VEY (Pty) Ltd..
47. Rajaratnam, N., Subramanya, K. & Muralidhar, D., 1968. Flow profiles over sharp-crested weirs. *Journal Hydraulics Division ASCE*, 94(HY3), pp. 843-847.
48. Riley, J. D. & Rhoads, B. L., 2012. Flow structure and channel morphology at a natural confluent meander bend. *Geomorphology*, Volume 163-164, p. 84-98.
49. Rouse, H., 1936. Discharge characteristics of the free fall. *Civil Engineering*, Volume 6, p. 257.
50. Savage, B. & Johnson, M., 2001. Flow over Ogee Spillway: Physical and Numerical Model Case Study. *Journal of Hydraulic Engineering*, 127(8), pp. 640-649.
51. Şentürk, F., 1994. *Hydraulics of Dams and Reservoirs*. 1st ed. Highlands Ranch, Colorado: Water Resources Publication.
52. Smoak, G., 1997. *Guide to Concrete Repair*. Denver: US Dept. of the Interior.
53. Tatro, S. B. et al., 1994. Compendium of Case Histories on Repair of Erosion-Damaged Concrete in Hydraulic Structures. *American Concrete Institute*, ACI 210.1(R-94), pp. 210.1R-1 - 210.1R-33.
54. Thandaveswara, B., 2006. *Indian Institute of Technology*, Madras: National Programme on Technology Enhanced Learning (NPTEL).
55. Tropea, C., Yarin, A. L. & Foss, J. F., 2007. *Springer Handbook of Experimental Fluid Mechanics*. 1st ed. Berlin: Springer-Verlag Berlin Heidelberg.

56. U.S. Army Corps of Engineers, 2009. *Dam Safety Risk Analysis Best Practices Training Manual*. Version 2.2 - April 2011 ed. Denver, Colorado: U.S. Department of Interior Bureau of Reclamation.
57. USACE (a), 1987. *Hydraulic Design Criteria: Overflow Spillway Crest*, Vicksburg, Mississippi: U.S. Army Engineers Waterways Experiment Station.
58. USACE (b), 1987. *Hydraulic Design Criteria: Elliptical Crest Spillway Co-ordinates*, Vicksburg, Mississippi: U.S. Army Engineer Waterways Experiment Station.
59. USACE, 1970. *Hydraulic Design Criteria*, Vicksburg, MI: Army Waterways Experiment Station.
60. USACE, 1992. *Engineering and Design - Hydraulic Design of Spillways*. EM 1110-2-1603 ed. Washington: Department of the Army U.S. Army Corps of Engineers.
61. USBR, 1987. Chapter 9: Spillways. In: *Design of Small Dams*. 3rd ed. Washington: U.S. Government Printing Office, pp. 339-434.
62. van Vuuren, L., 2012a. *Water Research Commission: Press Release Lani van Vuuren*. [Online] Available at:
<http://www.wrc.org.za/News/Pages/NewbookexploreshistorybehindSouthAfrica%E2%80%99smostimpressivebulkwaterinfrastructure.aspx>
[Accessed 1 October 2012].
63. van Vuuren, L., 2012b. *Water Research Commission: News Lani van Vuuren*. [Online] Available at:
<http://www.wrc.org.za/News/Pages/ThehistorybehindSouthAfrica%E2%80%99slargedams.aspx>
[Accessed 1 October 2012].
64. van Vuuren, L., 2012c. *New book explores history behind South Africa's most impressive bulk water infrastructure*. [Online] Available at:
<http://www.wrc.org.za/News/Pages/NewbookexploreshistorybehindSouthAfrica%E2%80%99smostimpressivebulkwaterinfrastructure.aspx>
[Accessed 20 July 2012].
65. van Vuuren, S. J., 2010. *Model Study of the Neckertal Dam - Namibia*, Pretoria: Sinotech CC.
66. van Vuuren, S., Steyn, G., Pilz, N. & Koch, H., 2011. *Influence of 3D approaching flow on a curved ogee spillway section - Neckartal Dam Namibia*. Stellenbosch, UP Printers.
67. Vischer, D. & Hager, W., 1999. In: *Dam Hydraulics*. s.l.:John Wiley and Sons, pp. 40-44.
68. Wahl, T. L., Frizell, K. H. & Cohen, E. A., 2008. Computing the Trajectory of Free Jets. *Journal of Hydraulic Engineering* © ASCE, 10.1061(2), pp. 256-260.

69. Wiltshire, R. L., Gilbert, D. R. & Rogers, J. R., 2010. *Hoover Dam 75th Anniversary History Symposium*. 1st ed. Las Vegas, Nevada: American Society of Civil Engineers.
70. Yahoo! Inc., 2011. *Flickr from Yahoo!*. [Online]
Available at: <http://www.flickr.com>
[Accessed 07 October 2012].

APPENDIX A: POPULATED DATA SHEETS